Ultra-Short Pulsed Non-Equilibrium Atmospheric Pressure Gas Discharges

.....

by

James Leon Walsh

A Doctoral Thesis

Submitted in partial fulfilment of the requirements

for the award of

Ph.D. of Loughborough University

01/04/2008

Abstract

This thesis presents experimental studies of various non-thermal atmospheric pressure gas discharges generated using short pulsed excitation as an alternative to widely used sinusoidal excitation. Several pulse generators are detailed that provide high voltage pulses ranging from hundreds of microseconds to less than ten nanoseconds in duration. A key enabler to the generation of a stable discharge is a suitably high repetition rate; this prerequisite precludes many conventional pulsed power technologies. Fortunately, recent advances in semiconductor technology have made it possible to construct solid state switches capable of producing high voltage pulses with repetition rates of many kilohertz. Pulsed excitation introduces many opportunities to tailor the applied voltage and consequently enhance the discharge which are not possible with sinusoidal excitation sources. Through detailed electrical and optical analysis it is shown that pulsed excitation is not only more energy efficient than a comparable sinusoidal source but produces a higher flux of excited species that are essential in many applications. When pulse widths are reduced to a sub-microsecond timescale a novel barrier-free mode of operation is observed. It is shown that diffuse large area plasmas are easily produced at kilohertz repetition rates without the usually indispensable dielectric barriers. Experimental results show that a short pulse width prevents the onset of the undesirable glow-to-arc transition thus introducing an added degree of stability. A further benefit of pulsed excitation is the ability to produce gas discharges with a high instantaneous peak power yet low average power consumption, resulting in a high density plasma that exhibits room-temperature characteristics. Finally, as an acid test to highlight the many benefits of pulsed excitation several real-world applications are considered. It is shown that in all cases pulsed gas discharges provide real benefits compared to their sinusoidal counterparts.

Key words: gas discharge, atmospheric, pulsed, nanosecond, plasma jet, experimental, helium, argon, polymer, bio-decontamination.

Acknowledgements

This thesis would not be possible without the tireless support and encouragement from my supervisor, Professor Michael Kong, who introduced me as an undergraduate student to the fascinating world of plasma. I appreciate greatly the conversations we had, the invaluable advice he shared with me, and his never ending confidence in my abilities.

I also wish to thank Loughborough University for the financial support provided in the form of a four year scholarship; this PhD would not have been possible without it.

My sincere thanks go to the numerous people that have helped me considerably over the past four years. Special thanks go to my colleagues within the Plasma and Pulsed Power group, Dr Jianjun Shi, Dr Xuatao Deng, Dr Felipe Iza, and Mr David Liu. Their knowledge and experience has benefited my work considerably.

Finally, but certainly not least I would like to express my deepest thanks to my family and friends for their support and encouragement over the past four years.

Journal Publications:

[1] Walsh J.L, Shi J.J, Kong M.G, 'Contrasting characteristics of pulsed and sinusoidal cold atmospheric plasma jets', Applied Physics Letters, Vol.88, Iss.17, No.171501, 2006.

[2] Walsh J.L, Shi J.J, Kong M.G, 'Submicrosecond pulsed atmospheric glow discharges sustained without dielectric barriers at kilohertz frequencies' Applied Physics Letters, Vol.89, Iss.16, No.161505, 2006.

[3] Walsh J.L, Kong M.G, 'Sharp bursts of high-flux reactive species in submicrosecond atmospheric pressure glow discharges', Applied Physics Letters, Vol.89, Iss.23, No.231503, 2006.

[4] Walsh J.L, Kong M.G, 'Room-temperature atmospheric argon plasma jet sustained with submicrosecond high-voltage pulses', Applied Physics Letters,Vol.91, Iss.22, No.221502, 2007.

[5] Walsh J.L, Kong M.G, '10 ns pulsed atmospheric air plasma for uniform treatment of polymeric surfaces', Applied Physics Letters, Vol.91, Iss.25, No.251504, 2007.

[6] Walsh J.L, Kong M.G, 'Frequency Effects of Plasma Balls in Atmospheric Glow Discharges', IEEE Transactions on Plasma Science, Accepted for publication.

[7] Perni S, Shama G, Hobman J.L, Lund P.A, Kershaw C.J, Hidalgo-Arroyo G.A, Penn C.W, Deng X.T, Walsh J.L, Kong M.G, 'Probing bactericidal mechanisms induced by cold atmospheric plasmas with Escherichia coli mutants', Applied Physics Letters, Vol.90, Iss.7, No.073902, 2007.

Conference Publications:

[1] Walsh, J.L, Chalise, P.R, Kong, M.G, 'Microprocessor-Controlled Nanosecond Pulser System for Cell Manipulation'Plasma Science, 2005. ICOPS '05. IEEE Conference Record - Abstracts. IEEE International Conference on 20-23 June 2005, pp.242 - 242.

[2] Walsh, J.L, Shi, J.J, Kong, M.G, 'Characteristics of nonthermal atmospheric plasma jets with kilohertz voltage excitation', Technical plasma workshop, Edinburgh, Dec 2005.

[3] Walsh, J.L, Shi, J.J, Kong, M.G, 'Characteristics of a nonthermal atmospheric plasma jet with pulsed excitation' International Workshop on Microplasmas, Greifswald, 2006.

[4] Walsh, J.L, Shi, J.J, Kong, M.G, 'Cold atmospheric plasma jet sustained with nanosecond voltage pulses', Plasma Science, 2006. ICOPS 2006. IEEE Conference Record - Abstracts. The 33rd IEEE International Conference on 2006, pp.260 - 260.

[5] Walsh, J.L, Shi, J.J, Kong, M.G, 'Nanosecond pulsed atmospheric glow discharges without dielectric barriers', Plasma Science, 2006. ICOPS 2006. IEEE Conference Record - Abstracts. The 33rd IEEE International Conference on 2006, pp.3 - 3.

[6] Walsh, J.L, Kong, M.G, 'Sub-microsecond and nanosecond pulsed atmospheric pressure glow discharges' Technical plasma workshop, Manchester, Dec 2006.

[7] Walsh, J.L, Kong, M.G, 'Near room-temperature sub-microsecond pulsed plasma jet in flowing atmospheric argon', XXVIII International Conference on Phenomena in Ionized Gases, Prague 2007.

[8] Walsh, J.L, Kong, M.G, 'Ultra-short pulsed excitation: an efficient route to highly reactive, tens kilowatts, and near room-temperature atmospheric glow discharges', 18th International Symposium on Plasma Chemistry, Kyoto, 2007.

[9] Walsh, J.L, Kong, M.G, 'Ultra short pulsed glow discharges for the uniform treatment of polymeric surfaces' Technical plasma workshop, Belfast, Dec 2007.

Contents

1 Introduction

1.1 A historical perspective

Plasma, known as the forth state of matter,[1.1] is typically obtained when a significant amount of energy is applied to a gas. Within the gas, electrons are detached from atoms allowing positive and negative charges to move more freely; as electrons are small they are rapidly accelerated and consequently produce more electrons via collisions. When the amount of free electrons increases such that the electrical properties of the gas are affected it is called a plasma or an ionised gas.

It is estimated that approximately 99% of all matter in the universe is in the form of ionised gas.[1.2] It is worth noting however that not all plasmas are equal, they differ significantly in terms of temperature and density. Figure 1-1 illustrates typical parameters of naturally occurring and laboratory plasmas.[1.3]

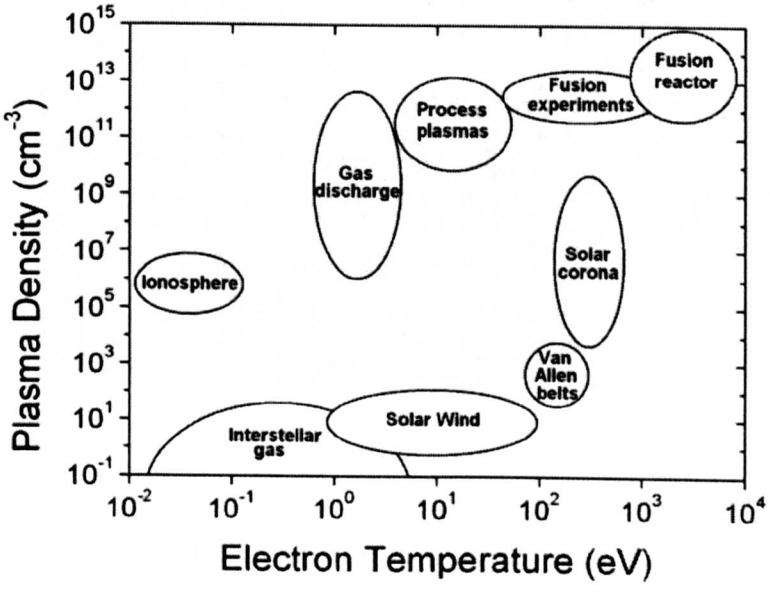

Fig 1-1: Typical parameters of naturally occurring and laboratory plasmas.

The term plasma was first used by Irving Langmuir in 1928 but the study of gas discharges can be traced back to the 17th century.[1.4,1.5] Naturally occurring gas discharges, such as lightening and the aurora, are commonly observed and have fascinated people for many centuries. The desire to discover the reasons behind naturally occurring gas discharges led early pioneers in the field to construct apparatus which enabled discharges to be studied in the laboratory.

Discharges due to frictional charge were observed by the Greek philosophers but it was not until the 17th and 18th centuries that real progress and understanding was achieved.[1.5] Notably, around this time significant progress was made on charge storage devices, such as batteries and capacitors. The ability to store electrical energy and discharge it when required was fundamental for those wishing to study gas discharges, at the time no other means of providing the necessary ionisation energy existed.

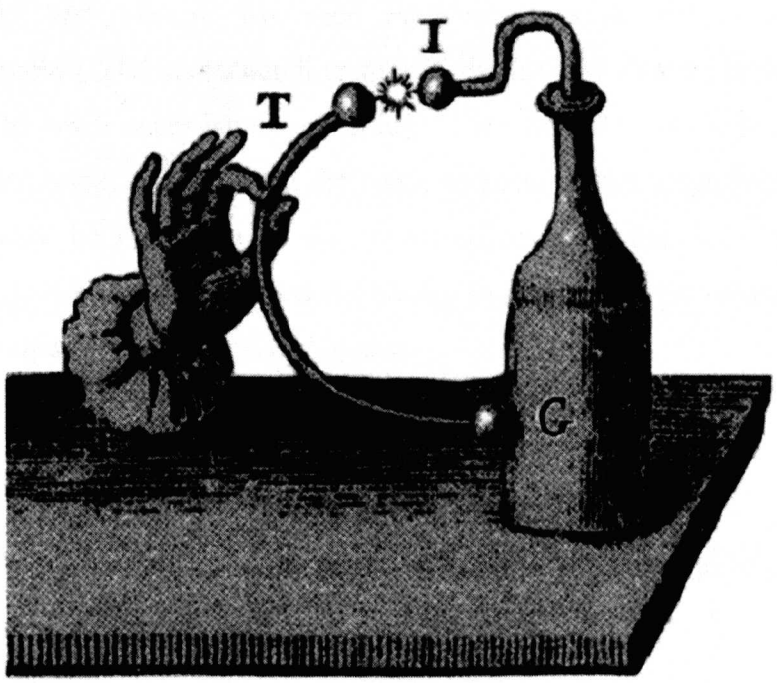

Fig 1-2: Arc discharge device, developed in 1775.

Figure 1-2 shows an early arc discharge device, the apparatus consisted of a charge storage device known as a Leyden jar and two metallic electrodes.[1.6] The touching of one electrode to another caused the stored

charge to rapidly discharge thus producing a 'spark'. The Leyden jar was developed by von Kleist and van Musschenbroek in 1745. Later in 1800, Volta produced a working electrochemical battery.[1.7] These devices provided the energy for many of the early gas discharge devices, such as the continuous arc discharge demonstrated by Petrov in 1803.[1.8]

During the 19th century significant progress was made on energy storage devices and vacuum systems. By 1830 Faraday was conducting extensive investigations into gas discharges within evacuated glass tubes,[1.9] the forerunner to today's vacuum plasmas. In the latter years of the 19th century and early 20th century a significant understanding of gas discharges had been reached. It was known how to produce and to control a discharge, also that the discharge was in the form of a partially ionised gas consisting of neutral, positive, and negative particles.

The 20th century has seen rapid progress in the development, characterisation, and understanding of gas discharges. Plasma is no longer confined to small scale laboratory study. It is often the case that industrial applications, especially those in the semiconductor industry, prove to be the driving force behind many of the recent advances in the field. Typically industrial processes depend upon the ability to generate large volume, stable gas discharges at the lowest possible cost.

1.2 Introduction to gas plasmas

A plasma can be characterised in terms of its level of ionisation, known as the ionisation degree, which can be calculated with equation (1.1)

$$Ionisation\ degree = \frac{n_i}{n_i + n} \tag{1.1}$$

where n_i and n are the densities of ionised particles and neutral atoms respectively. A plasma is classified as being weakly ionised when its ionisation degree is less than 10^{-2}, as the ionisation degree reaches unity the plasma is said to be fully ionised.

Using the ionisation degree allows a plasma to be classified into three types of discharge,[1.1] each with distinct properties and characteristics. Very weakly ionised gas is known as a dark discharge as it is invisible to the eye. As the ionisation degree increases the discharge transits into the glow discharge regime. Glow discharge plasmas are the basis of this thesis and will be discussed extensively in future chapters. Further ionisation leads to transition into the arc discharge regime, such plasmas are generally very hot and consume significant amounts of power.

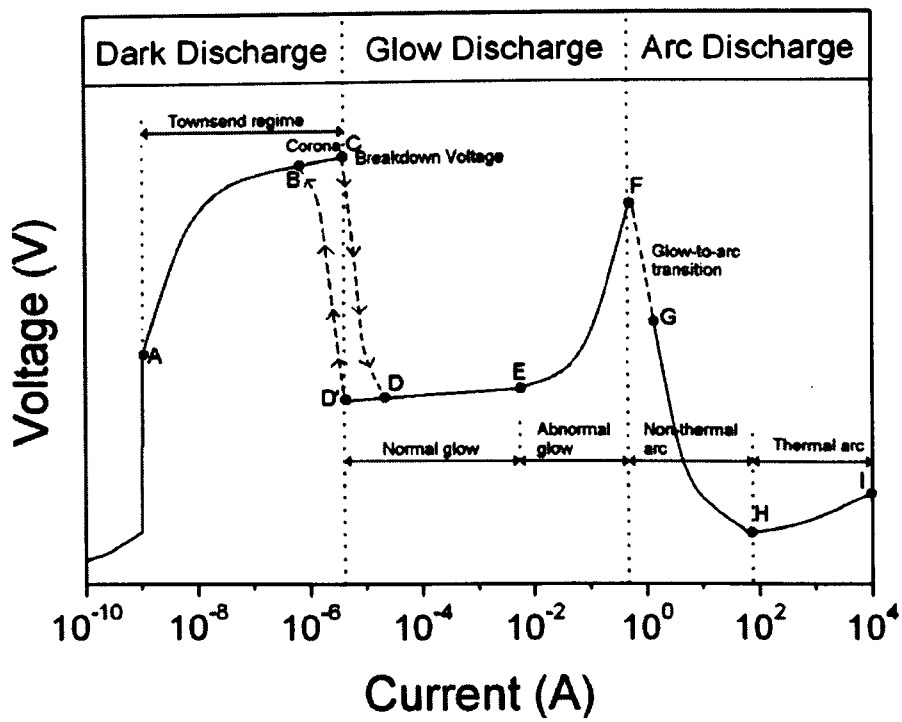

Fig 1-3: Typical voltage-current characteristics of a DC low-pressure discharge.

Figure 1-3 shows a typical voltage-current characteristic for a low pressure, usually less than 1 Torr,[1.3] DC electrical discharge.[1.10] In the figure the section preceding A is a non-self-sustaining discharge. A low voltage across the gap causes electrons, ionised by external sources (such as UV), to be accelerated toward the anode resulting in a very small current in the external circuit. Section A-C denotes the Townsend discharge regime, in which the discharge is self-sustaining. The high applied voltage causes free electrons within the gap to ionise gas molecules by electron impact, the result

is a multiplication of electrons and ions within the gas gap. As positive ions collide with the cathode, electrons are emitted via secondary electron emission. The emitted electrons are drawn to the anode and may collide with one or more gas atoms on route. As voltage is increased the rate of electron multiplication increases rapidly meaning small changes in voltage can cause a large rise in current, this corresponds to the section B-C in figure 1-3.

As the breakdown voltage is reached the effect of space charges becomes significant. As ion mobility is considerably lower than that of electron mobility a large concentration of positive ions form in front of the cathode. This is known as a cathode fall or sheath region. The voltage drop across the cathode fall is usually comparable to that across the discharge gap, as the cathode fall region is small the electric field is much higher than when distributed equally across the gap.[1.11] A higher electric field leads to increased electron multiplication resulting in a greater number of free electrons and a higher electrical conductivity. As such a lower applied voltage is capable of sustaining the discharge, which explains the drop in the applied voltage observed from C to D.

In the section D to E the cathode fall region is fully formed and the applied voltage is low. A small increase in applied voltage leads to a sharp rise in the discharge current. The current density in the glow discharge remains at a constant; it is the size of the discharge that varies. Initially only a small portion of the electrode gap may contain the discharge, as current is increased the discharge spreads to fill the gap. It should be noted that when current is reduced from point E the discharge will travel back to point D'. This hysteresis suggests that the discharge is dependant upon it's initial conditions.

At point E the discharge fully covers the entire electrode surface, a further increase in the discharge current leads to a decrease in the size of the cathode fall region. This results in a rapid voltage increase across the electrodes up to point F. As current is increased beyond point F the uniform glow discharge transits into a narrow channel known as an arc. In arc plasma

various processes such as gas heating and thermionic electron emission become dominant. Transition to arc is accompanied with a rapid drop in the voltage needed to sustain the discharge.

1.2.1 Gas breakdown

Fundamental to any gas discharge is the breakdown point; this is the point at which a plasma is initiated. In steady state plasma, such as a radio frequency generated glow discharge, the breakdown phase only occurs once; following breakdown the system descends in to a steady state. In transient plasma, such as the pulsed DC plasmas discussed in this thesis, the breakdown event takes up a considerable portion of the plasma lifetime.

Early studies on gas breakdown conducted by Paschen in 1889 showed that the voltage needed to break down a gas was a function of three variables.[1.12] The separation between the two electrodes, d, the pressure of the gas, p, and the type of gas used. Figure 1-4 highlights Paschen curves for various gases.[1.10]

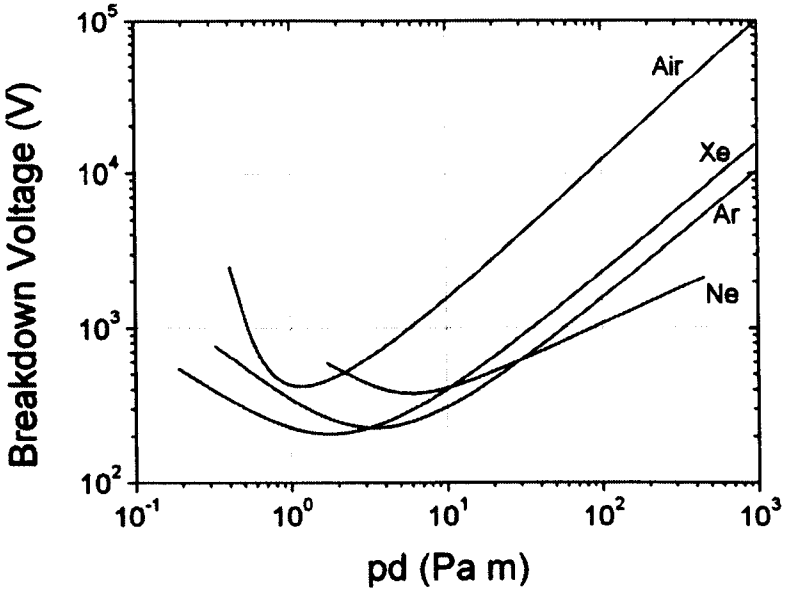

Fig 1-4: Paschen curves showing the breakdown voltage as a function of pd for various gases

Paschen curves were obtained experimentally in 1889 but the underlying processes involved in gas breakdown were not explained until Townsend proposed a theory in 1909. The theory was based on ionisation and electron multiplication and explained the results obtained by Paschen well. The Townsend theory is still commonly used today to describe low pressure discharges; however as the pressure is increased the theory no longer agrees with experimental observations. A new theory, known as streamer breakdown was developed by Loeb,[1.13] Meek,[1.14] and Raether.[1.15] In the streamer breakdown theory space charge effects inside electron avalanches are considered, resulting in thin, weekly-ionised channels, known as streamers.

1.2.2 Characteristics of glow discharges

Glow discharges play a vital role in many scientific and industrial applications. Due to the widespread usage of the glow discharge it is necessary to have a clear understanding of its distinguishing features and characteristics. The method of plasma generation determines the principal characteristics of the discharge; however, there are common features which can be observed in all glow discharges. Figure 1-5 shows the typical structure for a low pressure DC discharge.[1.3]

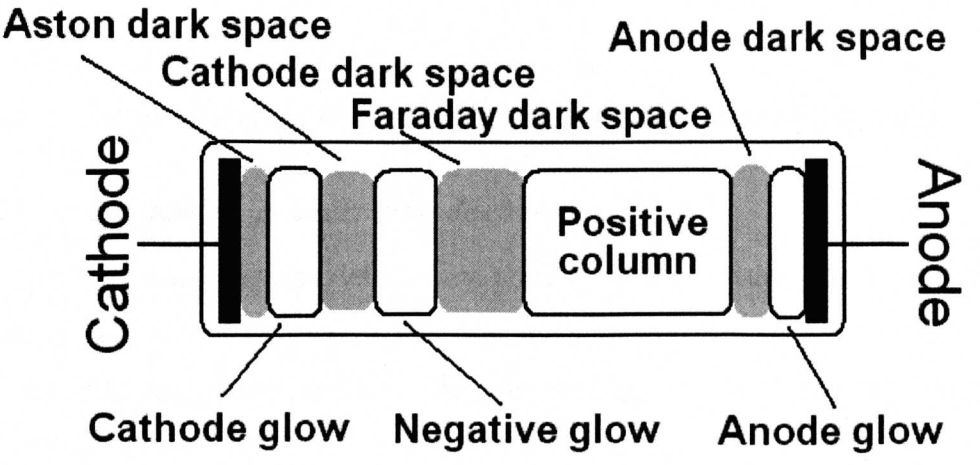

Fig 1-5: Typical structure of a low-pressure DC discharge

As shown in figure 1-5 the structure of a DC glow discharge is that of several dark and bright luminous layers that form along the discharge gap between the anode and cathode.[1.16] The cathode glow is observed as a bright band above the cathode which indicates the presence of a cathode fall region. Due to a high local electric field between the cathode and the cathode glow, a region of very few ions and fast moving electrons is produced, this is typically known as a sheath region.

When a high frequency alternating voltage, for example in the MHz range, is applied to a gas filled gap a discharge is produced. The use of radio frequency (RF) excitation has been studied extensively and is perhaps one of the most widespread techniques for generating a glow discharge. A unique feature of the RF discharge is that the high excitation frequency tends to trap electrons within the electrode gap.[1.17] Examination of an RF discharge over one cycle of the applied voltage shows the formation of a sheath over the instantaneous cathode, similar to that seen in a DC discharge. Due to the alternating applied voltage, the sheath appears to form over one electrode in one half-cycle and then over the other electrode in the next half-cycle. As sheaths are formed on the same timescale as the applied RF voltage, typically 10-100ns, they appear to co-exist simultaneously when viewed by the naked eye.

1.3 Current trends in atmospheric pressure glow discharges

1.3.1 Atmospheric pressure glow discharges

The previous sections detail some common low pressure gas discharges, the generation and control of low and medium pressure plasma is notably easier than at higher pressures. As gas pressure is raised the number of atoms/molecules increases proportionally, consequently more electron collisions occur and ionisation rate increases significantly. At atmospheric pressure it is often difficult to maintain a stable discharge as the high breakdown voltage combined with high gas density leads to rapid ionisation

causing gas heating and consequently a glow to arc transition. To generate stable atmospheric pressure gas discharges, APGD, it is often necessary to use noble gases such as helium as it is particularly stable and has a very low breakdown voltage when compared to other gases.[1.18]

1.3.2 Generation Techniques

In general APGD is generated using either capacitive coupling, or inductive coupling techniques. Inductively coupled plasma (ICP) tends to require high power, high frequency, and high cost excitation sources. ICP discharges also tend to have very high gas temperatures which can often be a disadvantage in many practical applications.[1.19,1.20] Capacitive coupling requires less power and can be achieved at much lower excitation frequencies. It's the relative ease of generation over inductively coupled plasma that has led to such widespread use of the capacitively coupled gas discharge.[1.21]

A distinct drawback of atmospheric pressure gas discharges is the tendency for the discharge to undergo the glow-to-arc transition far easier than their low pressure counterparts. To prevent the rapid transition between glow to arc at sub-MHz excitation frequencies the use of resistive electrodes or dielectric barriers is often essential.[1.22,1.23] A dielectric layer limits the magnitude of discharge current by reducing the voltage drop across the discharge gap. A resistive electrode has a similar current limiting effect, as the discharge current increases the voltage dropped across the resistive electrode increases thus reducing the voltage drop across the gas gap. When a dielectric barrier is used to stabilise an APGD the discharge is known as a dielectric barrier discharge (DBD). A DBD has a unique current-voltage characteristic of one discharge event in every voltage rising phase, using a conventional kHz sinusoidal source results in two discharge events per applied voltage cycle. The basic concept of the DBD is to control the electron avalanche process by limiting the voltage applied to the gas gap.[1.24] In radio frequency APGD the glow to arc transition is prevented through the trapping of electrons and ions within the gas gap. As the applied voltage oscillates faster than the majority of

electrons can traverse the gap there is a current limiting effect which prevents arcing.[1.25] This thesis will detail the use of pulsed excitation as a method for generating stable APGD. Using short high voltage pulses offers a unique method of preventing the glow to arc transition, careful choice of pulse width allows the applied voltage to be removed before the glow discharge transits to an arc resulting in a high current yet stable APGD.[1.26, 1.27]

1.3.3 Applications

For many years low pressure glow discharges have been used extensively in materials processing applications, especially in the area of microelectronics fabrication.[1.21] Recent studies have shown that APGD's are capable of deposition,[1.28] and etching,[1.29] also the use of atmospheric DBD in surface treatment of polymers is widespread.[1.29] The rapid development and understanding of APGD systems suggests that it could potentially become an alternative to the currently indispensable low pressure plasma systems used in so many industrial applications. The shift from low pressure plasma processing to atmospheric pressure plasma processing would represent a huge saving in terms of cost and energy, as there is no longer the need for a vacuum system.

The use of APGD as a tool for sterilisation in biomedical applications is currently an area of intensive research. It has been shown that APGD is an effective tool for tissue processing and repair,[1.30] decontamination of cavities in teeth,[1.31] and protein removal from surgical instruments.[1.32] Food safety is also an area that benefits from the ability of APGD to inactivate biofilm-forming bacteria.[1.33]

1.4 Scope of thesis

This thesis provides the reader with an experimental study of a novel APGD generated using short bursts of high voltage electricity. Pulsed gas discharges, such as those used in spark gap switches, have been studied at

length by others for many years; the physics behind such discharges is well understood. This work takes advantage of recent advances in semiconductor technology to show experimentally that it is possible to produce a stable, uniform, and room-temperature APGD using high repetition rate voltage pulses. The pulse generating devices used in the experiments detailed within this thesis are all based on 'off the shelf' semiconductor devices, many systems used have been developed 'in-house'. The research described employs modern diagnostic equipment that is capable of capturing the highly transient nature of pulsed APGD. Through analysis of the recorded data it has been possible to propose theories for the physical mechanisms behind pulsed generation of APGD.

A notable feature of this thesis is that it is divided in to two distinctive parts; this reflects two of the major areas of active research in the field of APGD. The generation of a gas discharge between parallel electrodes is widely used both in laboratories and industrial processes. The simplistic geometry of two flat plates is highly conducive to the production of a uniform discharge due to the uniformity of the electric field across the gap. Industrial processes often make use of a parallel plate electrode configuration for 'in-situ' processing; where an object is place between the electrodes and exposed to the plasma.

A recently developed electrode geometry, known as the plasma jet, has captured the attention of many working within the field. The benefit of using a jet like configuration is that plasma is generated in a region of stable inert gas and then flushed in to a region of highly reactive gas; thus simultaneously achieving stability and reactivity. Figure 1-6 highlights the impact of electrode configuration on the characteristics of an APGD. It is clear that electrode geometry is of fundamental importance in the study of APGD and as such the parallel plate and jet configuration are considered separately.

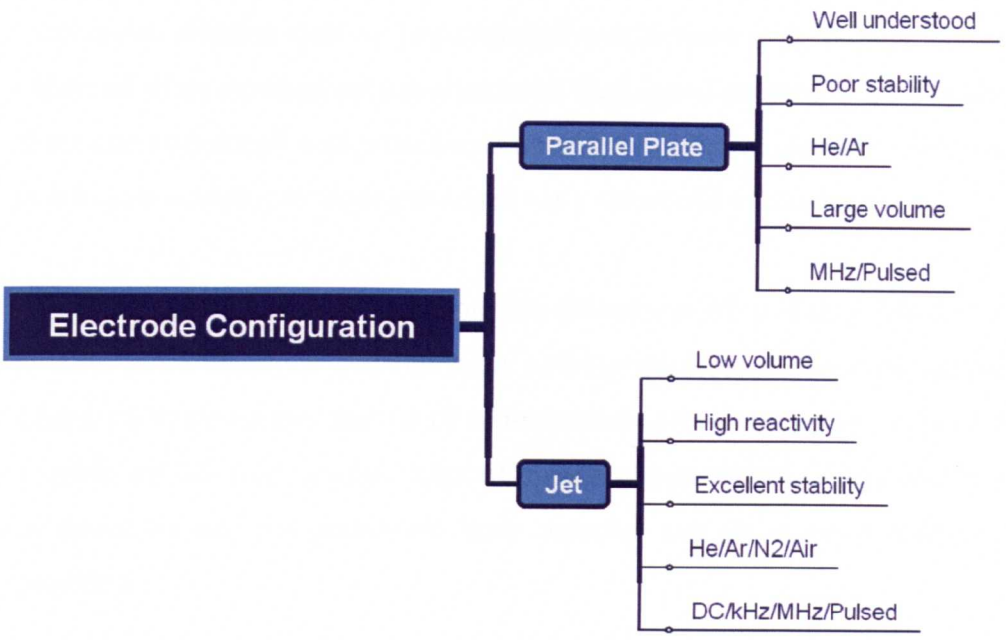

Fig 1-6: Effect of electrode geometry on the characteristics of an APGD.

1.5 Thesis outline

As discussed in the preceding section this thesis is divided into two distinct parts to reflect the current trend in APGD research. Following a brief review of pulse generation technologies in Chapter 2; Chapters 3, 4, and 5 are dedicated to investigations on pulsed excitation of a plasma jet device. Chapter 3 presents detailed experimental results to highlight the advantages of using pulsed excitation over the commonly used kHz sinusoidal excitation.

Chapter 4 details experimental observations of sub-microsecond pulsed plasma jets operating with helium or argon as a base gas and the effects of varying the applied voltage, pulse width and repetition frequency. Also considered are the effects of adding various reactive gases to the base gas in order to achieve a higher flux of reactive species within the discharge.

Chapter 5 is the concluding chapter on the jet configuration and presents observations of the actual plasma plume produced using a typical plasma jet. Previous studies have indicated that a high velocity 'plasma bullet' phenomenon is observed; however, a complete theory to describe the bullet

mechanism remains elusive. Experimental results show that 'bullets' are also observed when a pulsed excitation is used, high speed imaging is used to show that bullets produced with pulsed excitation have different characteristics, such as a higher velocity, to those generated via a sinusoidal excitation.

Chapters 6 and 7 focus on the generation of a stable APGD in a parallel plate electrode configuration without the use of dielectric barriers. Chapter 6 demonstrates the use of sub-microsecond voltage pulses to generate a stable APGD, over a wide range of operating parameters. This novel mode of operation had not previously been reported and an in-depth analysis is provided.

Chapter 7 investigates the benefits of employing ultrashort pulsed plasma in various real world applications. It is shown that the many benefits discussed in previous chapters actually translate into clear improvements in application efficiency. Several of the key areas in which atmospheric pressure plasma are used, such as biomedicine, ultraviolet light production, and surface modification are considered. Finally, a conclusion and future work is discussed in Chapter 8.

1.6 Contributions of thesis

Over the thesis period of 36 months, 5 journal papers have been published and the work has been presented numerous times at leading international conferences. The key contributions reported in this thesis can be summarised as follows:

1. Advantages of pulsed excitation over sinusoidal excitation:
   The work detailed in Chapter 3, shows compelling evidence that pulsed excitation is a more efficient means of generating an APGD than an equivalent sinusoidal source. Following the publication of simulation data in 2000,[1.34] there had been some speculation in the community that pulsed excitation was more efficient however it was never proven until the results

in this chapter were published in 'Contrasting characteristics of pulsed and sinusoidal cold atmospheric plasma jets' J.L. Walsh, J.J. Shi, M.G. Kong. *Applied Physics Letters*. Vol.88 Iss.17 No.171501 2006.

2. Cold atmospheric pressure pulsed argon jet:
   The work detailed in Chapter 4 is the first reported study on the operation of a cold APGD jet that uses Argon as a working gas. Due to the nature of pulsed excitation it is possible to generate a stable, room-temperature Argon plasma plume that is flushed in to open air for various applications. Many of the results published in the section appeared in 'Room-temperature atmospheric argon plasma jet sustained with submicrosecond high-voltage pulses' J.L. Walsh, M.G. Kong. *Applied Physics Letters*. Vol.91, Iss.22, No.221502, 2007

3. Frequency effects on the plasma bullet:
   Chapter 5 investigates the transport mechanisms behind the plasma jet; it is shown that the plume consists of discreet plasma bullets moving at very high velocities. The exact nature of the plasma bullets is the subject of intensive research by many groups, the work detailed within Chapter 5 highlights for the first time the effects of excitation frequency upon the plasma bullets. Many of the results from this chapter are accepted for publication in IEEE Transaction on Plasma Science.

4. Observation of barrier-free APGD sustained with short pulses:
   A prerequisite for any sub-MHz APGD is generally at least one dielectrically coated electrode. Recent studies have shown that it is possible to operate a stable discharge in the kHz range without a barrier, but only over a very small range of operating parameters thus limiting its potential usefulness. The work described in Chapter 6 is the first reported study of a barrier free APGD that is stable over a wide range of operating parameters which does not rely upon RF excitation. Many of the results from this chapter appear in ' Submicrosecond pulsed atmospheric glow discharges sustained without dielectric barriers at kilohertz frequencies'

J.L. Walsh, J.J. Shi, M.G. Kong. *Applied Physics Letters* Vol.89 Iss.16 No.161505 2006. And in 'Sharp bursts of high-flux reactive species in submicrosecond atmospheric pressure glow discharges' J.L. Walsh, M. G. Kong. *Applied Physics Letters* Vol.89 Iss.23 No.231503 2006.

5. Application of ultra short pulsed APGD in real world applications:
   Chapter 7 details several applications where pulsed APGD makes a significant improvement over conventional sinusoidal excitation. It is shown that pulses on a nanosecond scale are capable of generating cold and diffuse air plasma that is well suited to the surface modification of polymeric materials. Several of the results from this chapter were published in '10 ns pulsed atmospheric air plasma for uniform treatment of polymeric surfaces' J.L. Walsh, M.G. Kong. *Applied Physics Letters* Vol.91 Iss.25 No.251504 2007.

References

[1.1] Roth J.R, 'Industrial plasma engineering: I Principals' IOP, 1995.

[1.2] Gurnett D.A, Bhattacharjee A. 'Introduction to plasma physics: With space and laboratory applications' Cambridge University Press, 2005.

[1.3] Lieberman M.A, Lichtenberg A.J, 'Principals of plasma discharges and materials processing' John Wiley & sons inc. 1994.

[1.4] Tonks L, 'The birth of plasma' American Journal of Physics, Vol.35, Iss.9, pp.857-858, 1964.

[1.5] Anders A, 'Tracking down the origin of arc plasma science I. Early pulsed and oscillating discharges' IEEE Transactions on plasma science, Vol.31, No.4, pp.1052-1059, 2003.

[1.6] Schiffer M.B, Bell C.L. 'Draw the lightening down: Benjamin Franklin and electrical technology in the age of enlightenment' Univ. California press, 2003.

[1.7] Volta A, 'On the electricity excited by the mere contact of conducting substances of different kinds' Abstracts of the Papers Printed in the

Philosophical Transactions of the Royal Society of London, Vol.1, pp.27-29, 1800-1814.

[1.8] Anders A, 'Tracking down the origin of arc plasma science-II. Early continuous discharges' IEEE Transactions on plasma science, Vol.31, No.4, pp.1060-1069, 2003.

[1.9] Faraday M, 'Experimental researches in electricity-Thirteenth series' Abstracts of the Papers Printed in the Philosophical Transactions of the Royal Society of London, Vol.4, pp.54-56, 1837-1843

[1.10] Raizer Y.P, 'Gas discharge physics' London: Springer, 1997.

[1.11] Wagenaars E, Bowden M.D, Kroesen G.M.W, 'Plasma emission imaging of a low-pressure argon breakdown' Plasma Sources Science and Technology, Vol.14, Iss.2, pp.342-350, 2005.

[1.12] Becker K. H, 'Non-equilibrium air plasma at atmospheric pressure' IOP Publishing, 2005.

[1.13] Loeb L.B, & Meek J.M, 'The mechanism of spark discharge in air at atmospheric pressure' Journal Applied Physics, Vol.11, pp.438-447, 1940.

[1.14] Meek J.M, Crags & J.D, 'Electrical Breakdown of gases' Oxford(Clarenden press), 1953.

[1.15] Raether H, 'Electron avalanches and breakdown in gases' London:Butterworth 1964.

[1.16] Udelson J.B, Creedon J.E, 'Comparison of electron density in different regions of a dc glow discharge' Physical Review, Vol.88, Iss.1, pp.145-145, 1952.

[1.17] Raizer Y.P, 'Radio-Frequency Capacitive Discharges' CRC Press, 1995.

[1.18] Park J, Henins I, Herrmann H.W, Selwyn G.S, 'Gas breakdown in atmospheric pressure an RF capacitive plasma source' Journal Applied Physics, Vol.89, Iss.1, pp.15-19, 2001.

[1.19] Long M.L, 'Power efficiency oriented design of high density CCP and ICP sources for semiconductor RF plasma processing equipment' IEEE Transactions on Plasma Science, Vol.34, No.2, pp.443-454, 2006 .

[1.20] Tuszewski M. 'Planar inductively coupled plasma operated with low and high radio frequencies' IEEE Transactions on Plasma Science, Vol.27, No.1, pp.68-69, 1999.

[1.21] Anders A, 'Plasma and ion sources in large area coating: A review' Surface & Coatings technology, Vol.200, Iss.5-6, pp.1893-1906, 2005.

[1.22] Laroussi M, Alexeff I, Richardson J.P, Dyer F.F, 'The resistive barrier discharge' IEEE Transactions on Plasma Science, Vol.30, Iss.1, pp.158-159, 2002.

[1.23] Kanazawa S, Kogoma M, Moriwaki T, Okazaki S, 'Stable glow plasma at atmospheric pressure' Journal Of Physics D-Applied Physics, Vol.21, Iss.5, pp.838-840, 1988.

[1.24] Mangolini L, Anderson C, Heberlein J, Kortshagen U, 'Effects of current limitation through the dielectric in atmospheric pressure glows in helium' Journal Of Physics D-Applied Physics, Vol.37, Iss.7, pp.1021-1030, 2004.

[1.25] Yuan X.H, Raja L.L, 'Computaional study of a capacitively coupled high-pressure glow discharges in helium' IEEE Transactions on Plasma Science, Vol 31, Iss.4, pp.495-503, 2003.

[1.26] Walsh J.L, Shi J.J, Kong M.G, 'Submicrosecond pulsed atmospheric glow discharges sustained without dielectric barriers at kilohertz frequencies' Applied Physics Letters, Vol.89, Iss.16, No.161505, 2006.

[1.27] Walsh J.L, Kong M.G, 'Sharp bursts of high-flux reactive species in submicrosecond atmospheric glow discharges' Applied Physics Letters, Vol.89, Iss.23, No.231503, 2006.

[1.28] Massines F, Gherardi N, Fornelli A, Martin S, 'Atmospheric pressure plasma deposition of thin films by Townsend dielectric barrier discharge' Surface & Coatings technology, Vol.200, Iss.5-6, pp.1855-1861, 2005.

[1.29] Choi H.S, Rybkin VV, Titov V.A, Shikova T.G, Ageeva T.A, 'Comparative actions of a low pressure oxygen plasma and an atmospheric pressure glow discharge on the surface modification of polypropylene' Surface & Coatings technology, Vol.200, Iss.14-15, pp.4479-4488, 2006.

[1.30] Stoffels E, '"Tissue processing" with atmospheric plasmas' Contributions to Plasma Physics, Vol.47, Iss.1-2, pp.40-48, 2007.

[1.31] Stoffels E, (Stoffels, E.), Kieft I.E, (Kieft, I. E.), Sladek R.E.J, van den Bedem L.J.M, van der Laan E.P, Steinbuch M. 'Plasma needle for in vivo medical treatment: recent developments and perspectives' Plasma Sources Science & Technology, Vol.15, Iss.4, pp.S169-S180, 2006.

[1.32] Deng X.T, Shi J.J, Chen H.L, Kong M.G, 'Protein destruction by atmospheric pressure glow discharges' Applied physics letters, Vol.90, Iss.1, No.013903, 2007.

[1.33] Vleugels M, Shama G, Deng X.T, Greenacre E, Brocklehurst T, Kong M.G, 'Atmospheric plasma inactivation of biofilm-forming bacteria for food safety control' IEEE Transactions on Plasma Science, Vol. 33, Iss.2. pp.824-828, 2005.

[1.34] Kong M.G, Deng X.T, 'Electrically efficient production of a diffuse nonthermal atmospheric plasma', IEEE Transactions On Plasma Science, Vol. 31, Iss.1, pp.7-18, Part 1, 2003.

2 Pulse generation techniques and applications

2.1 Current trends in pulsed power research

The generation of short, high voltage pulses has been an area of intensive research since the late 1930's.[2.1] Early radar systems directed short bursts of intense electrical energy into the sky as a means of detecting enemy aircraft and the field of pulsed power was born. The development of radar technology has progressed at a rapid rate in the post war decades, so much so, that it is now integral part of everyday life. The use of pulsed power is no longer limited to radar technology, the following sections detail several novel applications that rely on the principles and technologies developed in the field of pulsed power.

2.1.1 Military applications of pulsed power technology

Pulsed power technology plays a fundamental role in many military applications. Almost all areas of military technology, be it weapons or communications, require high energy sources. Recent examples of pulsed power technology employed in military applications includes the development of highly intense laser pulses to assist in the development of nuclear weapons without the need for testing with radioactive materials. Using advanced pulse power techniques, its possible to produce picosecond duration laser pulses with Petawatt energy densities. [2.2]

Another example of pulsed power technology employed in a military application is that of exploding wires. Large currents are pulsed through a wire causing it to vaporise, the resultant plasma is extremely dense and a large shockwave is produced.[2.3] A novel application of exploding wire technology is

that of canopy shattering and cutting; by embedding a wire within the canopy of a cockpit it is possible to shatter the canopy thus rapidly separating it from the aircraft it is attached to.[2.4]

2.1.2 Biological applications of pulsed electric fields

The application of pulsed electric fields is used extensively in molecular biology as a means of increasing the permeability of cellular membranes. Electrical pulses of several kV/cm in magnitude with durations from microseconds to milliseconds have the effect of opening pores on a cellular membrane thus allowing the introduction of foreign substances such as drugs or DNA.[2.5] The method, known as electroporation, is commonly used and many commercial devices are available.

Recent advances in pulsed power technology have opened the gateway to a new type of field-cell interaction, by means of sub-microsecond electrical pulses at electric fields exceeding 50 kV/cm the sub-cellular functions and structures of living cells can be manipulated. The ability to disrupt cellular signalling pathways has numerous applications; however, of significant interest is the ability to initiate cell suicide, known as apoptosis, in cancer cells.[2.6] It is often the case that cancer cells have mutated in such a way as to prevent the bodies attempts to destroy them. Potentially, high intensity nanosecond electrical pulses could offer a novel means of inducing apoptosis in cancer cells thus becoming a revolutionary cancer treatment.

The ability of high intensity pulsed electric fields to destroy micro-organisms is regarded as one of the most promising technologies in the areas of food processing and food safety.[2.7] A significant advantage of using pulsed electric fields as a sterilisation method over conventional techniques such as pasteurisation is the non-thermal nature of the treatment. In general, heat treatment of food alters the taste which is highly undesirable, pulsed electrical field treatment generates very little heat and is consequently a highly attractive technique. Generation of pulsed electric fields in excess of 30kV/cm with

microsecond duration has the effect of inducing a large cellular transmembrane potential that can lead to an electroporation effect and consequently destruction of the microrganism.[2.8] Recent studies have employed higher applied fields and shorter pulse durations to give an insight into the mechanisms behind the destruction of bacterial agents using pulsed electrical fields.[2.9]

2.1.3 Pulsed corona and other pulsed discharges

A corona discharge is a special kind of non-equilibrium plasma discharge with a low current density that forms in the presence of a highly non-uniform electric field.[2.10] The typical corona discharge device consists of a cathode-wire and a flat anode plate, a pulsed excitation source is usually used to apply negative high voltage pulses to the cathode. The discharge develops very much like a DC discharge, positive ions are accelerated towards the cathode where secondary electrons are emitted and accelerated, causing further ionisation by collision. A prerequisite for any pulsed corona discharge is that the pulse duration must be shorter than the time necessary for an arc to form. When each pulse ends, the discharge is extinguished before it becomes too conductive. Figure 2-1 shows a typical pulsed corona streamer formed in ambient air using a point to plane configuration. Pulsed corona discharges are widely used for the plasma assisted modification of surfaces, for example the deposition of hard coatings on a polymeric surface, [2.11] or the nitriding of steel. [2.12]

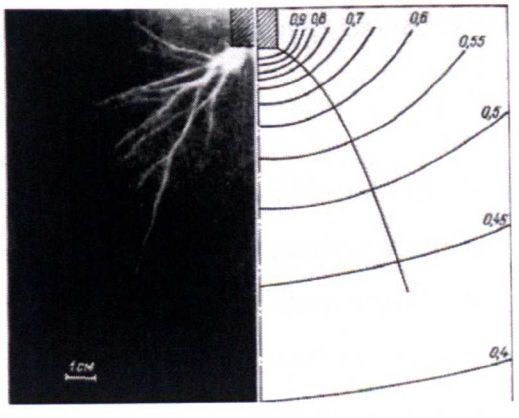

Fig 2-1: Photograph showing streamer produced from a rod to plane at a distance of 150cm. Applied voltage is 125kV. Schematic shows equipotential surfaces. [2.13]

The use of pulsed gas discharges is commonplace in the fields of plasma assisted ignition and plasma combustion. Experimental evidence has shown that low temperature plasmas can reduce the ignition delay time of combustible mixtures, intensify ignition, and sustain combustion of lean mixtures.[2.14] Recent studies have shown that the efficiency of combustion can be increased significantly by employing a low power, low temperature pulsed discharge to stabilise the flame,[2.15] the results obtained have far reaching consequences for large scale combustion processes.

2.1.4 Pulsed APGD

Relatively few studies exist in the area of pulsed atmospheric glow discharges. A computational investigation carried out in 2003 suggested that appropriate tailoring of the applied voltage waveform could permit a 50% reduction in the power required to sustain a an APGD whilst maintaining levels of electron and metastable densities.[2.16] The simulation results suggested a more efficient applied voltage waveform could be in the form of a rectangular pulse. Experimental data produced in 2004 showed that it was possible to generate and maintain a stable glow discharge using pulsed excitation at atmospheric pressure albeit with the use of dielectric barriers.[2.17] It was not until the publication of the work presented in this thesis that an exhaustive study was provided to highlight the several advantages of pulsed excitation over conventional sinusoidal excitation.[2.18] Experimental data obtained showed that not only was pulsed excitation significantly more electrically efficient, but also, the plasma generated contained a high flux of reactive species.

Experimental results detailed within this thesis highlight the use of sub-microsecond pulsed excitation to generate a stable glow discharge without the need for dielectric coatings on the electrodes.[2.19] This work employs the fast switching devices associated with modern pulsed power technology and the principals of gas discharge physics to generate intense, room-temperature, gas discharges.

2.2 Common Pulsed Power Switching Technologies

All pulsed power systems have two critical elements that dictate their entire systems characteristics. Every system must employ some kind of energy storage mechanism, allowing energy to be accumulated slowly and released rapidly. All devices used within this thesis, which are detailed later in the Chapter, make use of capacitive energy storage. This is a widely used technique involving the gradual charging of a capacitor to a high potential followed by a rapid discharge into the load. An alternative energy storage technique involves the use of energy stored within the magnetic field of an inductor; this often requires a more complex circuit design and has not been used within this body of work.

The second defining characteristic of a pulsed power system is the switching device used to discharge the stored energy. In most cases the switch determines the generator performance. For example, the switching devices used in the experimental studies conducted within this thesis must be capable of nanosecond switching and be rugged enough to handle instantaneous powers in excess of several kilowatts. In larger pulsed power systems nanosecond duration pulses with peak powers in excess of 10GW are often necessary for high power microwave sources.[2.20] The remainder of this section briefly describes some of the most common switching techniques employed in modern pulsed power systems that could be of potential use in generating repetitive high voltage pulses (<15kV) at rates from hundreds to many thousand pulses per second.

2.2.1 Reed switches

A Reed switch is an electro-mechanical switching device developed by W.B. Elwood in 1936.[2.21] It consists of two ferromagnetic contact blades hermetically sealed within an evacuated glass tube, for faster switching times the tube can be filled with various gases such as Hydrogen or SF_6. On the outside of the tube a coil of wire is wound. As an electric current flows

through the coil an electromagnet is formed, causing the contacts within the tube to be drawn together. Figure 2.2 shows a simple pulsed power system employing a reed switch and an energy storage capacitor. In the circuit, the capacitor C is gradually charged to the applied voltage. On application of a low voltage control signal the reed switch closes and the electric charge held within the capacitor is dumped into the load. The resistor, $R_{s/c}$, is used to protect the high voltage DC power source from being connected directly to ground via the low impedance load.

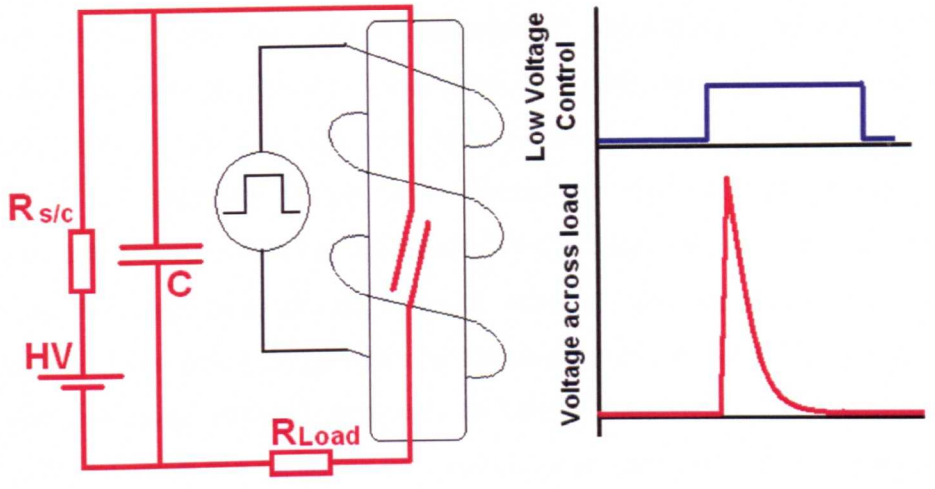

Fig 2-2: Simple pulsed power circuit using reed switch. High voltage components shown in red.

For example, in the circuit shown, if the applied voltage is 10kV and the load resistance is 1000Ω then the peak current would be 10A resulting in a peak instantaneous power of 100kW. The duration of the pulse is determined by the discharge time constant of the load and capacitor combination, consequently large energy storage capacitors and high impedance loads result in long pulses and low repetition rates.

Reed switches typically switch within a few nanoseconds, however, by carefully controlling the pressure and composition of the background gas within the switch, switching times as low as 50ps have been recorded.[2.21] Commercially available reed switches are capable of withstanding very high voltages, in excess of 20kV, however the hold-off voltage is inversely

proportional to the repetition rate of the device. A limited repetition rate severely limits the usefulness of the reed switch in many high-speed pulsed power applications, including the case of pulsed APGD. A further consideration is the lifetime of the device, which may be as low as 10^6 transitions.

2.2.2 Spark gaps

Spark gaps are widely used in pulse power applications, they can take many forms, from the simple automotive 'spark-plug' to the complex pressurised, laser triggered, pico-second switching device. Spark gaps vary considerably in their design and construction however in most cases the principal of operation is the same. When the electric field between two electrodes increases above the breakdown voltage an electron avalanche occurs. The electron avalanche forms a weakly ionised streamer that reaches across the inter-electrode gap joining the two electrodes. Once fully formed a complex heating mechanism occurs and the voltage across the gap falls to zero, at this point the switch is considered closed and very large currents can flow.

The simplest form of spark gap is the over-voltage gap, where the applied voltage is increased above the breakdown voltage thus causing the switch to close. A triggered spark gap typically makes use of a three electrode arrangement, two electrodes form the switch and a third is inserted into the gap between them. The applied voltage is held slightly below the breakdown voltage of the gap, when the switch is to be closed a high voltage pulse is sent into the third electrode causing the ionisation of nearby gas molecules. The weak discharge around the third electrode introduces additional electrons into the gap which has the effect of reducing the breakdown voltage such that the switch closes. More elaborate triggering methods, such as laser-triggering, can be employed to decrease switching time and jitter, yet they are all based upon the same principals. [2.22]

Typically spark gaps have two drawbacks when high repetition rate switching is considered. Most importantly, the discharge between the two electrodes must be fully extinguished before the system can begin to recharge. The dependence of switching rate on the lifetime of the plasma between the electrodes generally means that the repetition rate of a spark gap is limited to the sub-kHz. Through careful design and the use of a fan to blow the plasma from the gap switching rates in the low kHz range have been demonstrated, [2.21] however such systems are rather complex and expensive. A second disadvantage is that the electrodes in the system are subjected to extreme forces during normal operation and become rapidly degraded, this effects switching performance significantly.

2.2.3 Thyratrons and similar devices

A thyratron is a type of gas filled tube that is often used as a high energy electrical switch. The device was developed in the 1920's and is based on the vacuum tubes of the time. Small thyratron devices were manufactured on a mass scale and used in a variety of applications. Advances in semiconductor technology has virtually eliminated the use of small gas thyratrons, however, large thyratrons are still used in a variety of pulsed power applications that require rapid switching of high peak powers.

A typical hot-cathode thyratron uses a heated filament cathode, which is positioned below a control grid. The voltage on the control grid effects the electric field between the anode and the cathode which is held at the cathode potential when the devices is in the off state. If a positive voltage is applied to the control grid the gas between anode and cathode ionises and a current flows, at which point the switch is said to be on. The gas in large thyratrons is typically hydrogen and is at a fraction of the pressure of air at sea level; 15 to 30 millibars is typical. Modern thyratrons can switch hundreds of kilovolts and kiloamps in a few nanoseconds and are often found in radar systems and x-ray machines. For example, the E2V CX1594M Deuterium filled ceramic envelope thyratron is capable of switching 155kV and 10kA.

2.2.4 Semiconductors

The number of semiconductor devices that can be used as switches in pulsed power applications is numerous. Rapid development and new fabrication processes mean new devices are capable of switching higher powers in faster times than ever before. Common semiconductor switches include thyristors, bipolar junction transistors (BJT), metal-oxide-semiconductor field effect transistors (MOSFET's), insulated gate bipolar transistors (IGBT's), plus numerous diode devices. As the pulsed APGD work detailed within this thesis is based upon semiconductor technology the following section is dedicated to a discussion of some of the most common types of semiconductor switches employed in pulsed power applications.

2.3 Semiconductor switches

Compared to many other pulsed power switching devices semiconductors are a recent invention, yet one that has had inconceivably far reaching consequences. This section gives a introduction into several of the most common semiconductor switching devices and the typical applications they are used in. The work detailed in this thesis is entirely reliant upon semiconductor switching technology, as such, the remainder of this section highlights the properties of individual devices. The following section covers several topologies in which semiconductor switches are combined to produced a single high power switch.

2.3.1 Thyristor

The thyristor is a four-layer semiconductor device first conceived in 1950; it consists of alternating N-type and P-type doped silicon, for example P-N-P-N. A thyristor usually has three terminals, an anode, a cathode and a control terminal known as the gate which is connected to a P-type section near the cathode.

Essentially the thyristor can be thought of as a controllable diode. In one direction the diode blocks the flow of electrical current just as a regular diode does, in the opposite direction the diode can conduct, but only if the gate signal has been applied. Once a thyristor is conducting it cannot be turned off, this is a very significant property. After triggering a thyristor remains in the on-state regardless of the gate signal, the only way to reset a thyristor is to remove the current flowing through the device. In applications such as AC rectification this is not a problem as the voltage is periodically returned to zero thus resetting the device. However, in applications that require the pulse width to be controlled, thyristors are not best suited.

Thyristors can switch many kilo-amperes and several thousands of volts, typical applications include controllable rectification for large DC motors and 'crowbar' devices, which protect sensitive components within a power supply when the output is short circuited. As such they are generally designed to operate in a single shot or low repetition mode, typically 50/60Hz.

The switching characteristics of a thyristor and slow switching speeds, typically milliseconds, tend to preclude the use of thyristors in pulsed power applications including generation of a stable glow discharge. The thyratron discussed previously is the vacuum tube equivalent of the thyristor and has very similar characteristic, except switching speed, which may be several orders of magnitude shorter.

2.3.2 Bipolar Junction Transistor

A BJT is a three-terminal device constructed of a doped semiconductor material that is often used in amplifying or switching applications. Typically BJT's are produced using three layers of doped silicon, they can be manufactured such that the structure is either NPN or PNP.

BJT's can be summarised as current amplification devices. The current flowing into the base region controls the current flowing between the collector

and the emitter. Typically a base current of a few milliamps controls collector-emitter currents of several orders of magnitude larger, leading to a typical current gain of 50-1000. For applications where precise replication of the base waveform is required, the transistor is biased such that the maximum amplitude of the base signal is within the linear amplification region of the BJT. For applications where a BJT is used as a switch no biasing is required, the transistor is used in its saturation region and is either fully on or fully off.

The manufacture and design of transistors has improved significantly over the decades and modern transistors can switch significant amounts of power and have a very wide bandwidth. In general, the use of conventional transistors in pulsed power applications is limited as small BJT's are fast (typically nanosecond rise times) but have limited power handling capability, and large BJT's are too slow. Recent advances in MOSFET technology make BJT's less attractive to system designers (MOSFET's are detailed in the next section). One area in which the use of a BJT's is highly advantageous over a MOSFETs is RF amplification. The base of a BJT appears as a very high impedance load at RF and is relatively easy to drive, a MOSFET gate appears as a large capacitance which is almost impossible to drive above a few MHz.

A unique mode of operation, known as the avalanche breakdown, is observed in BJT transistors,[2.25] this allows very fast switching of high voltage signals. BJT's operated in the avalanche mode are used in many pulsed power systems for the generation of kilovolt pulses with sub-nanosecond switching times. This mode of operation is discussed further in section 2.4.

2.3.3 FET's & Power MOSFET

The field-effect transistor (FET) is a type of transistor that relies on an electric field to control the shape and hence the conductivity of a 'channel' in a semiconductor material. The concept of the field effect transistor predates the bipolar junction transistor (BJT), however FETs were implemented after BJTs

due to the limitations of semiconductor materials and relative ease of manufacturing BJTs compared to FETs at the time.

A FET controls the flow of electrons from the source to drain by affecting the size and shape of a "conductive channel" created and influenced by the voltage (or lack of voltage) applied across the gate and source terminals. There are numerous types of FET devices available, each with distinctive properties; by far the most commonly used in the area of power electronics is the metal oxide field effect transistor (MOSFET).

MOSFETs have been used in power electronics applications since the early 80's due to their appreciable current carrying capability, high blocking voltage, and low on-state resistance. They have managed to replace BJTs in many applications due to their simple gate drive requirements and positive temperature coefficient. As devices warm up they become increasing resistive, consequently when devices are paralleled there is little chance for thermal runaway in a single device, this is not the case with BJTs.

N-channel enhancement type power MOSFETS are the most popular for use in power switching circuits and applications. The drive voltage is applied between the gate and the source to switch the MOSFET on, this must exceed a threshold value which is usually around a few volts. Essentially a MOSFET gate behaves like a capacitor, once it is charged it will remain charged indefinitely. Also like a capacitor, the time it takes to charge the gate (and consequently turn-on the device) relates directly to the current applied. A typical 1nF MOSFET gate will require several amperes of drive current to switch in a nanosecond time scale. Fortunately commercially available MOSFET drivers are capable of delivering tens of amps to rapidly charge the gate. Fast switching is essential within a MOSFET as the majority of power dissipation occurs during the switching transition of the device.

Modern MOSFET's such as the IXYS Technologies INC DE475-102N21A are capable of switching 1kV, with a continuous current of 24A,

with transition times of 5ns. It should be noted that the gate capacitance of such MOSFETs (5.6nF) is highly prohibitive and requires extreme drive circuitry (tens of amperes) to obtain the short switching times stated on the datasheet. Many of the pulse generators detailed within this thesis are based on arrays of power MOSFET combined to increase the drain to source voltage above that of a single device and will be discussed in section 2.4.3.

2.3.4 IGBT

The Insulated Gate Bipolar Transistor (IGBT) is a relatively recent invention (1990's) which combines the simple gate drive characteristics of the MOSFETs with the high current and low saturation voltage capability of bipolar transistors. This is achieved by combining an isolated gate FET for the control input, and a bipolar power transistor as a switch, in a single device. The IGBT is used in medium to high power applications, typically from 1-10kW, such as switched-mode power supplies, motor control and induction heating systems.

Large IGBT modules typically consist of many devices in parallel and can have very high constant current handling capabilities, in the order of hundreds of amperes with blocking voltages of up to 6kV. In general the switching speed of an IGBT is inversely proportional to its power handling capability. Larger IGBT's tend to be employed in applications where switching in the low kHz range is required. Certain circuit topologies, such as zero-voltage-switching (ZVS), allow large IGBT's to switch at several hundreds of kHz increasing their potential for use in high frequency pulsed power applications.

IGBT devices have very high peak current ratings, often several kiloamperes. This makes them attractive for high energy pulsed power applications, where repetition rates are not an issue. In the context of this thesis, it is thought that medium power IGBT's could potentially replace MOSFETs in many of the devices used in the experimental studies presented.

However, it is unlikely that the small additional benefits would make significant impact on the experiments and consequently they have not been used.

2.4 Circuit topologies

2.4.1 Stacked MOSFET

In general semiconductor switches tend to be low impedance devices, having a low switching voltage yet a high current capability. To develop a semiconductor switch capable of switching high voltages the obvious solution appears to be the series connection of several devices. Through careful circuit design it is possible to serially connect many power semiconductor devices such that the voltage across each device is within acceptable limits yet the total switching voltage is significantly higher than that of a single device. It should be noted that the peak current handling capability of the switch is still limited to that of a single device, to increase current handling ability it is necessary to parallel semiconductor devices. High power semiconductor switches often employ arrays of parallel and series connected devices to increase voltage and current switching capabilities.

In principle the series connection of devices is simplistic however in practice the precise timing required to trigger all devices simultaneously is difficult to achieve. An additional complication is introduced when there is a slight variation in the switching times between each device due to variations in manufacturing processes between production batches.

For example figure 2.3 shows a series 'stack' of three 1kV MOSFET devices, if one device is triggered slightly before the other two devices a voltage of 1.5kV appears across the remaining 'off-state' MOSFET's thus exceeding the maximum operating conditions and resulting in certain destruction of the devices. One solution is to transformer couple the gates of each MOSFET device in the series circuit. To achieve simultaneous switch-on

a transformer using a single primary winding and a separate secondary winding for each device is required. A drawback of this topology is the complexity of the transformer; it will usually consist of multiple, closely coupled, secondary windings yet must withstand voltages in excess of the maximum switching voltage.

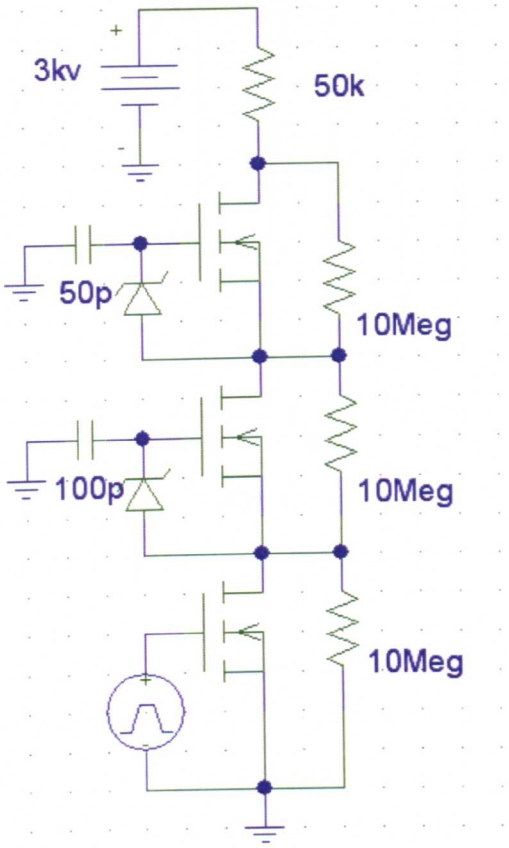

Fig 2-3: Stacked MOSFET circuit topology

Figure 2-3 shows a transformerless method of coupling MOSFET gates first proposed by R.J. Baker in 1992.[2.23] A capacitor is inserted between the gate and the ground of each MOSFET, except for the bottom MOSFET in the stack. Using a single input voltage signal to trigger the bottom MOSFET, a voltage division across the network of device capacitance and inserted capacitances triggers the entire series stack reliably.

A PSpice analysis of the circuit, highlighted in figure 2-4, clearly shows that the circuit is capable of switching voltages equal to several times

that of a single device. The repetition rate in the simulation is 5kHz, the rise time is controlled by an RC time constant and is approximately 30μs, the fall time is controlled by the MOSFET device and is 25ns.

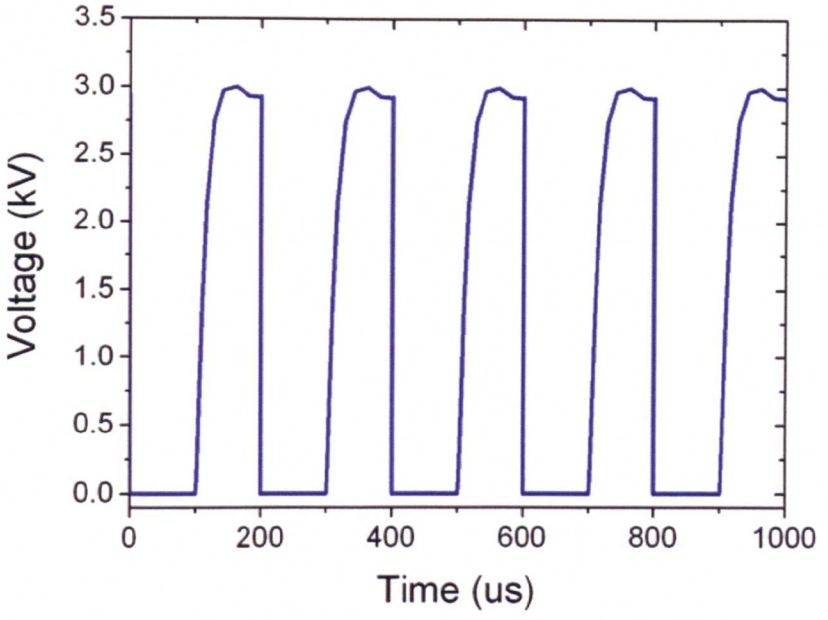

Fig 2-4: PSpice analysis of a 3kV stacked MOSFET circuit

A drawback of the circuit depicted in figure 2-3 is the slow rise time of the voltage waveform, which arises as a result of a charging time constant created by the MOSFET input capacitance and the 50kΩ resistor used to limit current. When the MOSFETs are in the on-state and are conducting, the entire supply voltage is across the current limiting resistor which must dissipate a considerable amount of energy as heat, thus making this topology highly inefficient. The slow rise time of this particular circuit topology was exploited in Chapter 3 of this thesis. Components were chosen such that the voltage rising phase mimicked that of a sinusoidal excitation source. The nanosecond voltage fall phase is on a similar scale to previously published studies on a pulsed DBD, thus a clear comparison is obtainable.

2.4.2 *Push-Pull MOSFET*

An improvement on the series stacked MOSFET circuit topology is the push-pull arrangement shown in figure 2-5. The circuit still requires very precise control of the MOSFET gates yet it is much more efficient as there is no power dissipation in a large current limiting resistor.

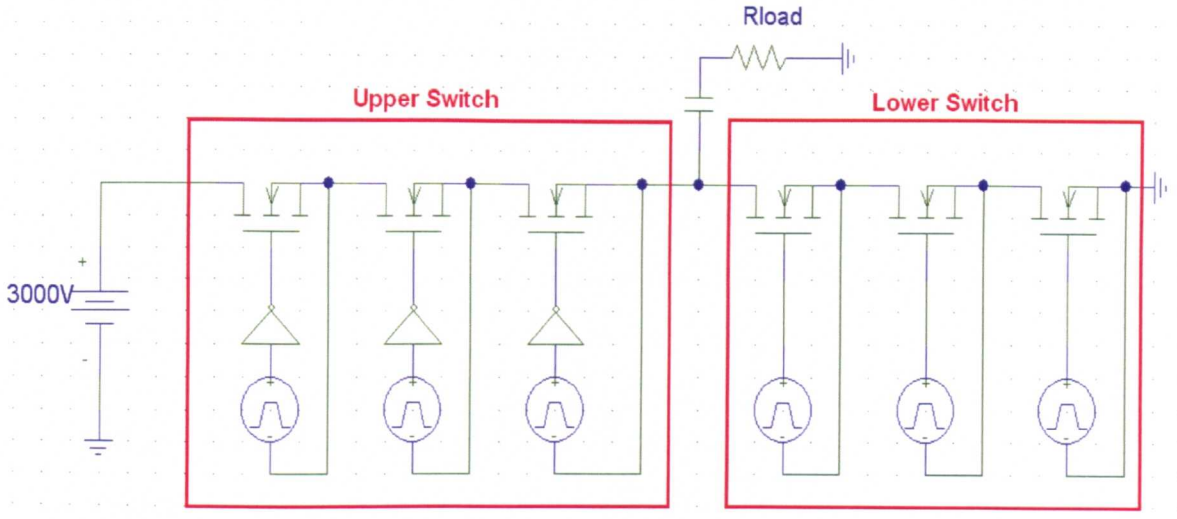

Fig 2-5: Stacked MOSFET Push-pull topology

Essentially, the circuit shown in figure 2-5 consists of two switches, each employing three serially connected 1kV MOSFET's. When the upper switch is closed and the lower switch open, the load is at the potential of the applied voltage. Alternatively the upper switch is open and the lower switch is closed resulting in the load being at ground potential. It is worth noting that should both switches be closed simultaneously then the supply will be shorted to ground resulting in certain damage to the semiconductor switches.

In the push-pull circuit shown the major challenge is the control of each MOSFET gate, the obvious choice would appear to be either transformer coupling or capacitive coupling. Unfortunately neither are ideally suited because the non-ground referenced MOSFET's in the lower switch are often required to be held in the off-state for a substantial amount of the pulse width. Consider the example of generating a 1μs pulse repeated at 1kHz, The

MOSFET's in the lower switch must be held on for 999μs and switched off for just 1μs, this represents a duty cycle of 0.1% which is unobtainable using a simple transformer arrangement and practically impossible for a capacitive coupling topology. A possible method to overcome this problem is via the use of an opto-isolator and isolated DC power supply. This method is relatively simple to implement however the cost and size of such a system increases substantially as devices are added; each device requires its own isolated voltage supply capable of withstanding the high applied voltages within the circuit.

An alternate approach is presented in an application note published by International Rectifier INC.[2.24] It employs transformer coupling and an additional MOSFET to hold the gate at a particular potential until it is discharge by a second pulse. This method allows very high duty cycles to be transformer coupled, which is highly advantageous. A disadvantage is the need for additional components and considerable design effort. Figures 2-6 shows the proposed circuit used to obtained very high duty cycle ratios. The circuit employs a small 1:1 transformer wound on a ferrite core and a low power, low cost MOSFET, M1, to control the switching signals applied to the power MOSFET M2. The circuit provides excellent isolation between the low voltage drive signal and the non-ground referenced power MOSFET.

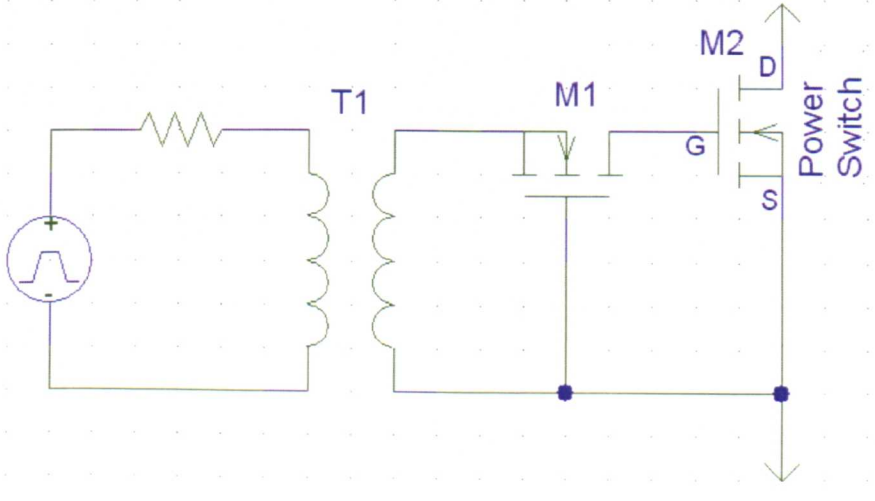

Fig 2-6: Transformer coupled circuit allowing large duty cycle operation

The operation of the circuit is explained through the voltage waveforms shown in figure 2-7. The low voltage control signal to be switched by M2 is denoted the drive signal and is shown in the top graph. When this voltage is applied to the primary of T1 the waveform is supported by changing the core flux until saturation occurs as shown by the waveform in the second graph. At this time the winding voltages fall to zero and remain so until the core flux is reversed by the negative-going portion of the drive signal.

During the positive portion of the secondary waveform, which is a replica of the drive signal, the intrinsic diode of Ml is in forward conduction. M2 receives a positive gate drive voltage with a source impedance equal to that of the primary side of the transformer plus the intrinsic diodes forward impedance.

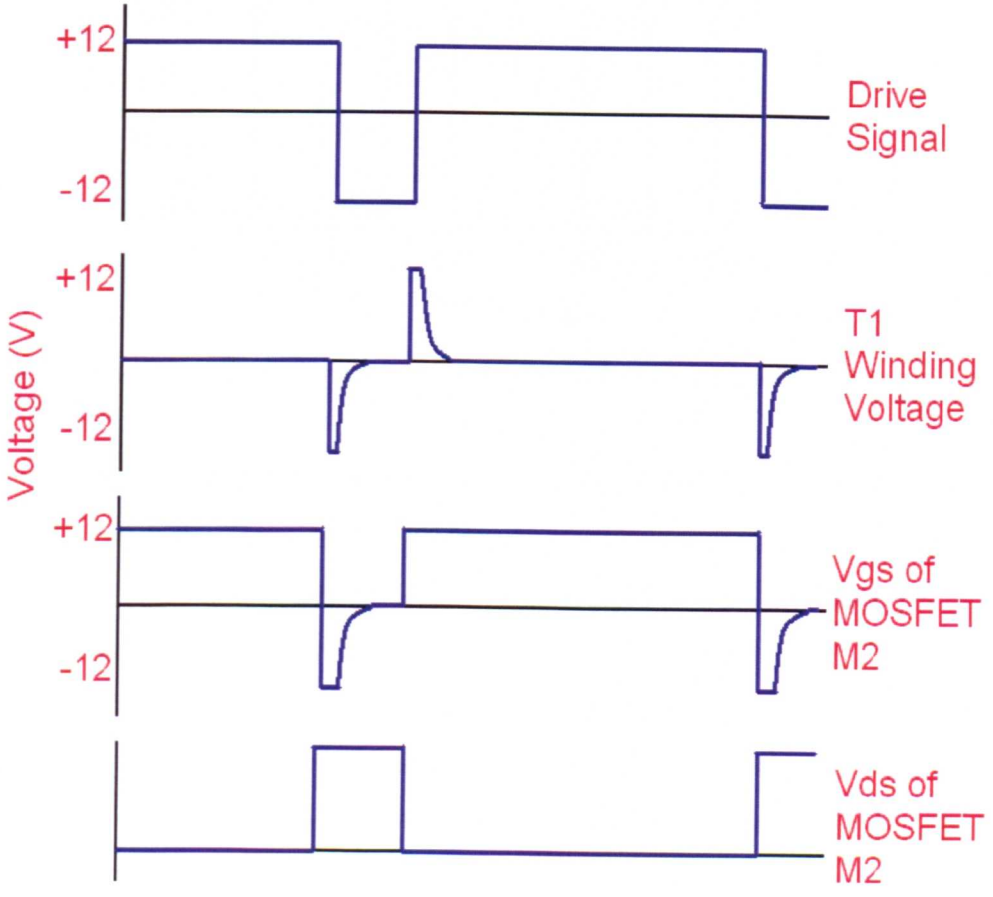

Fig 2-7: Voltage waveforms obtained from circuit shown in figure 2-6

When T1 saturates, the intrinsic diode of M1 isolates the collapse of voltage at the winding from the gate of the power device; the input capacitance of the power switch holds the gate bias at the fully enhanced condition for a time limited only by the gate leakage current of M2, essentially meaning that the power switch remains in the on-state indefinitely. When the drive signal goes to -12V MOSFET M1 becomes fully enhanced; and the power switch M2 will be turned off at approximately -12V with a source impedance equal to the primary impedance plus the on resistance of MOSFET M2.

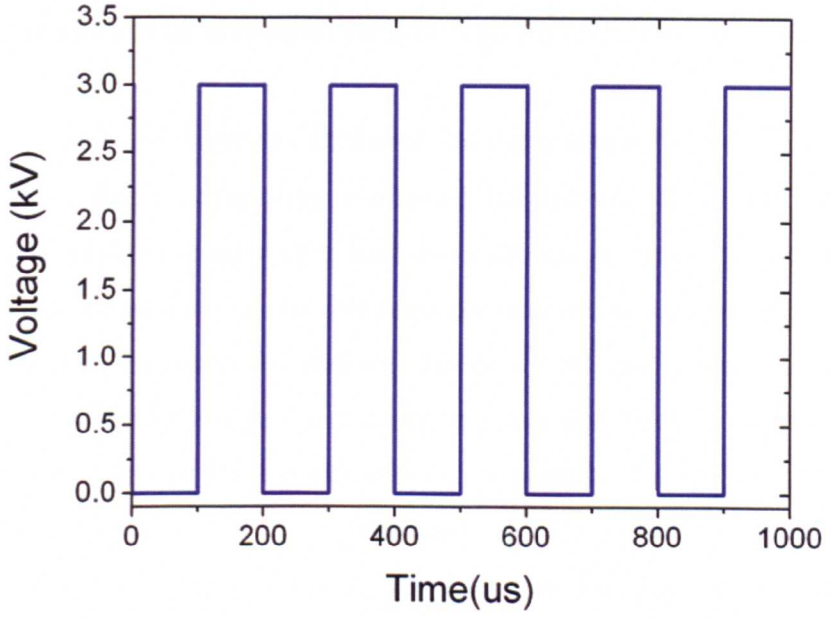

Fig 2-8: PSpice analysis showing output from stacked MOSFET push-pull circuit

Figure 2-8 shows a PSpice simulation of the stacked MOSFET push-pull circuit. It is clear that the waveform is highly rectangular compared to that shown in figure 2-4, rise and fall times are around 25ns. Using this topology it is possible to achieve pulses with rises times in the nanosecond range with voltages in excess of 20kV. A further advantage of the circuit is its high efficiency; no resistors are required to 'burn' excess power. Devices, based upon this topology, capable of switching up to 15kV and handling peak currents of 60A at kilohertz repetition rates, have been used extensively in the experiments detailed within this thesis.

2.4.3 Avalanche transistor Marx bank

The simple bipolar junction transistor is the backbone of today's computer age, however transistors are often overlooked as switching devices in pulsed power systems as their power handling capabilities tend to be low. Current mode secondary breakdown, also known as avalanche breakdown, is often assumed to be destructive to a transistor, however, if the amount of time a BJT is subjected to the breakdown is limited then the device will survive undamaged. The avalanche breakdown process in a BJT occurs when the maximum collector-emitter voltage is exceeded such that the electric field within the semiconductor junction is so high (MV/m) breakdown occurs.

Initial investigations attributed the p-n junction breakdown as a similar process to that of spark-gap avalanche breakdown, hence the name. This theory is not consistent with recent experimental studies that show transition times can be as low as 30 picoseconds which are unexplainable with the conventional avalanche breakdown theory.[2.25] A new theory that ionisation occurs as a wave through the p-n junction was proposed by Gerkhov.[2.25] The theory states that as the ionisation wave propagates through the junction, the voltage is held off by an increasingly thinner layer of material but no significant current flows until the wave reaches the other side of the junction and the insulating layer collapses very quickly.

Many low power BJT devices exhibit non-destructive avalanche breakdown and can typically switch several hundred volts in sub-nanosecond time scales. By combining many devices with similar avalanche voltages together a single high voltage switch is formed. For example ten serially connected NPN ZTX451 transistors can switch 1.5kV and tens of amperes when in the avalanche breakdown mode. This is quite surprising considering the maximum collector emitter voltage specified for a single device is only 60V, the maximum collector current is stated at 1A, and the maximum power dissipation is 1W.

Increasing the number of serially connected devices increases the avalanche voltage of the entire chain; however, as the total voltage is increased, the current through each device is increased thus power dissipation in each device increases. At some point the loss matches the voltage gained through adding an extra device, at which point adding additional devices becomes futile.

When a relatively high impedance load is considered and the current through each device is not very high, 20-30 BJT's can be serially connected to form a single high voltage switch. To achieve even higher voltages a Marx bank topology can be used. A Marx bank consists of several fast switches and charged capacitors; figure 2-9 gives a simple example. Initially all the capacitors are charged in parallel from the 10kV supply voltage. When the first switch in the system is closed, capacitors C1 and C2 become connected serially via the low impedance switch, this has the effect of combining the two 10kV voltages to produce a 20kV pulse. If the switches employed are spark gaps the high-voltage pulse causes rapid breakdown of the second switch resulting in all three capacitors being serially connected, thus producing an output voltage of 30kV which is delivered to the load. This topology requires the sequential operation of each switch within the Marx bank, which is simplistic when over-voltage spark gaps are used, however the situation is more complex when semiconductor switches are used as precise triggering is essential.

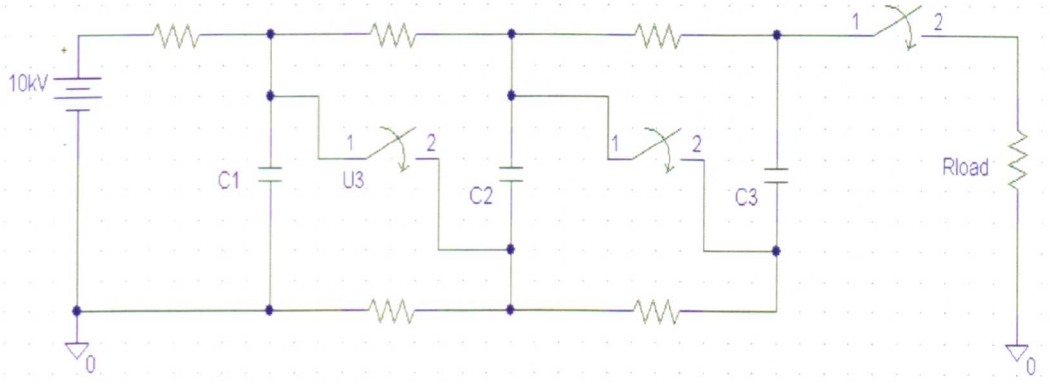

Fig 2-9: Simple three capacitor Marx bank topology.

The advantage of replacing spark gap switches with semiconductor switches in a Marx bank is the ability to obtain much higher repetition rates. Typically several kHz are achievable, the addition of elaborate cooling systems coupled with a careful circuit design can permit repetition frequencies up to 100kHz. Commercial units are available that deliver a 2ns pulse with 10kV magnitude at 100kHz.[2.26]

Figure 2-10 shows a typical transistorised Marx bank consisting of three stages each containing four serially connected devices, the circuit has been used in several of the investigations detailed within this thesis as a means of generating kilovolt nanosecond pulses. Several Marx bank devices were constructed for pulsed APGD experiments, through experience it was found that a six stage Marx bank formed with 15 BJT devices per stage proved to be the optimum, producing 8kV pulses with rise times less than 2 nanoseconds. In theory the rise time of such a device should be significantly faster than 2ns, as the impedance of a plasma is dynamic it is impossible to accurately match it to the impedance of the pulse generator thus causing a 'blurring' of the waveform.

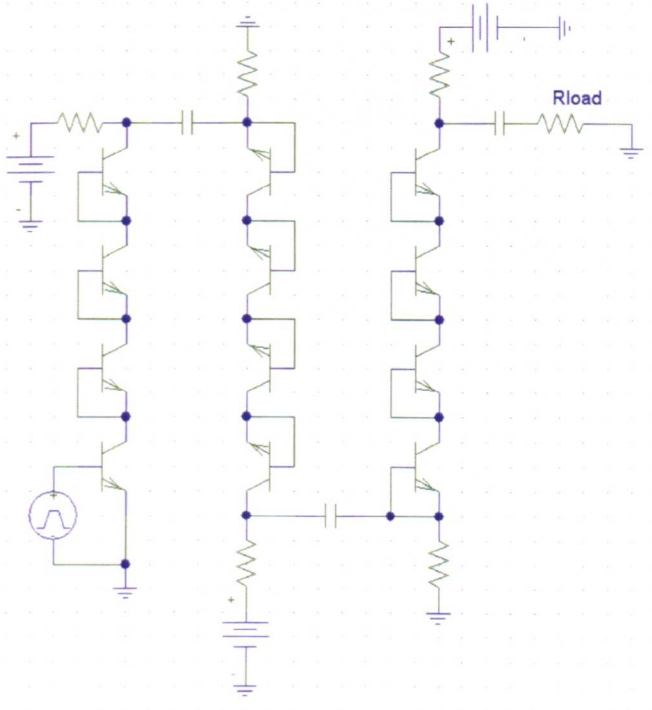

Fig 2-10: Three stage transistorised Marx bank circuit.

Figure 2-11 shows the output of an avalanche transistor Marx bank, consisting of four 450V stages simulated on PSpice. It is worth noting that the pulse is not rectangular, in order to obtain a rectangular pulse transmission line capacitors are required. Unfortunately, transmission lines have a fixed impedance and the plasma does not, this precludes their use for rectangular pulse forming in this particular application.

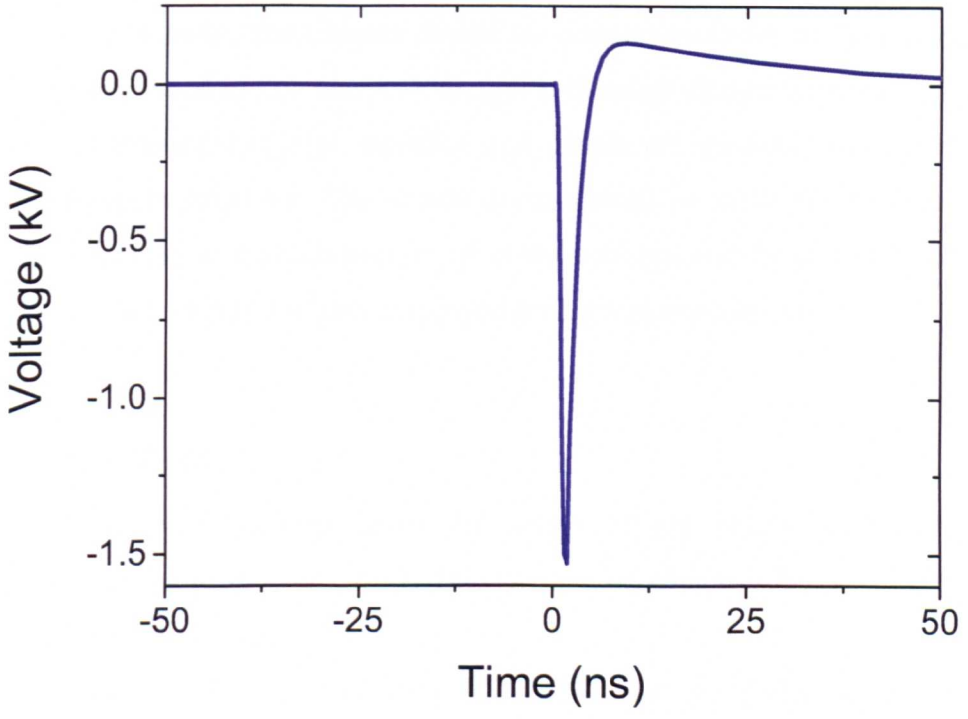

Fig 2-11: PSpice simulation of a four stage transistorised Marx bank.

2.5 Summary

This Chapter has aimed to give the reader a brief review of current pulsed power applications that are relevant to the subject of this thesis. Many modern applications of pulsed power require significantly higher peak powers than are necessary for the generation of APGD and consequently have not been discussed.

Essential to any pulsed power system is the switching method used to rapidly discharge stored energy into the load. A substantial portion of this Chapter has been dedicated to the various switching options currently available. The experiments detailed in this thesis have all used semiconductor switching devices primarily because they are low cost and allow for high repetition rates. Other switching devices, such as thyratrons, were considered but deemed inappropriate due to their cost and complexity.

Finally, this Chapter details the circuit topologies of the pulsed-power systems used in this thesis. Although a thorough design methodology has not been presented, design equation and details are available in several of the references provided. The details given should be sufficient to highlight the advantages and disadvantages of each topology and give justification as to why each circuit has been employed for a given experiment.

References

[1.7] Anders A. 'Tracking down the origin of arc plasma science-II. Early continuous discharges' IEEE Transactions on plasma science, Vol 31, No 4, pp.1060-1069, 2003.

[2.1] Brown L. 'A Radar History of World War II: Technical and Military Imperatives' Institute of Physics Publishing, 1999.

[2.2] Perry M.D, Pennington D, Stuart B.C, Tietbohl G, Britten J.A, Brown C, Herman S, Golick B, Kartz M, Miller J, Powell H.T, Vergino M, Yanovsky V, 'Petawatt laser pulses' Optics Letters, Vol.24, Iss.3, pp.160-162, 1999.

[2.3] Kotov Y.A, 'Electric explosion of wires as a method for preparation of nanopowders', Journal Of Nanoparticle Research, Vol.5, Iss.5-6, pp.539-550, 2003.

[2.4] Novac B.M, Smith I.R, Downs P.R, Marston P, Fahey D, 'Cockpit canopy shattering using exploding wire techniques' Journal Of Physics D-Applied Physics, Vol.40, Iss.7, pp.2217-2222, 2007.

[2.5] Tsong T,Y. 'Electroporation of cell-membranes' Biophysical Journal, Vol.60, Iss.2, pp.297-306, 1991.

[2.6] Beebe S.J, Schoenbach K.H, 'Nanosecond pulsed electric fields: A new stimulus to activate intracellular signaling' Journal Of Biomedicine And Biotechnology, Iss.4, pp.297-300, 2005.

[2.7] Jeyamkondan S, Jayas D.S, Holley R.A, 'Pulsed electric field processing of foods: A review' Journal Of Food Protection, Vol.62, Iss.9, pp.1088-1096, 1999.

[2.8] Beveridge J.R, MacGregor S.J, Anderson J, Fouracre R.A, 'The Influence of Pulse Duration on the Inactivation of Bacteria Using Monopolar and Bipolar Profile Pulsed Electric Fields' IEEE Transactions On Plasma Science, Vol.33, Iss.4, pp.1287-1293, Part 1, 2005.

[2.9] Chalise P.R, Perni S, Shama G, Novac B.M, Smith I.R, Kong M.G, 'Lethality mechanisms in Escherichia coli induced by intense sub-microsecond electrical pulses' Applied Physics Letters, Vol.89, Iss.15, No.153902, 2006.

[2.10] Tendero C, Tixier C, Tristant P, Desmaison J, Leprince P, 'Atmospheric pressure plasma: A review' Spectrochimica Acta Part B-Atomic Spectroscopy, Vol.61, Iss.1, pp.2-30, 2006.

[2.11] Beer T.A, Laimer J, Stori H, 'Study of the ignition behavior of a pulsed dc discharge used for plasma-assisted chemical-vapor deposition' Journal Of Vacuum Science & Technology A - Vacuum Surfaces And Films, Vol.18, Iss.2, pp.423-434, 2000.

[2.12] Guiberteau E, Bonhomme G, Hugon R, Henrion G, 'Modelling the pulsed glow discharge of a nitriding reactor' Surface & Coatings Technology, Vol.97, Iss.1-3, pp.552-556, 1997.

[2.13] Raizer Y. P, 'Gas discharge physics' London: Springer, 1997.

[2.14] Starikovskaia S.M, 'Plasma assisted ignition and combustion' Journal Of Physics D-Applied Physics, Vol.39, Iss.16, pp.R265-R299, 2006.

[2.15] Pilla G, Galley D, Lacoste D.A, Lacas F, Veynante D, Laux C.O, 'Stabilization of a turbulent premixed flame using a nanosecond repetitively pulsed plasma' IEEE Transactions On Plasma Science, Vol.34, Iss.6, pp.2471-2477, Part 1. 2006.

[2.16] Kong M.G, Deng X.T, 'Electrically efficient production of a diffuse nonthermal atmospheric plasma' IEEE Transactions On Plasma Science, Vol.31, Iss.1, pp.7-18, Part 1, 2003.

[2.17] Laroussi M, Lu X, Kolobov V, Arslanbekov R 'Power consideration in the pulsed dielectric barrier discharge at atmospheric pressure' Journal Of Applied Physics, Vol.96, Iss.5, pp.3028-3030, 2004.

[2.18] Walsh J.L, Shi J.J, Kong M.G, 'Contrasting characteristics of pulsed and sinusoidal cold atmospheric plasma jets' Applied Physics Letters, Vol.88, Iss.17, No.171501, 2006.

[2.19] Walsh J.L, Shi J.J, Kong M.G, 'Submicrosecond pulsed atmospheric glow discharges sustained without dielectric barriers at kilohertz frequencies' Applied Physics Letters, Vol.89, Iss.16, No.161505, 2006.

[2.20] Novac B.M, Istenic M, Luo J, Smith I.R , Brown J, Hubbard M, Appelgren P, Elfsberg M, Hurtig T, Moller C, Larsson A, Nyholm S.E, 'A 10-GW pulsed power supply for HPM sources' IEEE Transactions On Plasma Science, Vol.34, Iss.5, pp.1814-1821, Part 1, 2006.

[2.21] Mankowski J, Kristiansen M, 'A review of short pulse generator technology' IEEE TransactionsOn Plasma Science, Vol.28, Iss.1, pp.102-108, 2000.

[2.22] Frolov O, Kolacek K, Bohacek V, Straus J, Schmidt J, Prukner V, 'Gas-filled laser-triggered spark gap', Czechoslovak Journal Of Physics, vol.54, pp.309-313, Part 1-3, Suppl.C, 2004.

[2.23] Baker R.J, Johnson B.P, 'Series Operation Of Power Mosfets For High Speed, High-Voltage Switching Applications' Review of Scientific Instruments, Vol.64, Iss.6, pp.1655-1656, 1993.

[2.24] 'Transformer-Isolated Gate Driver Provides very large duty cycle ratios' International Rectifier Application Note: AN-950.

[2.25] Ataev B.M, Grekhov I.V, Magomedov M.A, Mutalibov S.R, 'Mechanism For Secondary Breakdown On The Surface Of High-Voltage Silicon P-N-Transitionsc' Zhurnal Tekhnicheskoi Fiziki, Vol.49, Iss.8, pp.1768-1770, 1979.

[2.26] http://www.fidtechnology.com/products/fpg-nanosecond.html

3 Microsecond pulsed APGD jet

3.1 Introduction

Many applications involving the use of plasma require efficient reaction chemistry and excellent plasma stability, two properties which are often difficult to achieve simultaneously.[3.1] One solution is to generate APGD in an inert gas which is then flushed into a region of reactive gas, thus achieving both stability and reactivity simultaneously. A common technique to achieve this is the jet configuration. The vast majority of APGD jets reported previously employ some form of sinusoidal excitation.[3.2-3.11] Simulation data produced in 2003, and summarised in figure 3-1, indicates that non-sinusoidal excitation can be used to improve the electrical efficiency whilst maintaining a constant electron density.[3.12] Recent studies, have explored the use of pulsed excitation as an alternative to sinusoidal and highlighted some of the similarities and differences between them. [3.4, 3.10, 3.13]

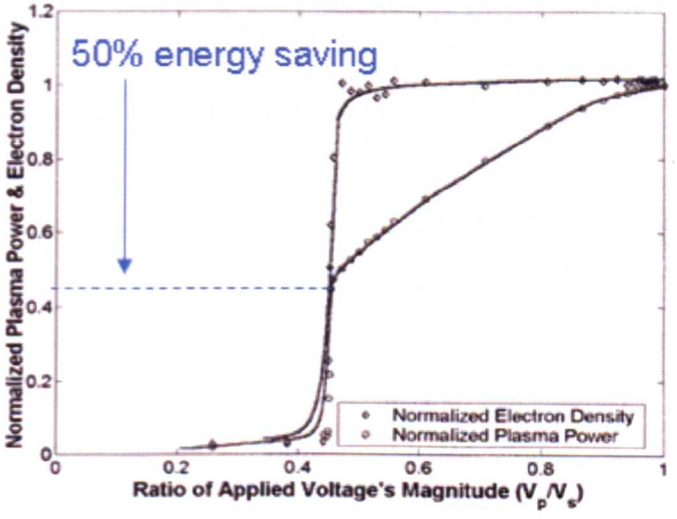

Fig 3-1: Graph showing effect on power consumption and electron density of waveform shaping. The ratio V_p/V_s indicates the amount by which a sinusoidal waveform can be reduced in magnitude before electron density is adversely effected.[3.12]

It is suggested that pulsed excitation may be a more efficient means of generating APGD compared to sinusoidal excitation,[3.14] however, a comparison between the two was not conducted. Given that pulsed APGD jets introduce additional system parameters, such as pulse width, pulse rise/fall time, and repetition rate, the scope for tailoring a pulsed discharge for maximum efficiency is considerable. A necessary first step is to provide a direct comparison between the two as the lack of a direct comparison casts uncertainty on whether a pulsed APGD jet offers any significant advantages over its sinusoidal counterpart. The remainder of this Chapter presents experimental results of a pulsed APGD helium jet and provides a direct comparison with a sinusoidal excited APGD jet.

3.2 Atmospheric pressure plasma jet review

As mentioned previously, atmospheric pressure plasma jets exhibit excellent potential for many industrial applications. As such the amount of research effort directed toward understanding and enhancing their properties is increasing at a rapid rate. Figure 3-2 shows the number of journal articles published between 1989 and December 2007 that contain the key words 'atmospheric pressure plasma jet.' From 2000 onwards a steep rise in the number of published studies is observed, this indicates a rapid increase in the number of research groups investigating the plasma jet, it is likely that this trend will continue for many years to come.

Out of the 353 publications up to December 2007 containing the key words mentioned above, it is possible to divide the number of plasma jets detailed into three distinct categories based on their excitation method. An even split between DC plasma jets, DBD jets (including pulsed), and RF plasma jets is observed, a few studies make use of microwave excitation to produce a plasma 'torch' however these are typically very hot at atmospheric pressure so are not considered here. The following subsections review each excitation method and discuss its advantages and disadvantages.

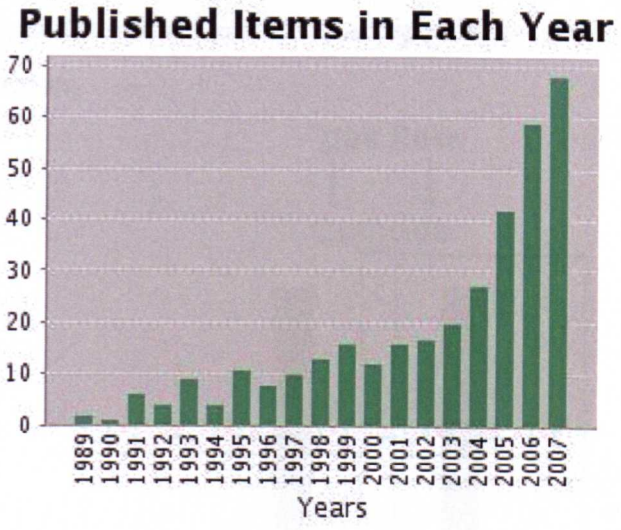

Fig 3-2: Graph showing number of papers published containing the key words 'atmospheric pressure plasma jet' obtained from Web of Science.

3.2.1 DC Plasma Jets

A DC excited plasma jet is possibly the simplest to construct and analyse of all the plasma jets considered. All that is required is a DC source and two metallic electrodes through which gas is somehow flushed. Figure 3-3 shows a typical DC plasma jet configuration, the cathode usually consists of a sharpened metallic rod that is housed in a structure through which gas can be flushed at high velocities. A metallic anode is usually placed at a suitable distance downstream. As the DC voltage is increased the gap between the anode and the cathode breaks down, as no form of current limiting is employed the breakdown rapidly becomes an arc plasma. Typically, DC plasma jets tend to operate at low voltages with high current densities, consequently the plasma is very dense which translates into a high operating temperature.[3.15] Efforts to limit the discharge current,[3.16] or cool the plasma using gas flow, have reduced the temperature of DC plasma jets down to a level suitable for many materials processing applications. As such DC plasma jets are widely used in chemical vapour deposition, CVD, applications where it is necessary that the substrate being treated is at an elevated temperature.[3.17] Unfortunately, the cooling mechanisms reported are insufficient to reduce the

plasma temperature down to a level acceptable for applications such as bio-decontamination.

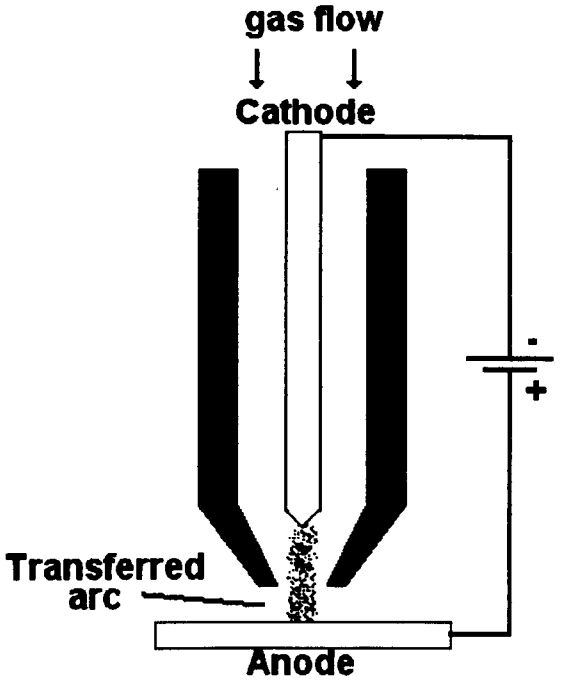

Fig 3-3: Schematic showing a typical configuration of a DC plasma jet.

3.2.2 RF Plasma Jets

Another widely used configuration is that of an RF excited plasma jet, these typically use MHz excitation between two metallic electrodes to produce a high intensity discharge which is then flushed out of the jet structure using a high gas flow.[3.5] A typical coaxial RF plasma jet configuration is shown in figure 3-4, a variation on that shown is the production of a plasma between two parallel plate electrodes which is then flushed out.[3.18] In both cases the plasma is produced between two electrodes and then flushed into another region. A drawback of these configurations is that the plasma is usually produced between two vertical electrodes, meaning the electric field is in a horizontal direction, to get the plasma from between the electrodes requires the gas flow push the plasma in a vertical direction thus at a tangent to the field, which is difficult. Very high flow rates are often employed yet plume lengths are typically only around a few millimetres,[3.19] also, the plume only

contains neutral species as charged species remain trapped in the electric field between the electrodes.

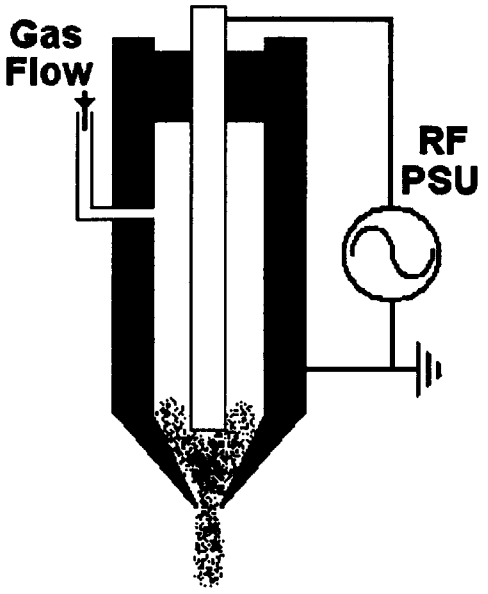

Fig 3-4: Schematic showing a typical configuration of an RF plasma jet

A variation on the RF plasma jet is known as the plasma needle.[3.20] The device employs a single pin like electrode which produces a very small area discharge at the tip.[3.21] The small area of the plasma needle prevents it from being of much use in many industrial applications, however it can be a benefit for certain biomedical applications. Recently it has been used to treat cavities in teeth which would be inaccessible using larger plasma systems.[3.22]

3.2.3 DBD Plasma Jets

Many studies focus upon the use of a dielectric barrier jet employing kHz sinusoidal or pulsed excitation. The configuration of the plasma jet used varies somewhat however the majority employ a dielectric tube through which the base gas flows, a powered electrode is attached to the outside of the tube to ionise the gas flow.[3.28] This configuration is depicted in figure 3-5. A slight variation on that shown is the addition of a second electrode on the tube which is grounded.[3.25] A grounded electrode on the tube generally reduces the influence of any objects placed downstream in the plasma plume.

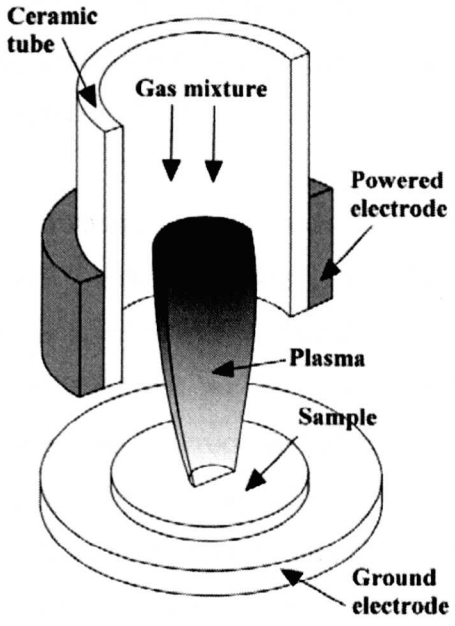

Fig 3-5: Schematic showing typical configuration of kHz DBD plasma jet.

The dielectric barrier jet is the focus for the first part of this thesis due to its beneficial operating properties, typically low temperature operation coupled with highly reactive chemistry.[3.25] Due to these properties the DBD jet is an ideal candidate for many biological decontamination applications.[3.24, 3.28] The following sections will examine operation of a kHz sinusoidal and kHz pulsed DBD jet in further detail.

3.3 Experimental Setup

The APGD jet used for this study employed a dielectric tube 6 cm in length, one end of which was wrapped with a concentric copper belt of 1 cm wide as the powered electrode. A stainless steel plate, either dielectrically insulated or naked, was used as the ground electrode and placed at 3 – 5 cm away from the gas exit point of the dielectric tube. As shown in figure 3-5, the electrode configuration was essentially that of a dielectric-barrier discharge jet. Atmospheric helium gas was fed to flow at 5 standard litres per minute (SLM) through the dielectric tube, which became ionised by the high voltage externally applied to the copper electrode. The ionised helium gas was flushed

out of the dielectric tube into the surrounding ambient air, where the excited helium species transferred their energy to the ground-state oxygen and nitrogen molecules and created excited oxygen and nitrogen species such as atomic oxygen, OH and excited N_2/N_2^+.

Electrical measurements were made using a Tektronix digital oscilloscope (TDS 5054B) with a 500MHz bandwidth. A 75MHz Tektronix P6015A voltage probe, rated at 40kV, was used to measure the high applied voltages. A Pearson 2877 current probe with a 200MHz bandwidth was attached between the grounded electrode and earth. Figure 3-6 is a schematic of the experimental layout. Optical measurements were performed with an Andor DH720/Shamrock system with a grating of 600/1200/2400 g/mm depending on the spectral resolution required.

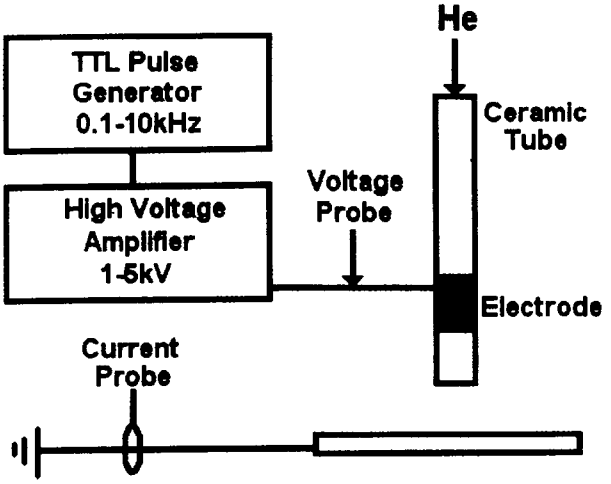

Fig 3-6: Schematic showing the experimental setup of a kHz excited DBD plasma jet

The generated plasma jet was very stable and could be sustained for many hours. Its volumetric appearance near the gas exit point seemed to depend largely on the applied voltage and the helium flow rate, relatively independent of the ground electrode.

Figure 3-7 shows the plasma jet in operation as observed using a Canon digital camera with the exposure set to $1/60^{th}$ of a second, the

appearance of the plasma plume is that of a purple glow that extends from the tube exit to several centimetres into the open air. Clearly objects can be placed within the plasma plume and exposed to the reactive species with relative ease. As the high voltage electrode is insulated from the plasma via the dielectric tube, arcing is not an issue; hence it is safe to put conductive objects within the plasma plume, including biological matter (such as a human finger). When a ground electrode is employed, primarily to enable a satisfactory current measurement to be obtained, it is found that the plasma terminates upon the surface. If the ground electrode has a dielectric coating the terminating plasma has the appearance of spreading out across the dielectric surface. If the ground electrode is a naked metallic surface the plasma plume terminates in a single small bright spot.

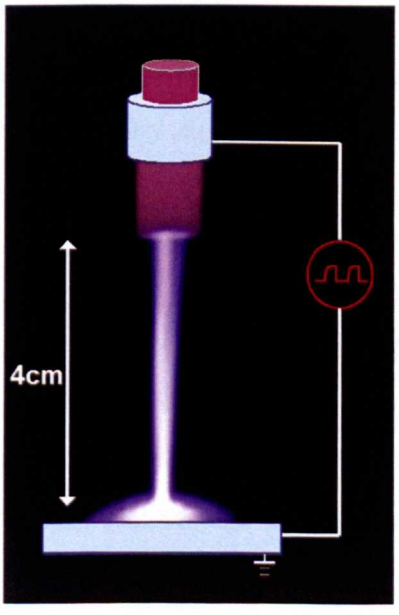

Fig 3-7: Photograph of an atmospheric pressure helium plasma plume (1/60 sec exposure).

3.4 Comparative study

To facilitate a direct comparison of sinusoidal and pulsed excitation, a simple sinusoidal voltage source was developed and constructed. The device consisted of a half-bridge MOSFET switching power supply and a high-voltage ignition transformer, commonly used in the automotive industry. The sinusoidal output had a variable output of 1-10kV with a variable excitation

frequency of 1 – 10 kHz but nominally at 7 kHz. A pulse generator was also developed and constructed, based on the circuit shown in figure 2-3. The device was capable of generating unipolar voltage pulses up to 5kV with a variable duty cycle of 20-80% and a pulse repetition frequency up to 10kHz.

For all results presented here, the sinusoidal source had a peak-to-peak voltage of 7.3 kV and the pulsed source delivered a unipolar pulse train having a peak voltage of 4 kV, thus both with similar voltage spans. To facilitate direct comparison, the pulse width of the pulsed source was fixed at 71μs which yielded a duty cycle of 49% and equates to a frequency of 7kHz, identical to that of the sinusoidal source.

3.4.1 Electrical comparison

A significant advantage of in-house design and construction of the pulse generator was the ability to closely control certain properties of the generated waveform. In this study it was desirable to ensure the amplitude; frequency and rise time of the pulse closely resemble that of the sinusoidal source. A 10kΩ resistor was combined with the MOSFET's 3nF input capacitance to give a charging time of 30μs, the MOSFET fall-time controlled the fall time of the pulse and as such was less than 100ns. The contrasting rise and fall times provided a clear contrast with each other *and* also enabled easy comparison with the sinusoidal voltage that nominally required 35μs to climb from zero to the next peak. The pulsed voltage source was designed to have a rise time similar to one pulsed APGD jet study and a fall-time similar to the other,[3.4,3.13] thus enabling a comparison with these previous studies. The discharge current and the applied voltage characteristics are shown in figure 3-8 for both pulsed and sinusoidal excitations. The applied voltage is measured in kV and is shown in blue, the current is measured in mA and is shown in green.

With the pulsed excitation, two discharge current pulses were induced during one voltage pulse – one in the voltage-rising phase and the other in the

voltage-falling phase. Although the pattern of two current pulses per one voltage pulse was not explicitly mentioned in previous studies of pulsed APGD jets,[3.4,3.13] it was observed with a pulsed DBD APGD between parallel-plate electrodes.[3.14] It is expected that this temporal character is likely to be observable in most previously reported pulsed APGD jets.[3.4,3.13] As shown in figure 3-8a, the peak current is 12.1 mA in the voltage-raising phase and 12.9 mA in the voltage-falling phase. The difference in the peak discharge current is insignificant, suggesting that the timescale of the voltage variation, 30μs and 100 ns respectively, was unlikely to be the only influencing factor. The pattern of the discharge current was highly periodic with the peak current being the same from one voltage pulse to another.

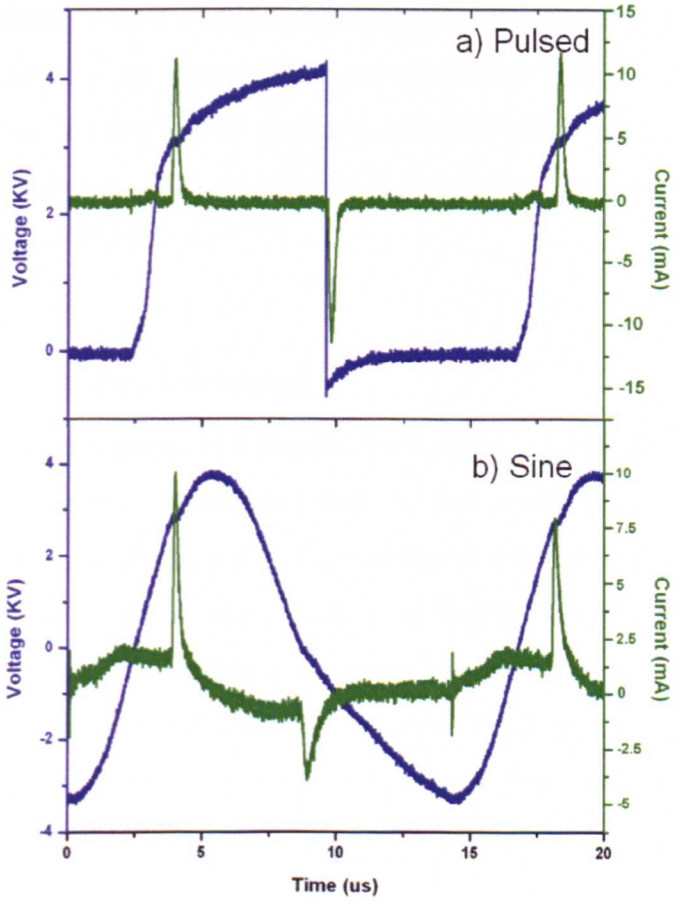

Fig 3-8: Current & Voltage characteristics of a) pulsed, and b) sinusoidal excited jets

With the sinusoidal excitation, the discharge pattern seen in figure 3-8b has one discharge current pulse per half cycle of the applied voltage and the

current pulses occurred always at a voltage-rising phase. This is similar to that in APGD sustained between two parallel-plate electrodes.[3.26] The discharge events were periodic, though the peak current appeared to vary from one cycle of the applied voltage to another. When the applied voltage was positive, the peak discharge current varied between 7.9 mA and 12.0 mA. When the applied voltage was negative, the peak discharge current became smaller. The difference in the peak discharge current is however not uncommon among parallel-plate APGD.[3.26] In general, the discharge current achieved with the pulsed APGD jet was higher than that in the sinusoidal APGD jet but the difference was not large. The averaged power was 74 mW in the pulsed APGD jet and 370 mW in the sinusoidal APGD jet, representing superior energy efficiency by a factor of 5 with the pulsed excitation for the same peak discharge current. This is significantly higher than a theoretical evaluation of a sinusoidal APGD and a comparable pulsed APGD both sustained between parallel-plate electrodes.[3.12] The plasma power dissipated in the pulsed APGD jet was more than one order of magnitude lower than that found in previous studies of pulsed APGD jets.[3.10, 3.13]

3.4.2 Gas temperature comparison

The gas temperature in a plasma discharge is often difficult to measure, common measurements techniques such as thermocouples cannot be used reliably. For example, the insertion of a thermocouple into the discharge often causes disruption to the plasma, leading to arcing. Additionally, the high-voltage, high frequency excitation is often a source of electromagnetic noise which interferes with the delicate electronics of the measuring device. An alternative, non-invasive, temperature method involves the use of an optical emission spectroscopy (OES) technique.

By comparing measured and simulated optical emission from suitable excited species it is possible to determine the rotational temperature of gas molecules in the discharge. At atmospheric pressure the energy required to reach rotational excitation is low and the transition time from the ground state

is also short.[3.27] As a result, gas molecules in the rotational states and the neutral gas molecules, in the ground state, can be considered to be in equilibrium. Hence the gas temperature can be estimated directly from the rotational temperature obtained via OES.

As the plasma jet is flushed into the ambient air, hydroxyl (OH) molecular band and the nitrogen monopositive ion N first negative system are observed in the emission spectrum due to water molecules in the air and nitrogen from the air composition, respectively. In this investigation the emission of the diatomic molecule OH was measured and compared to simulation data produced using a program known as LIFBASE,[3.30] developed by Jorge Luque. LIFBASE has been designed to compile the information available from transition probability calculations on the diatomic molecules OH, OD, CH and NO. The output of the program furnishes Einstein emission and absorption coefficients, radiative lifetimes, transition probabilities, and frequencies for many bands of OH (A-X), OD (A-X), CH (A-X, B-X, C-X), NO (A-X, D-X). The software allows for interactive modification of many parameters; most significantly in this investigation, the rotational and vibrational temperatures can be adjusted and the effect on the spectral data observed. [3.30]

Using the emission of the OH band around 309nm, simulation data can be fitted to the experimental results with a high degree of accuracy, it has been shown that rotational temperatures can be estimated to within as little as 2.4% error using this method.[3.27] To achieve such high levels of accuracy the spectrometer grating must be very fine thus giving a high spectral resolution, unfortunately the grating of the spectrometer employed in this investigation was relatively low thus only permitting a rough estimation of rotational temperature.

In this investigation, emission of the OH band was recorded using a spectral resolution of 0.3 nm, gas temperature was found to be between 290 and 350 K but closer to 290 K, in both the pulsed and sinusoidal APGD jets.

Figure 3-9 shows the experimental data and synthetic data calculated at various rotational temperatures. Essentially the difference in the measured gas temperature was insufficient to differentiate the pulsed and sinusoidal APGD jets, possibly because both plasma jets had their gas temperature either at or very close to room temperature. The dielectric tube was thermally safe to handle even after several hours of plasma operation, with both the sinusoidal and pulsed excitations.

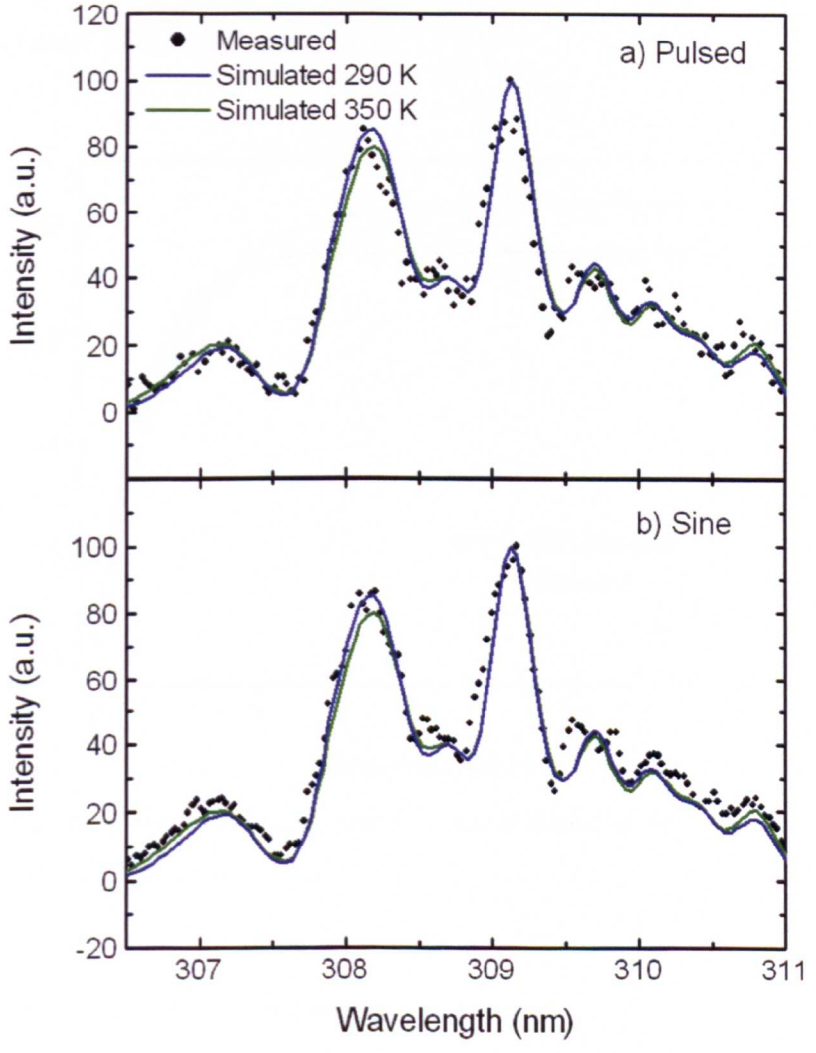

Fig 3-9: Gas temperature data for a) pulsed, and b) sinusoidal excited jets, experimental data obtained using an optical grating of 2400 groves/mm.

For further clarification, an infrared thermocouple was employed to continuously monitor the temperature of the dielectric substrate (focused approximately 1mm from plasma plume) during operation of the jet. After

several minutes of operation the temperature of the ceramic plate rose steadily and then reached a plateau at which the temperature stayed indefinitely. A slight difference was observed between the temperature of the pulsed jet and sinusoidal jet, however it was not significant. The temperature recorded by the thermocouple, shown in figure 3-10, is in close agreement with those obtained using the OES method. From the two sets of temperature data it is clear to see that there is very little difference between the pulsed and sinusoidal APGD jets. Both are just slightly above room temperature highlighting the non-thermal nature of the discharge.

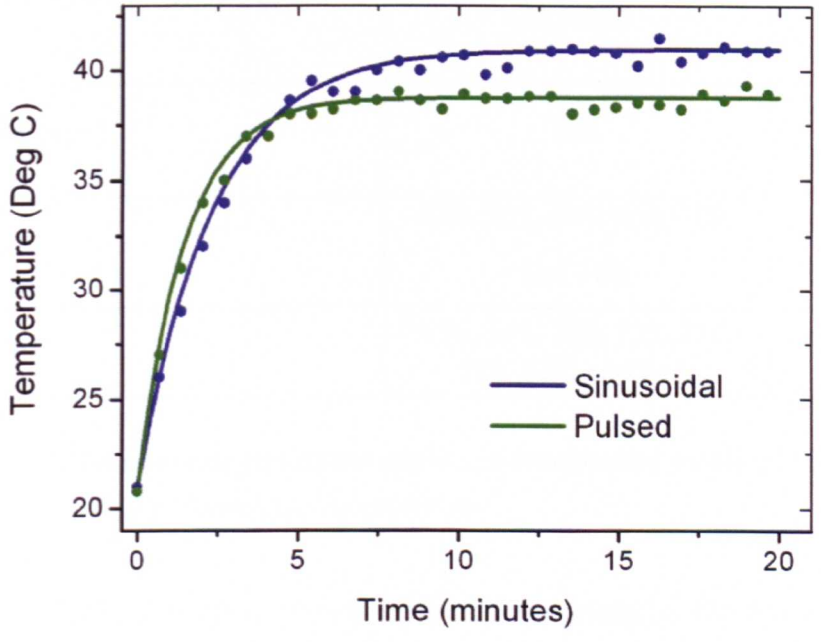

Fig 3-10: Substrate temperature of pulsed and sinusoidal excited jets obtained using an infrared thermocouple.

3.4.3 Plasma reactivity comparison

Optical emission spectroscopy provides a relative measurement of the optical emission from excited atoms to determine the chemical composition of a plasma. The use of OES relies upon atoms within the plasma having a sufficient energy such that they are in an excited state. The atoms decay back to lower levels by emitting light which is collected via a fibre optic cable and analysed by a spectrometer. Since the transitions are between distinct atomic

energy levels, the emission lines in the spectra are narrow. The spectrum of a typical helium plasma jet is often very congested due to the excitation of the background air, which has a rich chemical composition. Since all atoms in the plasma are excited simultaneously, they can be detected simultaneously; this is a major advantage of emission spectroscopy over other methods, such as absorption spectroscopy.

Species	**Wavelength (nm)**	**Ref**
Hydroxyl (OH)	306-310	3.20
Nitorgen N_2 2^{nd} positive series	315-385	3.17, 3.19
Nitrogen N_2+	391	3.17, 3.19
Helium	446, 501, 587, 668, 706, and 728;	3.5, 3.19
Oxygen	616, 645, 700, 725, 777, 794, 822, and 845;	3.5

Table 3-1: Table showing predominate species and corresponding wavelengths in a helium APGD jet flushed into the ambient air.

Table 3-1 gives typical emission wavelengths for the predominate species observed in an APGD jet that is flushed into the background ambient air. An Andor optical emission spectroscopy system using a grating of 600g/mm was used to detect various excited plasma species within the jet plume and figure 3-11 gives spectral data for both pulsed and sinusoidal excitation sources. In general, atomic oxygen, OH and various nitrogen species were observed, this is typical of APGD plasma jets that are flushed in to the ambient air and consequently excite oxygen, nitrogen and other molecules that are generally not present in a pure helium discharge.[3.5,3.10,3.13]

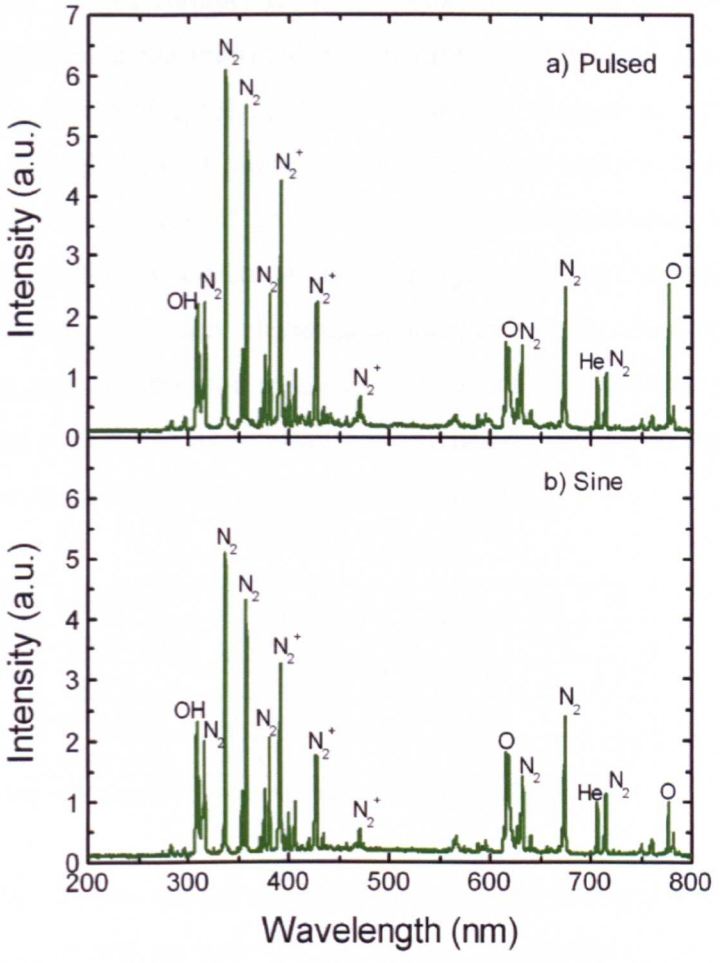

Fig 3-11: Emission spectrum of a) pulsed, and b) sinusoidal excited jets. Data obtained using a grating of 600 groves/mm.

The general emission spectra were similar for the pulsed and sinusoidal APGD jets. In the spectral range of 200 – 300 nm, there were very weak emission lines with their magnitudes at most a couple of percent of the nitrogen emission line at 337 nm. Therefore UV photons were not a major plasma species in the two APGD jets studied. Additional spectroscopic measurements with greater gratings were performed (not shown) and the findings confirmed the above conclusion. It is worth mentioning that UV emission was found similarly weak in other studies of pulsed APGD jets.[3.10, 3.13] This suggests that the APGD jets considered in this study are likely to enable applications through their reactive plasma species.

Recent studies conducted into various applications of APGD plasma jets have highlighted the importance of hydroxyl species and atomic oxygen species. In many biological applications atomic oxygen is of paramount importance, a high flux of atomic oxygen has been shown to significantly increase the effectiveness of an APGD jet in the inactivation of bacterial spores.[3.28] For surface modification the hydroxyl group is of particular interest, use is often made of a water electrode to increase it's presence in APGD.[3.29] Interestingly, optical emission intensities of several key application enabling species in the pulsed APGD jet were equivalent or greater than the sinusoidal jet despite having a lower average power consumption.

Species	OH	N_2	N_2	O	He	O
Wavelength (nm)	309	337	391	616	706	777
Pulsed	2.22	6.09	4.26	1.59	1	2.52
Sinusoidal	2.33	5.09	3.24	1.83	1	1
Intensity ratio,	0.97	1.20	1.31	0.87	1	2.52

Table 3-2: Relative intensities of key excited species in APGD Jets

Table 3-2 lists optical emission intensities of OH radicals at 309 nm, atomic oxygen at 616 nm and 777 nm, helium metastable at 706 nm, excited N_2 at 337 nm and excited N_2^+ at 391 nm, measured with a fixed optical set-up with the same alignment and distance between the spectrometer and the plasma jet. As shown in table 3-2, the most significant difference lies with the optical emission intensity of the atomic oxygen line at 777 nm – the emission intensity from the pulsed jet is 2.5 times greater than that from the sinusoidal jet. While the optical intensity at 616 nm was about 13% less in the pulsed jet than that in the sinusoidal jet, most oxygen atoms were produced via the channel associated with the 777 nm line. Therefore the pulsed jet was capable of producing more oxygen atoms. Similarly, the production of all other listed plasma species was more abundant with the pulsed plasma jet. This is both significant and desirable, as it offers unambiguous evidence of the advantage of pulsed excitation of APGD jets as a more efficient producer of reactive plasma species.

3.4.4 Visual comparison

To make a valid visual comparison it is necessary to employ an intensified charge-coupled device (ICCD), which is essentially a CCD that is fiber-optically connected to a micro-channel plate (MCP) to increase the sensitivity. In an ICCD camera a photo-cathode in front of the MCP converts photons to electrons which are multiplied by the MCP. Following the MCP a phosphor screen converts the electrons back to photons which are fibre-optically guided to a standard CCD. The advantage of using an ICCD camera over a standard CCD is two-fold, primarily the sensitivity is much greater, allowing the capture of events that would otherwise be invisible. Secondly, the exposure time at which an ICCD can operate can be extremely short. Imaging of plasma often requires exposure times in nanoseconds to capture specific events in the breakdown process.

Figure 3-12 shows a series of images of a plasma jet captured in 200ns steps starting 200ns before the pulse of current observed in the waveform shown in figure 3-8a. The exposure time of the ICCD camera was set to 2ns and each single image is the culmination of 100 individual shots. It is clear to see that the plasma plume is not a continuous 'stream' of plasma, as it appears to the naked eye, but comprises of a discrete ball of plasma that travels with a high velocity. Similar observation have been made previously and the term 'plasma-bullet' was coined.[3.11] The plasma 'bullet' exits the dielectric tube and travels vertically downwards toward a grounded electrode. The velocity of the bullet is dependant on several factors such as excitation method and gas type. Notably, one factor which has no effect on bullet velocity is the velocity of the background gas, which is typically only a few m/s whereas the bullet velocity is measured in the km/s range. A similar sequence of images is observed regardless of pulsed or sinusoidal excitation, the visible plume is always a product of rapid plasma bullets ejected from the dielectric tube. The production of a plasma bullet is always associated with a pulse of current through the circuit. As mentioned previously, the excitation method has a

significant effect on the properties of the plasma bullet; this will be re-visited in latter chapters.

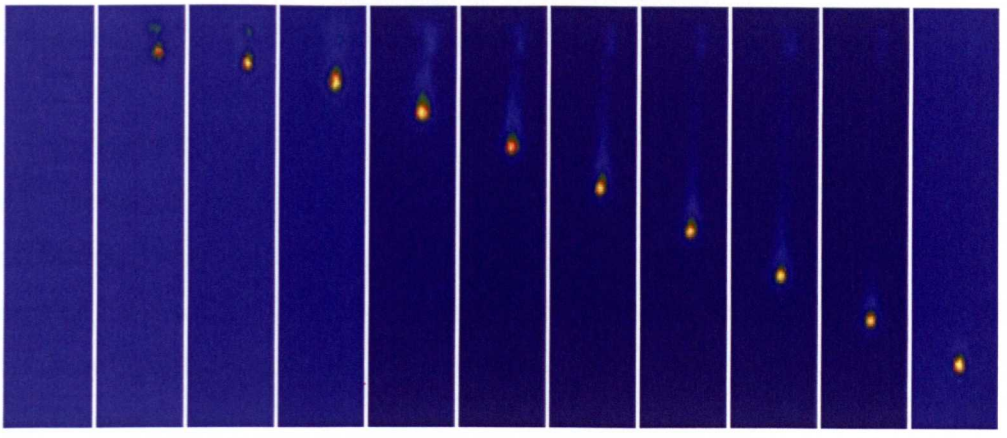

Fig 3-12: High-speed imaging of plasma plume (2ns Exposure, 200ns steps)

3.5 Summary

In this Chapter, a comparison study of pulsed and sinusoidal cold atmospheric plasma jets through electrical characterisation, gas temperature measurement, and optical detection of reactive plasma species has been reported. This has been the first direct comparison between pulsed and sinusoidal excitation methods, the results show conclusively that pulsed excitation is highly advantageous.

Using current and voltage measurements it has been shown that pulsed excitation has an average power consumption fives times lower than that of an equivalent sinusoidal source. This is attributed to a lower displacement current in a pulsed scenario compared to the displacement current that is continuously generated in the sinusoidal case. Optical emission spectroscopy was employed to determine the gas temperature of the plasma plume for each excitation method. Comparison between experimental measurements and simulated spectral data of the OH emission showed the gas temperature to be between 290 and 350K, this was confirmed using an infrared thermometer. The temperature for each excitation method was found to be roughly the same. OES was also used to investigate the chemical composition of the excited

species within the plasma plume. The technique gave a relative measure of the excited species within the plasma and it was found that pulsed excitation produced 2.5 times more emission of excited atomic oxygen which is known to be a key application enabler.

Using the energy consumption data and OES data it has been shown that electrical energy consumption can be reduced by a factor of 12 for producing the same amount of oxygen atoms. This is a highly significant finding for many applications employing APGD technology and will have far reaching consequences for the choice of excitation method in future applications.

References

[3.1] Shi J.J, Kong M.G, 'Expansion of the plasma stability range in radio-frequency atmospheric-pressure glow discharges' Applied Physics Letters, Vol.87, Iss.20, No.201501, 2005.

[3.2] Walsh J.L, Shi J.J, Kong M.G, 'Contrasting characteristics of pulsed and sinusoidal cold atmospheric plasma jets' Applied Physics Letters, Vol.88 Iss.17, No.171501, 2006.

[3.3] Babayan S.E, Jeong J.Y, Tu V.J, Park J, Selwyn G.S, Hicks R.F, 'Deposition of silicon dioxide films with an atmospheric-pressure plasma jet' Plasma Sources Science & Technology, Vol.7, Iss.3, pp.286-288, 1998.

[3.4] Cui N.Y, Brown N.M.D, 'Modification of the surface properties of a polypropylene (PP) film using an air dielectric barrier discharge plasma' Applied Surface Science, Vol.189, Iss.1-2, pp.31-38, 2002.

[3.5] Wang S, Schulz-von der Gathen V, Dobele H.F, 'Discharge comparison of nonequilibrium atmospheric pressure Ar/O-2 and He/O-2 plasma jets'Applied Physics Letters,Vol.83, Iss.16, pp.3272-3274, 2003.

[3.6] Yalin A.P, Yu Z.Q, Stan O, Hoshimiya K, Rahman A, Surla V.K, Collins G.J, 'Electrical and optical emission characteristics of radio-frequency-driven hollow slot microplasmas operating in open air' Applied Physics Letters,Vol.83, Iss.14, pp.2766-2768, 2003.

[3.7] Moon S.Y, Choe W, Kang B.K, 'A uniform glow discharge plasma source at atmospheric pressure' Applied Physics Letters,Vol.84, Iss.2, pp.188-190, 2004.

[3.8] Deng X.T, Shi J.J, Shama G, Kong M.G, 'Effects of microbial loading and sporulation temperature on atmospheric plasma inactivation of Bacillus subtilis spores' Applied Physics Letter,Vol.87, Iss.15, No.153901, 2005.

[3.9] Zhu W.C, Wang B.R, Yao Z.X, Pu Y.K, 'Discharge characteristics of an atmospheric pressure radio-frequency plasma jet' Journal Of Physics D-Applied Physics, Vol.38, Iss.9, pp.1396-1401, 2005.

[3.10] Leveille V, Coulombe S, 'Design and preliminary characterization of a miniature pulsed RF APGD torch with downstream injection of the source of reactive species' Plasma Sources Science & Technology, Vol.14, Iss.3, pp.467-476, 2005.

[3.11] Teschke M, Kedzierski J, Finantu-Dinu E.G, Korzec D, Engemann J, 'High-speed photographs of a dielectric barrier atmospheric pressure plasma jet' IEEE Transactions On Plasma Science, Vol.33, Iss.2, pp.310-311, Part 1, 2005.

[3.12] Kong M.G, Deng X.T, 'Electrically efficient production of a diffuse nonthermal atmospheric plasma' IEEE Transactions On Plasma Science, Vol.31, Iss.1, pp.7-18, Part 1, 2003.

[3.13] Laroussi M, Lu X, 'Room-temperature atmospheric pressure plasma plume for biomedical applications' Applied Physics Letters, Vol.87, Iss.11, No.113902, 2005.

[3.14] Laroussi M, Lu X, Kolobov V, Arslanbekov R 'Power consideration in the pulsed dielectric barrier discharge at atmospheric pressure' Journal of Applied Physics, Vol.96, Iss.5, pp.3028-3030, 2004.

[3.15] Bibinov N, Dudek D, Awakowicz P, Engemann J, 'Characterization of an atmospheric pressure dc plasma jet' Journal Of Physics D-Applied Physics, Vol.40, Iss.23, pp.7372-7378, 2007.

[3.16] Pan W.X, Zhang W.H, Ma W, Wu C.K, 'Characteristics of argon laminar DC plasma jet at atmospheric pressure' Plasma Chemisrty And Plasma Processing, Vol.22, Iss.2, pp.271-283, 2002.

[3.17] Kurihara K, Sasaki K, Kawarada M, Koshino N, 'High-Rate Synthesis Of Diamond By DC Plasma-Jet Chemical Vapour-Deposition' Applied Physics Letters, Vol.52, Iss.6, pp.437-438, 1988.

[3.18] Park J, Henins I, Herrmann H.W, Selwyn G.S, Hicks R.F, 'Discharge phenomena of an atmospheric pressure radio-frequency capacitive plasma source' Journal Of Applied Physics, Vol.89, Iss.1, pp.20-28, 2001.

[3.19] Kikuchi T, Hasegawa Y, Shirai H, 'Rf microplasma jet at atmospheric pressure: characterization and application to thin film processing' Journal Of Physics D-Applied Physics, Vol.37, Iss.11, pp.1537-1543, 2004.

[3.20] Stoffels E, Flikweert A.J, Stoffels W.W, Kroesen G.M.W, 'Plasma needle: a non-destructive atmospheric plasma source for fine surface treatment of (bio)materials' Plasma Sources Science & Technology, Vol.11, Iss.4, pp.383-388, 2002.

[3.21] Brok W.J.M, Bowden M.D, van Dijk J, van der Mullen J.J.A.M, Kroesen G.M.W, 'Numerical description of discharge characteristics of the plasma needle' Journal Of Applied Physics, Vol.98, Iss.1, No.013302, 2005.

[3.22] Sladek R.E.J, Stoffels E, Walraven R, Tielbeek P.J.A, Koolhoven R.A, 'Plasma treatment of dental cavities: A feasibility study' IEEE Transactions On Plasma Science, Vol.32, Iss.4, pp.1540-1543,Part 2 , 2004.

[3.23] Panousis E, Clement F, Loiseau J.F, Spyrou N, Held B, Thomachot M, Marlin L, 'An electrical comparative study of two atmospheric pressure dielectric barrier discharge reactors' Plasma Sources Science & Technology, Vol.15, Iss.4, pp.828-839, 2006.

[3.24] Xu L, Liu P, Zhan R.J, Wen X.H, Ding L.L, Nagatsu M, 'Experimental study and sterilizing application of atmospheric pressure plasmas' Thin Solid Films, Vol.506, pp.400-403, 2006.

[3.25] Lu X, Jiang Z, Xiong Q, Tang Z, Hu X, Pan Y, 'An 11 cm long atmospheric pressure cold plasma plume for applications of plasma medicine' Applied Physics Letters, Vol.92, No.081502, 2008.

[3.26] Kunhardt E.E, 'Generation of large-volume, atmospheric-pressure, nonequilibrium plasmas' IEEE Transactions On Plasma Science, Vol.28, Iss.1, pp.189-200, 2000.

[3.27] Moon S.Y, Choe W, 'A comparative study of rotational temperatures using diatomic OH, O-2 and N-2(+) molecular spectra emitted from atmospheric plasmas' Spectrochimica Acta Part B-Atomic Spectroscopy, Vol.58, Iss.2-3, pp.249-257, 2003.

[3.28] Deng X.T, Shi J.J, Kong M.G, 'Physical mechanisms of inactivation of Bacillus subtilis spores using cold atmospheric plasmas' IEEE Transactions On Plasma Science, Vol.34, Iss.4, pp.1310-1316, Part 2, 2006.

[3.29] Choi H.S, Shikova T.G, Titov V.A, Rybkin V.V, 'Surface oxidation of polyethylene using an atmospheric pressure glow discharge with liquid electrolyte cathode' Journal Of Colloid And Interface Science, Vol.300, Iss.2 pp.640-647, 2006.

[3.30] Foltin V, Lestinska L, Machala Z, 'Spectroscopic investigations of atmospheric pressure microwave torch nitrogen plasma jet' Czechoslovak Journal Of Physics, Vol.56, pp.B712-B720, Part 4, Suppl. B, 2006.

4 Sub-Microsecond Pulsed APGD jets

4.1 Introduction

The previous chapter provided a detailed comparison between pulsed and sinusoidal excitations of an APGD jet. Conclusive evidence indicated that pulsed excitation is significantly more electrically efficient than the sinusoidal excitation; furthermore it was observed that despite lower power consumption a higher flux of reactive species was obtained. The use of pulsed excitation offers a greater level of flexibility by altering certain pulse parameters, for example pulse width and rise time, to achieve the highest efficiency possible. This chapter focuses upon the reduction of pulse width down to a sub-microsecond scale and highlights the benefits of using increasingly short pulsed excitation. Potentially, reduction of the pulse width will further enhance the electrical efficiency of plasma generation and could introduce additional benefits such as greater stability, higher reactivity, and lower gas temperatures.

The first part of this chapter explores the use of sub-microsecond pulsed excitation of a helium APGD jet. The few published studies on sub microsecond pulsed APGD have all focused upon parallel plate electrode geometries,[4.1-4.5] whilst the excitation method is identical the effects of introducing a complex geometry, such as the plasma jet configuration, are unknown. Through electrical and optical measurements the advantages of sub-microsecond pulsed excitation are highlighted for an APGD jet and compared to previous studies of pulsed APGD employing parallel plate electrode configurations. In the second part of this chapter, focus is directed towards the use of argon as a carry gas as it is economically more desirable than helium which has commonly been used for the generation of APGD.[4.6] So far, the use

of argon has been found to considerably increase the gas temperature of APGD jets leading to a danger of instability through thermal runaway.[4.9] Significantly, pulsed excitation has been shown to reduce the minimum energy consumption, at a given density of reactive plasma species.[4.7] This should, in principle, help mitigate or even eliminate the development of a thermal runaway instability. Given that most previously reported pulsed APGD studies have been produced in a helium-dominant working gas,[4.1-4.4] pulsed argon APGD's are of particular interest [4.6] The latter part of this chapter discusses the production of a stable argon APGD jet sustained with sub-microsecond pulses repeated at kilohertz frequency.

4.2 Experimental setup

The APGD jet considered in this chapter consisted of a quartz tube wrapped with a 1cm band of copper foil as the powered electrode, either argon or helium was flushed through the tube at a rate determined via a mass flow controller. A grounded copper electrode was placed vertically below the tube outlet at a maximum distance of 2 cm but nominally 1 cm, a 2mm ceramic sheet was placed on the surface of the grounded electrode to form a second dielectric barrier. Figure 4-1 depicts the electrode arrangement and the overall apparatus, it should be noted that the configuration shown is identical to that used in Chapter 3. The inner diameter of the quartz tube was 3 mm, and the outer diameter 4mm. Quartz was chosen as it is able to withstand high-temperatures and is optically transparent to short wavelength light allowing OES to be performed inside and outside of the jet structure. Plasma images were taken with an exposure time down to 1 ns using an iCCD camera (Andor i-Star DH720), optical emission spectra were obtained using a spectrometer system (Andor Shamrock) with a focal length of 0.3 m and a grating of 600 grooves/mm.

The pulsed power supply was home built and is based upon the push-pull stacked MOSFET circuit shown in section 2.4.2. The device consists of thirty 1kV MOSFETs arranged as two switching elements thus resulting in an

output voltage up to 15 kV. The MOSFET devices employed have switching transition times around 20ns so the rectangular pulses produced have equivalent rise and fall times. As the repetition frequency is increased device heating becomes significant and this limits the maximum repetition frequency to 5kHz. The discharge current and the applied voltage were measured with a wideband current probe (Pearson 2877) and a wideband voltage probe (Tektronix P6015A), respectively. Their waveforms were recorded on a digital oscilloscope (Tektronix TDS 5054B).

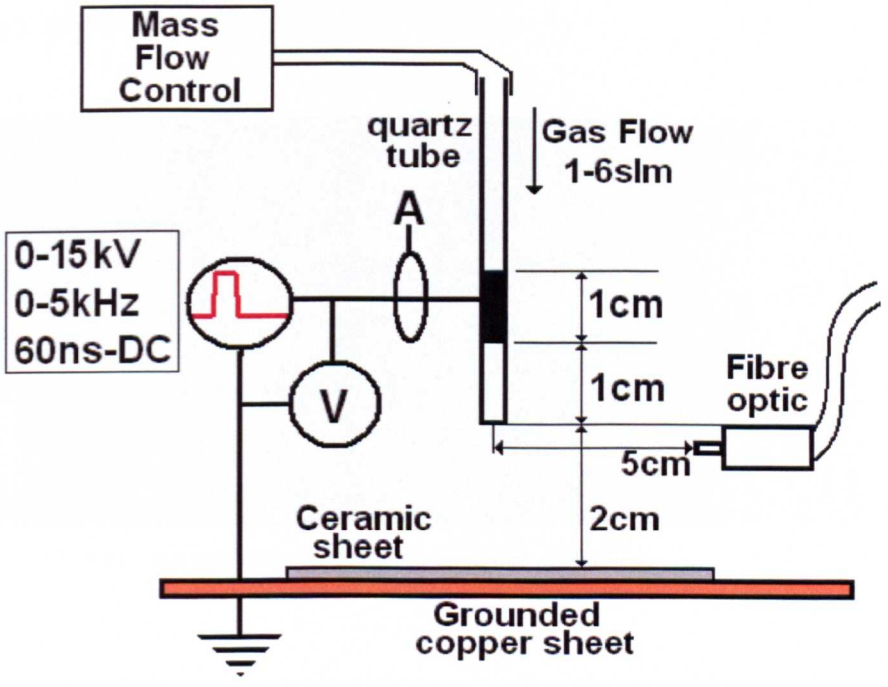

Fig 4-1: Schematic showing the experimental setup of helium / argon pulsed APGD jet.

In all experiments conducted the optical fibre was fixed to focus at a point 5mm below the tube exit, horizontal from the axis of the ceramic tube. The fibre was placed 5cm away from the plume to avoid direct contact with the plasma. A prerequisite for any comparative study is the reliable and repeatable placement of the fibre optic cable, a slight adjustment in position can translate into a big variation in the measured emission spectrum.

4.3 Helium APGD Jet

This section details observations made of a sub-microsecond pulsed helium APGD jet. Figure 4-2 shows an image of the plasma plume taken with a Canon digital camera, in this image no ground electrode has been used and consequently the plume extends for 7 cm which is exceptional long. Typically, the maximum plume length observed in an APGD jet flushed into the ambient air is less than 5cm.[4.7] A markedly different plume length with a similar gas flow rate and comparable maximum applied voltage suggests that the reduction of the pulse width is likely to have a large impact on the properties of the APGD jet.

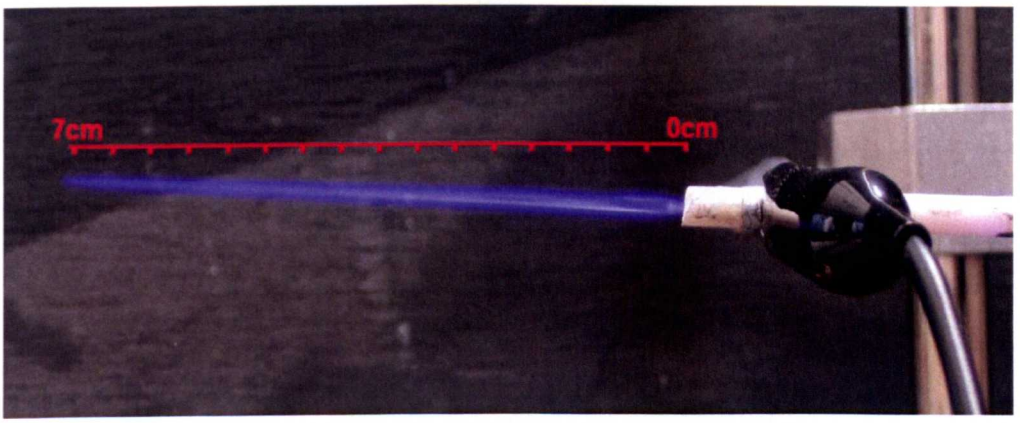

Fig 4-2: Digital image of a sub-microsecond pulsed helium APGD Jet

4.3.1 Electrical characteristics

Figure 4-3 shows a typical applied voltage waveform on a microsecond scale, each voltage pulse has a width of 500ns and is repeated at 350μs intervals. This yields a repetition frequency of almost 3kHz and a duty cycle of 0.14%. As the applied voltage is only present over very short time periods the energy unnecessary for plasma generation is reduced significantly.

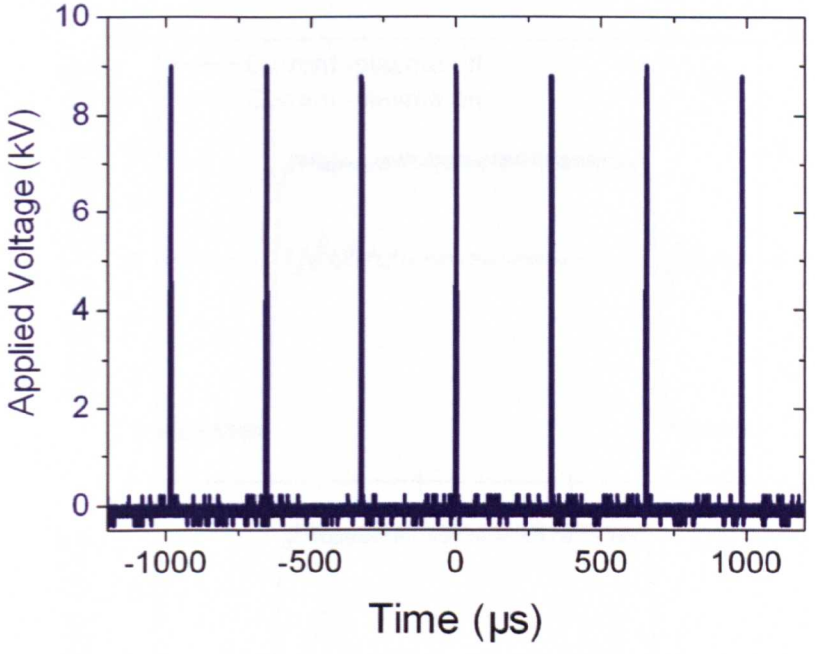

Fig 4-3: Graph showing the voltage waveform of a pulsed helium APGD jet on a microsecond scale.

The power consumption discussed in previous chapters relates to the electrical power required to sustain the plasma, i.e. the power dissipated within the plasma itself, no mention was given to the actual power requirements of the entire system. Wall-plug efficiency, which is defined as the ratio of the output power to the input power of the entire system is of paramount importance when APGD systems are considered on an industrial scale. A significant advantage of the sub-microsecond pulse generator arises from the use of a push-pull circuit topology, no energy is wasted in heating large DC blocking resistors hence the wall-plug efficiency is increased substantially.

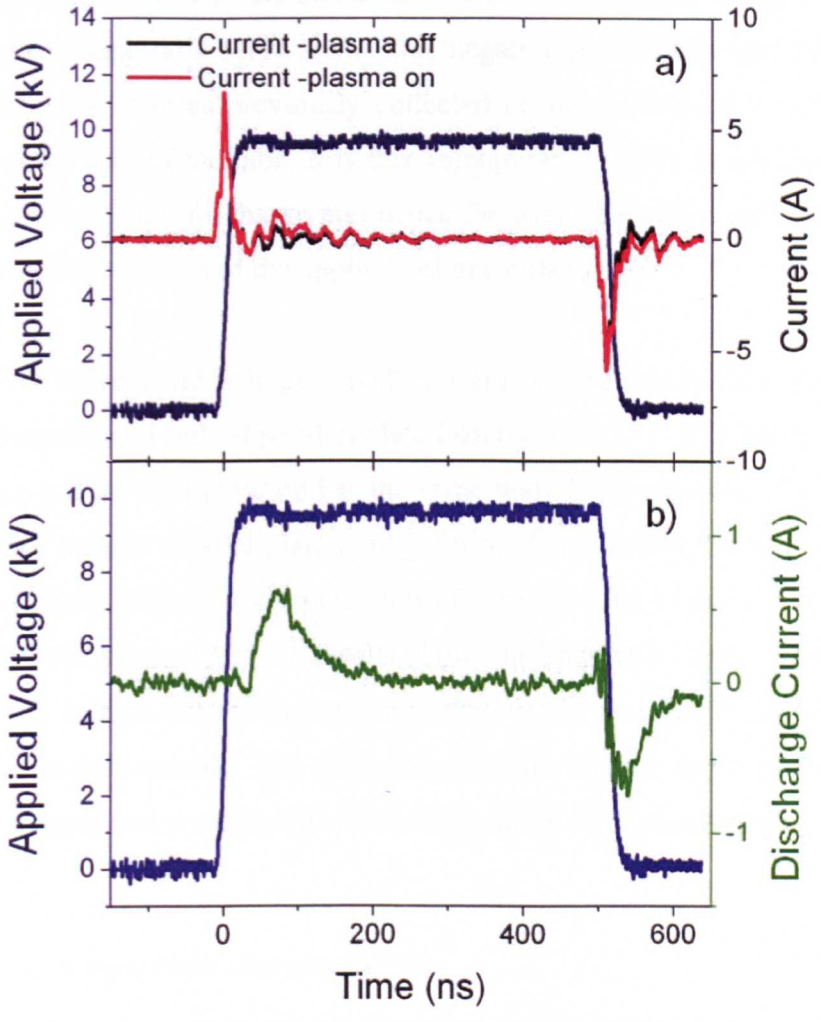

Fig 4-4: The applied voltage, displacement current and discharge current measured in a pulsed helium APGD Jet

Figure 4-4a shows the applied voltage pulse in blue, the current without plasma (no gas flow), in black, and the current with plasma (recorded with helium flow), in red. Figure 4-4b shows the applied voltage, and the actual discharge current, in green, which was obtained by subtracting the displacement current (due to the cable capacitance, the dielectric equivalent capacitance, and the gas gap equivalent capacitance) from the total measured current.[4.2] Two distinct current pulses indicating two consecutive discharges are clearly visible. The first pulse occurs shortly after the rising edge of the voltage pulse and the second current pulse occurs at the falling edge of the voltage.[4.1] These two current pulses are each approximately 100 ns wide. Due

to the capacitive effect of the dielectric barrier as the applied voltage falls the actual gas voltage falls below zero. This negative pulse of the gas voltage is induced by the charges previously collected on the surface of the dielectric plate and the wall of the tube. It is this voltage pulse which is responsible for the re-ignition of the discharge and hence the occurrence of a second current pulse at the falling edge of the applied voltage pulse.

The current and voltage waveforms are very similar to those presented in sub-microsecond pulsed parallel plate DBD studies.[4.1,4.2] It is likely that the discharge in a jet configuration has the same underlying physical mechanisms as that in a simple parallel plate configuration. One curiosity worth noting is the delay of the initial current pulse from the rising edge of the voltage pulse, which was not observed in the results shown in Chapter 3. This is unusual as the applied voltage has reached it's maximum value and yet breakdown does not occur instantaneously. The next section of this chapter explores this delay in further detail and presents a possible explanation for its occurrence.

4.3.2 Gas temperature characteristics

Using optical emission data from the excited hydroxyl molecular band at 307-311 nm, the rotational temperature and consequently the gas temperature has been obtained by means of best-fit between experimental and simulated data. Figure 4-5 presents the measured spectrum obtained using a high resolution optical grating of 2400 grooves/mm and two sets of simulated data, one at a rotational temperature of 300K and the other at 350K. As expected, the temperature is low, approximately room temperature, however this fails to show any advantage gained by using sub-microsecond pulses over other excitation techniques.[4.7,4.11] This is partly due to the fact that the technique of comparing measured and simulated spectra is not particularly effective in resolving small temperature variations when the gas temperature is close to room temperature. It is expected that the advantages of pulsed APGD will be clearer when other carry gases are used. Discharges in gases such as

argon and nitrogen tend to be significantly hotter than those generated in helium, hence the advantage of short pulse excitation may be more distinct.

Figure 4-6 provides further confirmation of the low temperature nature of the pulsed helium APGD jet. A finger placed into the plasma feels no discomfort and can be held within the plume for a long time. The effect of such atmospheric pressure plasmas on biological matter is of great importance in many APGD applications. For example, the use of APGD to decontaminate wounds,[4.12] depends upon the plasma not causing any undue damage to the biological matter. Thermal instability leading to an increase in temperature beyond a level that is painful to humans must be avoided, equally important is the limitation of current flowing through the discharge. As the discharge current increases the glow discharge transitions to an arc, notable for high temperatures and high currents which could potentially lead to the patient receiving an electric shock. As the pulse width is reduced an inherent stability is introduced into the gas discharge system, gas heating is reduced and glow-to-arc is less likely to occur.[4.4]

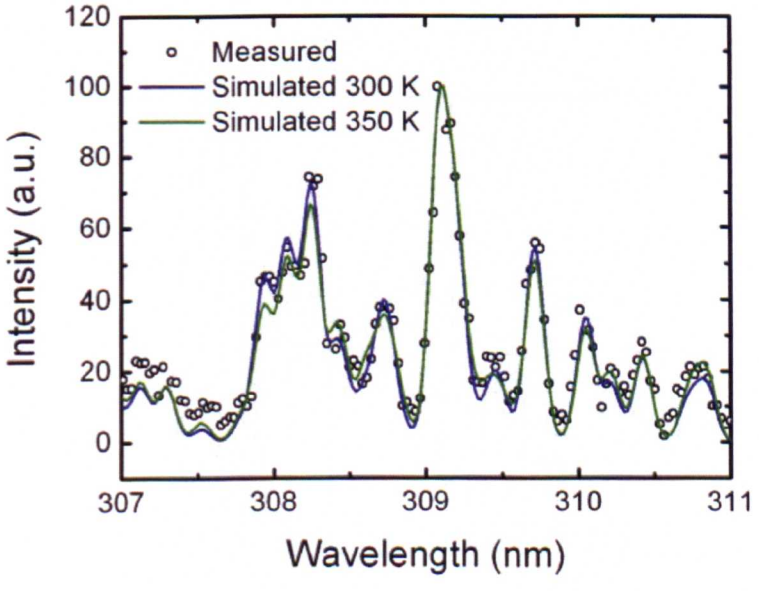

Fig 4-5: Measured and simulated data used to determine the rotational temperature in a 500ns pulsed helium APGD jet.

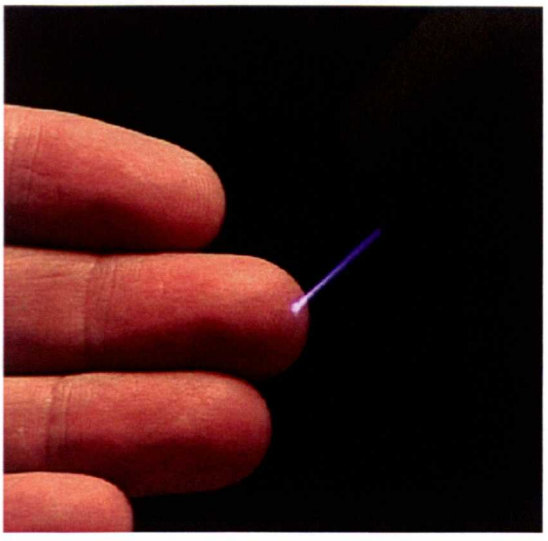

Fig 4-6: Image of a sub-microsecond pulsed helium APGD jet directed on to a finger.

4.3.3 Plasma reactivity characteristics

Figure 4-7 shows optical emission spectroscopy results obtained from the 500ns pulsed helium jet, a grating of 600grooves/mm was used to record the spectrum in the 250-900nm range. As in the case of the sinusoidal helium APGD jet discussed in the previous chapter and other reported studies,[4.7,4.9] the spectrum is rich in emission lines from excited nitrogen and oxygen species.

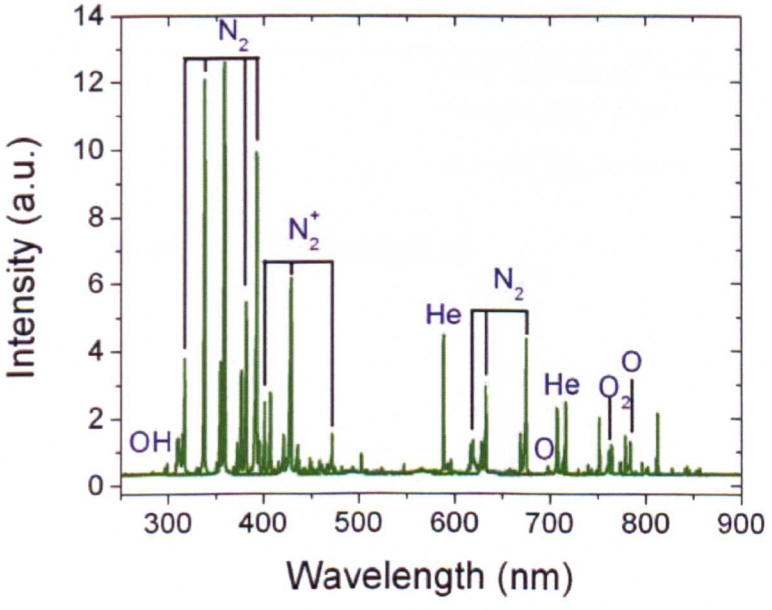

Fig 4-7: Measured spectrum of the pulsed 500ns helium APGD jet.

It is not possible to directly compare the OES results shown in figure 4-7 with the data given in Chapter 3 as the position of the fibre optic probe was different. It is worth noting however that the discharge current measured within the sub-microsecond pulsed jet is several orders of magnitude above that normally observed in a DBD discharge;[4.7,4.8] this is consistent with previously reported sub-microsecond pulsed APGD.[4.1,4.2] As the discharge current may be used to give a rough indication of the electron density, it can be concluded that there are more electrons and consequently a higher density of excited species in the sub-microsecond pulsed APGD.

The OES data given in figure 4-7 was obtained using an exposure time of 1ms, this is substantially longer than a single discharge event thus resulting in a time averaged spectrum. The OES instrument consists of two separate parts, the spectrometer and the iCCD camera. The camera allows exposure times as low as 1ns hence it is possible to obtain time resolved emission spectroscopy. By monitoring the evolution of excited species within the transient discharge a far greater understanding can be achieved in comparison to the simple time averaged OES highlighted previously. Figure 4-8 shows typical time resolved OES data for the 500ns pulsed APGD jet of figure 4-4.

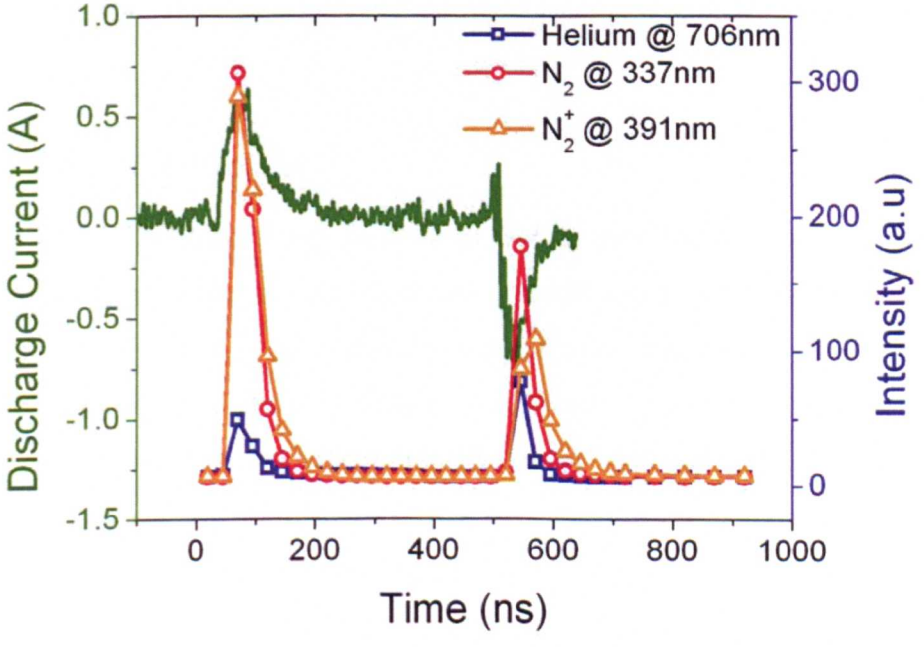

Fig 4-8: Time resolved OES data of the 500ns pulsed helium APGD jet.

With an exposure time of a few nanoseconds it is possible to obtain a very high temporal resolution allowing for the evolution of species to be tracked precisely over one pulse of the applied voltage. This method is used extensively throughout the remainder of this thesis; however, just a brief example is given here to highlight the potential of the technique. Figure 4-8 shows the evolution of three particular excited species over a single voltage pulse. Metastable helium at 706nm and ionic nitrogen at 391nm, both of which are considered to be indicative of energetic electrons within an APGD.[4.13] Also excited molecular nitrogen at 337nm is tracked, this is typically the strongest emission line observed in an APGD jet flushed in to ambient air and plays an important role in many applications.[4.13] From the time resolved data it is clear to see that the production of the excited helium and nitrogen species is closely related to the discharge current. This makes sense, as the current increases more electrons flow through the gas gap reflecting a greater level of ionisation within the background gas. It is worth noting that the levels of excited species within the plasma rapidly fall in absence of the discharge current, this is consistent with the observations of nanosecond imaging, presented in section 3.3.4. At each discharge event a plasma 'bullet' is ejected and rapidly travels toward the grounded electrode. The photons emitted from the plasma bullet can only enter the fibre optic when the bullet is within the viewing angle of the fibre, as such the time resolved OES appears to rise and fall very rapidly.

4.4 Argon APGD Jet

For APGD technology to become widely used on an industrial scale, efforts must be made to use more economical gases such as argon and nitrogen.[4.6,4.9] Helium is prohibitively expensive for large-scale applications, almost five times more costly than argon; however the characteristics of a helium gas discharge, such as low temperature and inherent stability make it a very attractive choice. The use of pulsed excitation to introduce stability and lower gas temperatures could potentially open the gateway to large volume, low temperature APGD processing without using expensive helium gas.

Figure 4-9 shows an argon APGD jet flushed in to the ambient air. It is clear to see that the generated plasma is very stable and visually free from streamers. Similar to a helium APGD jet, the discharge has a spreading effect on the dielectric sheet, this is clearly visible in the photo.

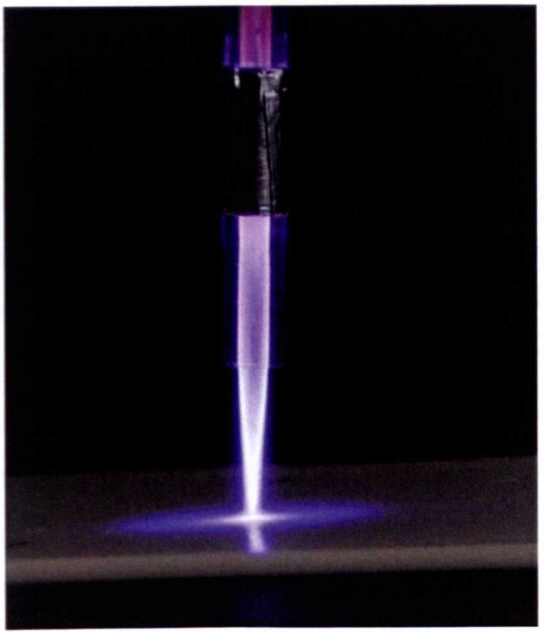

Fig 4-9: Digital image of a pulsed argon APGD Jet

To confirm the uniformity of the pulsed argon jet nanosecond imaging was used, figure 4-10 shows a sequence of images taken at 5ns intervals over a single discharge event with an exposure time of 2ns. It is clear from the images that the discharge is free from streamers. It is also worth noting that the plume appears to be continuous unlike that of a helium APGD jet, where the plume consists of discrete 'bullets'. This could be a consequence of the higher applied voltage and is investigated further in the next chapter.

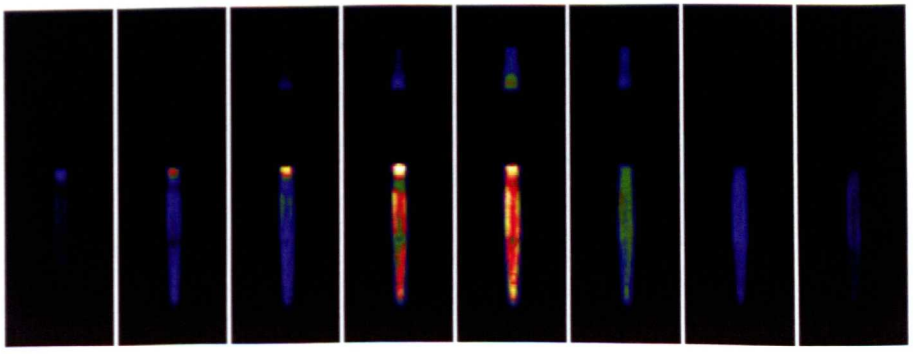

Fig 4-10: Images taken with a 2ns exposure at 5ns intervals over a discharge current pulse.

4.4.1 *Electrical characteristics*

As the breakdown voltage of argon is notably higher than that of helium the amplitude of the applied pulse must increase compared to that of the helium APGD detailed in section 4.3. It was found that the stable operating range of the argon jet was between 8kV right up to the pulse generator maximum of 15kV. Figure 4-11 shows the current and voltage characteristics of the pulsed argon jet for which the peak applied voltage is 12.0 kV, the voltage pulse width measured as full width at half maximum amplitude is 505 ns and the repetition frequency is 4 kHz. The rise and the fall times of the applied voltage pulse are very short at 15 ns and 22 ns, respectively, causing a large displacement current to be established at each of the voltage-rising and the voltage-falling edges. The two displacement current peaks are respectively 6.7 A and -6.0 A at 138 ns and 648 ns, at which the corresponding total current peaks are 7.1 A (This value and the displacement current are the same on the rising edge, because the discharge current is offset) and -7.5 A, respectively. In addition, the total current reaches a peak of 4.5 A at 192 ns where the main discharge event occurs.

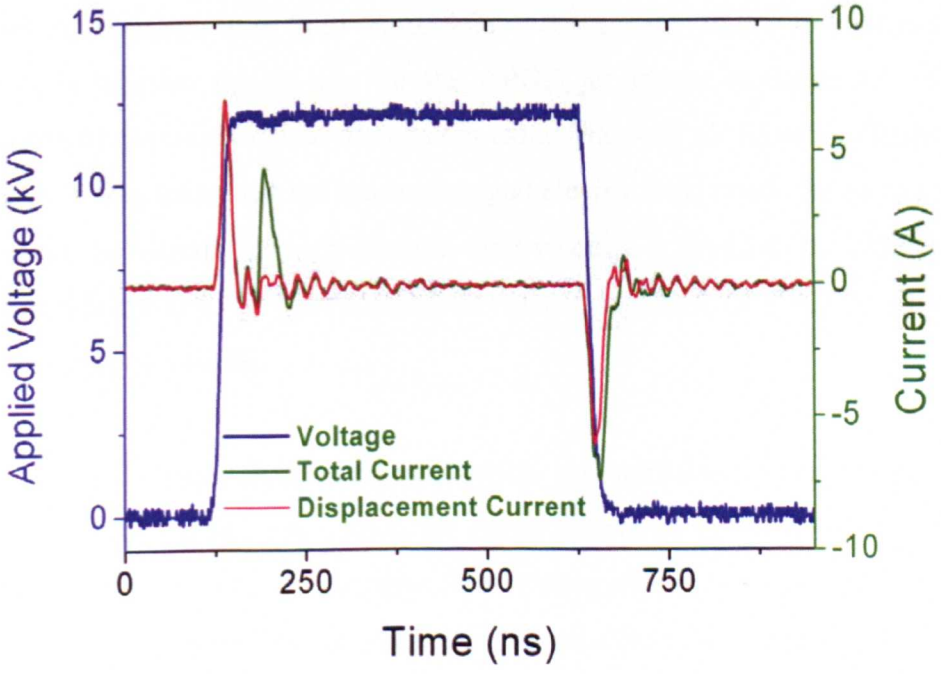

Fig 4-11: Applied voltage, displacement current and discharge current measured in a pulsed argon APGD jet

It is of interest to note that the current peak of 4.5 A occurs some 75 ns after the onset of the voltage pulse at 117 ns. This delay is likely to be related to a pre-ionization phase in which a weak Townsend discharge takes place to accumulatively increase the space charges in the quartz tube and subsequently elevate the local electric field above the threshold for gas breakdown. The delay of the current pulse from the onset of the voltage pulse was also observed in sub-microsecond pulsed APGD between two parallel bare electrodes.[4.3,4.4]

Following the pre-ionization phase, the 4.5A current pulse reaches its peak and then falls to form a 33 ns short pulse from 182 ns to 215 ns even though the applied voltage remains at 12 kV. This is because electrons generated from gas ionisation inside the quartz tube travel to and arrive at the inner wall of the quartz tube, and the resulting voltage across the quartz tube wall is at the opposite direction to the applied voltage thus reducing the gas voltage. Consequently, the ionization process is stopped and this causes the fall in the discharge current. This is typical of dielectric barrier discharges,[4.8,4.10] and one half of the current pulse width is comparable to the electron transition time from the middle of the gas gap to the quartz tube. To examine whether this is true for the APGD jet shown in figure 4-9, a 2D electrostatic simulation was undertaken using Maxwell SV (Ansoft, Pittsburgh USA). It was found that the space-averaged electric field inside the quartz tube is about 40 kV/cm at which electron drift velocity is found to be 107cm/s in atmospheric argon.[4.14] This corresponds to 15 ns, similar to one half of the 38 ns current pulse width.

As the gas voltage is reduced below the breakdown voltage, electrons generated during gas breakdown are either stored on the wall of the quartz tube or left to drift inside the tube. The drifting electrons can in principle be carried by the argon flow to reach the ground electrode and register a small current peak. To assess this possibility, we performed a 2D electrostatic computation of the electrode structure shown in figure 4-9 using the Ansoft simulation package. Figure 4-12 shows the simulation results. At an applied

voltage of 12kV, the electric field along the passage of the argon flow was found at about 7.2 – 10.8 $x10^3$ V/cm at which the electron drift velocity is calculated to be about 2 – 3 $x10^6$ cm/s in atmospheric argon.[4.14]

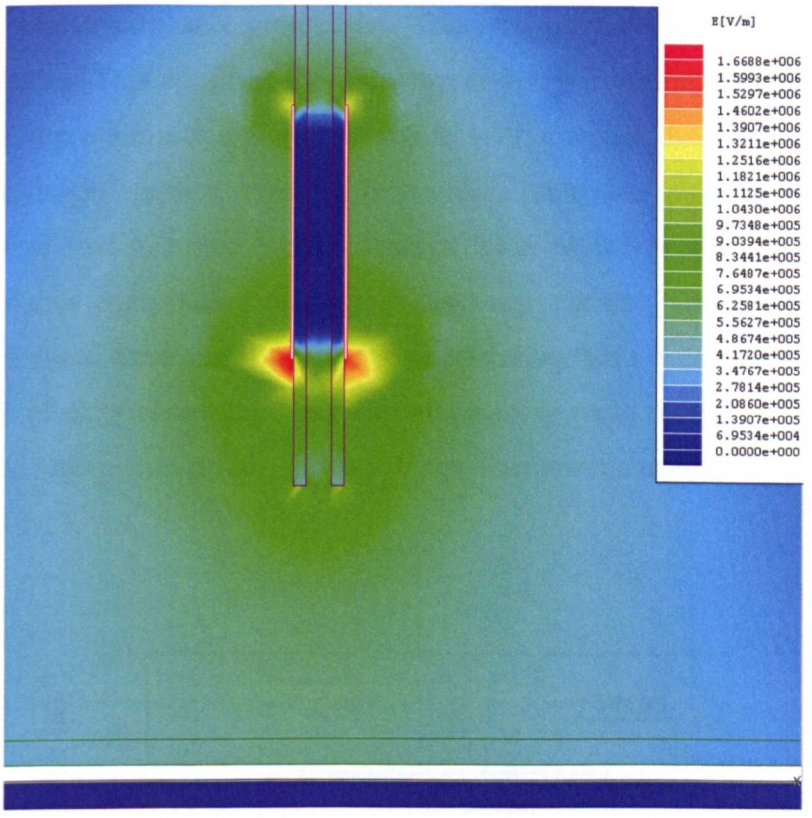

Fig 4-12: Electrostatic simulation of the 500ns plasma argon APGD jet

As the nozzle-side of the powered electrode is 1.5 cm away from the ground electrode, an electron is likely to take 500 – 750 ns to travel from the plasma generating region to the grounded electrode. This is markedly longer than the interval of 398 ns from the end of the 4.5 A current pulse to the beginning of the voltage pulse fall. Therefore, the drifting electrons cannot reach the grounded electrode to register a current pulse before the fall of the voltage pulse. At the fall of the voltage pulse, they add to the displacement current pulse to increase the total current pulse.

The above interpretation can be further supported by changing the applied voltage. As the applied voltage decreases, the onset of the current pulse should occur at a more delayed instant from the onset of the voltage

pulse because a longer pre-ionization phase is needed at a smaller applied voltage to the threshold for gas breakdown. Figure 4-13 shows the traces of the discharge current obtained by subtracting the displacement current from the total current, at an applied voltage of 13.3, 11.4, and 9.4 kV for which the current pulse occurs at a progressively delayed point from the onset of the voltage pulse. This confirms that the current delay from the voltage pulse is related to a pre-ionization phase. In figure 4-13, the peak discharge current is larger at larger applied voltage, but with a narrower pulse width. It is conceivable that a larger applied voltage leads to the production of more electrons thus contributing to a larger discharge current. The availability of more generated electrons at a larger applied voltage also cause more efficient diffusion of electrons to the tube wall and a more rapid reduction of the gas voltage to reduce the current. This results in a narrower current pulse as shown in figure 4-13.

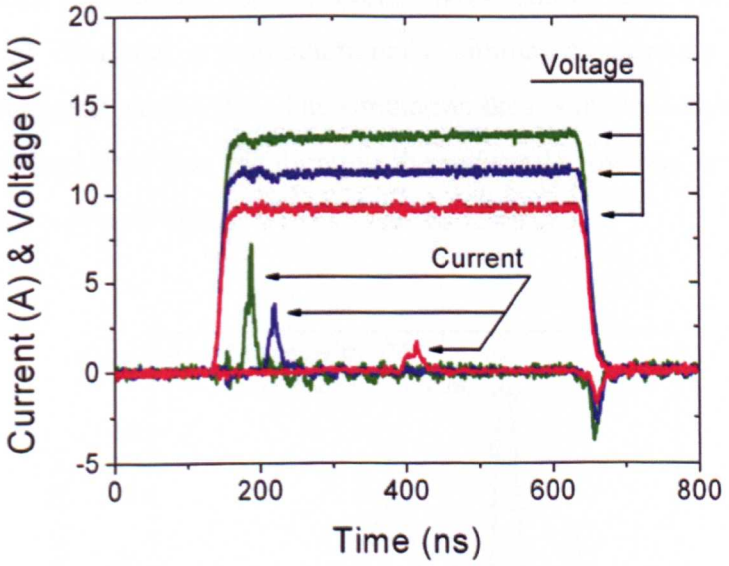

Fig 4-13: Variation of discharge current with applied voltage for a pulsed argon APGD jet.

4.4.2 Gas temperature characteristics

It is widely understood that atmospheric pressure argon discharges have gas temperatures in excess of 100°C,[4.9] when using conventional

sinusoidal excitation at frequencies in the kHz[4.15], MHz,[4.9] or microwave range.[4.16] A small proportion of the previous studies published on argon APGD jets have claimed room temperature operation can be achieved using high gas flow rates;[4.16] however their claims have not been sufficiently substantiated. It is possible to use a very high gas flow rate, several tens of m/s, to rapidly cool objects placed within the plasma plume thus giving the *appearance of a room temperature* APGD. However this is not a true measurement of the plasma temperature but rather that of *the afterglow region* where the plasma is considerably less intense. In addition using gas flow to cool the discharge results in a large amount of gas wastage.

As discussed previously, a common method for determination of the gas temperature in an APGD is the use of optical emission spectroscopy. The emission intensities recorded are independent of gas flow rate and as such are more accurate than using a thermocouple to record the temperature of an object placed within the plume. Figure 4-14 shows that comparison of experimental data and a computationally simulated spectrum suggests a rotational temperature of 320K. The simulation data is in close agreement with the experimental data thus highlighting the unusually low temperature of the 500ns pulsed argon APGD.

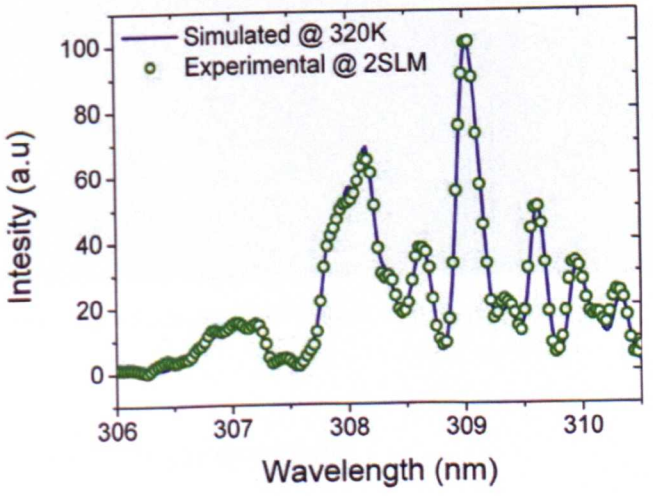

Fig 4-14: Measured and simulated data used to determine the rotational temperature of a 500ns pulsed argon APGD Jet.

To confirm that the OES temperature measurement method is independent of the flow rate the temperature of the generated APGD was determined for argon flow rates from 2 to 10 SLM. It was found that the temperature was within +/-10K of 320K in all cases thus confirming the reliability of the method.

Figure 4-15 shows a photo of a finger placed in the argon jet plume. Similar photos have appear in recently published studies on a microwave generated argon APGD jet.[4.16] However, it is worth noting that the argon flow rate used in this study is as little as 2 SLM and the finger can be held within the plume indefinitely without any discomfort. The flow rates used in reference 4.16 are significantly higher leading to a cooling effect on any objects placed within the plume, allowing a finger to be placed in a potentially hot plasma without discomfort.

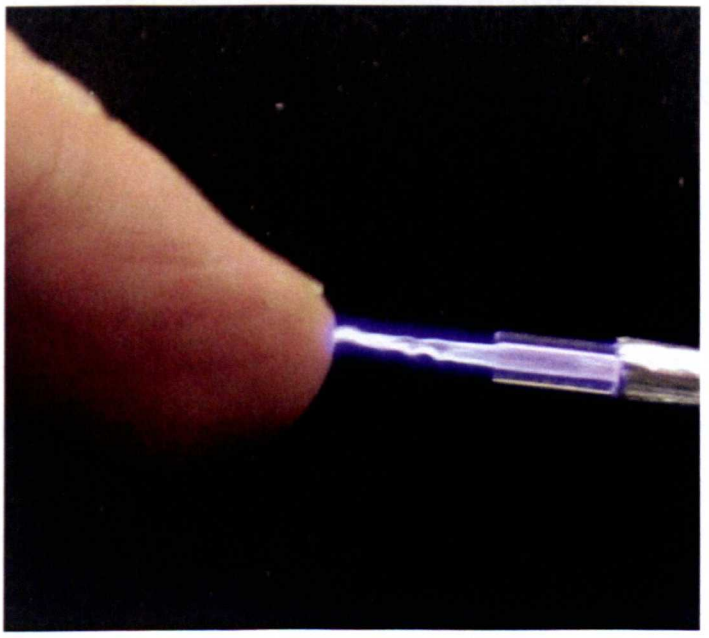

Fig 4-15: Image showing a finger in direct contact with Ar jet plume

4.4.3 Plasma reactivity characteristics

Fig. 4-16 shows optical emission spectrum data for of a pulsed argon jet at an applied voltage of 10 and 12 kV, in which there are strong emission

lines of OH, nitrogen, argon and atomic oxygen. This is distinctively different from pulsed helium APGD jets of which the optical emission spectra are dominated by nitrogen lines, figure 4-16 is strongly dominated by argon lines such as those at 696.5, 750.4, 763.5, and 772.4 nm.

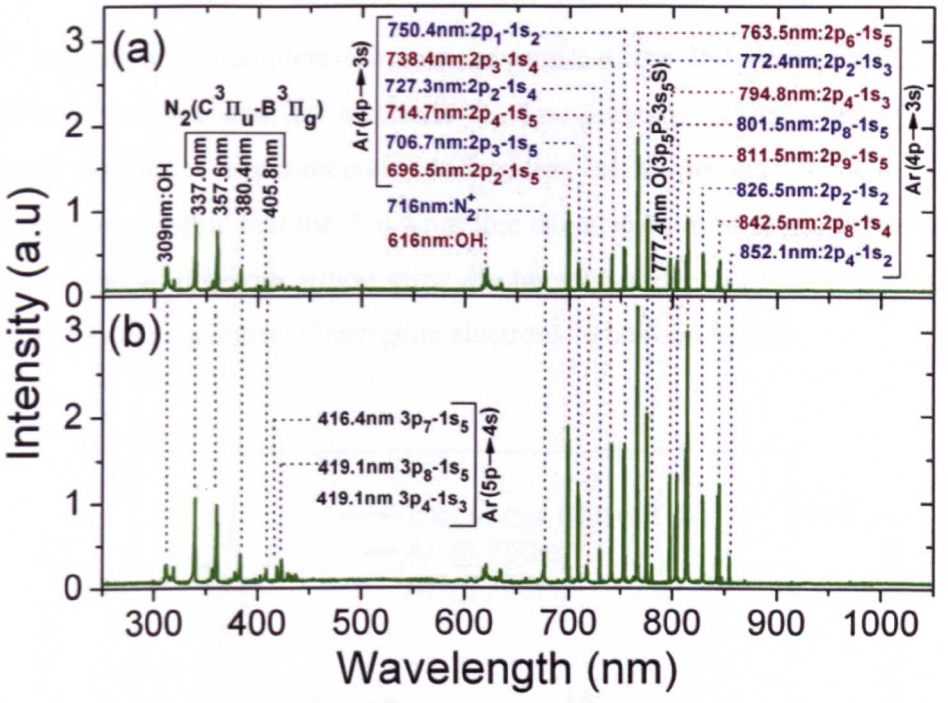

Fig 4-16: Time averaged emission spectrum of the pulsed argon jet at a)10kV and b)12kV.

Time-resolved emission intensities of two particular excited species are shown in figure 4-17 together with the measured current trace. In general, the line intensities reach their peak when the current pulse is just about to complete. This suggests that the timescale of the current pulse represents that of the entire discharge event during which the optical emission increases accumulatively. After the discharge event finishes and the line intensities reach their peak, no more excited plasma species are available to emit photons and increase further the intensity of relevant emission lines. Therefore, the rising phase of the line intensities is comparable to the pulse width of the discharge current and is about a few tens of nanoseconds. Their falling phase, on the other hand, is much longer and perhaps indicative of the timescale for relevant excited plasma species to decay to their ground states. These

observations were confirmed using nanosecond imaging, it was seen that the discharged reached its maximum intensity in 20-30ns and then gradually decayed over many hundreds of nanoseconds. This is in stark contrast to a pulsed helium jet where the plasma is observed as a discrete lump ejected at a time coinciding with the discharge current pulse and is rapidly extinguished.

It is of particular interest to note the profile of the 750.4 nm argon line, which has been related to electrons in low-pressure argon plasmas.[4.17] Although no direct experimental confirmation is at present available in literature, it is possible that the 750.4 nm line can also be used as the signature of electrons in atmospheric argon glow discharges similar to the 706 nm line being used as the signature of energetic electrons in helium APGD.

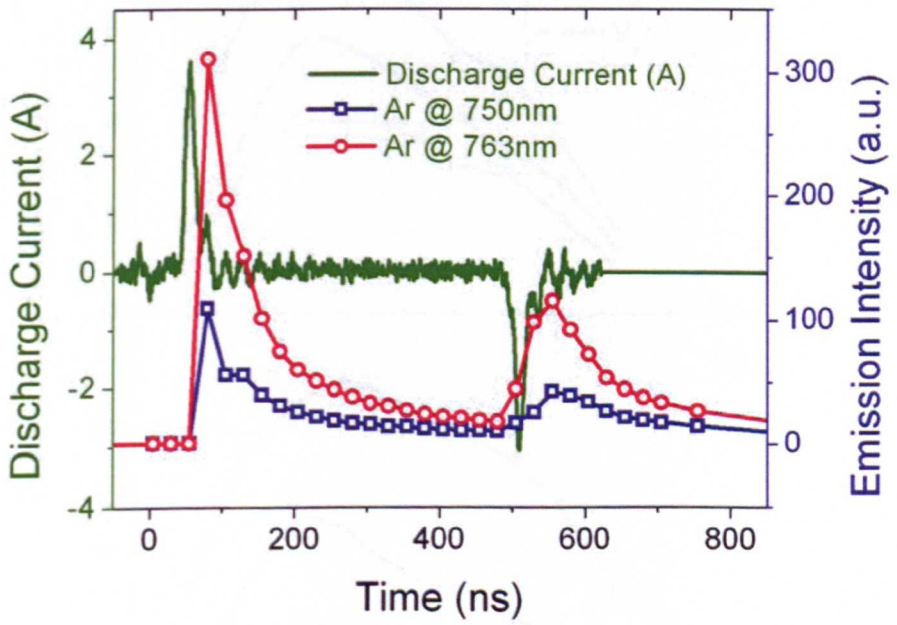

Fig 4-17: Time resolved OES data of pulsed Argon Jet

4.5 Gas Mixtures

The mixture of small amounts of a reactive gas to the chemically inert base gas necessary for stable APGD generation is often seen as a way to improve the reactivity of the discharge. Many applications of APGD rely upon a high flux of atomic oxygen.[4.9,4.18] Using a jet configuration allows the

discharge to be flushed in to the oxygen rich background air, which is an excellent way of increasing oxygen content. However, small amounts of oxygen can also be added to the base gas without having a significant effect on the stability of the discharge.

Figure 4-18 shows the effect on the emission of exited atomic oxygen when small amounts of oxygen are mixed with the argon base gas. As expected a small amount of added O_2 increases the level of emission, however this trend is quickly reversed when excessive O_2 is added.

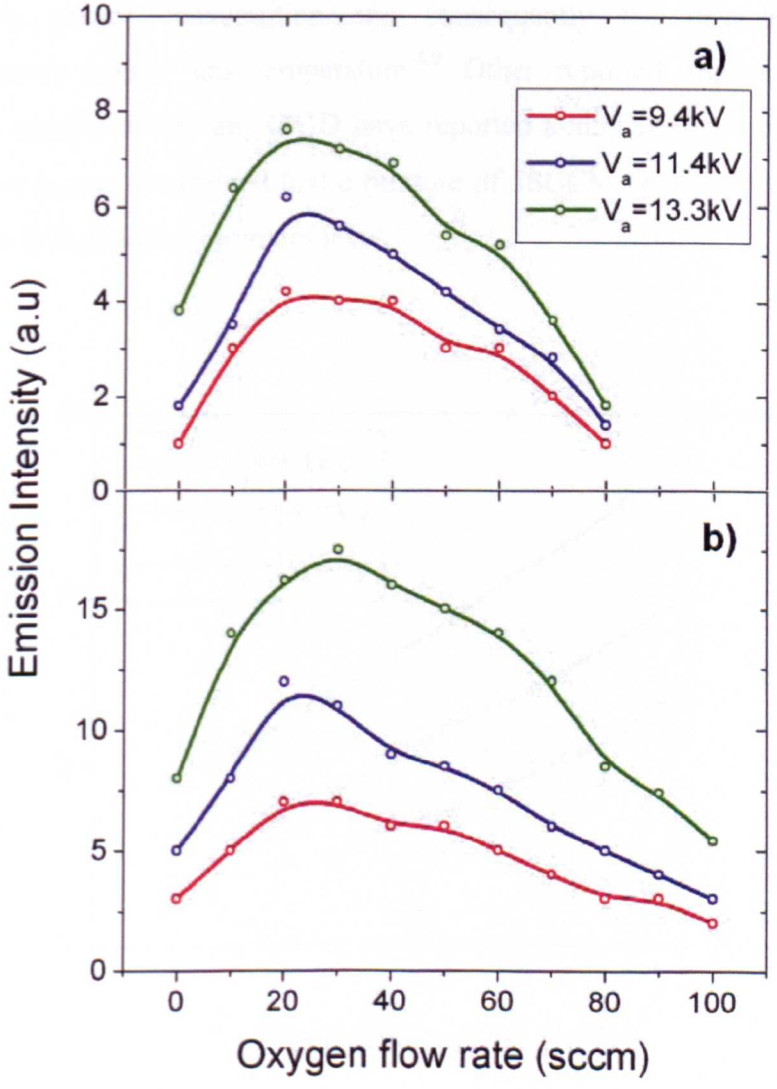

Fig 4-18: Impact of adding small amounts of O_2 on the emission intensity of a)777nm and b)845nm.

The results shown in figure 4-18 are consistent with expectation, oxygen is highly electronegative and has a very strong quenching effect on the discharge.[4.19] As oxygen is added to the background argon flow the breakdown voltage of the gas increases substantially.[4.19] As the pulse amplitude is fixed, increasing oxygen content effectively shifts the gas voltage down toward the breakdown voltage, resulting in a reduction in the optical emission intensity. Figure 4-18 highlights the dangers of mixing too much reactive gas in to the inert base gas. For example, a 9.4kV pulse with 20SCCM of Oxygen added produces a higher flux of reactive oxygen species compared to a 13.3kV with 100SLM of oxygen added. It is likely that the addition of too much O_2 increases power consumption and consequently the discharge has a significantly higher gas temperature.[4.9] Other reported studies observing oxygen species within an APGD have reported a similar trend, through trial and error it was determined that a mixture of 5SCCM O_2 for every 1SLM of inert gas is around the optimum level.

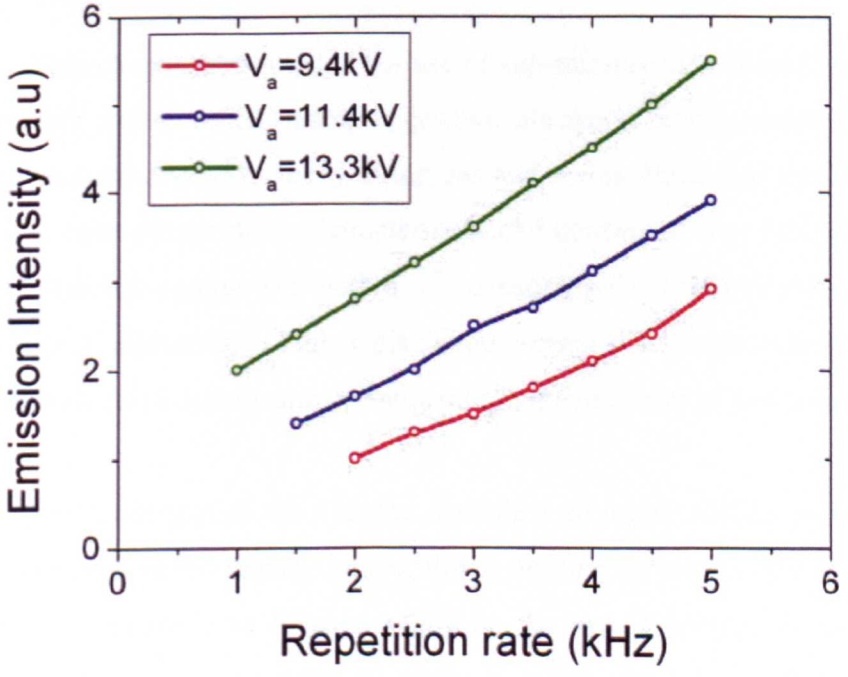

Fig 4-19: Repetition frequency effects on the emission intensity of excited atomic oxygen @ 777nm.

A simple and effective way to increase the flux of reactive species within a discharge is to increase the repetition rate of the applied voltage pulses. Figure 4-19 highlights the effect of repetition frequency on the emission of atomic oxygen at 777nm. Obviously, as the repetition rate increases more discharge events occur in a given time resulting in a linear increase of measured intensity. It is worth noting that the emission intensity of a single applied pulse is relatively independent of the repetition frequency.

It should also be pointed out that at low repetition rates, <1 kHz, it is very difficult to produce and sustain a stable discharge. At lower applied voltages the repetition rate needs to be increased substantially to initiate gas breakdown. This suggests that there is some kind of frequency dependence or threshold within the system, most likely due to the storage of charge on dielectric surfaces after each applied voltage pulse which accumulates to enhance the local electric field.

4.6 Summary

This chapter has detailed the use of sub-microsecond pulsed excitation to generate stable APGD using a jet-like electrode configuration. Initially helium was considered as the working gas and it was found that the discharge exhibited room-temperature characteristics and consumed very little electrical energy. A direct comparison with a microsecond pulsed jet was not possible, however the substantially higher discharge current is a rough indicator of an increased electron density and consequently a greater level of gas ionisation.

The latter part of the Chapter described an argon APGD jet sustained with sub-microsecond voltage pulses, this is the first reported study of its type, as previous studies have focused solely on the use of helium. A shift away from helium to more economical gases is highly desirable if APGD is to become a viable large scale processing technology, hence research in to argon APGD is of significant importance.

Sub-microsecond voltage pulses with amplitudes of 8-15kV were applied at repetition rates of 1-5 kHz and shown to generate a stable argon APGD. Using OES it was demonstrated that pulsed excitation of an argon APGD significantly reduces the gas temperature and consequently reduces the threat of thermal runaway. The discharge proved to be stable over a wide range of operating parameters. It was shown through optical emission data that the argon APGD jet plume is dominated by argon emission lines, this is in stark contrast to that of a helium APGD jet which is dominated by nitrogen lines. Nanosecond images were also used to highlight a difference in the way the discharge evolves. A pulsed argon APGD jet has a continuous plume unlike that observed in helium jets where the plume is in the form of discrete plasma bullets. It was shown that upon the application of an applied voltage pulse with a 10 – 20 ns rising phase, a pre-ionization phase was triggered and its subsequent development was necessary to elevate the local electrical field above the threshold for gas breakdown. Discharge currents of several amperes were reached and the plasma-enclosing dielectric tube acted as a switch to produce a short current pulse. The switching effect of a dielectric is common in all DBD's however the magnitude of the generated currents were significantly larger than those observed in conventionally excited DBD, this suggests a greater electron density may be achieved.

References

[4.1] Lu X P, Laroussi M 'Optimization of ultraviolet emission and chemical species generation from a pulsed dielectric barrier discharge at atmospheric pressure' Journal of Applied Physics, Vol.98, Iss.2, No.023301, 2005.

[4.2] Lu X.P, Laroussi M, 'Temporal and spatial emission behaviour of homogeneous dielectric barrier discharge driven by unipolar sub-microsecond square pulses' Journal Of Physics D-Applied Physics, Vol.39, Iss.6, pp.1127-1131, 2006.

[4.3] Walsh J.L, Shi J.J, Kong M.G, 'Submicrosecond pulsed atmospheric glow discharges sustained without dielectric barriers at kilohertz frequencies' AppliedPhysics Letters, Vol.89, Iss.16, No.161505, 2006.

[4.4] Walsh J.L, Kong M.G, 'Sharp bursts of high-flux reactive species in submicrosecond atmospheric pressure glow discharges' Applied Physics Letters, Vol.89, Iss.23, No.231503, 2006.

[4.5] Walsh J.L, Kong M.G, '10 ns pulsed atmospheric air plasma for uniform treatment of polymeric surfaces', Applied Physics Letters, Vol.91, Iss.25, No.251504, 2007.

[4.6] Walsh J.L, Kong M.G, 'Room-temperature atmospheric argon plasma jet sustained with submicrosecond high-voltage pulses', Applied Physics Letters, Vol.91, Iss.22, No.221502, 2007.

[4.7] Walsh J.L, Shi J.J, Kong M.G, 'Contrasting characteristics of pulsed and sinusoidal cold atmospheric plasma jets' Applied Physics Letters, Vol.88, Iss.17, No.171501, 2006.

[4.8] Gherardi N, Massines F 'Mechanisms controlling the transition from glow silent discharge to streamer discharge in nitrogen' IEEE Transactions On Plasma Science, Vol.29, Iss.3, pp.536-544, 2001.

[4.9] Wang S, Schulz-von der Gathen V, Dobele H.F, 'Discharge comparison of nonequilibrium atmospheric pressure Ar/O-2 and He/O-2 plasma jets Applied PhysicsLetters, Vol.83, Iss.16, pp.3272-3274, 2003.

[4.10] Kong M.G, Deng X.T, 'Electrically efficient production of a diffuse nonthermal atmospheric plasma' IEEE Transactions On Plasma Science, Vol.31, Iss.1, pp.7-18, Part 1, 2003.

[4.11] Laroussi M, Lu X, 'Room-temperature atmospheric pressure plasma plume for biomedical applications' Applied Physics Letters, Vol.87, Iss.11, No.113902, 2005.

[4.12] Stoffels E, '"Tissue processing" with atmospheric plasmas' Contributions To Plasma Physics,Vol.47, Iss.1-2, pp.40-48, 2007.

[4.13] Nersisyan G, Graham W.G, 'Characterization of a dielectric barrier discharge operating in an open reactor with flowing helium' Plasma Sources Science & Technology, Vol.13, Iss.4, pp.582-587, 2004.

[4.14] Lisovskiy V, Booth J.P, Landry K, Douai D, Cassagne V, Yegorenkov V 'Electron drift velocity in argon, nitrogen, hydrogen, oxygen and ammonia in strong electric fields determined from rf breakdown curves' Journal Of Physics D-Applied Physics, Vol.39, Iss.4, pp.660-665, 2006.

[4.15] Chen G.L, Chen S.H, Zhou M.Y, Feng W.R, Gu W..C, Yang SZ, 'The preliminary discharging characterization of a novel APGD plume and its application in organic contaminant degradation' Plasma Sources Science & Tecnology,Vol.15, Iss.4, pp.603-608, 2006.

[4.16] Goch M, Jasinski M, Zakrzewski Z, Mizeraczyk J, 'New microwave source of microdischarges in noble gases at atmospheric pressure' Czechoslovak Journal Of Physics, Vol.56, pp.B795-B802, Part 4, Suppl. B, 2006.

[4.17] Ray P.P, Chaudhuri P, 'Optical emission spectroscopy used to study the characteristics of the capacitive radio-frequency, discharge in argon' Czechoslovak Journal Of physics, Vol.53, Iss.3, pp.229-234, 2003.

[4.18] Deng X.T, Shi J.J, Shama G, Kong M.G, 'Effects of microbial loading and sporulation temperature on atmospheric plasma inactivation of Bacillus subtilis spores' Applied Physics Letters,Vol.87, Iss.15, No.153901, 2005.

[4.19] Leveille V, Coulombe S, 'Design and preliminary characterization of a miniature pulsed RF APGD torch with downstream injection of the source of reactive species' Plasma Sources Science & Technology,Vol.14, Iss.3, pp.467-476, 2005.

5 Plasma jet propagation mechanisms

5.1 Introduction

Plasma jets operated at atmospheric pressure are being used in an increasing number of applications, especially in the areas of biological decontamination and materials processing.[5.1,5.2] The unique configuration of the plasma jet allows plasma to be generated in a region of high stability and be transported in to a region of high chemical reactivity. This ability gives a significant advantage over conventional parallel plate plasma reactors where the sample being treated is placed between the two electrodes which often has the detrimental effect of disturbing the stability of the plasma.

Many studies have been reported on atmospheric pressure plasma jets. Some focus upon the excitation method used, such as DC,[5.3] kHz sinusoidal,[5.4] kHz pulsed,[5.5] or radio frequency.[5.6] Other studies focus upon the applications made possible using a plasma jet, in such studies the plasma jet itself is often considered as a tool and the emphasis is placed upon the application. Very few studies have investigated the transport mechanism within the plasma jet that makes it possible for plasma to be generated in one region and then moved to another. The few studies reported so far focus upon the kilohertz range of excitation frequencies and report that the plasma plume is not a continuous discharge as it appears to the naked eye, but consists of discreet packets of plasma ejected at a rate equal to that of the excitation frequency.[5.7,5.8,5.9] The phenomena has been termed plasma bullets and was mentioned briefly in Chapters 3 and 4; very little is understood as to the exact nature of the plasma bullet and what its underpinning physical mechanisms are.

This Chapter aims to investigate various features of the plasma plume produced in a kHz excited plasma jet in an attempt to build upon the limited body of knowledge currently available. Section 5.2 describes the configuration of the plasma jet used, both a single wrapped electrode configuration and pin like electrode configuration have been employed to allow for a simplified analysis. In section 5.3 the various modes of operation are discussed, it's shown that the plasma jet can be operated in one of three modes; it is determined that the plasma bullet mode is the most suited to many applications. Section 5.4 details the plasma bullet propagation mechanism including experimental observations to give the reader an insight into the physical properties of the plasma bullet phenomena. Finally, section 5.5 highlights several interesting observations made of the plasma bullet which remain inexplicable.

5.2 Experimental Setup

In order to fully investigate the propagation mechanism of the plasma jet it is necessary to employ both pulsed and sinusoidal excitation sources. As discussed in the previous chapters, the vast majority of reported studies have focused exclusively upon sinusoidal excitation sources as a means of generating a plasma plume. A considerable disadvantage of sinusoidal excitation is its continuous wave nature, there is no voltage off period, just a zero crossing point, this complicates the analysis of the plasma plume. The long off time associated with pulsed excitation allows each pulse to be treated as an isolated event, unaffected by the preceding pulse; this simplifies the analysis of the plasma plume. The pulse generator used in this investigation was based upon a MOSFET push-pull topology discussed in Chapter 2, and was capable of delivering voltage pulses up to 15kV in magnitude, with pulse widths down to 150ns at repetition rates up to 5kHz. A simple sinusoidal source was constructed which employed a low voltage DC-AC converter and a high voltage transformer. The sinusoidal source was capable of delivering a 3-10kHz sinusoid up to 30kVp-p in magnitude.

The configuration of the plasma jet used is similar to that discussed in previous chapters, consisting of a single metallic electrode wrapped around a dielectric tube through which helium flows. The ground electrode consisted of a polished metallic disc and a removable ceramic dielectric sheet, typically the ground electrode was placed at some distance, 1 to 2 cm, downstream from the plasma jet. While this configuration works well, and is simple to construct it is not ideal for a detailed analysis of the plasma jet. A simplified construction was devised employing a pin like electrode inserted within a dielectric tube, typically made of quartz glass. Figure 5-1 shows a schematic of the revised plasma jet configuration. The central electrode is a sharpened tungsten welding rod with a diameter of 2mm. The tip of the rod is fixed 2cm above the ground electrode which can be dielectrically coated (using a ceramic tile) or bare metallic.

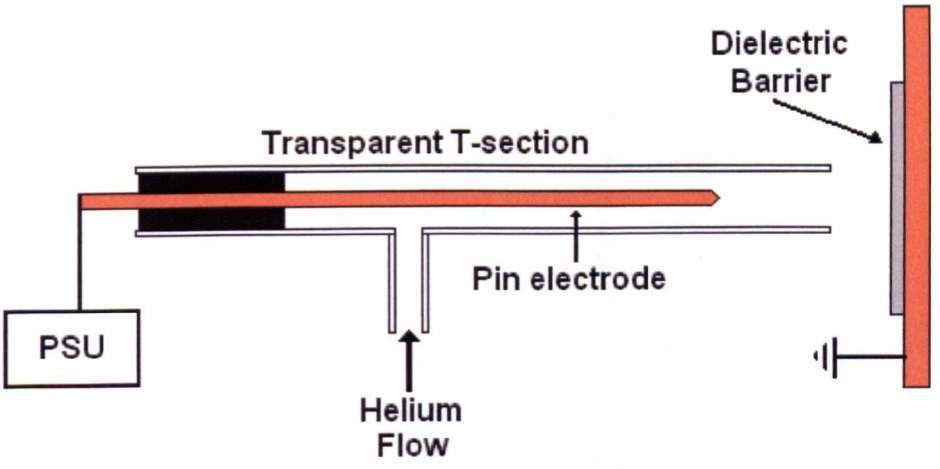

Fig 5-1: Schematic of simplified plasma jet configuration

The revised configuration allows the evolution of the plasma plume to be viewed inside and outside of the jet structure; this is a significant improvement over the conventional configuration where the electrode is on the outside of a ceramic tube. A further benefit of the simplified configuration is that the discharge always ignites from the same point, the tip of the centre rod, thus allowing the iCCD camera to be focused accordingly. A drawback of the simplified configuration is that it is not an exact representation of the configuration used in previous Chapters; fortunately the propagation

mechanism is almost certainly the same regardless of the electrode configuration.

All electrical measurements were made using a Tektronix TDS 5054B oscilloscope with a 500MHz bandwidth. A Tektronix P6015A voltage probe, rated at 40kV DC, was used to measure the applied voltage. A Pearson 2877 current monitor, with a 200MHz bandwidth was used to measure the current between the power source and the powered electrode. It was often necessary to employ multiple turns through the current probe to amplify the signal to a measurable level. Typically, the currents associated with a plasma jet are only on the order of tens of milliamps, the Pearson 2877 outputs 1V per Amp, hence 1 milliamp equates to 1 millivolt, such a low value is hard to distinguish due to the electrical interference produced by the high frequency power source. Optical measurements were performed using an Andor iStar iCCD camera capable of exposure times less than 2ns and a triggering precision of 200ps.

5.3 The three modes of the plasma jet

Despite the large number of previously reported studies employing a plasma jet configuration there appears to have been little investigation into its various modes of operation.[5.2] The different modes within the plasma jet were first encountered whilst conducting biological decontamination experiments using a simple 30kHz sinusoidal DBD plasma jet; as the applied voltage was gradually increased an abrupt change in plasma intensity was observed which led to a significant rise in gas temperature. Unfortunately, a sharp rise in gas temperature leads to thermal destruction of the biological media under test thus masking the true effects of the plasma chemistry. For atmospheric pressure plasma jets to be of real benefit in biological applications near room temperature operation is highly desirable, therefore an ability to control the plasma jet and a clear understanding of its modes of operation are essential.

Figure 5-2 shows two images taken of a typical, wrapped electrode, APGD helium jet using a 1/60s exposure setting, the plasma plume shown in figure 5-2a is clearly much less intense than the plume shown in figure 5-2b. The jump in intensity occurs abruptly at a given voltage which is dependant on the distance between the powered and ground electrodes.

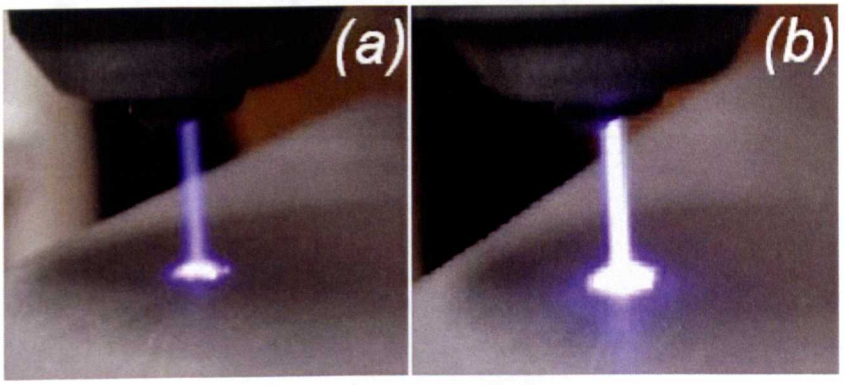

Fig 5-2: Digital images of a helium plasma jet operating in different modes.

Figures 5-3 and 5-4 show the current and voltage waveforms relating to the images shown in figures 5-2a and 5-2b respectively. In figure 5-3 the applied voltage is 8kVp-p, there are two distinctive current pulses per half cycle, whilst this current pattern is unusual it has been observed in previous studies,[5.5] each current pulse relates to a distinct discharge event. In figure 5-4 the applied voltage is 8.3kVp-p, less than 4% higher than the applied voltage shown in figure 5-3, yet the peak current has increased 100%, jumping from 35mA to 70mA.

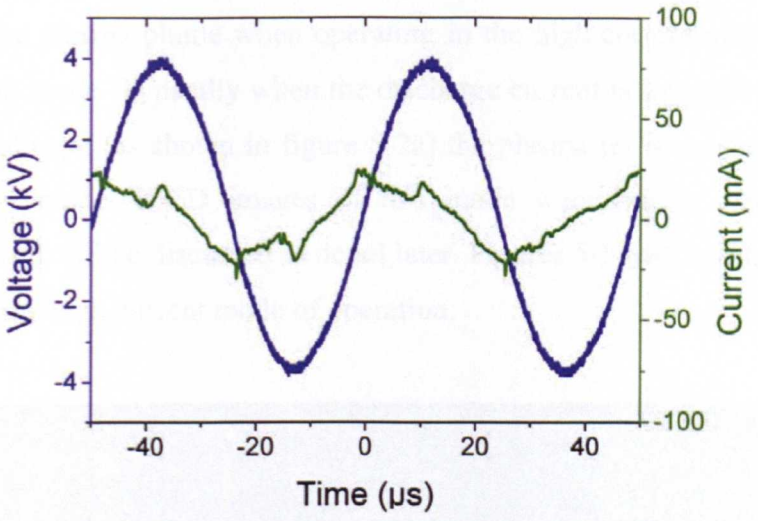

Fig 5-3: Current and voltage waveforms of the plasma jet shown in figure 5-2a.

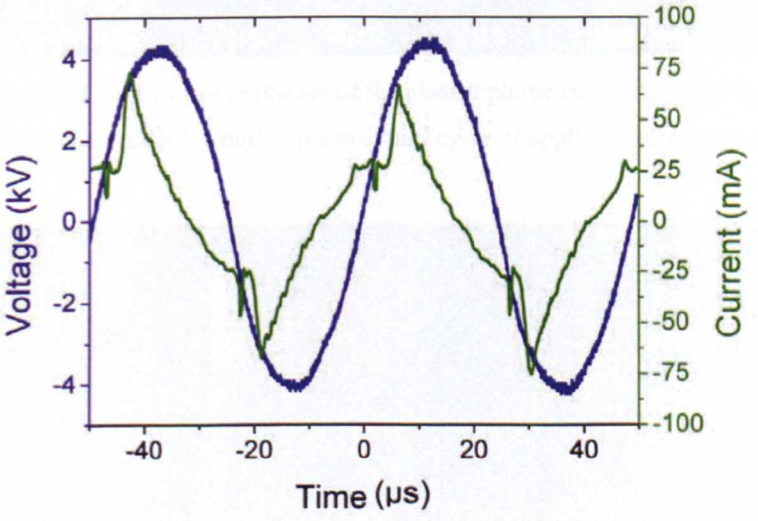

Fig 5-4: Current and voltage waveforms of the plasma jet shown in figure 5-2b.

The shape of the current pulse shown in figure 5-4 differs to that observed in figure 5-3. The two small current pulses have become a single large current pulse repeated every half cycle. This pattern is far more representative of a conventional dielectric barrier discharge,[5.10] where the gas voltage is rapidly reduced following each discharge through the accumulation of space charge on dielectric surfaces. A sharp rise in the measured current which corresponds to a small change in the applied voltage and a change in the current waveform are both highly indicative of a change in the operating mode

of the plasma. To further investigate the mode transition iCCD images were taken of the plasma plume when operating in the high-current mode and the low-current mode. Typically when the discharge current is low and the plume looks translucent (as shown in figure 5-2a) the plasma jet is operating in the low-current mode, iCCD images of this mode were briefly discussed in chapter 3 and will be discussed in detail later. Figures 5-5 and 5-6 show iCCD images of the high current mode of operation.

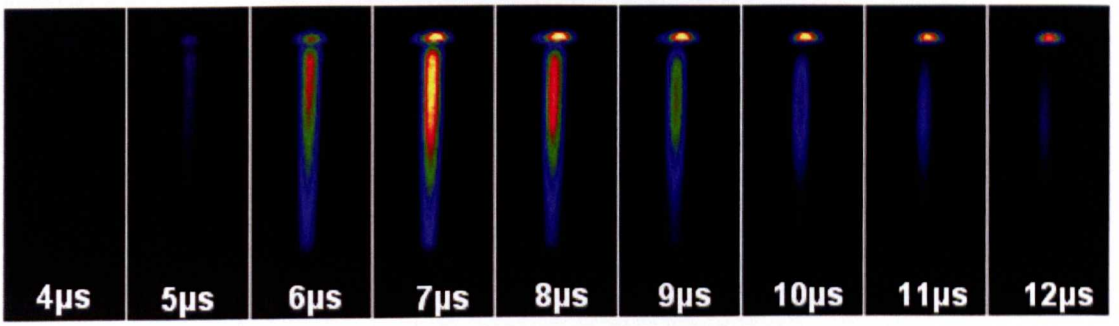

Fig 5-5: Normalised 20ns exposure images of the plasma plume operating in the high-current mode. Images recorded during positive half cycle of applied voltage (see figure 5-4)

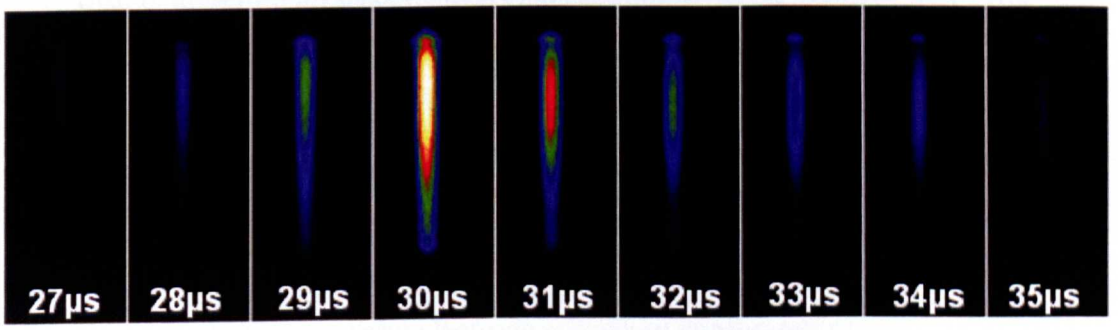

Fig 5-6: Normalised 20ns exposure images of the plasma plume operating in the high-current mode. Images recorded during negative half cycle of applied voltage (see figure 5-4)

In figures 5-5 and 5-6 the top of each image is a grounded metallic disc and the bottom of the image is the exit of the ceramic tube upon which the powered electrode is mounted. The images are normalised such that the intensity of each image is comparable to all the others in the sequence, but the gain is reduced by a factor of two between figures 5-5 and 5-6, as such the intensities are not directly comparable. The iCCD camera was triggered using the applied voltage waveform and as such the time displayed in each image

directly relates to the waveforms shown in figure 5-4. The images taken from 4μs to 12μs cover the plasma produced in the positive half cycle of the applied voltage, during which the grounded metal disc is less positive than the powered electrode hence can be considered the instantaneous cathode. The plasma plume appears within the gap as the applied voltage increases, it doesn't seem to ignite at one electrode and travel to the other electrode like in the low current, plasma bullet mode, shown in section 3.4.5. During the positive half cycle a distinctive bright region can be seen just above the cathode, this is likely to be a cathode glow region formed due to the presence of a sheath region in which electrons are rapidly accelerated. Such structures have been widely reported in DC,[5.11] kHz,[5.12] pulsed,[5.13] and RF APGD.[5.14]

The images in figure 5-6 were taken between 27μs to 35 μs and show the plasma produced during the negative half cycle of the applied voltage. During this period the powered electrode is more negative than the grounded disc and as such can be considered the instantaneous cathode, the grounded disc is therefore an instantaneous anode. Similar to the positive half cycle, the discharge forms within the electrode gap, however the distinctive cathode glow region is no longer visible. As the cathode glow region always forms directly above the cathode it is likely produced above the powered electrode and is consequently hidden by the ceramic tube. Figure 5-7 shows a diagram highlighting the differences between the positive and negative half cycles in the conventional wrapped electrode APGD jet configuration.

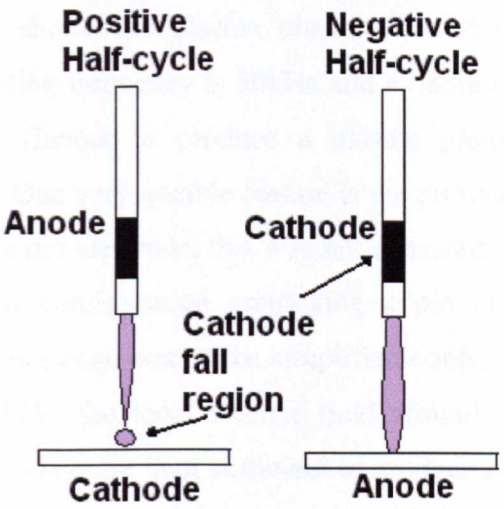

Fig 5-7: Diagram showing differences between positive and negative half-cycles in a conventional wrapped electrode plasma jet configuration.

To further enhance the understanding of the transition from a low-current mode that exhibits *'bullet'* like characteristics to a high-current mode exhibiting *'continuous'* characteristics the simplified plasma jet configuration was adopted. Initial test confirmed that the two modes of operation were both clearly identifiable when using the simplified configuration. Figure 5-8 shows digital images taken at different applied voltages with a fixed operating frequency and electrode separation.

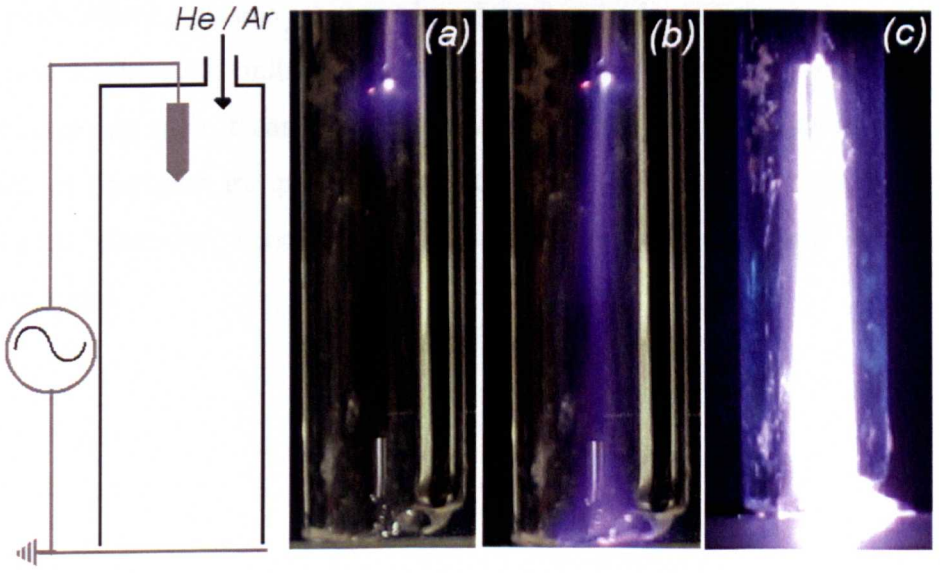

Fig 5-8: Digital images showing the plasma plume with applied voltages of (a)7.5kVp-p (b)8kVp-p (c) 8.5kVp-p

Figure 5-8a shows the plasma plume when the applied voltage is 7.5kVp-p, the operating frequency is 30kHz and a helium flow rate of 5SLM, this voltage is insufficient to produce a plasma plume that reaches the grounded electrode. One very notable feature is the presence of a small corona discharge around the pin electrode, this was not expected and is only observed using the simplified configuration employing a pin electrode. Figure 5-9 shows an electrostatic simulation of the simplified configuration at an applied DC voltage of 3.75kV, the local electric field around the pin electrode is almost 1.6MV/m, this is more than sufficient to produce a corona discharge in helium. It should be noted that the dimensions of the simulated configuration are close to those used in the experimental configuration however the sharpness of the tip is hard to quantify, consequently the simulated electric field may be slightly over estimated.

Electrostatic simulations of the conventional plasma jet configuration, shown in the previous chapter (figure 4-12), also indicate the presence of a very high local electric field around the powered electrode edges. In both configurations, it is likely that at low applied voltages some corona is formed around any sharp edges; the resultant free electrons produced are likely to play an important role in the plume propagation mechanism. It is expected that in all cases where a plasma jet is employed, be it pulsed or sinusoidally excited, a corona discharge is initially produced and acts as a starting point for the discharge, as such it can be considered the first mode of operation. In this mode of operation the plasma plume does not propagate very far from the powered electrode hence it is unlikely to be of much use for many applications.

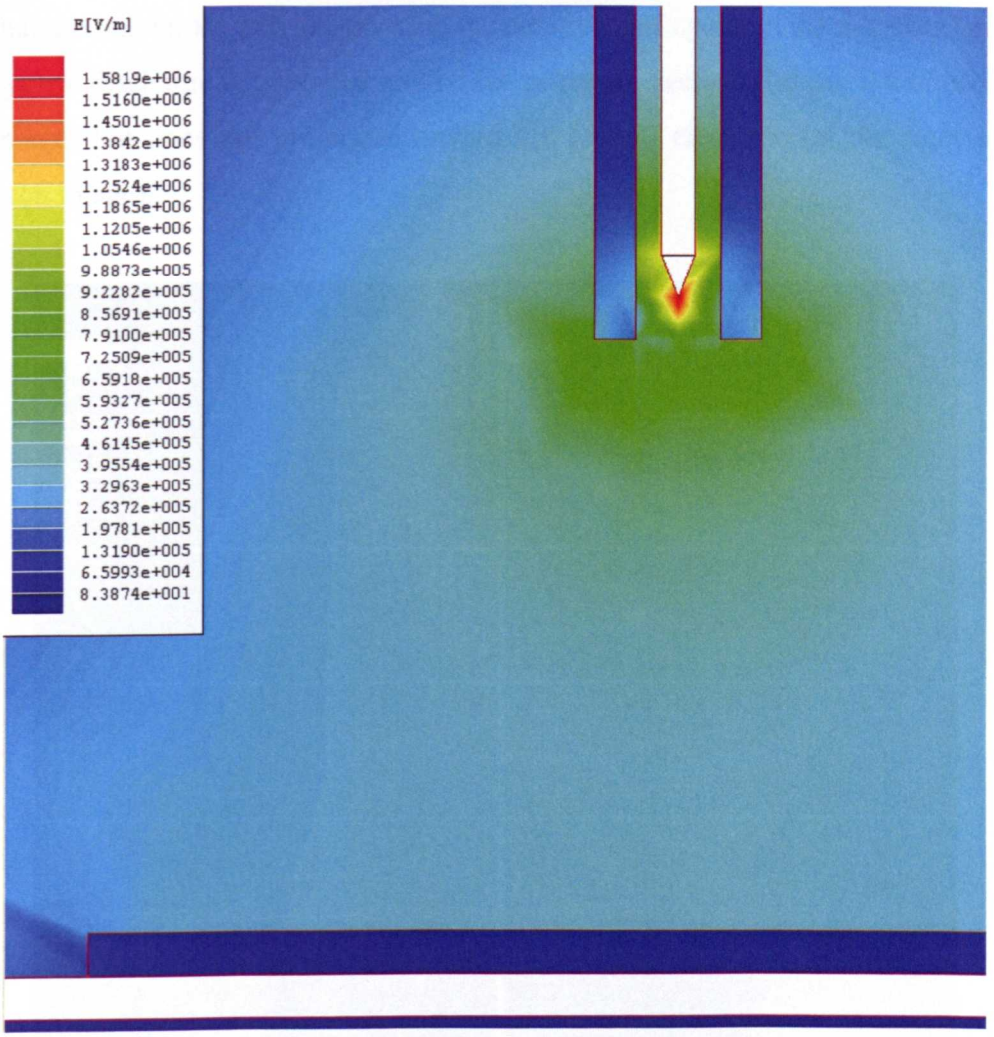

Fig 5-9: Electrostatic simulation of simplified jet configuration with an applied voltage of 3.75kV. Rod diameter 2mm, suspended 4cm from ceramic tile on ground plate,

As the applied voltage is increased from 7.5kVp-p to 8kVp-p the corona mode abruptly transitions in to the plasma 'bullet' mode which extends to reach the ground electrode, shown in figure 5-8b. As discussed previously, in this mode the plume appears as bullet like balls of plasma being ejected from the powered electrode and travel toward the grounded electrode. Figure 5-10 shows 10ns exposure iCCD images taken of the plasma plume while operating in the plasma bullet mode. In Figure 5-10a, argon is used as the working gas and in 5-10b helium is used. The images are notable as plasma bullets have not been previously reported in gases other than helium, this has led some to believe that the plasma bullet effect may be partly attributed to helium metastable accumulation, this is obviously not the case. Also notable is

that the bullets are only observed in the positive half cycle, in the negative half cycle a discharge is produced around the powered electrode (at the left of each image) but does not propagate toward the ground electrode (at the right of each image).

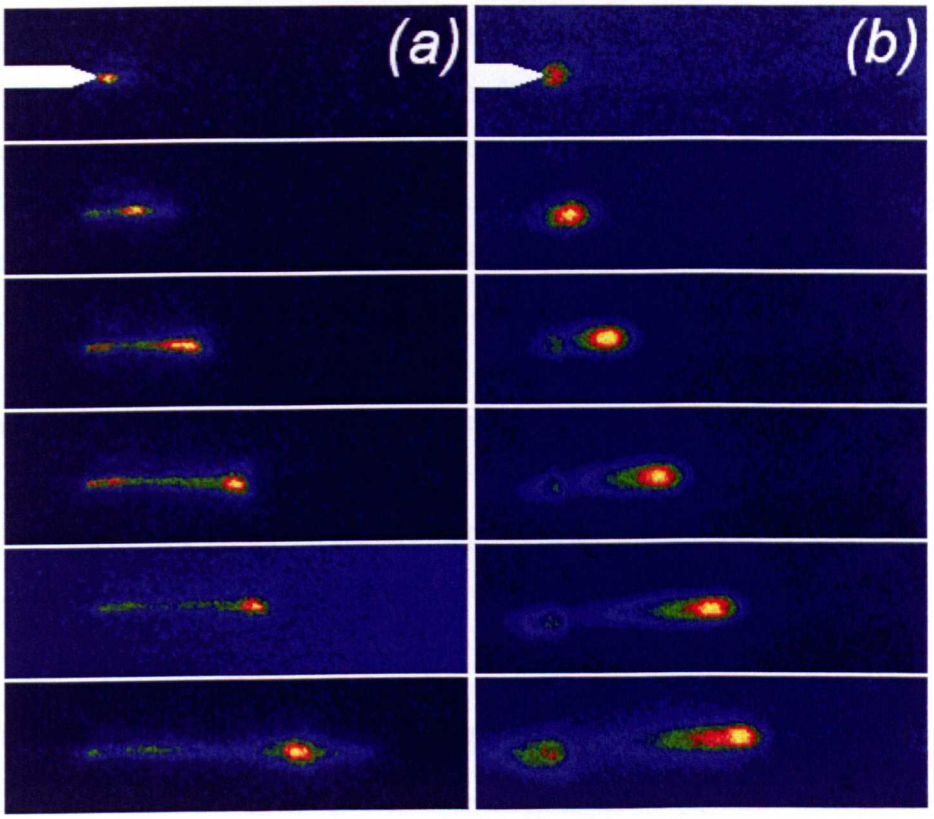

Fig 5-10: 10ns exposure iCCD images of the plasma plume taken every 500ns in (a) argon and (b) helium. Powered electrode drawn in white on first image of each sequence.

From figure 5-10 it is clear to see that initially a small corona like discharge forms around the powered electrode, after 500-1000ns the voltage has increased such that the discharge begins to propagate away from the electrode, this confirms that the first mode of operation is indeed the production of a small area corona discharge. The images were all taken during the rising portion of the positive half cycle, as such the voltage in each image is higher than in the preceding image. Due to the increasing voltage the corona grows in size and intensity. In the helium case the discharge begins to move toward the ground electrode at approximately 3.9kV, this value is slightly higher in argon. The point at which the corona discharge begins to propagate

away from the powered electrode is discussed in greater detail within the next section.

In summary, this section has highlighted the presence of three distinctive modes of operation within the plasma jet. Initially as the applied voltage is increased a corona like discharge forms around the sharp edges of the powered electrode. As the applied voltage is further increased the discharge begins to propagate away from the powered electrode and forms a bullet-like plasma ball. It is the bullet mode of operation that is of most interest for many applications as the plasma produced is highly reactive yet maintains a low temperature. Finally, at high applied voltages the discharge becomes continuous, plasma fills the entire region between powered and grounded electrodes. During this mode of operation the discharge current is high and gas temperature is well above ambient room temperature; this mode is less useful for low-temperature applications however other applications, such as materials processing, could benefit from the elevated temperatures.

5.4 Physical properties of the plasma plume

As discussed in the previous section, it is the plasma bullet mode of operation that is often considered to be the most useful for low-temperature applications; accordingly the means by which the plasma propagates is investigated further within this section. The first observations of plasma bullets in a kHz excited DBD helium plasma jet were reported by Teschke *et al.* in 2005.[5.7] An iCCD camera was used to image the plasma bullet at microsecond intervals with a 100ns exposure time, the velocity of the plasma bullet was calculated to be 15km/s, several orders of magnitude above the gas velocity of 16.5m/s. No explanation as to the origin of the plasma bullet was proposed however it was stated that the bullet phenomena was only observed during the positive half cycle of the excitation voltage, this finding is similar to the results presented in the previous section. Figure 5-11a shows current and voltage waveforms forms of a pulsed helium APGD jet. Figure 5-11b shows 18 single shot iCCD images of the plasma plume generated using the pulsed

waveform shown in figure 5-11a propagating into ambient air obtained at a 3kHz repetition rate. Each image was taken with a 10ns exposure time at 50ns intervals starting at the point the bullet exits the dielectric tube.

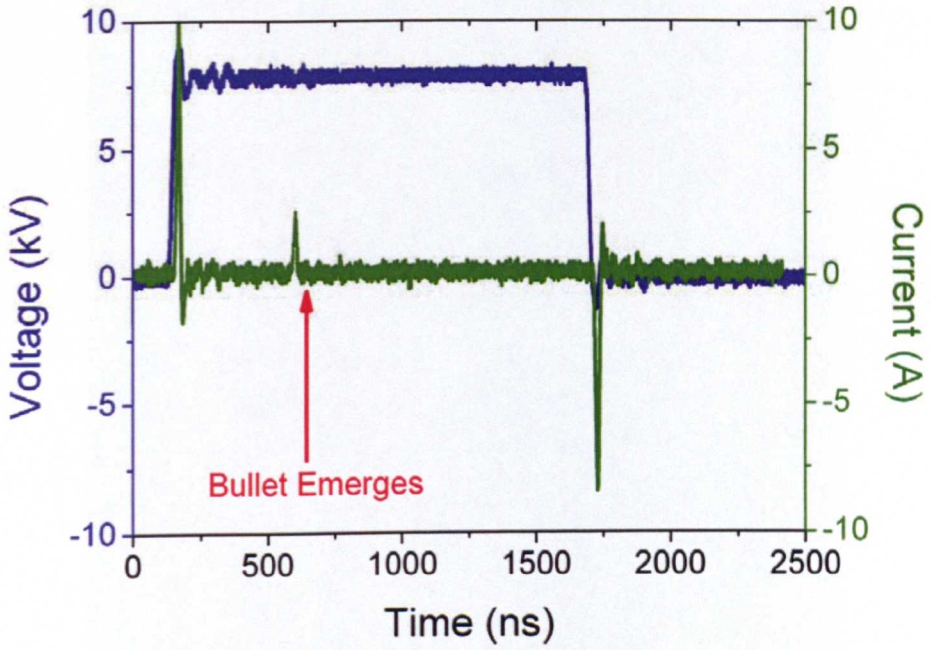

Fig 5-11a: Current and voltage waveforms of pulsed helium APGD jet.

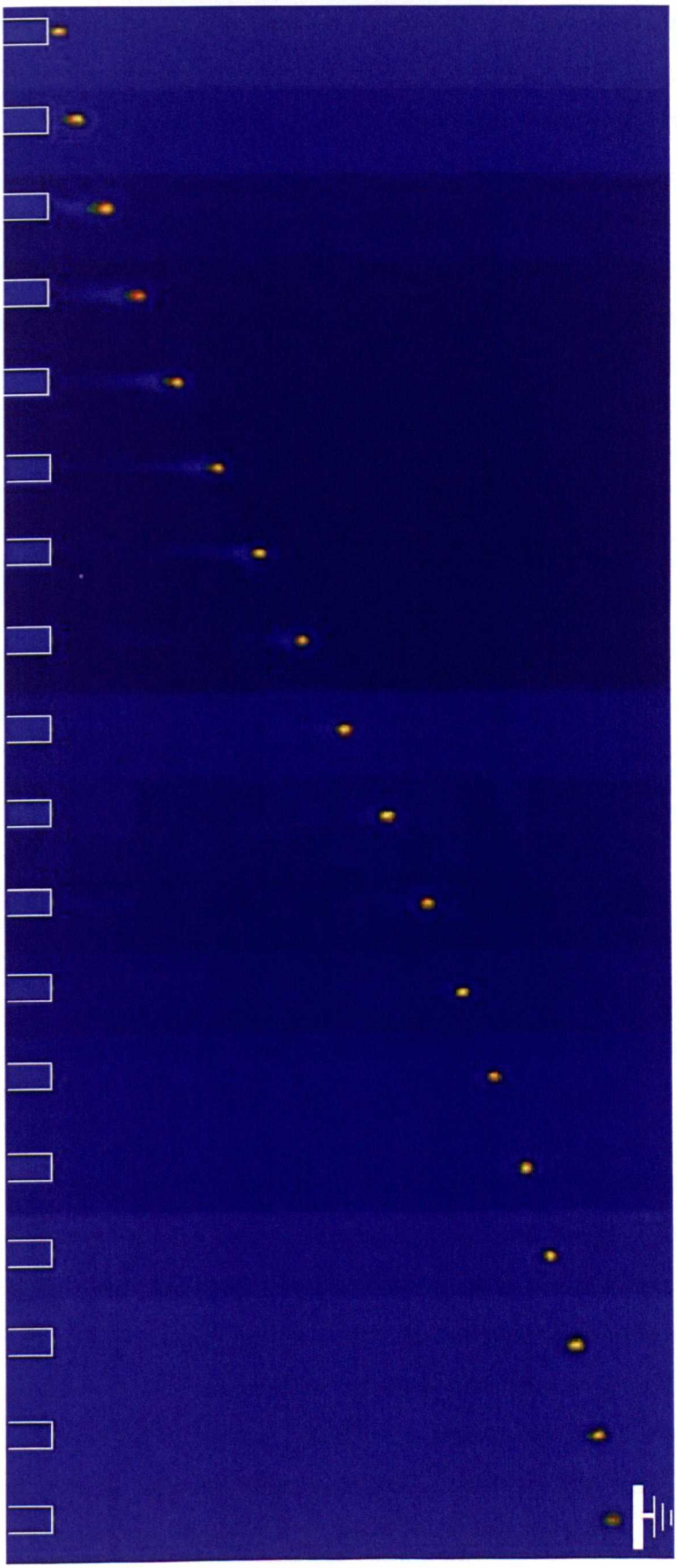

Fig 5-11b: 10ns exposure iCCD images of the plasma plume taken every 50ns.

From Figure 5-11b it is clear to see that the plasma bullet takes a very similar form to that presented in other studies, consisting of a high intensity tip which propagates away from the powered electrode, there is no visible link between the tip and the powered electrode.[5.7,5.9] From the images it is possible to see that the velocity profile is non-uniform, the bullet accelerates rapidly at first and then slows until its intensity drops below the minimal observable level. Figure 5-12 shows the velocity and intensity of the plasma bullet as it propagates.

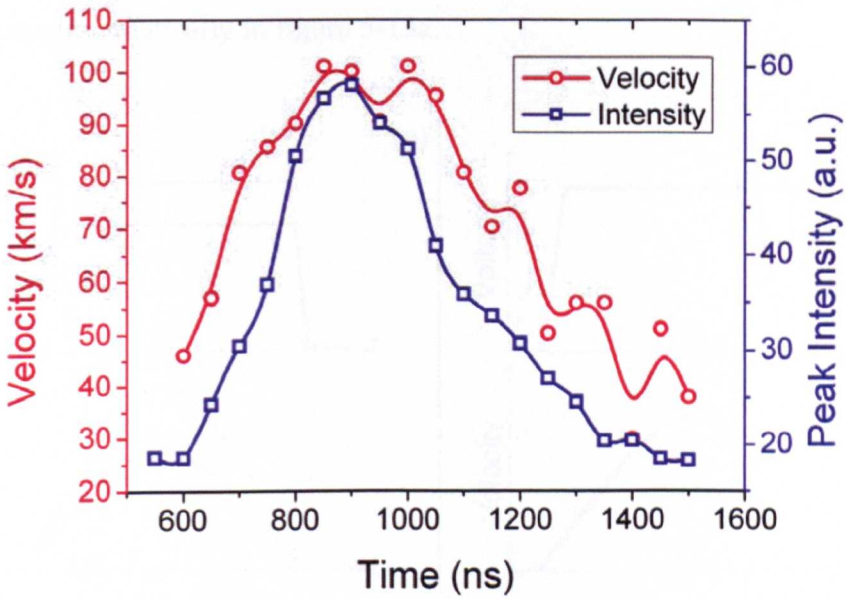

Fig 5-12: Velocity and intensity profile of a plasma bullet generated with 8kV, 2μs voltage pulse.

The velocity is determined from the iCCD images by calculating how far the bullet centre moves from one image to the next image. The intensity was determined from the peak photon count in each iCCD image, typically this was at the centre of the plasma bullet. An interesting point to note is the differences in the velocity reported in this study and those in previous studies, Teschke *et al.* reported an average bullet propagation velocity of 15km/s, Lu *et al.* reported a peak velocity of almost 160km/s.[5.8] In this study the peak velocity is calculated to be around 100km/s, very similar to that presented by Lu *et al.* a likely explanation for the differences observed is due to the type of

excitation used. Both this study and that of Lu *et al.* employed fast rising pulsed excitation whereas Teschke *et al.* used a more conventional sinusoidal source. Experiments using the same configuration but employing sinusoidal excitation showed that bullet velocity to be significantly reduced even though the peak applied voltage was held constant; the reason for this remains illusive. Another point worth noting is the effect of the applied voltage magnitude, higher applied voltages produce faster plasma bullets compared to lower applied voltages; this translates into a longer plume length as the time the bullet propagates seems to remain fixed for a fixed pulse width. This is shown diagrammatically in figure 5-13a.

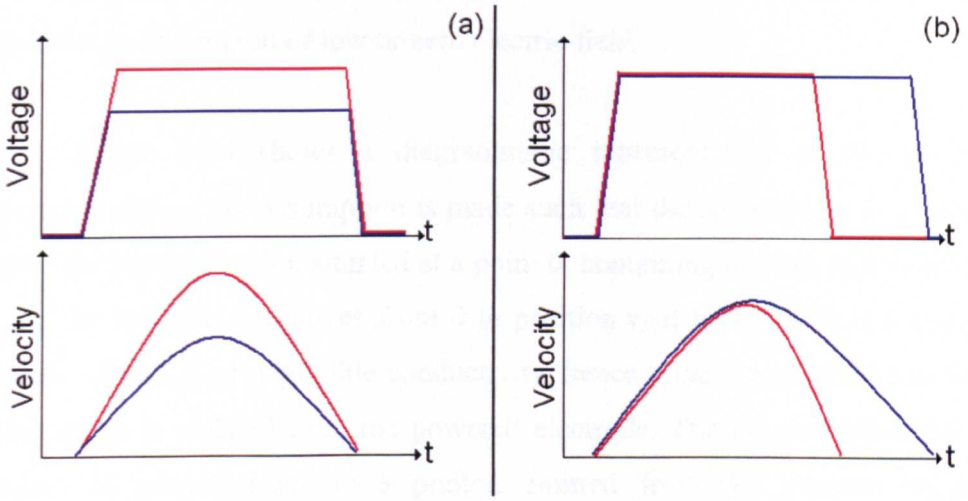

Fig 5-13: Diagram showing effects of changing (a) applied voltage & (b) pulse width on plasma bullet velocity

Figure 5-13b shows another interesting property of the plasma plume observed when pulsed excitation is employed; at a fixed applied voltage the propagation time of the plasma bullet is directly proportional to the voltage pulse width. The plasma bullet propagation is rapidly terminated as the applied voltage reduces, this has not been reported previously, and will be re-examined in the following sections.

5.4.1 Dawson's theory of suppressed corona streamers

Lu *et al.* suggested a possible mechanism for the propagation of the plasma plume based on a theory first proposed by Dawson and Winn in 1965.[5.15] Dawson investigated the effect of positive voltage pulses applied to a pin like electrode in ambient Air. It was found that at voltages near the theoretical breakdown voltage of a large air gap, a streamer would form at the anode and propagate toward the cathode. Using a photomultiplier tube it was determined that the streamer travelled for some time after the applied voltage had been removed, this indicated that propagation could continue in a zero electric field situation. A theory was proposed based on photo-ionisation that was capable of explaining the propagation of a streamer at extremely high velocities in to a region of low or zero electric field.

Figure 5-14 shows a diagrammatic representation of the photo-ionisation theory. An assumption is made such that the streamer tip is a small positively charged region situated at a point 0, containing n^+ ions, and a radius r_0. As the streamer tip moves from 0 to position r_2 it leaves behind a quasi-neutral tail that is of negligible conductivity, hence it can be assumed that the streamer tip is isolated from the powered electrode. The tip propagates by a process of photo-ionisation; a photon emitted from the positive region produces a free electron at a distance, r_1, away from the centre of the positive region. The negatively charged electron is accelerated toward the positive region due to the high localised electric field, at atmospheric pressure the collisional frequency between electrons and gas molecules is extremely high, consequently the free electron rapidly collides with a gas molecule and initiates an electron avalanche.

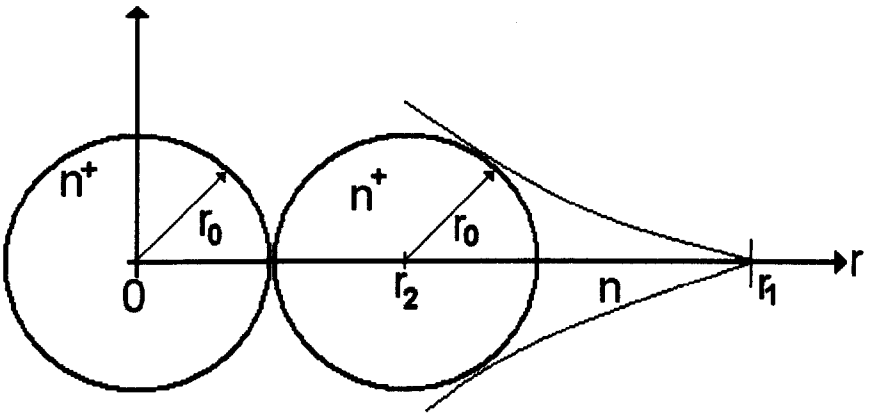

Fig 5-14: Diagram showing Dawson's photo-ionisation theory.

As the electron avalanche initiated at r_1 travels toward the positive region it is exponentially amplified:

$$n = \exp \int_{r_2}^{r_1} \alpha.dr$$

Where α is Townsend's first ionisation coefficient. If the number of electrons, n, is equal to the number of positive charges, n+, in the streamer tip all the positive ions will be neutralised. A consequence of the neutralisation process is the formation of a new positive region centred somewhere between r_1 and r_2, this new positive region can then be considered a new streamer tip and the process repeats. Due to the extremely high electric field between the positive region and electrons in the avalanche, the electron drift velocity, which is a product of the electron mobility and the electric field is very high. The streamer propagates at a velocity determined by the drift velocity of electrons in the avalanche head which is dependant on the density n^+ and independent of the applied field. This explains why the velocities measured are orders of magnitudes higher than the drift velocity calculated using the externally applied electric field. As shown in the previous section, the magnitude of the applied electric field does slightly influence the propagation velocity; this is possibly due to the higher applied field producing more positive charge which in turn produces a higher localised electric field between positive region and electron avalanche.

Dawson states three requirements that must be satisfied in order to explain streamer propagation in regions of low electric field. Firstly, the number of new positive charges created by the electron avalanche must equal the number of ions in the original sphere. Secondly, the diffusion radius of the electron avalanche must not become greater than radius, r_0, of the original sphere. Finally, the electron avalanche must reach the required amplitude before the two charge regions overlap, $2r_0<r_2$. Based on these three rules Liu *et al.* calculated the radii r_0 and r_2 as a function of the initial number density of positive ions, n^+. The results indicated that the condition of $2r_0<r_2$ is only met when the number of positive charges in the initial sphere is greater than $3x10^9$, consequently the streamer head can only self propagate in low electric fields if the initial charge density is above $3x10^9$. It is also pointed out that energy needed for the ionisation of a new volume of gas replaced by the streamer channel can only be derived from an external source. Therefore the propagation of the streamer in a region of low electric field is not a steady state process, eventually the electrostatic energy of the sphere of charges will be lost through the ionisation process and streamer propagation will terminate. Dawson showed this to be true by focusing the streamer through a series of metallic rings; each ring was pulsed to a high voltage as the streamer passed through. This had the effect of replenishing the charges in the tip allowing the streamer to propagate several times its original length.

An interesting point to note is the effect of further increasing the applied electric field. The results detailed within section 5.3 show that plasma bullets are only observed up to a given applied voltage and then a transition occurs in to a continuous glow discharge mode. A potential explanation of this is suggested on page 335 of Raizer's book,[5.16] as the number of charges in the streamer tip increases the tail of the streamer becomes increasingly conductive, upon reaching the cathode a partially conductive channel exists between the anode and the cathode, if the conductivity is sufficiently high the link between anode and cathode rapidly becomes a spark channel. In the case of a plasma jet there is a dielectric barrier between the conductive channel and the anode, as such no spark can form however in such circumstances a glow

discharge is possible; this fits well with experimental observations. For this explanation to hold true, in the case of high applied voltages one would expect to see a plasma bullet reach the cathode followed by an increase in intensity of the streamer tail. iCCD images of the continuous mode of operation, shown in figure 5-6, don't reveal any streamer head reaching the cathode prior to the formation of a glow discharge. One possible explanation could be that the streamer head is moving so fast, because of the high applied field, that it is missed by the iCCD camera; as such the gap between the anode and the cathode appears to instantaneously fill with plasma.

5.4.2 Experimental evidence of Dawson's propagation theory

Dawson initially proposed his streamer propagation theory in 1965, at that time diagnostic equipment was less advanced; iCCD cameras had not been invented and the semiconductor technology was in its infancy meaning signal processing techniques were confined to the analogue domain. Modern diagnostic equipment makes it is possible to investigate the streamer propagation mechanism with high temporal resolution giving a far greater level of detail than possible in 1965.

A consequence of Dawson's theory is that the streamer should appear to propagate in discreet steps; it takes time for an electron to be produced at a suitable distance, the avalanche to reach the positive region, and the neutralisation of the positive region to occur. During this time the motion of the heavy positive ions can be assumed to be negligible. Using an iCCD camera it might be possible to see this process in action, figure 5-15 shows a sequence of images taken of the plasma bullet with the shortest possible exposure time of 1ns. It is clear to see that the intensity of the bullet changes from high to low at approximately 3ns intervals, this pattern is highly repeatable and can be observed not only in single shot images but images consisting of many hundreds of accumulated images. This pulsing of intensity could well be an indicator of Dawson's theory in action, however caution

should be aired as light emission is not a direct indicator of electrons or positive ions.

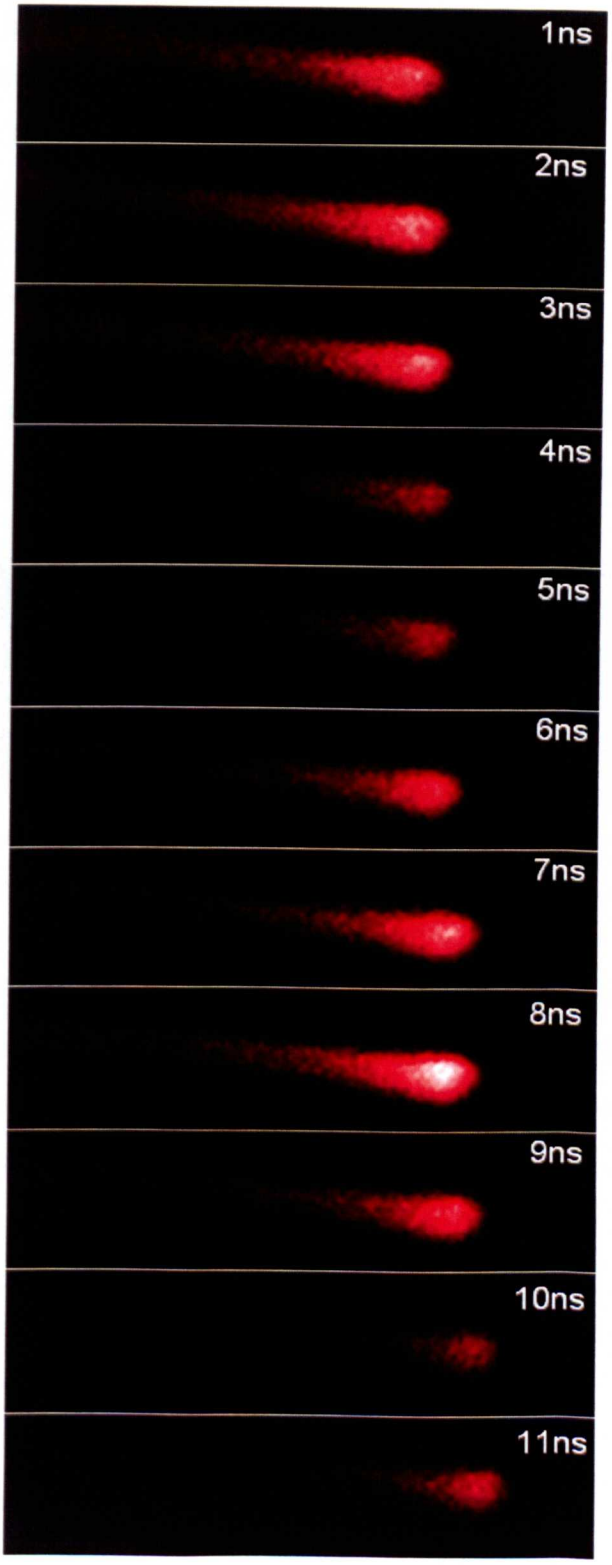

Fig 5-15: 1ns exposure, single shot iCCD images of the plasma plume taken at 1ns intervals.

Figure 5-16 shows an iCCD image that has been post-processed using a technique known as Abel inversion. This process applies a log scale to the intensity of an image, allowing very low intensity regions to been seen equally well as high intensity regions. Typically, unprocessed iCCD images are dominated by the plasma bullet centre, the peak intensity at the centre of the bullet is orders of magnitude above that of the tail, it is impossible to display this information using a standard colour scheme where image intensity relates to pixel colour. By applying Abel inversion it becomes possible to see details that were previously invisible. From the figure it is clear that the bullet has a long tail that extends right back to the powered electrode at the right of image. The tail region is orders of magnitude less intense than the bullet tip, this fits well with Dawson's explanation of an electrically isolated streamer tip.

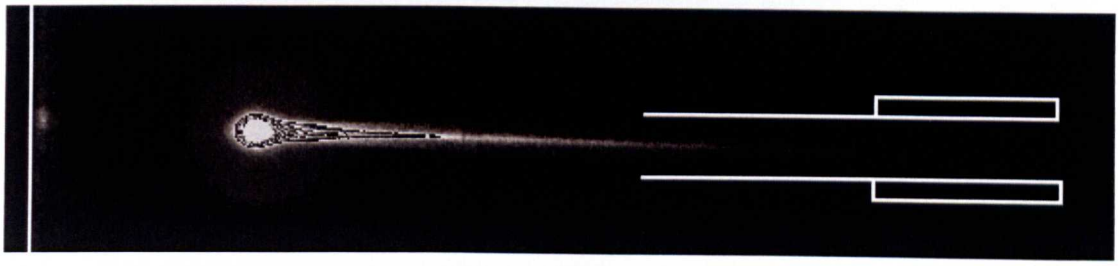

Fig 5-16: 10ns exposure, single shot Abel inverted iCCD image of the plasma plume. Cathode to left of image.

Figure 5-16 also highlights another interesting feature around the plasma bullet tip; a faint spherical luminous region is clearly visible. This glow could be a consequence of photons emitted from the positive bullet tip, as the tip is spherical it can be assumed to be an isotropic radiator and as such photons should be emitted in all directions. In the case of a plasma jet employing both the anode and the cathode it is reasonable to assume that the streamer will always take the shortest path to reach the cathode and consequently travels in a straight line. In the case of a plasma jet operated with a single powered electrode and no clearly defined cathode the situation is less clear. If the photons are emitted in an isotropic manner what dictates the direction of the streamer? This is easily explained in the case of a helium jet flushed into ambient air, the plasma will always be confined to the region

where helium concentration is highest, thus maintaining a collimated beam like appearance. The situation of a helium plasma jet being flushed into a helium atmosphere has not been reported previously, in theory the photons radiated from the positive tip are all equally likely to initiate an avalanche and as such the direction of the streamer should be randomised. The photo shown in figure 5-17 shows this not to be the case.

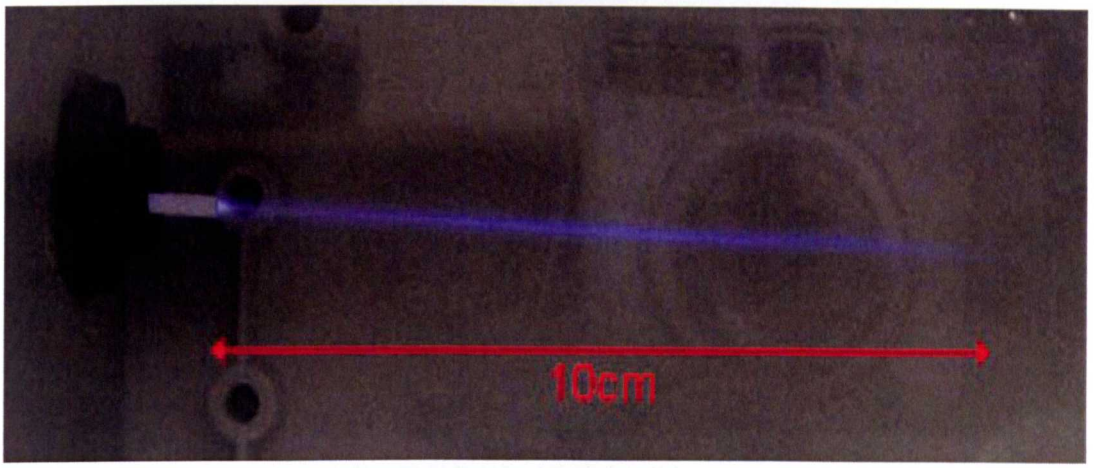

Fig 5-17: Image of helium plasma plume flushed into a helium atmosphere.

It is clear from the photo that the plasma plume remains a collimated beam over a significant distance in the pure helium atmosphere. This is unexpected and highlights a discrepancy in the theory predicted by Dawson, the reasons why the beam remains collimated in this situation are still unknown.

5.5 Interesting observations of the plasma bullet

While investigating the properties of the plasma bullet several interesting observations have been made which are not always explicable, however it is worthwhile including them within this thesis to enhance the body of knowledge on the subject. Figure 5-18 shows a series of iCCD images of a single powered electrode wrapped around a quartz tube through which helium is flushed. The electrode used consisted of a polymer coated with indium tin oxide (ITO); a unique property of ITO is that it is electrically conductive yet

optically transparent. Employing such an electrode on a transparent quartz tube allows the evolution of the plasma bullet to be observed completely.

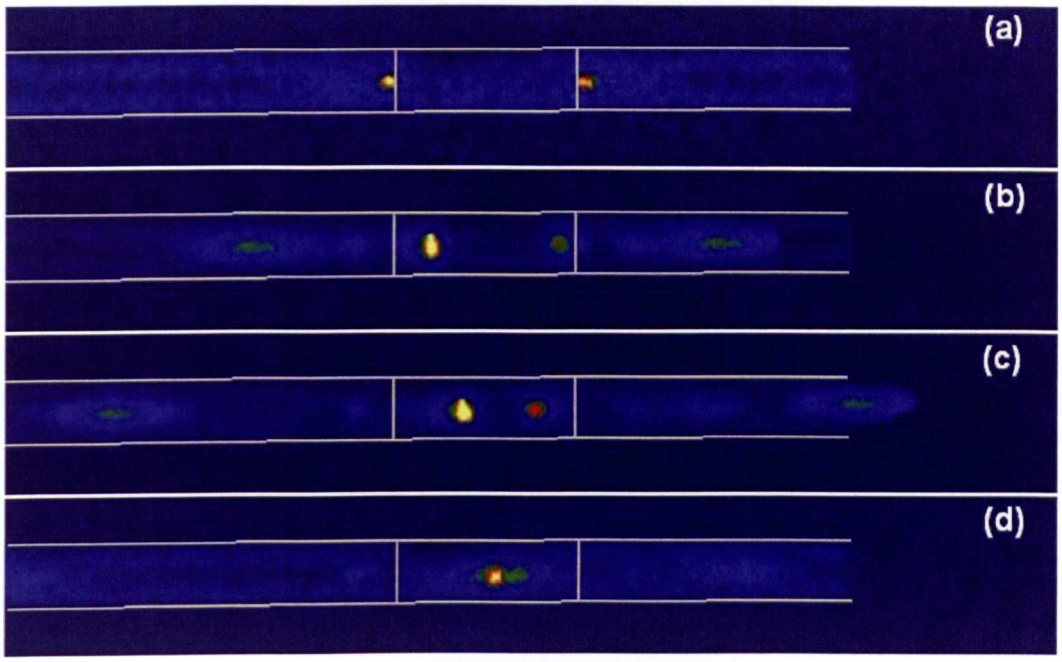

Fig 5-18: 10ns exposure iCCD images of plasma jet employing ITO transparent electrode.

The images in figure 5-18 were taken at 250ns intervals on the rising slope of the positive half-cycle. From 5-18a its possible to see two corona discharges forming at each end of the powered electrode, this fits well with the theory that a corona discharge initiated at the electrode edges is the starting point of the plasma jet. In figure 5-18b the voltage has increased such that the corona discharge begins to move, this fits with Dawson's theory, as the voltage increases the number of positive ions increases until it reaches a point where it can self-propagate. What is unexpected is that the two corona discharges produce four plasma bullets. Two bullets travel away from the powered electrode, these have been observed in many other studies. Unexpectedly, two plasma bullets are observed travelling towards the centre of the electrode, these are significantly more intense than the plasma bullets travelling away from the electrode. In images 5-18c and 5-18d it is possible to see the bullets travelling away from the electrode are moving very rapidly and eventually move out of the cameras view. The bullets travelling toward the centre of the electrode collide and form a stationary plasma ball in the centre

of the electrode that lasts for several hundreds of nanoseconds. This unusual pattern of four plasma bullets is a likely consequence of the single electrode configuration, if a grounded electrode had been placed at the exit of the tube it is likely that only one plasma bullet would have been formed. It should be noted that in all the images in figure 5-18 the gas flow is from left to right, as such the bullets travelling from right to left are actually moving against the gas flow.

As Dawson's theory suggests the plasma plume consists of a region of positive charge it is likely that any external electric field will influence the direction of propagation. Figure 5-19 shows three images of the plasma jet directed between two charge parallel plates. It's clear to see that the plume bends toward a negatively charged plate and bends away from a positively charged plate. It seems reasonable to assume that a negative charged plate will attract positive ions resulting in a bending of the beam towards the plate. Conversely, a strong positive field is likely to repel positively charged ions thus bending the beam away from the positively charge plate.

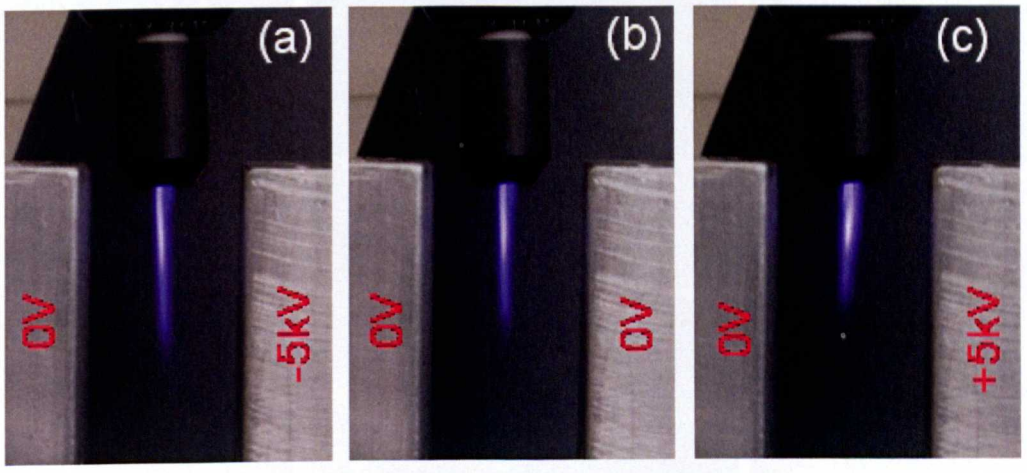

Fig 5-19: Effect of external electrostatic field on plasma plume direction.

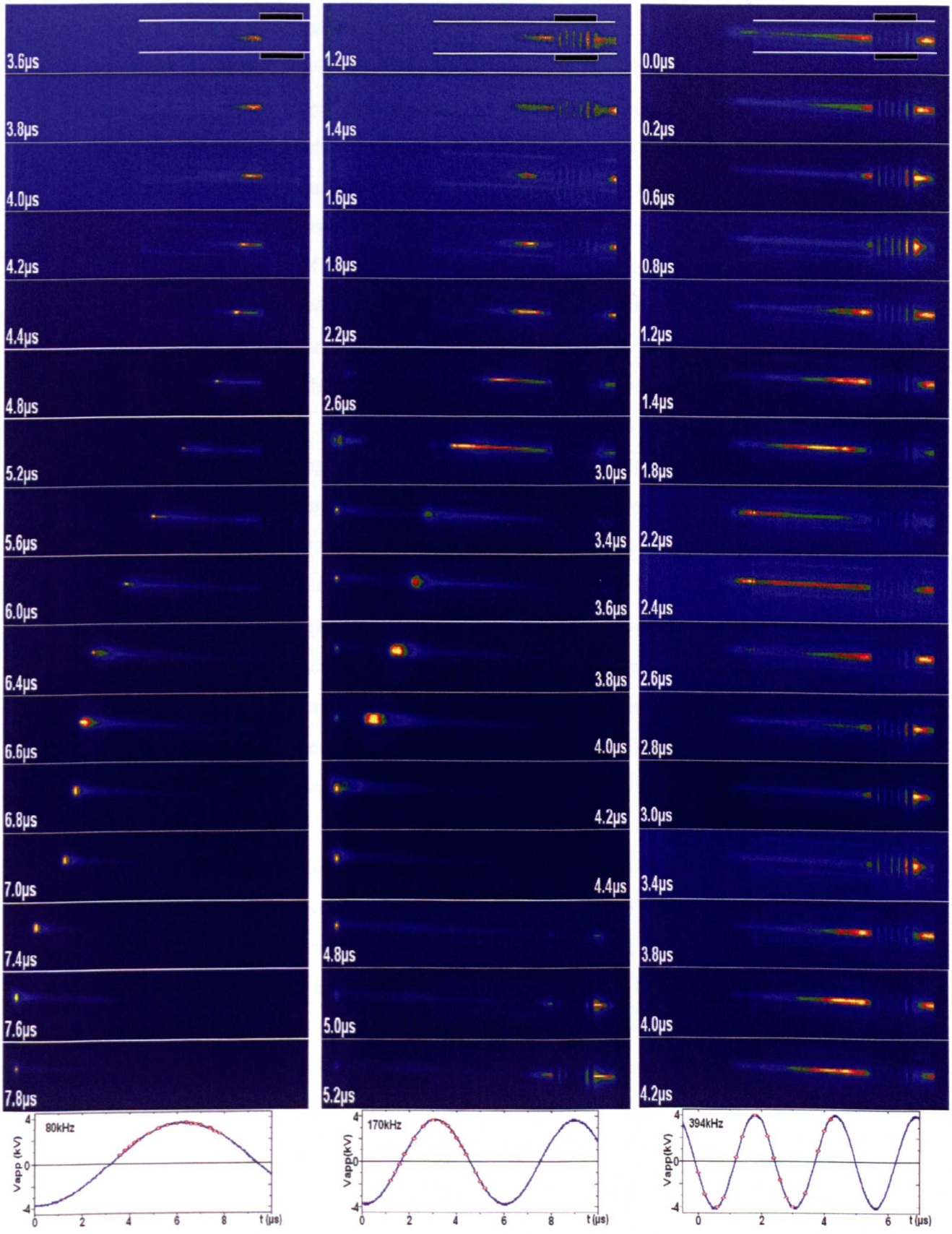

Fig 5-20: 10ns iCCD images of a helium plasma jet generated using different excitation frequencies.

As discussed in previous sections, the plasma jet is a widely used tool, typically 1-50 kHz excitation or 1-30 MHz excitation is employed to generate the plasma plume. Very few studies use frequencies outside the two stated ranges, as such the effect of excitation frequency on the plasma bullet is unknown. Using several air cored transformers with various self-resonant frequencies it was possible to generate a plasma plume from 50 – 1000 kHz. Figure 5-20 shows iCCD images of the plasma plume generated using three different excitation frequencies, in each case the configuration is the same, a single powered electrode consisting of multiple turns of wire on a quartz tube and a ground electrode placed several centimetres downstream. In the first column of figure 5-20 an excitation frequency of 80kHz was examined, each image was taken during the positive half-cycle of the applied voltage. During 3.6 – 4.2 μs, the plasma appeared as a strip with no obvious head and no movement. As the applied voltage is far from reaching its peak, the plasma density is low. The number of charges is likely to be too low to allow the streamer to self propagate. As the applied voltage increases, the plasma moves toward the ground electrode. After approximately 1.6 μs the plasma emerges from the quartz tube and continues to propagate until striking the grounded electrode. Its appearance outside the tube is very typical of plasma bullets observed below 50 kHz. [5.7]

When the frequency is increased to 170 kHz (images in the second column), the plasma becomes strip-like within the tube. During 1 – 1.6 μs, the powered electrode has a negative polarity thus acting as an instantaneous cathode and trapping the discharge. There was light emission from the gap between any two adjacent windings and the plasma appeared on both sides of the coil electrode, this suggests that a discharge is produced during the negative cycle, but it is incapable of self propagation. After 1.6 μs the applied voltage becomes positive, the plasma starts to move towards the ground electrode and appears as a long strip several centimetres in length, much longer and much brighter than that in the 80 kHz case. This is likely due to a much stronger discharge at higher frequencies; higher frequency operation means less time between consecutive discharges hence more charges are likely

to be stored on dielectric surfaces. Similar to the 80 kHz case, it takes approximately 1.4 μs for the plasma to emerge from the quartz tube, once the bullet is ejected from the tube it becomes more point-like with a long tail. Of interest are images at 3.0 – 4.0 μs when there is a distinct plasma near the cathode even though the plasma bullet is yet to reach the ground electrode. A possible explanation could be that the plasma bullet acts as a virtual anode thus enhancing the electric field at the ground electrode and creating a second discharge. At 3.2 μs, the plasma produced on the cathode is of a higher intensity than the plasma bullet itself. As frequency is increased to 394 kHz, the point-like plasma bullet is no longer observed (images in the third column of figure 5-20). The plasma remains strip-like in all images and its travel outside the tube is limited to only 0.5 cm. In the 80 kHz and 170 kHz cases, the time for the plasma to gather adequate pace and leave the tube was about 1.4 – 1.6 μs after the voltage became positive. This is longer than the half-period at 394 kHz (1.27 μs), and may be responsible for the plasma bullet being prevented from reaching the grounded electrode.

5.6 Summary

This chapter has covered the physical aspects of the plasma plume produced by various types of atmospheric pressure plasma jet. Section 5.3 highlights for the first time the three very distinctive modes of operation observed within the plasma jet. It was shown that the discharge is initiated as a low intensity corona discharge, as applied voltage increases the discharge is able to self propagate and forms a plasma bullet that moves away from the powered electrode. Finally, at high applied voltages the discharge becomes a continuous glow discharge which exhibits features similar to those observed in parallel plate barrier discharges.

For many low temperature applications, such as biological decontamination, it is essential the plasma jet be operated in the plasma bullet mode of operation. The corona mode is too weak to have the necessary chemical reactivity for decontamination of biological media. The continuous

glow mode is highly reactive, yet the gas temperature is so high that it thermally destroys the biological media. Only the plasma bullet mode exhibits room temperature operation and efficient reaction chemistry. As the plasma bullet mode of operation is of such importance its propagation mechanism was investigated in section 5.4. A theory first developed by Dawson and Winn in 1965 regarding the propagation of cathode directed streamers was adopted to explain the curious nature of the plasma bullet propagating in regions of low electric field. Dawson's theoretical predictions seemed to fit well with most experimental observations. However, no explanation was found to explain why a helium plasma bullet travelling through a helium atmosphere does not disperse.

Finally, section 5.5 reported several novel experimental observations of the plasma bullet. Whilst not all can be sufficiently explained at the current time it is hoped that the observations will form the basis for future investigations into the plasma bullet phenomena.

References

[5.1] Laroussi M 'Nonthermal decontamination of biological media by atmospheric-pressure plasmas: Review, analysis, and prospects' IEEE Transactions On Plasma Science, Vol.30, Iss.4, pp.1409-1415, Part 1, 2002.

[5.2] Schutze A, Jeong J.Y, Babayan S.E, Park J, Selwyn G.S, Hicks R.F, 'The atmospheric-pressure plasma jet: A review and comparison to other plasma sources' IEEE Transactions On Plasma Science, Vol.26, Iss.6, pp.685-1694 1998.

[5.3] Bibinov N, Dudek D, Awakowicz P, Engemann J,' Characterization of an atmospheric pressure dc plasma jet' Journal Of Physics D, Vol.40, Iss.23, pp.7372-7378, 2007.

[5.4] Walsh J.L, Shi J.J, Kong M.G, 'Contrasting characteristics of pulsed and sinusoidal cold atmospheric plasma jets, Applied Physics Letters,Vol.88, No. 171501, 2006.

[5.5] Walsh J.L, Kong M.G, 'Room-temperature atmospheric argon plasma jet sustained with submicrosecond high-voltage pulses' Applied Physics Letters, Vol. 91, Iss.22, No.221502, 2007.

[5.6] Stoffels E, Gonzalvo Y.A, Whitmore T.D, Seymour D.L, Rees J.A, 'A plasma needle generates nitric oxide' Plasma Sources Science & Technology, Vol.15, Iss. 3, pp.501-506, 2006.

[5.7] Teschke M, Kedzierski J, Finantu-Dinu E.G, Korzec D, Engemann J, 'High-speed photographs of a dielectric barrier atmospheric pressure plasma jet' IEEE Transactions On Plasma Science,Vol.33, Iss.2, pp.310-311, Part 1, 2005.

[5.8] Lu X , Laroussi M, 'Dynamics of an atmospheric pressure plasma plume generated by submicrosecond voltage pulses' Journal of Applied Physics, Vol.100, Iss.6, No.063302, 2006.

[5.9] Shi J.J, Zhong F.C, Zhang J, Liu D.W, Kong M.G, ' A hypersonic plasma bullet train travelling in an atmospheric dielectric-barrier discharge jet' Physics Of Plasmas,Vol.15, Iss.1, No.013504, 2008.

[5.10] Massines F, Rabehi A, Decomps P, Gadri R.B, Segur P, Mayoux C, 'Experimental and theoretical study of a glow discharge at atmospheric pressure controlled by dielectric barrier' Journal of Applied Physics, Vol.83 Iss.6, pp.2950-2957, 1998,

[5.11] Garamoon A.A, Samir A, Elakshar F.F, Nosair A, Kotp E.F, 'Spectroscopic study of argon DC glow discharge' IEEE Transactions On Plasma Science, Vol.35, Iss.1, pp.1-6, 2007.

[5.12] Zhu X.M, Kong M.G, 'Electron kinetic effects in atmospheric dielectric-barrier glow discharges' Journal of Applied Physics,Vol.97, Iss.8, No.083301, 2005.

[5.13] Walsh J.L, Shi J.J, Kong M.G,'Submicrosecond pulsed atmospheric glow discharges sustained without dielectric barriers at kilohertz frequencies' Applied Physics Letters, Vol.89, Iss.16, No.161505, 2006.

[5.14] Liu D.W, Shi J.J, Kong M.G, 'Electron trapping in radio-frequency atmospheric-pressure glow discharges' Applied Physics Letters, Vol.90, Iss.4, No.041502,2007.

[5.15] Dawson G.A, Winn W.P, 'A Model For Streamer Propagation' Zeitschrift Fur Physik, Vol.183, Iss.2, 1965

[5.16] Raizer Y.P 'Gas Discharge Physics' Springer 1991.

6 Pulsed APGD without dielectric barriers

6.1 Introduction

Atmospheric-pressure glow discharges offer a unique chamberless route to a wide range of highly desirable surface functionalities without wet chemistry and close to room temperature.[6.1] In the excitation frequency range of 1–300 kHz, dielectric insulation of electrodes has long been believed to be essential for stable APGD generation.[6.2] It is therefore of significant interest to study whether APGDs without dielectric barriers are fundamentally possible at kilohertz frequencies and, if so, whether barrier-free APGDs offer a different route to producing glow discharges at atmospheric pressure.

From an application standpoint, it is sometimes desirable to dispense the use of the electrode-insulating dielectric layers that may become contaminated after continuous usage and so potentially lose their ability to stabilise APGD. The vast majority of previous studies conducted in to barrier-free APGD have been achieved largely outside the 1–300 kHz range, either at the mains frequency using a large ballast resistor of various forms,[6.3,6.4] or at megahertz frequencies,[6.5–6.7] both techniques effectively stabilise the discharge by restricting current growth. Within the 1–300 kHz range, the only reported barrier-free APGD is achieved by maintaining the sinusoidal applied voltage close to the gas breakdown voltage.[6.8] A drawback of this method is the very limited operating range of the discharge, the applied voltage must be held just above the breakdown voltage and strictly regulated to prevent arcing.

This chapter details a novel barrier-free APGD discharge sustained at kilohertz frequencies by sub-microsecond voltage pulses, the discharge is shown to be stable over a wide operational range. Initially, section 6-3 details

the characteristics of the discharge using electrical and optical techniques. A comparison between pulsed barrier-free APGD and a kilohertz DBD is given in section 6.4. Perhaps the most widely used barrier-free atmospheric pressure discharge is the RF-APGD; section 6.5 provides a comparative study of RF-APGD and pulsed barrier-free APGD. Unlike sinusoidal excitation, pulsed excitation has many characteristics that can be tailored to enhance the efficiency of the discharge; the effects of pulse tailoring are explored in section 6.6. The penultimate section describes the breakdown mechanism observed in a pulsed barrier-free APGD. Pulsed excitation is shown to generate highly transient plasma in which gas breakdown occurs during every applied voltage pulse; hence a clear understanding of the breakdown mechanism is essential to enhance the properties of the discharge.

6.2 Experimental Setup

The sub-microsecond pulsed barrier-free APGD considered in this chapter was generated using two parallel stainless-steel electrodes with a surface area of 6 cm^2 and a separation distance of 0.5–1.5 cm. The two electrodes were naked without any dielectric barriers, and the electrode unit was housed within a Perspex box fed with a through flow of helium. A mass flow controller was used to regulate the gas flow and allow the addition of small amounts of various reactive gases such and oxygen and nitrogen. The Perspex box was not airtight; hence oxygen and nitrogen were present. In general the discharge was operated using a gas flow rate of 5 SLM helium with additional oxygen or nitrogen up to 300 SCCM.

In order to generate a high voltage train of sub-microsecond pulses a pulse generator was developed based on the push-pull stacked MOSFET topology discussed in chapter 2. The device was capable of delivering unipolar voltage pulses of up to +/-10 kV at 0.01–20 kHz. The pulse generator required an intricate matching network to cope with the dynamic impedance of the load. Initially, the load appears as a small capacitance and only displacement current flows, during the discharge the load becomes increasingly resistive and

several amps may flow; if instability occurs it is possible for many tens of amps to flow resulting in arc formation. The pulse generator must be capable of withstanding all the possible conditions of the discharge hence considerable effort was directed toward designing a rugged and robust device using the latest power MOSFET devices.

The generated plasma was found to be stable and repetitive for many hours of continuous operation. Water cooling was not needed, and the electrode temperature measured with an infrared thermocouple was found to be about 2 °C above room temperature. These observations suggest that the pulsed barrier-free plasma was essentially a room-temperature, homogeneous, atmospheric glow discharge. To understand the temporal behaviours of the sub-microsecond pulsed APGD, electrical measurements were performed electrical using a Tektronix oscilloscope (TDS 5054B) via wideband voltage and current probes. Figure 6-1 shows a schematic of the experimental setup, a trigger generator is employed to control the pulse width of the applied voltage and repetition frequency, a second function of the trigger generator is to provide a trigger signal to control the OES system and iCCD camera.

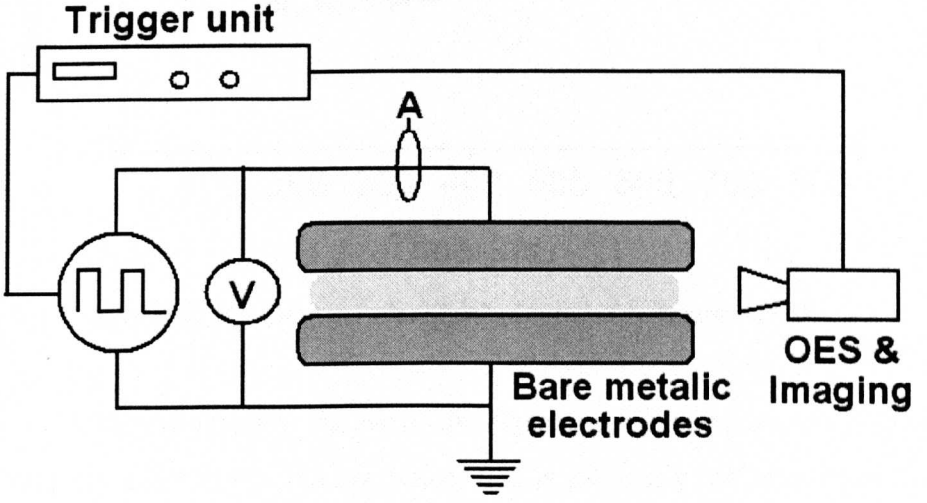

Fig 6-1: Schematic showing experimental setup for barrier-free APGD experiments.

6.3 Discharge characteristics

6.3.1 Electrical characteristics

The applied voltage was made of a train of -2 kV pulses repeated at 1 kHz and is shown in figure 6-2. Each voltage pulse had approximately a rise time of 100 ns, a falling time of 200 ns (between 10% and 90% of the peak voltage), and a pulse width of 360 ns (between two half-peak points). The duty cycle was very small at around 0.05%. The discharge current was also periodic and its pulse width was about 120 ns, markedly smaller than the voltage pulse width. Its peak was 4.84 A or 0.81 A/cm^2, much greater than that of atmospheric dielectric barrier discharges (DBDs) in He–O_2 mixtures.[6.9]

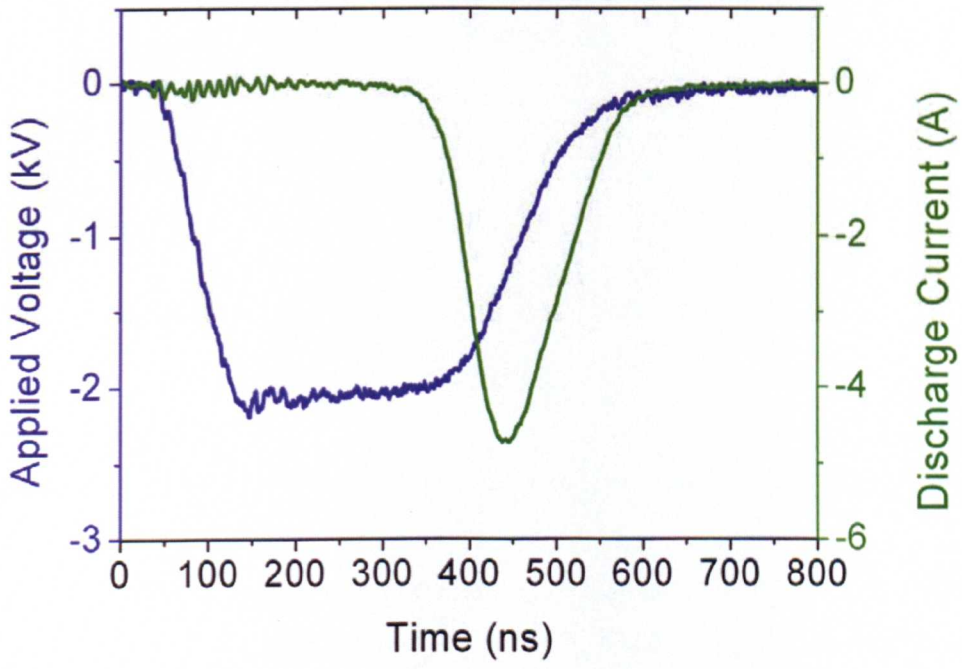

Fig 6-2: Current & voltage characteristics of pulsed barrier-free helium APGD.

A very distinctive feature of the discharge is the appearance of a single current pulse for every voltage pulse; this is markedly different from that of kilohertz sinusoidal excitation where two current pulses per cycle are seen.[6.9,6.10] Sub-microsecond pulsed excitation of a DBD jet employs voltage pulses with very similar characteristics to barrier-free APGD (see section 4),[6.12,6.13] however, two distinctive current pulses per applied voltage pulse are

observed, this suggests that the physical mechanisms behind the pulsed barrier-free APGD and other kilohertz APGD are very different.

Figure 6-3 highlights the discharge current on a microsecond scale. It is clear to see that at a repetition rate of 1kHz there is a distinct current pulse observed every 1ms. A single current is indicative of a single discharge event per applied voltage pulse; this is confirmed later in the chapter using nanosecond imaging techniques.

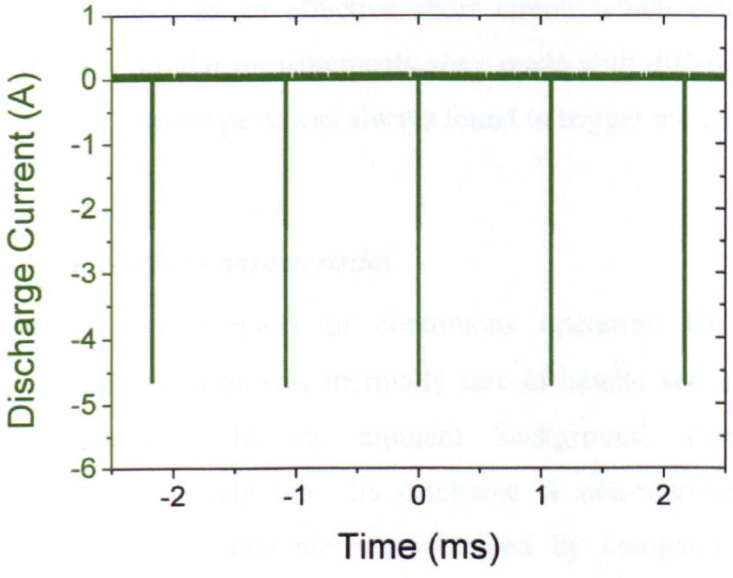

Fig 6-3: Discharge current of a pulsed barrier free APGD observed on a microsecond scale.

It is interesting to note that the current peak occurred in the falling phase of the applied voltage shown in figure 6-2. Suppose electron mobility is approximated to that in atmospheric helium, 1132 $cm^2\ V^{-1}\ s^{-1}$, and that the average electric field was 1kV/ 0.5 cm = 2 kV/cm in the voltage-rising phase. The time for an electron to transverse the electrode gap of 0.5 cm was about 221 ns. Hence the voltage-rising phase of 100 ns was not sufficiently long for electrons in the electrode gap, if any, to reach the anode and support a large current in the external circuit.

The displacement current made a similarly small contribution. With an electrode unit capacitance at 1.1 pF, the peak displacement current was 22 mA, 228 times below the peak current of 4.84 A in figure 6-2. So the discharge during the voltage-rising phase was supported by a very small current and was at most a Townsend discharge. After the applied voltage reached its plateau, gas ionization continued and produced more electron-ion pairs. Eventually at 350 ns, the discharge increased significantly and climbed to 4.84 A in about 100 ns. Because of the very large current, the conductivity of the plasma load increases very significantly and as a result is presented to the voltage source as an effective short circuit which causes the applied voltage to fall. Similar measurements were made with different voltage pulse widths and the current peak was always found to trigger the voltage fall.

6.3.2 Temperature characteristics

After several hours of continuous operation the electrode unit containing the discharge was thermally safe to handle and appeared to be a similar temperature to the ambient background. Considering these observations it is likely that the discharge is non-thermal in nature. As confirmation, gas temperature was obtained by comparing the measured spectrum and simulated data of the excited hydroxyl molecule at 309nm, figure 6-4 shows the results, a simulated spectrum with a rotational temperature of 320K closely fits the experimental data. A thermocouple employed to monitor the temperature over several hours of continuous operation recorded an increase of 2°C above the ambient room temperature. It is likely that the gas flow had a cooling effect upon the electrodes thus explaining the small discrepancy in the thermocouple and optical temperature measurement techniques.

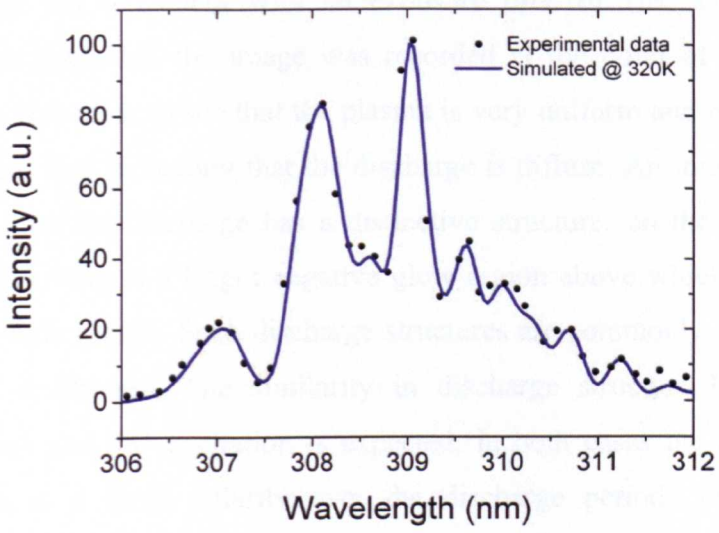

Fig 6-4: Measured and simulated spectrum of OH emission at 309nm.

6.3.3 Optical characteristics

If pulsed barrier-free APGD is to become a useful technology it is essential that the discharge be free from streamers to allow uniform processing of materials. Figure 6-5 shows an image taken using a Canon digital camera with an exposure time of 1/60s, visually the discharge appears to be free from streamers and highly uniform. To demonstrate the potential for large volume processing the electrode gap is set to approximately 1cm yielding 6cm^3 of plasma, in comparison to the needle like beam of an APGD jet this is quite a substantial amount.

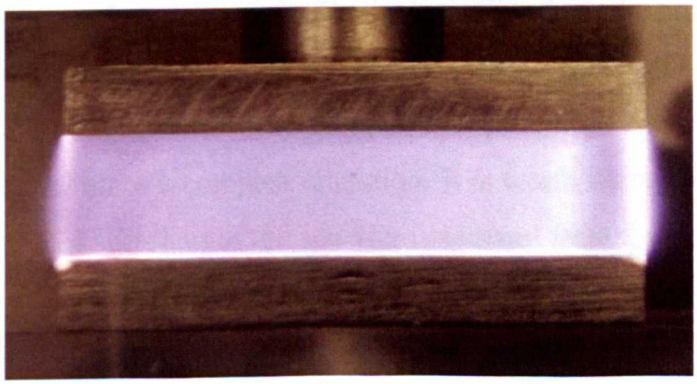

Fig 6-5: Photograph of pulsed barrier-free APGD.

Figure 6-6 shows an image of the pulsed barrier-free APGD taken using an iCCD camera with an exposure time of 1ns. The camera was triggered such that the image was recorded at the point of peak discharge current. It is clear to see that the plasma is very uniform and no streamers are observed, thus indicating that the discharge is diffuse. An interesting point to note is that the discharge has a distinctive structure; on the cathode (lower electrode) there is a bright negative glow region above which there is a less intense bulk region. Such discharge structures are commonly observed in DC plasma discharges. The similarity in discharge structure between pulsed excitation and DC excitation is expected, in both cases the applied voltage remains at a fixed polarity over the discharge period. This situation is markedly different from that of sinusoidal excitation, where the polarity of the applied voltage alternates during the discharge period.

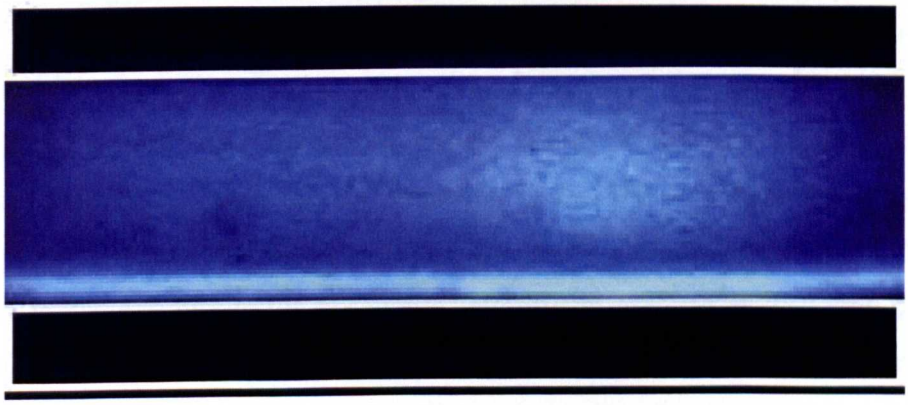

Fig 6-6: iCCD image of pulsed barrier-free APGD with a 1ns exposure.

OES measurements from 250nm to 800nm reveal a typical helium APGD spectrum, rich in nitrogen and oxygen species from the ambient air. To obtain a spectrum for a true pure helium discharge would require the evacuation of the background air from an airtight container prior to filling with helium, which is rather a complex operation. It is worth noting however, that unlike many APGD discharges the spectrum observed from the pulsed barrier-free APGD is dominated by oxygen emission at 777nm, this is unusual as excited nitrogen species tend to dominate kilohertz APGD.[6.13-6.15]

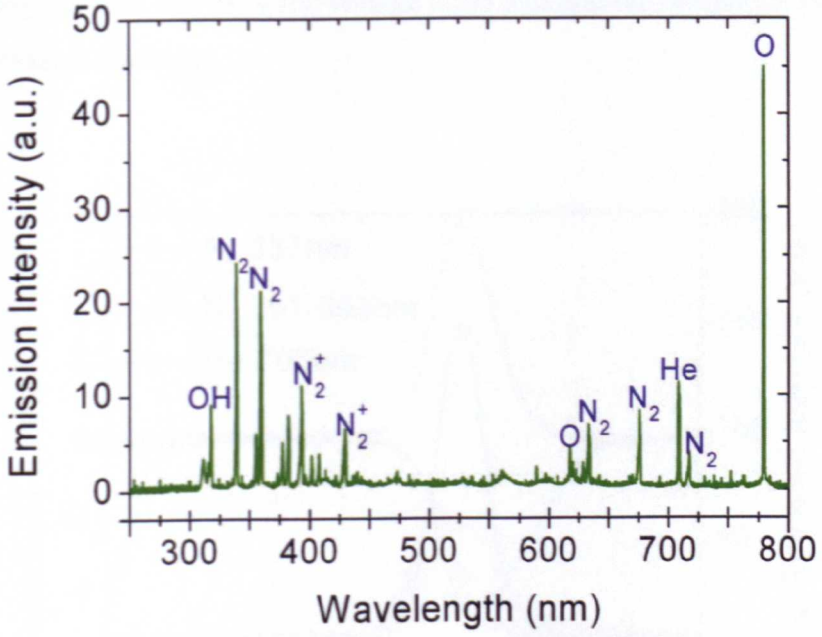

Fig 6-7: Emission spectrum of pulsed barrier-free APGD between 250nm and 800nm.

To further understand pulsed barrier-free APGD, optical signatures of three excited plasma species were plotted in figure 6-8 together with the discharge current and dissipated power, all as a function of time on a nanosecond scale. Since the N_2^+ emission in the 391 – 393 nm range is the most intensive among ionic species in figure 6-7, its absence from the first 300 ns in figure 4 suggests the absence of significant amount of ions and hence electrons in the electrode gap. This is consistent with the fact that the current pulse became significant only after 300 ns even though the voltage pulse had persisted for the first 250 ns (see figure 6-2). Emission in 391 – 393 nm is known to be resulted from N_2^+ ($B^2\Sigma_u^+$, v_b=0) transition to N_2^+ ($X^2\Sigma_u^+$, v_x=0), and the former is populated through the Penning reaction and the charge transfer from He^{2+} ions. The temporal profile of the 391 – 393 nm line therefore contains information of the evolution of the helium metastables and molecular ions.[6.16] Similarly, the helium line at 706 nm indicates the presence of either energetic electrons or He^{2+} ions and low energy electrons.[6.16] Again the absence of a strong 706 nm line before 300 ns supports the suggestion that there were insufficient electrons in the electrode gap to sustain a large current

during the first 300 ns of the voltage pulse and that the discharge was at most a Townsend discharge.

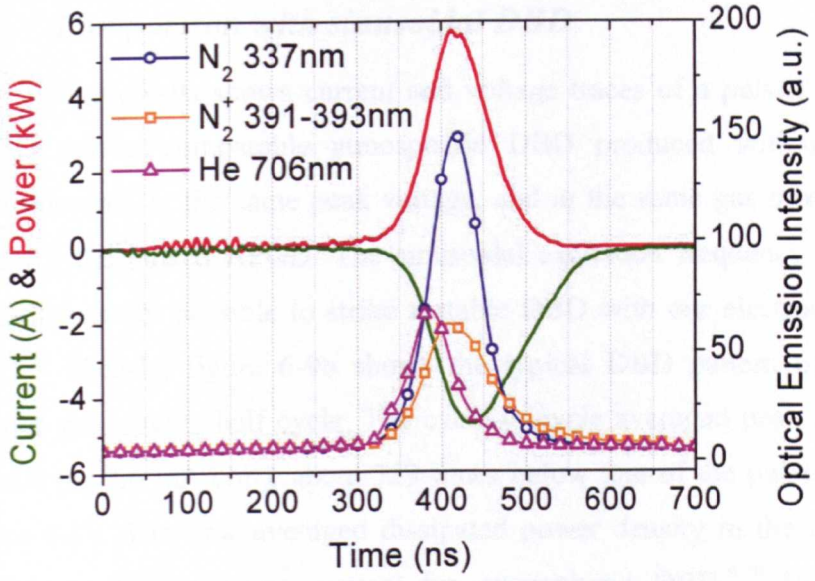

Fig 6-8: Optical signatures of N_2 @ 337nm, N_2^+ @ 391nm and He @706nm excited plasma species.

It is worth noting that the temporal profiles of all three plasma species are similar. The instants at which the three emission lines reached their peaks were different, and their fall times were also markedly different. For example, raw data suggest that the fall time of the 337 nm and 706 nm lines were 130 ns and 150 ns respectively. The ratio of their intensity integral over time in figure 6-8 was about 2, and compared well with the ratio of their time-accumulated intensity in figure 6-7. Difference in the temporal profiles of the three excited plasma species in figure 6-8 was probably related to their different life spans. It is also worth noting that their temporal profiles fit better with the power profile than the current profile. Given that the applied voltage tailed off during the current pulse in figure 6-2, it is possible that the average electron energy decreased in the latter phase of the current pulse and the profile of the dissipated power offers a more accurate indication of the dynamics of energetic electrons. This suggests that the profiles of excited plasma species

may be influenced by both their life times and the dynamics of energetic electrons.

6.4 Comparison with sinusoidal DBD

Figure 6-9a shows current and voltage traces of a pulsed barrier-free APGD and a comparable atmospheric DBD produced within the same electrode unit, at the same peak voltage, and in the same gas mixture as that used for the pulsed APGD. The sinusoidal excitation frequency was 8 kHz since it was not possible to strike a stable DBD with our electrode unit at 1 kHz.[6.11] Clearly, figure 6-9b shows the typical DBD pattern of one large current spike every half cycle. The cycle-to-cycle averaged peak current was 15 mA (or 2.6 mA/cm^2), about 323 times below that of the pulsed APGD in figure 6-9b. The time-averaged dissipated power density in the atmospheric DBD was 328 mW/cm^3, typical for atmospheric DBD.[6.10] However, the averaged power density in the pulsed barrier-free APGD was about one magnitude lower at 38 mW/cm^3. It is believed that the small duty cycle of the pulsed APGD was responsible for its smaller dissipated power even though its discharge current was much greater at the same applied voltage. Similarly, the pattern of one current peak per voltage pulse in figure 6-9a was different from that of pulsed atmospheric DBD in which two current peaks per voltage pulse were typical.[6.12,6.13] These suggest that the pulsed barrier-free APGD in figure 6-9a is unlikely to be assisted by any dielectric barrier effect.

Figure 6-10 shows the optical emission spectra of the pulsed barrier-free APGD and its corresponding atmospheric DBD, both with a peak applied voltage of 2 kV and measured with the same arrangement of an Andor Shamrock spectroscopy system at 1 ms exposure time. Both spectra exhibit spectral signatures of a very similar group of plasma species, for example the dominant helium line at 706 nm, the nitrogen ion line in 391 – 393 nm and the nitrogen line at 337 nm, the OH line at 309 nm, and the atomic oxygen line at 777 nm. Helium and oxygen lines were stronger in the pulsed APGD, and nitrogen lines were stronger in the atmospheric DBD.

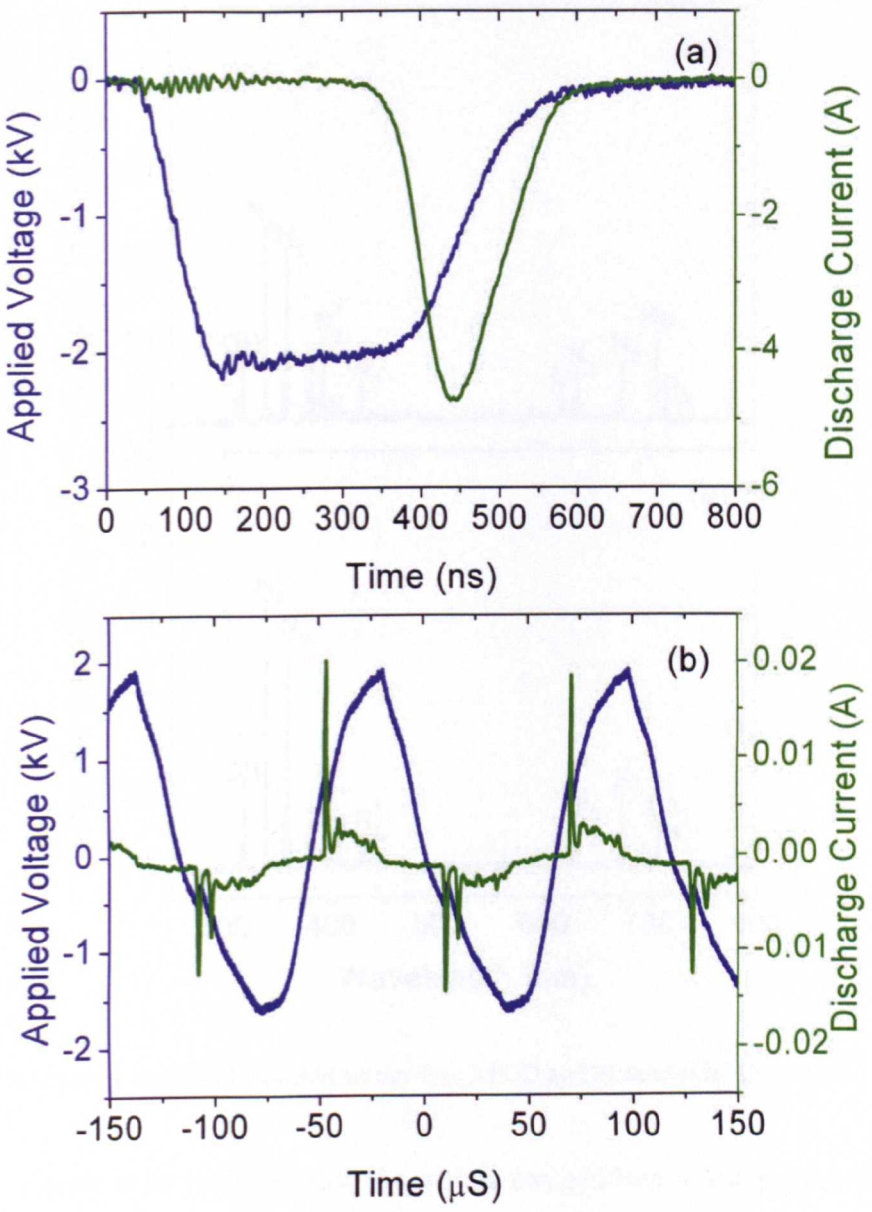

Fig 6-9: Current & Voltage traces for a) 400ns FWHM, 1kHz barrier free APGD and b)8kHz sinusoidal DBD.

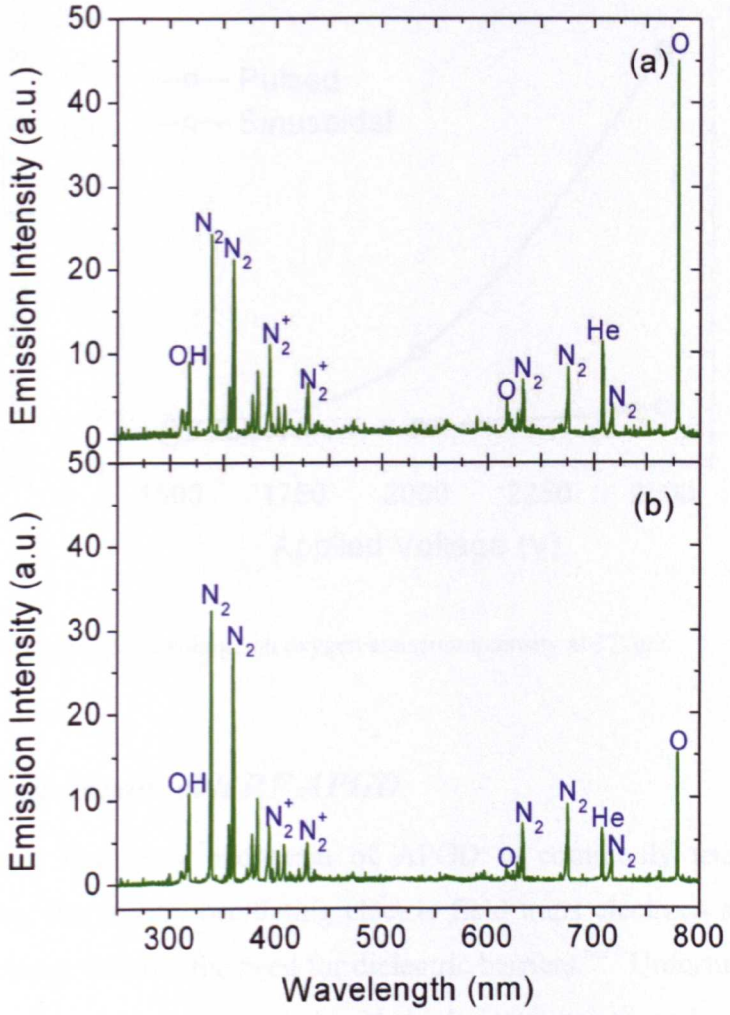

Fig 6-10: Emission spectra of a)pulsed barrier-free APGD and b) sinusoidal kHz DBD.

Figure 6-10 indicates that the atomic oxygen line in the pulsed APGD was about 3.7 times of that in the atmospheric DBD. This efficient production of oxygen atoms was found to improve further at larger applied voltages as shown in the figure 6-11. As the applied voltage increased to 2.5 kV, the intensity of the 777 nm line became about one magnitude higher in the pulsed APGD than that in the sinusoidal DBD. Hence the pulsed barrier-free APGD offers an energy-efficient route to the production of chemically reactive plasma species, such as atomic oxygen. Also compared to sinusoidal barrier-free APGD,[6.8] pulsed barrier-free APGD are much more versatile, operated over a wider voltage range and at higher currents.

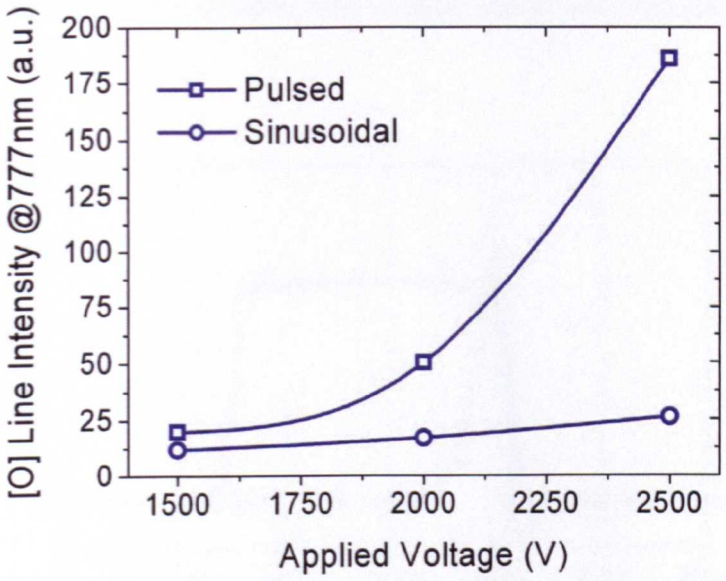

Fig 6-11: Effect of applied voltage on oxygen emission intensity at 777nm.

6.5 *Comparison with RF APGD*

Radio frequency excitation of APGD is commonly used in many applications; the rapidly oscillating electric field traps electrons and yields a stable discharge without the need for dielectric barriers.[6.27] Unfortunately, high frequency excitation is associated with high input power and consequently excessive gas heating; rendering RF-APGD unsuitable for applications involving temperature sensitive materials.[6.23] It is known that RF discharges produce significantly more reactive species compared to kHz excited barrier discharges, hence their attractiveness in many industrial applications. Potentially, pulsed barrier-free APGD could be an exciting alternative to RF-APGD, offering high fluxes of reactive species at greatly reduced input powers and consequently lower gas temperatures.

This section provides a comparison between pulsed barrier-free APGD and an RF-APGD generated using the same electrode unit, electrode separation, and gas flow. The RF excitation frequency was chosen to be 13.56MHz, as it is lies within the 13-14MHz band allowable for medical

devices and has been used extensively in previous studies of RF-APGD.[6.17,6.18] Figure 6-12 shows the current and voltage traces for both pulsed and RF excitation sources.

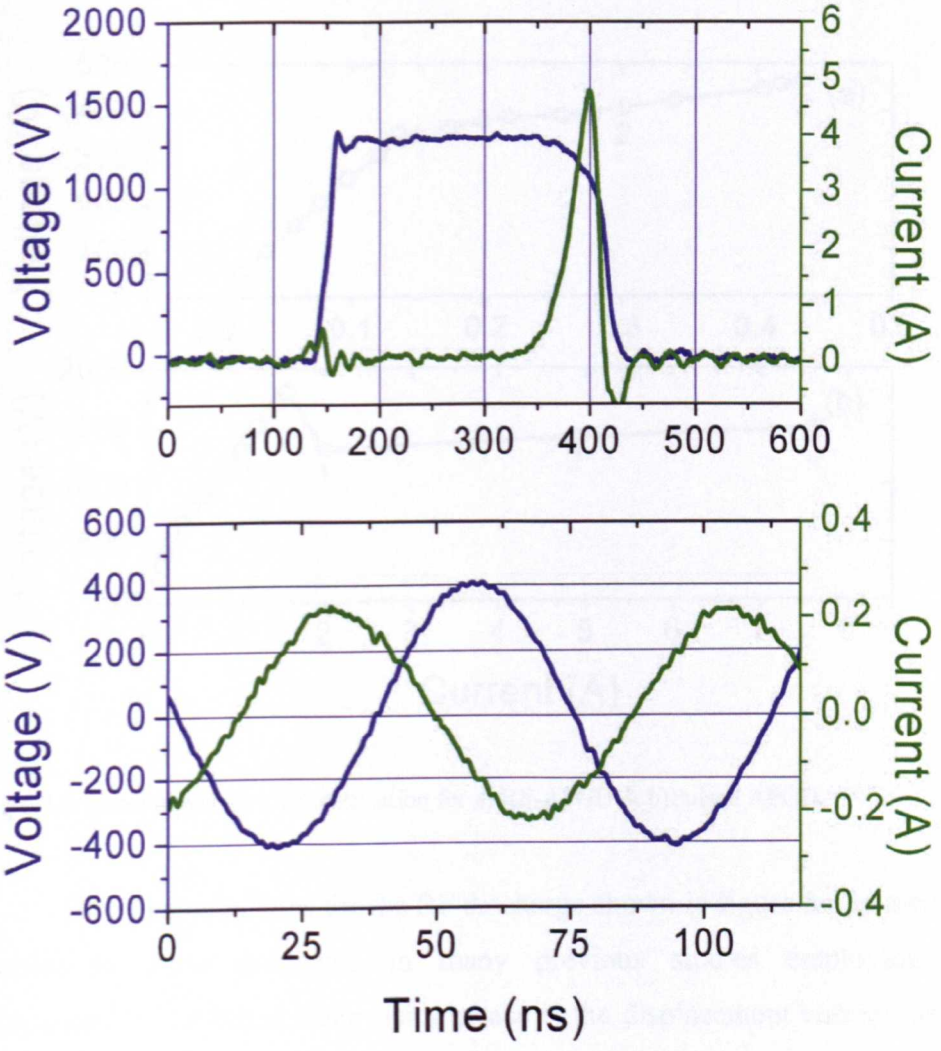

Fig 6-12: Current and voltage traces for pulsed-APGD and RF-APGD.

Typical of RF-APGD the discharge current leads the applied voltage; the phase difference indicates that the discharge has both a capacitive and resistive element.[6.17] Capacitances arise due to the formation of sheaths within the discharge and from the small separation of the two electrodes. The resistive element relates to the conductivity of the gas within the gap hence only becomes apparent after breakdown. Figure 6-13 provides a current-voltage-characterisation (CVC) for each discharge. Figure 6-13a highlights the

CVC for the RF-APGD, RMS currents and voltages are used. In figure 6-13b peak voltages and currents are used to characterise the pulsed discharge.

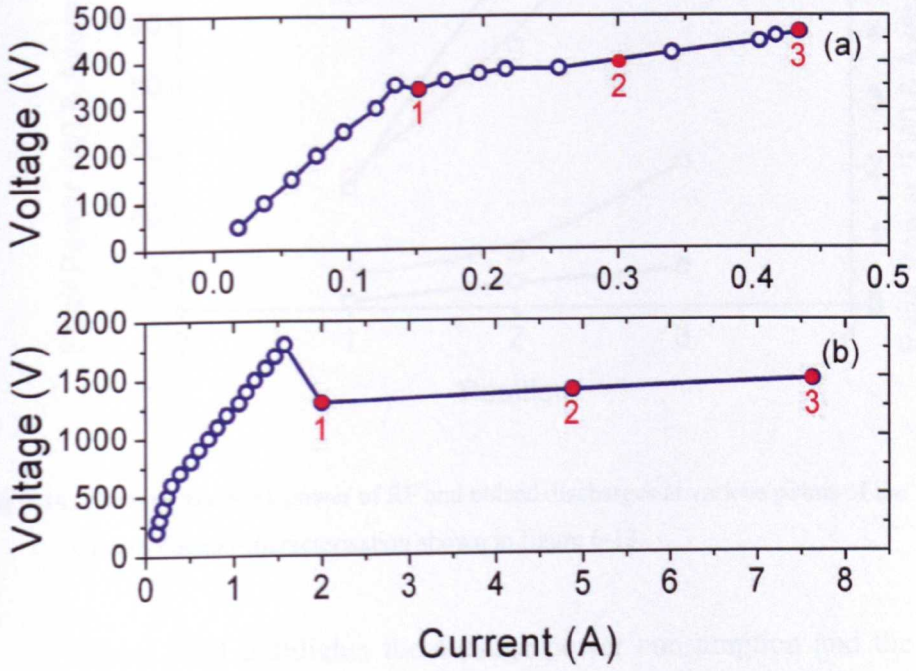

Fig 6-13: Current-voltage characterisation for a) RF-APGD & b)Pulsed APGD.

The characteristics for the RF discharge shown in figure 6-13a are very similar to those published in many previous studies employing RF excitation.[6.8] The initial steep rising phase is the displacement current, as the pulse-APGD has a steep rising edge this is considerable. At the breakdown point a small drop in voltage is observed (point 1); proceeding breakdown the discharge becomes increasingly conductive indicated by a large rise is current for a small increase in voltage (point 2). The furthest point at the right hand side of each CVC graph indicates the point at which the discharge exhibits instability and transitions to arcing (point 3).

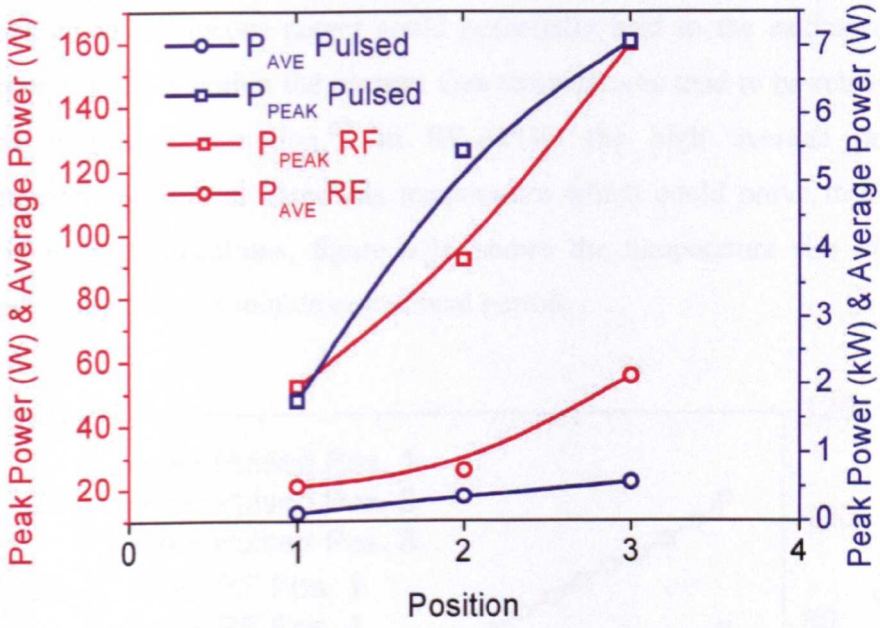

Fig 6-14: Average and peak power of RF and pulsed discharges at various points of the current-voltage characterisation shown in figure 6-13.

Figure 6-14 highlights the average power consumption and the peak power of each discharge at the three positions indicated on the CVC data shown in figure 6-13. It is clear to see that RF-APGD consumes a considerable amount of power and has a relatively low peak power, conversely, pulsed-APGD has a low average power and a very high peak power.

Excitation	V_{peak} (V)	I_{peak}(A)	P_{ave} (W)	P_{peak} (W)
Pulsed	1520	7.6	0.6	7000
Radio Frequency	460	0.45	58	160

Fig 6-15: Table summarising Current, voltage, and power consumption.

Figure 6-15 summarises the data shown in figure 6-14 at position 2, it lists the peak voltage, peak current, average power, and maximum instantaneous power measured for each excitation method. Of most practical interest is the average power consumed by each plasma, the RF APGD requires almost two orders of magnitude more power than that of the pulsed APGD, due primarily to the pulsed excitation method making use of a long voltage-off phase to reduce unnecessary power dissipation. It should be noted

that the maximum instantaneous power is 44 times higher in the pulsed case; such a high instantaneous power could potentially lead to the excitation of high energy species within the plasma. Gas temperatures tend to be related to average power consumption,[6.7] in RF-APGD the high average power consumption suggests elevated gas temperature which could prove to be an issue in many applications, figure 6-16 shows the temperature rise of the electrode body over a 5 minute operational period.

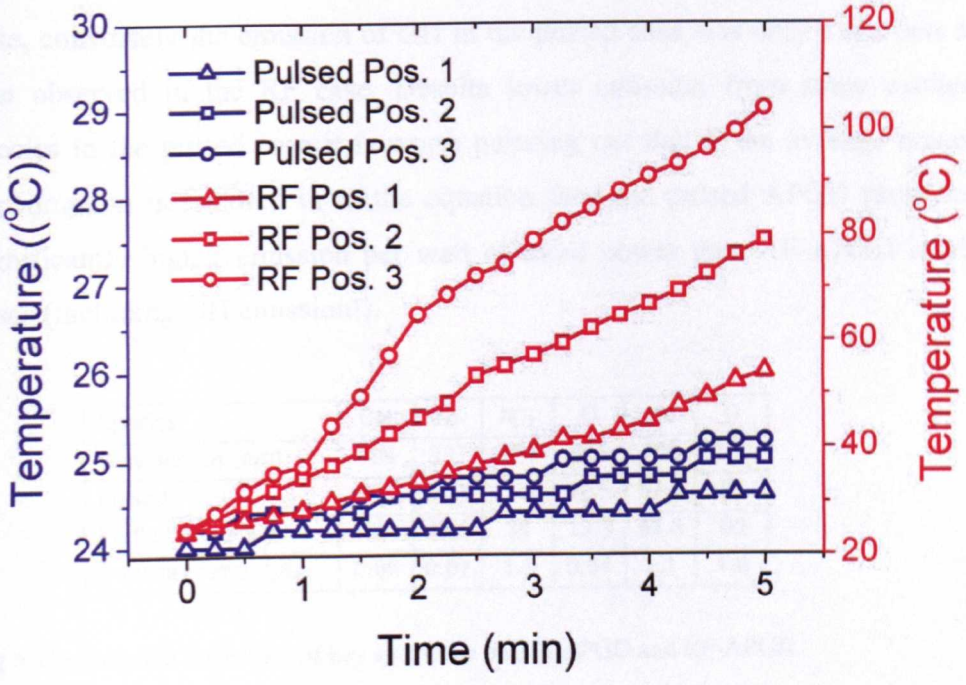

Fig 6-16: Temperature of electrode body in RF-APGD (Red) and pulsed APGD (Blue).

From figure 6-16 it is clear to see that in all case the RF discharge has significantly higher gas temperatures. After 5 minutes of operation the RF-discharge had elevated the electrode body temperature from 24°C to between 58°C and 110°C. Temperatures in excess of 100°C are commonly reported in helium RF-APGD studies.[6.7] Very little temperature rise was observed in the pulsed case, less than 1°C over the 5 minute period, highlighting the low power, non-thermal nature of the discharge.

Optical emission spectroscopy was used to detect various excited plasma species within each discharge. In general atomic oxygen, OH radicals and various nitrogen species were observed; the emission spectra were similar for the pulsed and RF-APGD cases. Figure 6-17 highlights the key species within each discharge recorded at point 3 on the CVC data shown in figure 6-13 (just prior to arcing) with an exposure time of 1ms. Apart from oxygen at 777nm and OH at 309nm the emission intensities are very similar. The emission of atomic oxygen in the pulsed case was almost twice that in the RF case, conversely the emission of OH in the pulsed case was only a fraction of that observed in the RF case. Despite lower emission from some excited species in the pulsed case it is worth pointing out that if the average power consumption is factored in to the equation then the pulsed APGD produces significantly higher emission per watt of input power than RF-APGD in all cases (including OH emission!).

Species	OH	N_2	N^+_2	O	He	O
Wavelength (nm)	309	337	391	616	706	777
Pulsed	5.5	41.5	42	12.5	67.5	90
Radio Frequency	90	47.5	38	13.3	61.5	50
Intensity ratio, I_p/I_{RF}	0.06	0.87	1.1	0.94	1.1	1.8

Fig 6-17: Emission intensities of key species in pulsed APGD and RF-APGD.

The results presented in this section give clear evidence that pulsed APGD is a viable alternative to the widely used RF-APGD. Electrical measurements show that power consumption is significantly lower yet the peak power is significantly higher. In industrial applications energy efficiency is often of paramount concern. Gas temperatures are also significantly lower in pulsed APGD meaning it can be used for the processing of heat sensitive materials. Optical emission results showed that pulsed APGD has a similar emission spectra to RF APGD however it produces double the amount of atomic oxygen emission which is essential in the field of plasma decontamination.[6.17]

6.6 *Enhancing characteristics*

In the previous sections, a kHz APGD generated with sub-microsecond high-voltage pulses between two naked electrodes have been reported. With a large current density of >0.5 A/cm^2, the pulsed APGD was shown to produce far more excited atomic oxygen emission at 777 nm than a comparable atmospheric DBD.[6.24] This is significant, given that reactive species such as atomic oxygen and OH radicals are key application enablers.[6.13,6.14,6.22,6.23] Therefore, it is of considerable interest to better understand and further develop pulsed APGD.

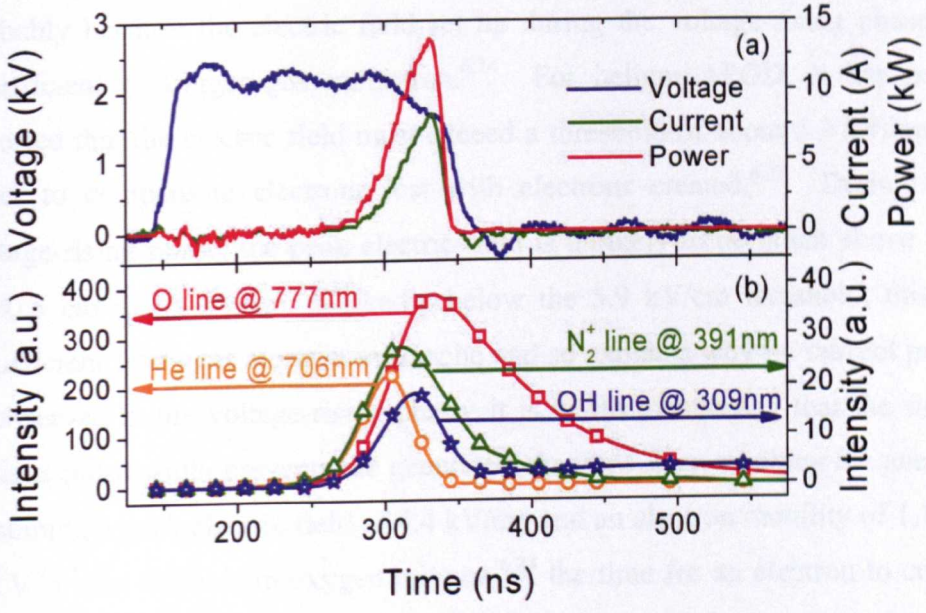

Fig 6-18: Electrical and time-resolved optical data for a pulsed barrier-free helium APGD.

Figure 6-18a shows electrical measurements of a 4 kHz sub-microsecond pulsed APGD. The mean peak voltage is Vp = 2.4 kV, the peak discharge current is Ip = 8.4 A, and the peak dissipated power is 13.7 kW. Similar to those reported previously,[6.24] nanosecond exposure images suggest that the pulsed atmospheric plasma was spatially uniform without unstable streamers and its spatial structure had a clear sheath region (image shown in figure 6-6). Compared to sinusoidal atmospheric DBD and indeed radio-frequency APGD, the pulsed APGD can be operated at very high peak power density of 1 – 5 kW/cm^3 without inducing any significant temperature rise.

Figure 6-18a shows that its voltage pulse has a rise time of 18 ns and a fall time of 55 ns, both measured between 10% and 90% of the peak voltage, and a pulse width of 190 ns measured as the full width at half maximum. The current pulse has a rise time of 43 ns, a fall time of 10 ns, and a pulse width of 30 ns. With a voltage rise time of 18 ns and a rig capacitance of 1.1 pF, the peak displacement current is 0.15 A and much less than the peak current of 8.4 A. Therefore, the discharge current shown in figure 6-18a is likely to be conduction current.

The discharge current pulse occurs in the voltage-falling phase, most probably because the electric field set up during the voltage-rising phase is insufficient to trigger gas ionization.[6.24] For helium APGD, it has been reported that the electric field must exceed a threshold of about 5.9 kV/cm in order to compensate electrons lost with electrons created.[6.25] During the voltage-rising phase, the peak electric field is unlikely to be much above 2.4 kV/0.5 cm = 4.8 kV/cm. Markedly below the 5.9 kV/cm threshold, this is insufficient to trigger electron avalanche and so explains why no current peak is observed in the voltage-rising phase. It is worth mentioning that the short voltage pulse width prevents the generated electrons from reaching the anode. Assuming a peak electric field of 4.4 kV/cm and an electron mobility of 1,132 $cm^2V^{-1}s^{-1}$ for the helium-oxygen mixture,[6.24] the time for an electron to cross the 0.5 cm electrode gap is found to be 100 ns – about 53% of the voltage pulse width. During the initial period of 100 ns, the generated electrons are trapped in the electrode gap and contribute to the build-up of space charges. This charge-accumulating period of 100 ns is similar to the time difference of 127 ns in the onset instant between the voltage and current pulses. In other words, a large portion of the voltage pulse is spent to build up space charges so that the maximum electric field is raised above the breakdown electric field to trigger electron avalanche.

The above discussion is supported by results of optical emission spectroscopy. It is known that the N_2^+ emission line at 391 nm line is strongly influence be excited helium species and as such it contains the optical

signature of helium metastables and molecular helium ions.[6.16] It is also known that the 706 nm line is linked to either energetic electrons or He^{2+} and low energy electrons.[6.16] Therefore, the temporal profiles of the 391 nm and 706 nm lines reflect that of either energetic electrons or molecular helium ions. As the most numerous ions in helium APGD are molecular helium ions,[6.26] these temporal profiles follow the profile of space charges. As shown in figure 6-18b, emission line intensities at 391 nm and 706 nm are negligible in the first 122 ns of the voltage pulse and so initially there are very few space charges in the gas gap to sustain a large current. The negligible emission period of 122 ns agrees very well with onset time of 127 ns.

Figure 6-18b also shows a pulse of the OH line at 309 nm and a pulse of the oxygen atom line at 777 nm, with their pulse width being 60.0 ns and 106.3 ns respectively. When compared to an atmospheric DBD using the same electrode unit, the same background gas and a very similar peak voltage, the intensities of the 307 nm and 777 nm emission lines in the pulsed APGD are up to 10 times greater (data not shown). Therefore, a distinct character of sub-microsecond pulsed APGD is their ability to produce high fluxes of reactive plasma species such as oxygen atoms and OH radicals. At a repetition frequency of 4 kHz, the half period is 125 μs and much longer than the electron transition time of 100 ns across the electrode gap. Therefore, electrons generated in one voltage pulse are most certainly lost to the electrodes and through ionic recombination well before the next voltage pulse. This suggests that reactive plasma species such as oxygen atoms and OH radicals are generated as a train of sharp and independent bursts. It is conceivable that such sub-microsecond windows of high-flux reactive species could facilitate surface modification with spatial or/and temporal selectivity. For example, surface pattern with sharp boundary could be realized by moving a pulsed APGD jet over a surface at a speed that translates the time scale of the windows to spatial dimensions of the surface pattern.

To enhance the production of reactive plasma species, the peak applied voltage can be varied so as to alter the discharge current. As the peak applied

voltage increases, figure 6-19 shows that the peak discharge current increases but the voltage pulse width decreases. The peak current is very high, ranging from 3 A to 6 A, and corresponds to a current density of 0.5 – 1.0 A/cm^2. It is probable that such a high discharge current could substantially increase electrical conductivity of the gas to short-circuit the gas gap, leading to a premature shortening of the voltage pulse.

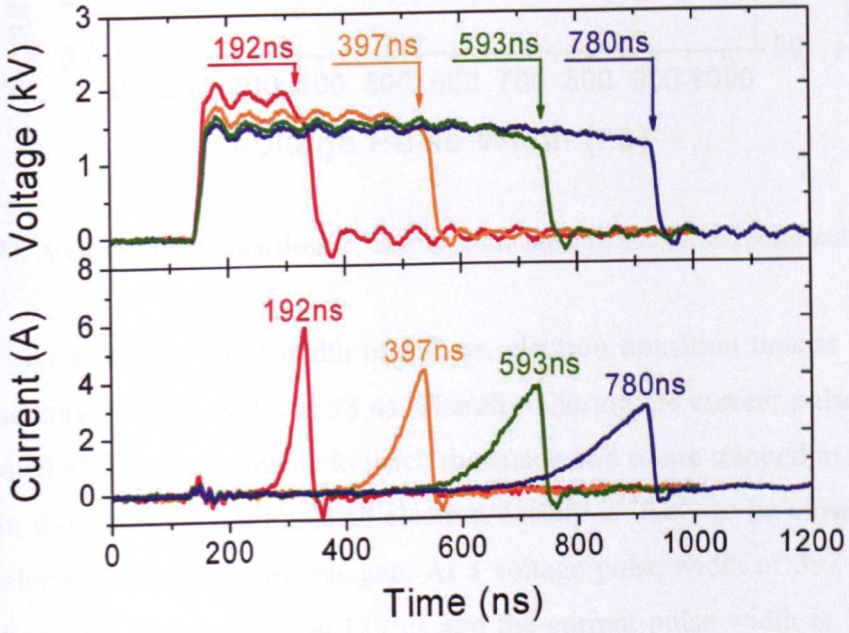

Fig 6-19: Applied voltage and discharge current traces for varying pulse widths.

To study this further, the current pulses in figure 6-19 were integrated to obtain the total accumulated electron density generated during one voltage pulse. This is shown in figure 6-20 together with the electron transition time across the electrode gap and the current pulse width, all as a function of voltage pulse width. While the voltage pulse width varies by a factor of more than 4, the total accumulated electron density varies only by a factor of 1.7 suggesting similar gas conductivity among all 4 cases.

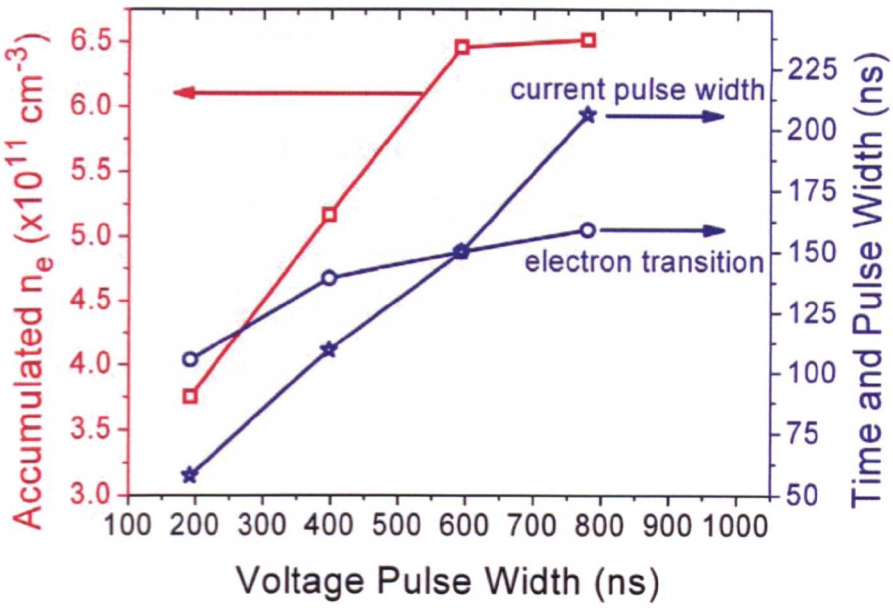

Fig 6-20: Accumulated electron density, electron transition time and current pulse width.

At a voltage pulse width of 192 ns, electron transition time is 106 ns and the current pulse width is 58 ns. Therefore during the current pulse, most generated electrons are unable to reach the anode and so are trapped in the gas gap. In this case, the accumulated electron density is likely to be close to the peak electron density in the gas gap. At a voltage pulse width of 397 ns, the transition time for electrons is 139 ns and the current pulse width is 109 ns. As the electron transition time is similar to the current pulse width, many generated electrons are trapped in the gas gap but the trapped electrons are proportionally fewer than those in the 192 ns voltage pulse width case. As a result, the peak electron density achieved during the current pulse is smaller than the accumulated electron density of 5.1×10^{11} cm^{-3} in figure 6-20. As the voltage pulse width increases to 593 ns, both the electron transition time and the current pulse width become 150 ns. This suggests that a significant proportion of generated electrons are now lost to the electrodes and the peak electron density reached during the current pulse is likely to be markedly smaller than the accumulated electron density of 6.5×10^{11} cm^{-3}. This difference is greater in the case of the 780 ns voltage pulse, for which electron transition time is 159 ns substantially less than the current pulse width 206 ns.

Therefore as the voltage pulse width increases, the peak electron density achieved during a current pulse becomes progressively less than its corresponding accumulated electron density in figure 6-20. This suggests that the peak electron density and hence and the maximum electrical conductivity of the gas gap remain relatively unchanged during the current pulse for all four cases of figure 6-20. It is therefore highly likely that narrow voltage pulse widths observed at high applied voltages are caused by plasma-induced short-circuiting of the gas gap.

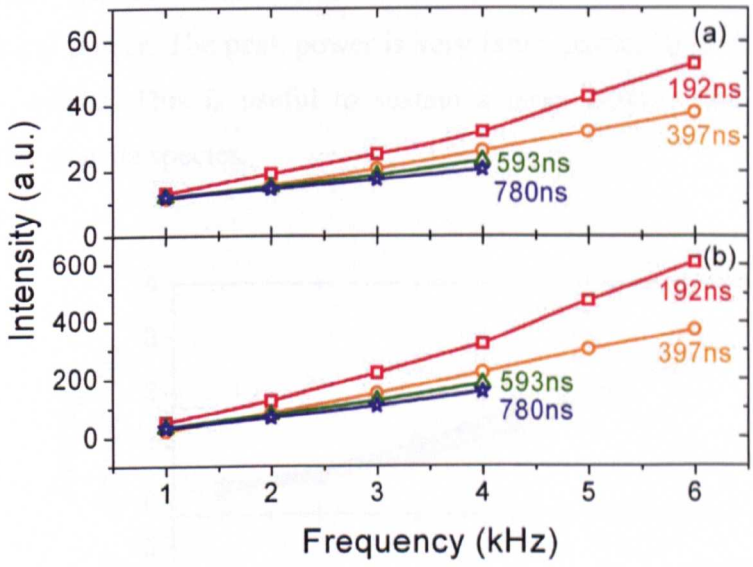

Fig 6-21: Effect of repetition rate and pulse width on emission intensity of a)OH at 309nm and b)atomic oxygen at 777nm.

Figure 6-21 shows that the optical emission intensity of the OH emission line at 309 nm and atomic oxygen line at 777 nm for the four different voltage pulse widths shown in figure 6-19. At a fixed frequency, stronger emission intensity is achieved with shorter pulse widths that is linked to a large peak current. At a given voltage pulse width, the emission intensity increases with increasing frequency. At a voltage pulse width of 192 ns, the 777 nm line intensity increases by a factor of 12 as the frequency increases from 1 to 6 kHz. A high frequency leads to more frequent production of sharp bursts of reactive plasma species and so to their greater accumulation over a

given time period. Also at long voltage pulse widths of 593 ns and 780 ns, stable APGD are achieved at frequencies up to 4 kHz. If the voltage pulse width is reduced to below 400 ns, stable APGD can be extended to above 6 kHz.

To place the above comparison in the context of energy budget, the average dissipated power is shown in figure 6-22 to increase with the frequency but change little with voltage pulse width. Combining this result with those in figure 6-21, it is clear that production of oxygen atoms and OH radicals can be increased substantially without consuming much more electrical power. The peak power is very large, particularly with short voltage pulse widths. This is useful to sustain a large current and a large flux of reactive plasma species.

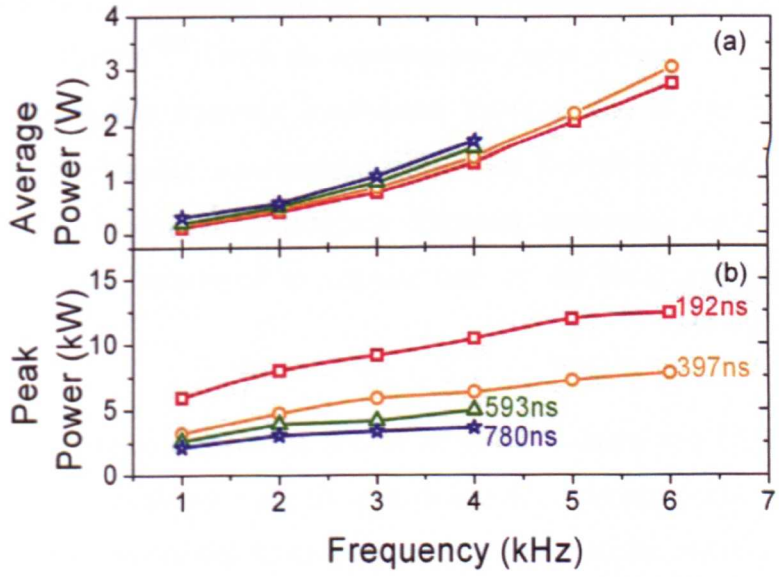

Fig 6-22: Effect of repetition frequency on average and peak power.

Curiously in figure 6-22b, the peak power varies with repetition frequency, this is unexpected. The duty cycle of the applied voltage is so low that it is assumed that pulses can be treated in isolation, such that one pulse is completely uninfluenced by the previous pulse. This is obviously not the case, as the voltage is fixed and the peak power increases with increasing frequency

it follows that the discharge current must increase. One possible explanation could be at higher repetition rates electrons from the previous discharge do not have time to completely recombine and hence add to the discharge current of the next pulse.

6.7 *Breakdown mechanism in pulsed APGD*

Plasma breakdown, the process by which a neutral gas becomes ionised is one of the fundamental processes in plasma physics. It occurs in every plasma at the time of ignition and is a highly transient process involving multiplication of electrons in avalanches and moving ionisation fronts. Although plasma breakdown has been studied for many years, many aspects remain poorly understood and it is still an area of active research. As mentioned in the introductory chapter, breakdown into a uniform glow discharge in low pressure can be accurately described with the Townsend breakdown theory.[6.27] From an experimental point of view it is difficult to capture the highly transient breakdown process, due to the limited time resolution of available experimental techniques. Recent advances in electrical and optical techniques mean that new diagnostic techniques and experimental methods can be employed to capture one of the most important plasma processes.

This section details the use of an iCCD camera and OES system to investigate the breakdown phenomena in sub-microsecond pulsed barrier-free APGD. The experimental setup consisted of two circular metallic electrodes with a diameter of 3cm and a separation of 3mm housed in a Perspex container. Helium was flown into the electrode enclosure at a rate of 5SLM. Voltage pulses were applied at a rate of 3 kHz with a pulse width of approximately 350ns. Figure 6-33 shows the applied voltage and discharge current. As the rise and fall times of the voltage are <20ns a substantial amount of displacement current is seen on the rising and falling edges of the pulse. The average maximum applied voltage is approximately 1450V, as the electrode separation is 3mm this produces an electric field of 4.8kV/cm, rather

high compared to those measured in the previous section; this explains the large 9.1A discharge current, equivalent to a current density of 1.27A/cm^2.

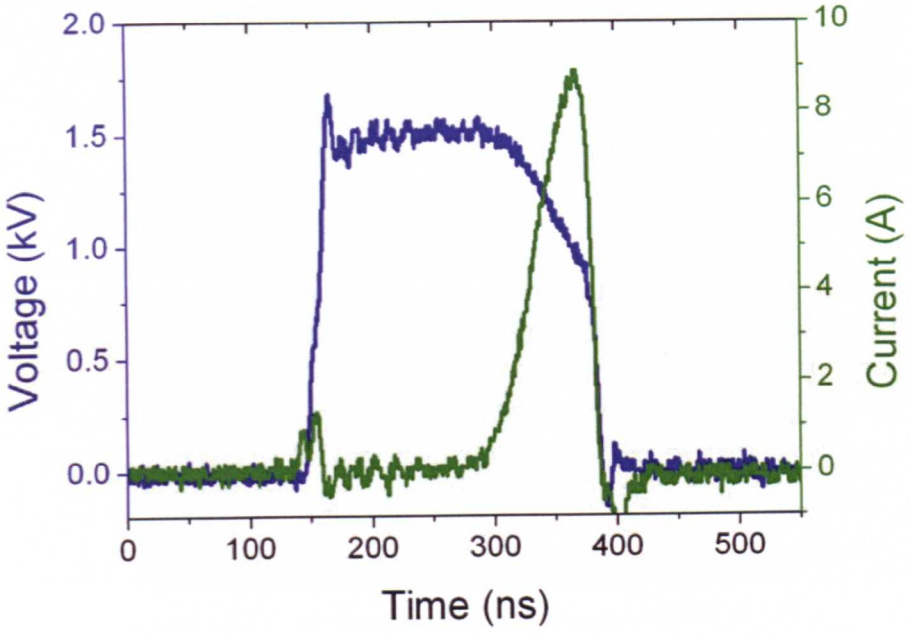

Fig 6-23: Current and voltage trace for pulsed APGD in 3mm gap.

By triggering the iCCD camera with a 1ns exposure time at regular intervals over the applied voltage period it is possible to get time, space, and intensity resolved data showing the evolution of the discharge. As discussed previously the breakdown mechanism should be similar to that in a DC discharge and can be characterised as Townsend breakdown. The high applied voltage causes free electrons within the gap to ionise gas molecules by electron impact, the result is a multiplication of electrons and ions within the gap. As the mobility of ions is substantially lower than that of electrons a large concentration of ions forms in front of the cathode leading to the formation of a cathode fall or negative glow region. Figure 6-24 shows images taken with an iCCD over the applied voltage period of 260ns to 300ns, it is worth noting that very little current flows during this period. The intensity of the light emitted from the discharge is very low and requires a substantial gain to be introduced by the camera.

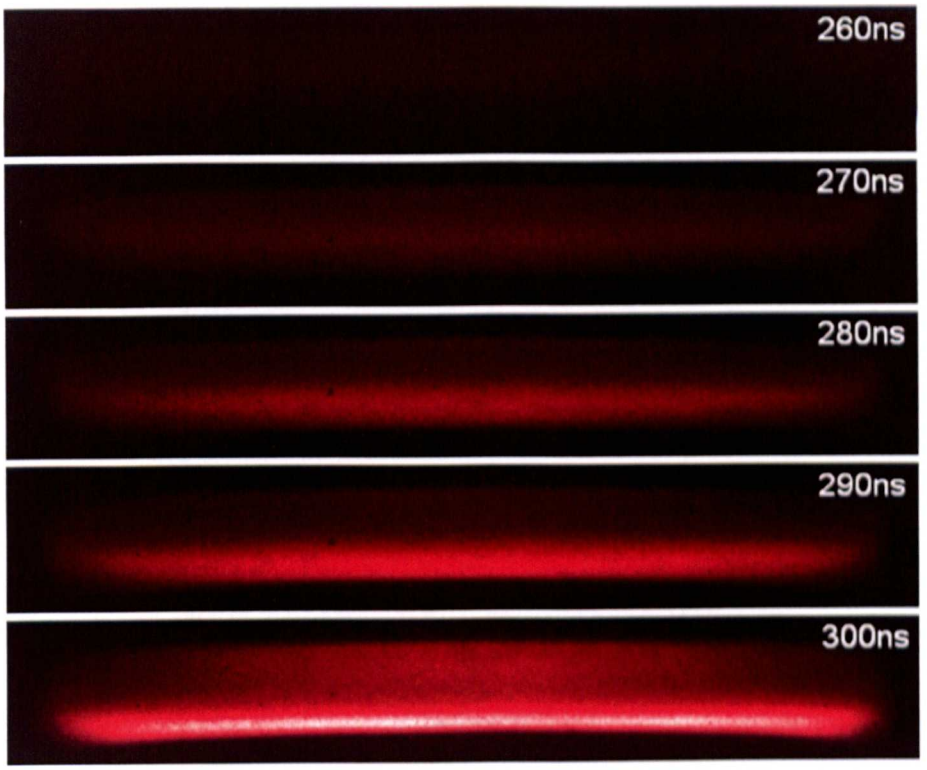

Fig 6-24: Images taken with a 1ns exposure time at 10ns intervals (260ns to 300ns), iCCD gain set at x100.

In figure 6-24 the cathode is at the bottom of each image and the anode at the top. The first image shows a very low intensity (barely visible) glow near the anode, as the discharge evolves this becomes brighter and descends toward the cathode and appears as an ionisation wave front. Around 50ns later ions reach the cathode and a bright negative glow region begins to form. It is worth noting that should it have been possible to increase the gain of the camera further it is likely that the gradual formation of ions within the gap would have been observable from the very start of the applied voltage pulse. The accumulation of space charge and formation of a negative glow region are highly consistent with Townsend breakdown theory.

To further our understanding, time resolved OES was employed to determine the spectral content of the discharge over the period 250-300ns. Again, a 1ns exposure time is used and the spectrum is recorded at 5ns intervals over the applied voltage pulse. Figure 6-25 shows the emission spectrum at 265ns taken with a 1ns exposure time, it is clear to see only one

distinctive emission line; it is no coincidence that this is the helium metastable emission at 706nm which is known to be an indicator of energetic electrons.[6.16]

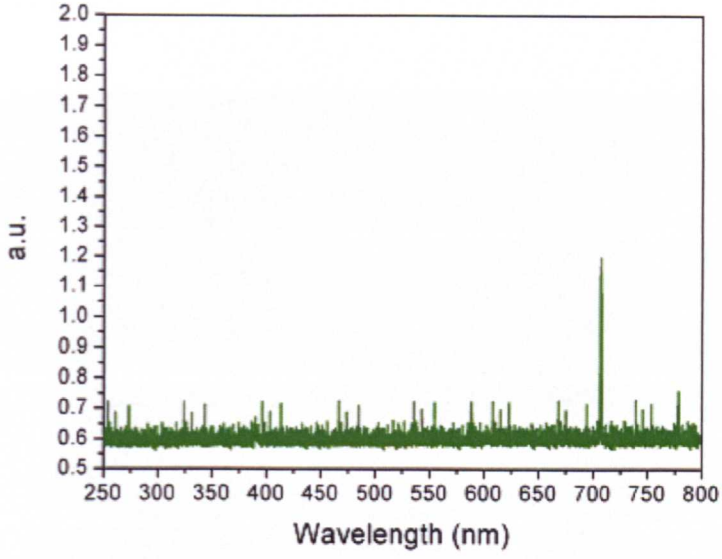

Fig 6-25: Emission spectrum of discharge recorded at 265ns. A single emission line observed at 706nm, indicating Helium metastables.

Throughout the time period 250-300ns, the only significant emission is from ionic nitrogen and excited helium species. The two most dominant lines are the helium metastable at 706 and ionic nitrogen at 391, these are plotted as a function of time in figure 6-26

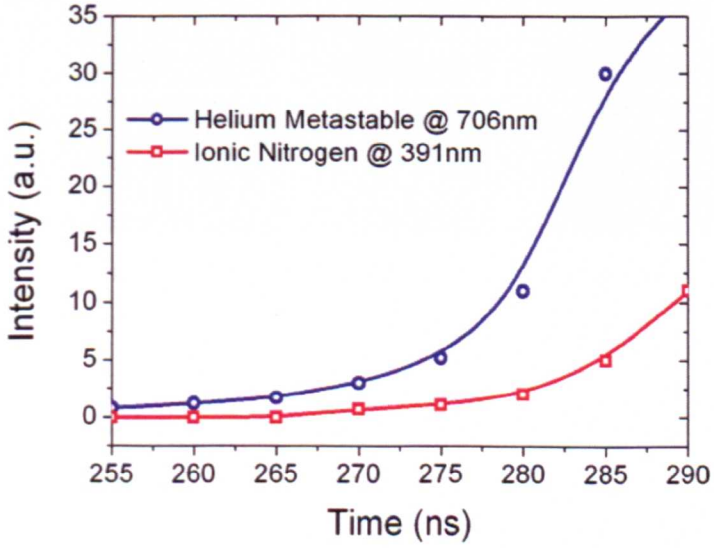

Fig 6-26: OES of helium metastable (706nm) & ionic Nitrogen (391nm) from 250ns to 290ns.

Figure 6-27 shows a sequence of images taken at 330ns to 400ns of the applied voltage shown in figure 6-23. The gain on the camera is reduced by a factor of 10 compared to the gain used in the previous images shown in figure 6-24.

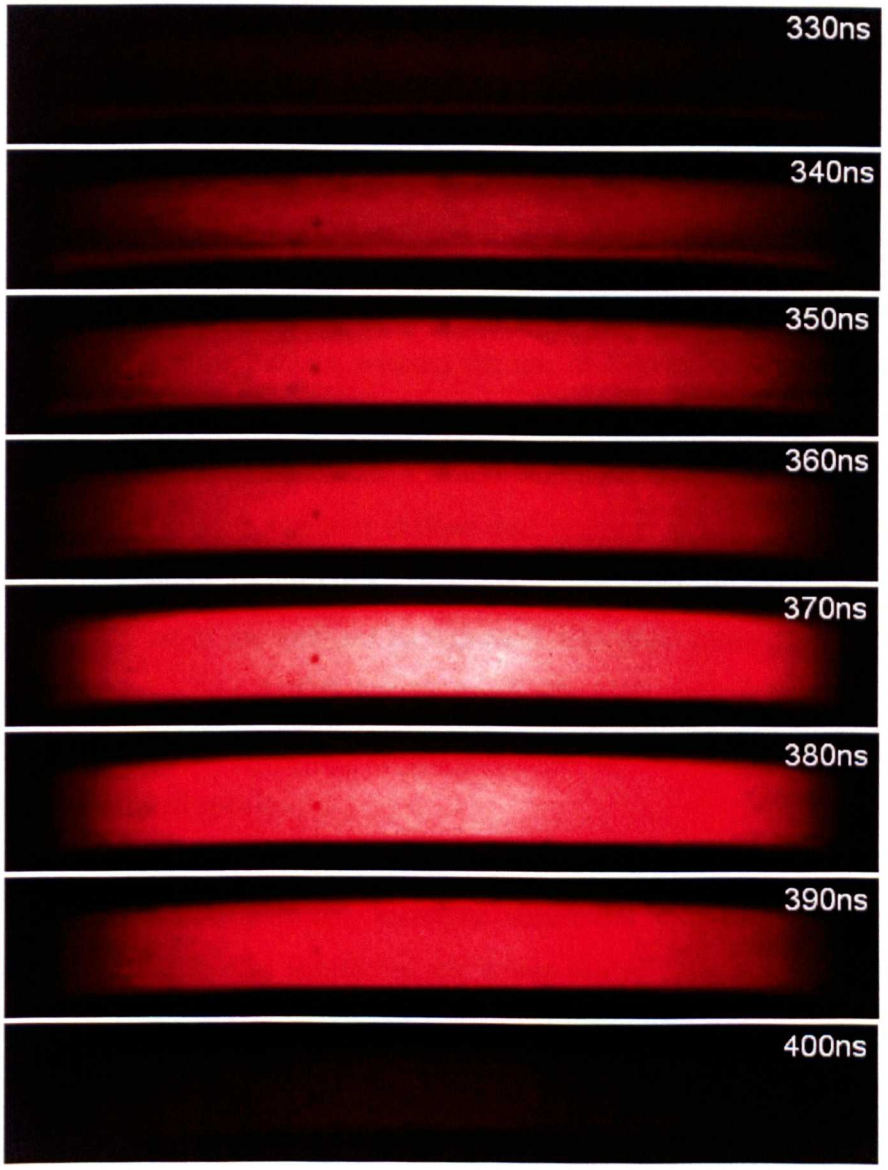

Fig 6-27: Images taken with a 1ns exposure time at 10ns intervals (330ns to 400ns) , iCCD gain set at x10.

Peak intensity is observed at 370ns, this is slightly before the maximum discharge current, as noted previously, peak emission coincides with peak dissipated power (almost 10kW). As the current reduces rapidly the discharge also diminishes in intensity. It is worth pointing out that if the

camera is returned to a high gain setting then it is possible to see light emission from the discharge for many hundreds of nanoseconds after the current pulse. Observations of the afterglow spectra indicate that the discharge is rich in oxygen and OH emission but there is very little emission from helium metastables and ionic nitrogen. This suggests that the discharge has very few energetic electrons and the light emission is related to the lifetimes of the excited species created during the applied voltage pulse.

6.8 Summary

This chapter has detailed a novel technique for the generation of APGD at kilohertz frequencies without the use of dielectric barriers. Using a home-built pulse generator capable of delivering sub-microsecond high voltage pulses it has been shown that stable APGD can be generated between two metallic electrodes which is diffuse and uniform over a wide range of operating parameters. Using OES it was determined that the gas temperature was similar to that of the ambient background. Electrical measurements show that pulsed barrier-free APGD has an unusually high current density which translates into a high electron density and consequently the generation of a high flux of excited species.

A comparison between kilohertz sinusoidal excitation and pulsed barrier-free excitation was conducted and it was shown that pulsed barrier-free APGD consumed less power than an equivalent kHz DBD and produced more atomic oxygen species. To become a widely used technology, pulsed barrier free APGD must be able to rival RF-APGD in terms of reactivity. It was shown through careful tailoring of the applied voltage pulse that it was possible to produce more atomic oxygen than an equivalent RF discharge. Other benefits of pulsed APGD over RF APGD included significant savings in power consumption and reduced gas temperatures, both highly attractive characteristics when large-volume plasma processing is considered.

A consequence of introducing a large voltage off period is that the nature of the discharge becomes transient and not steady state. Because of this, the breakdown process is of significant importance as it occurs every time a voltage pulse is applied. The breakdown process of pulsed barrier-free APGD was examined using nanosecond imaging and time resolved OES. It was determined that the process is very similar to that of a DC discharge, involving the accumulation of space charge and moving ionisation fronts. Nanosecond exposure images showed very clearly that the discharge structure consisted of a negative glow region above the cathode and a less intense bulk region. After each voltage pulse the intensity of the light emission was shown to diminish slowly, as there is no applied voltage or discharge current this implies that the emission is due to the lifetime of the excited species created.

In summary, the work detailed within this chapter shows that it is possible to create a stable APGD over a wide range of applied voltages at kilohertz frequencies using sub-microsecond pulsed excitation. The characteristics of the discharge were found to be very favourable compared to conventional kHz, and MHz excitation methods.

References

[6.1] Roth J.R, 'Industrial plasma engineering: I Principals' IOP, 1995.

[6.2] Kanazawa S, Kogoma S, Moriwaki T, Okazaki S, 'Stable glow plasma at atmospheric pressure', Journal Of Physics D-Applied Physics, Vol.21, Iss.5, pp.838-840, 1988.

[6.3] Okazaki S, Kogoma M, Uehara M, Kimura Y, 'Appearance Of Stable Glow-Discharge in Air, Argon, Oxygen AND Nitrogen at atmospheric-pressure using a 50-Hz source' Journal Of Physics D-Applied Physics, Vol.26, Iss.5, pp.889-892, 1993.

[6.4] Laroussi M, Alexeff I, Richardson J.P, Dyer F.F, 'The resistive barrier discharge', IEEE Transactions On Plasma Science, Vol.30, Iss.1, pp.158-159, Part.1, 2002.

[6.5] Baars-Hibbe L, Schrader C, Sichler P, Cordes T, Gericke K.H, Buttgenbach S, Draeger S, 'Micro-structured electrode arrays: high-frequency discharges at atmospheric pressure - characterization and new applications' VACUUM, Vol.73, Iss.3-4, pp.327-332, 2004.

[6.6] Shi J.J, Deng X.T, Hall R, Punnett J.D, Kong M.G, 'Three modes in a radio frequency atmospheric pressure glow discharge', Journal of Applied Physics, Vol.94, Iss.10, pp.6303-6310, 2003.

[6.7] Moon S.Y, Choe W, Kang B.K 'A uniform glow discharge plasma source at atmospheric pressure', Applied Physics Letters, Vol.84, Iss.2, p.p.188-190, 2004.

[6.8] Shi J.J, Kong M.G, 'Expansion of the plasma stability range in radio-frequency atmospheric-pressure glow discharges', Applied Physics Letters, Vol.87, Iss.20, No.201501, 2005.

[6.9] Radu I, Bartnikas R, Czeremuszkin G, Wertheimer M.R, 'Diagnostics of dielectric barrier discharges in noble gases: Atmospheric pressure glow and pseudoglow discharges and spatio-temporal patterns', IEEE Transactions On Plasma Science, Vol.31, Iss.3, pp.411-421, 2003.

[6.10] Kong M.G, Deng X.T, 'Electrically efficient production of a diffuse nonthermal atmospheric plasma', IEEE Transactions On Plasma Science, Vol. 31, Iss.1, pp.7-18, Part 1, 2003.

[6.11] Deng X.T, Kong M.G, 'Frequency range of stable dielectric-barrier discharges in atmospheric He and N-2', IEEE Transactions On Plasma Science, Vol.32, Iss.4, pp.1709-1715, Part 3, 2004.

[6.12] Laroussi M, Lu X, Kolobov V, Arslanbekov R, 'Power consideration in the pulsed dielectric barrier discharge at atmospheric pressure', Journal of Applied Physics, Vol.96, Iss.5, pp.3028-3030, 2004.

[6.13] Walsh J.L, Shi J.J, Kong M.G, 'Contrasting characteristics of pulsed and sinusoidal cold atmospheric plasma jets', Applied Physics Letters, Vol.88, Iss.17, No.171501, 2006.

[6.14] Moravej M, Yang X, Hicks R.F, Penelon J, Babayan S.E, 'A radio-frequency nonequilibrium atmospheric pressure plasma operating with argon and oxygen', Journal of Applied Physics, Vol.99, Iss.9, No.093305, 2006.

[6.15] Deng X.T, Shi J.J, Shama G, Kong M.G, 'Effects of microbial loading and sporulation temperature on atmospheric plasma inactivation of Bacillus subtilis spores', Applied Physics Letters, Vol.87, Iss.15, No.153901, 2005.

[6.16] Nersisyan G, Graham W.G, 'Characterization of a dielectric barrier discharge operating in an open reactor with flowing helium', Plasma Sources Science & Technology, Vol.13, Iss.4, pp.582-587, 2004.

[6.17] Deng X.T, Shi J.J, Kong M.G, 'Physical mechanisms of inactivation of Bacillus subtilis spores using cold atmospheric plasmas', IEEE Transactions On Plasma Science, Vol.34, Iss.4, pp.1310-1316, Part 2, 2006.

[6.18] Massines F, Gouda G, 'A comparison of polypropylene-surface treatment by filamentary, homogeneous and glow discharges in helium at atmospheric pressure', Journal Of Physics D-Applied Physics, Vol.31, Iss.24, pp.3411-3420, 1998.

[6.19] Babayan S.E, Jeong J.Y, Tu V.J, Park J, Selwyn G.S, Hicks R.F, 'Deposition of silicon dioxide films with an atmospheric-pressure plasma jet', Plasma Sources Science & Technology, Vol.7, Iss.3, pp.286-288, 1998.

[6.20] Yu Z.Q, Hoshimiya K, Williams J.D, Polvinen S.F, Collins G.J, 'Radio-frequency-driven near atmospheric pressure microplasma in a hollow slot electrode configuration', Applied Physics Letters, Vol.83, Iss.5, pp.854-856, 2003.

[6.21] Shi J.J, Kong M.G 'Evolution of discharge structure in capacitive radio-frequency atmospheric microplasmas', Physical Review Letters, Vol.96, Iss.10, No.105009, 2006.

[6.22] Roth J.R, 'Potential industrial applications of the one atmosphere uniform glow discharge plasma operating in ambient air', Physics Of Plasmas, Vol.12, Iss.5, No.057103, 2005.

[6.23] Vleugels M, Shama G, Deng X.T, Greenacre E, Brocklehurst T, Kong M.G, 'Atmospheric plasma inactivation of biofilm-forming bacteria for food safety control', IEEE Transactions On Plasma Science, Vol.33, Iss.2, pp.824-828, Part 2, 2005.

[6.24] Walsh J.L, Shi J.J, Kong M.G, 'Submicrosecond pulsed atmospheric glow discharges sustained without dielectric barriers at kilohertz frequencies', Applied Physics Letters, Vol.89, Iss.16, No.161505, 2006.

[6.25] Shi J.J, Kong M.G, 'Large-volume and low-frequency atmospheric glow discharges without dielectric barrier', Applied Physics Letters, Vol.86, Iss.9, No.091502, 2005.

[6.26] Shi J.J, Kong M.G, 'Mechanisms of the alpha and gamma modes in radio-frequency atmospheric glow discharges', Journal of Applied Physics, Vol.97, Iss.2, No.023306, 2005.

[6.27] Massines F, Gherardi N, Naude N, Segur P, 'Glow and Townsend dielectric barrier discharge in various atmosphere', Plasma Physics and Controlled Fusion, Vol.47, Sp.Iss.SI, Suppl.12B, pp.B577-B588, 2005.

[6.28] Liu D.W, Shi J,J, Kong M.G, 'Electron trapping in radio-frequency atmospheric-pressure glow discharges', Applied Physics Letters, Vol.90, Iss.4, No.041502, 2007.

7 Applications of pulsed APGD

7.1 Introduction

Throughout the preceding chapters it is hoped that the reader has gained a clear insight into the many benefits of pulsed excitation of atmospheric pressure glow discharges. In order for pulsed excitation to gain widespread acceptance as a viable plasma generation technique it must perform as well, if not better, than current plasma generation techniques employed in real-world applications. This Chapter is devoted to several applications where it is shown that pulsed excitation offers a significant advantage over conventional excitation mechanisms.

Section 7.2 explores the use of a sub-microsecond pulsed plasma jet for the removal of protein contamination on surgical instruments. It has been shown that gas discharges offer an efficient means of removing microscopic protein fragments that remain attached to surgical instruments after the conventional decontamination process. Such proteins are thought to be the main contributor to the transmission of Creutzfeldt-Jakob disease (CJD) betweens humans. It is shown that pulsed excitation almost doubles the rate of protein removal compared to a comparable sinusoidal excited plasma jet.

Section 7.3 details the use of barrier-free pulsed APGD employing helium-argon gas mixtures for the production of intense ultraviolet radiation. Compact and efficient light sources, especially those emitting in the UV region, are of intense industrial interest due to their potential for biomedical diagnostics and photochemical processing. It is observed that a reduction in

excitation pulse width increases ionisation efficiency and consequently enhances UV production.

Section 7.4 highlights the use of a nanosecond pulsed barrier discharge for the uniform processing of polymeric materials. By reducing pulse widths such that instabilities have insufficient time to develop it is possible to generate a uniform and diffuse discharge in ambient air over a large area. Such discharges are essential for the processing of polymeric films on an industrial scale.

7.2 Plasma sterilisation of surgical instruments

The use of ionised gas as a bacterial decontamination agent was first proposed in the late 1960's,[7.1] however at that time the technology required to produce large scale gas discharges was largely unknown. Over the past decade plasma decontamination technology has attracted serious attention due to the ease at which large scale, cold gas discharges can be generated. The vast majority of studies reported thus far investigate the effect of plasma upon various bacteria, whilst this is of considerable importance it must be noted that it is not just bacterial contamination that poses a risk to humans but also that of protein.

7.2.1 Decontamination of surgical equipment using pulsed APGD

Prion proteins are widely regarded as being responsible for the transmission of Creutzfeldt-Jakob disease, yet are extremely resistant to all current hospital decontamination procedures.[7.1] As a consequence the strategy of single-use surgical instruments is often employed at an unsustainably high cost to hospitals. Several attempts have been made to remove protein contamination using ionising radiation or wet chemical processes, however such techniques are often costly and pose a serious environmental hazard.[7.2] The application of APGD to remove protein from surgical instruments

represents one of the most promising decontamination technologies due to its ease of application and limited environmental impact.

Recent studies have shown plasma decontamination is capable of reducing protein contamination on stainless steel surfaces down to a femto mole level,[7.1,7.3] such small amounts significantly reduce the potential risk of protein contamination and infection. This study only focuses upon the difference in protein removal rate between a conventional kHz sinusoidal source and a pulsed source. While it is shown that the pulsed discharge does remove significantly more protein, the plasma properties have not yet been optimised hence the amount of protein removed from the surface is not comparable with those reported in reference 7.1 and 7.3.

7.2.2 Experimental procedure and results

In this investigation sinusoidal and pulsed excitation sources were used to generate an atmospheric pressure plasma plume in a dielectric tube, the ionised gas was allowed to flow into the ambient air thus introducing excited nitrogen and oxygen species. In order to perform a systematic comparison between pulsed and sinusoidal excitation the operating conditions in each case were fixed at a similar frequency, and a peak magnitude of 10kV (+/-10kV in the sinusoidal case). The pulsed source had a pulse width of 200ns, over 800 times less than a half cycle of the applied sinusoidal voltage. As the applied voltage was present for a significantly shorter time in the pulsed case the average sustaining power was substantially lower, approximately one tenth the level required for sinusoidal excitation.

Two methods of protein detection have been employed to enable the effect of plasma to be observed. The simplest technique is the use of a scanning electron microscope (SEM) coupled with electron energy dispersive x-ray analysis (XDS), this gives a qualitative measure of the effects of plasma treatment on protein samples. Figure 7-1 shows an SEM image of a real

surgical instrument that is deemed to be clean and due to be used upon the next patient. The high magnification of the SEM allows microscopic contamination to be observed, clearly, there is some kind of organic material still attached to the surface after the traditional decontamination process. The XDS functionality allows a rapid analysis of the elements which make up the surface, shown in figure 7-2. It is known that stainless steel usually contains less than 1% carbon, this is in stark contrast to the results of the XDS analysis shown in 7-2, carbon is by far the most dominant element, appearing to be many times greater than iron, sulphur or chromium. The only possible explanation for these results is that the structure observed in figure 7-1 is an organic material, comprised of carbon-oxygen containing amino acids,[7.4] that is attached to the surface which was not removed by the standard decontamination procedure. The size of the protein fragment is approximately 150μm x 50μm which is a substantial amount and is likely to be capable of transmitting disease from one patient to the next.

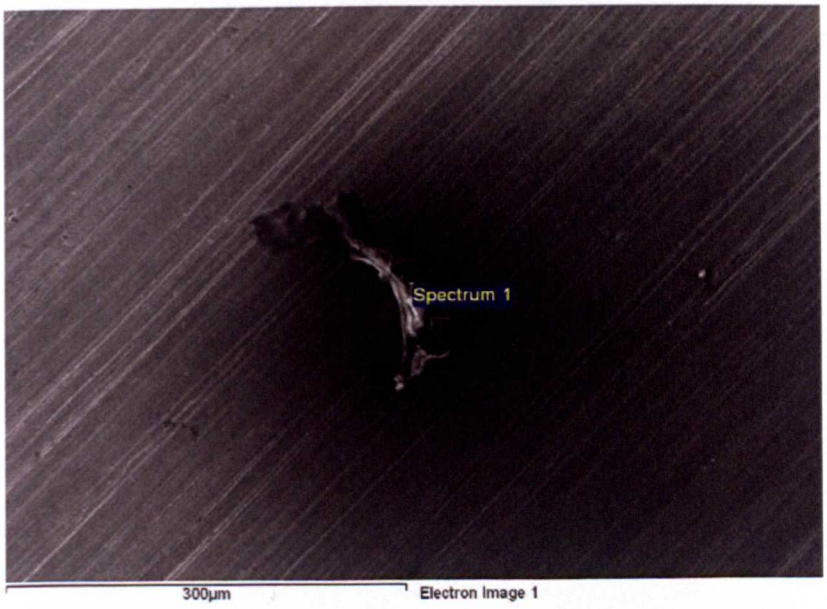

Fig 7-1: SEM image of contaminant on surgical forceps after traditional decontamination procedure.

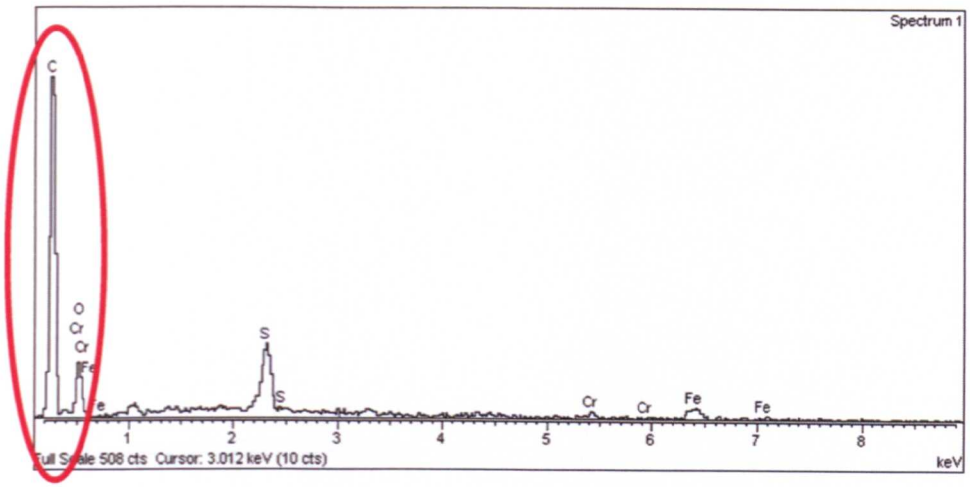

Fig7-2: XDS analysis of surface composition of surgical forceps.

Using this method of protein detection, both pulsed and sinusoidally excited plasma produced similar results. Figure 7-3 shows an SEM image of the surgical forceps following 60 seconds of exposure to plasma, it is clear that the bulk of the organic contamination has been removed. This is confirmed using XDS analysis, shown in figure 7-4. No longer is the surface composition dominated by carbon; iron and chromium clearly dominate which is much more representative of the composition of stainless steel. The amount of carbon remaining on the surface is undetectable using the XDS system suggesting a higher resolution detection technique is required.

Fig 7-3: SEM image of plasma treated surgical forceps.

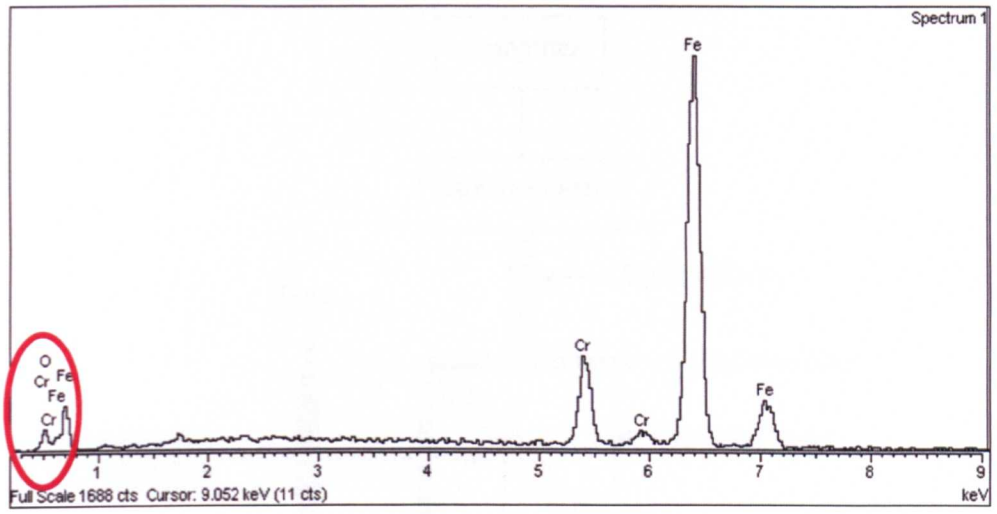

Fig 7-4: XDS analysis of plasma treated surgical forceps.

In order to enhance the comparison between pulsed and sinusoidal protein removal rates a quantitative means of determining the amount of protein residue remaining on the surface was necessary. Whilst standard biology laboratory methods are capable of measuring protein samples in solution they are not applicable to residue on a surface. A new method, based on laser induced fluorescence (LIF), was developed within the group.[7.3] Essentially, a model protein (Bovine Serum Albumin, BSA) is labelled with a fluorescent marker (FITC, fluorescein isothiocyanate) the marker emits light at 530nm when excited at 488nm. Once a known amount of tagged protein is dried on to the stainless steel surface it is possible to determine the amount of protein removed during plasma exposure using the reduction in fluorescence of the marker. Figure 7-5 shows a schematic of the protein detection system used, the excitation signal was provided by a laser diode (Ocean Optics LS 475) with a signal bandwidth of 460-490nm. The optical configuration of the system is of paramount importance and several wavelength filters are employed to ensure a high degree of accuracy. Calibration of the results with a photon counting fluorescence spectrometer confirmed reliable measurements of protein residue can be made down to 1.4 femtomole/mm^2.

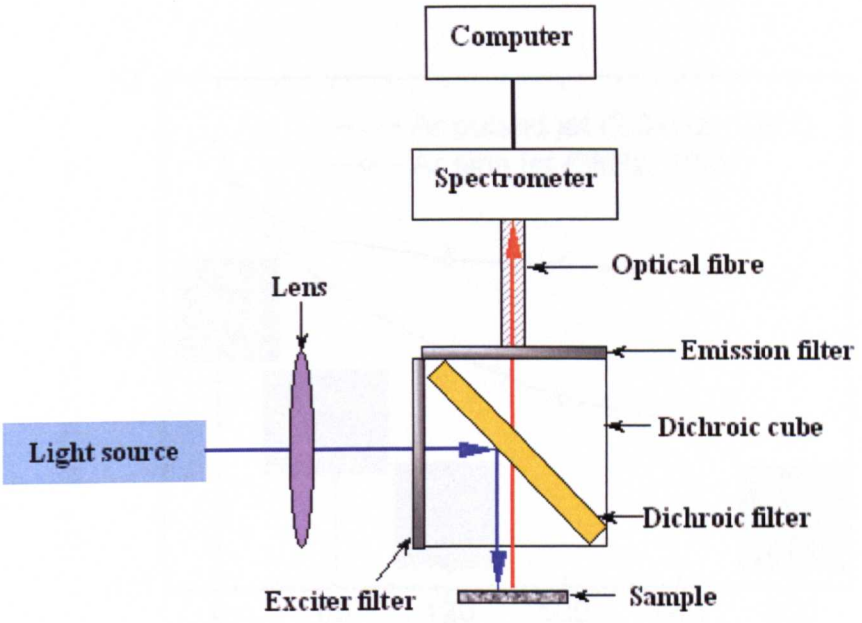

Fig 7-5: Schematic of laser induced fluorescence system used for surface protein measurement.

Figure 7-6 shows the removal rate of the model protein BSA tagged with an FITC marker from a stainless steel disc. In this investigation Argon was used as the working gas, results obtained using helium showed a similar trend (not shown). For many practical applications the use of helium is prohibitively expensive, conversely argon is one of the least expensive inert gases thus making it an attractive option for any commercial plasma application. From Figure 7-6 it is seen that the original concentration of protein on the disc was 15 picomole, after 300 seconds of treatment with the sinusoidal source the amount of protein was reduced to 10.8 picomole, representing a 28% reduction. After an exposure of 300 seconds to the pulsed plasma the amount of protein was reduced to 3.9 picomole, representing a 74% reduction. It is clear to see that pulsed excitation is more effective compared to its sinusoidal equivalent, this is likely to be a direct consequence of increased peak instantaneous power producing more oxygen species in the pulsed case compared to the sinusoidal case.

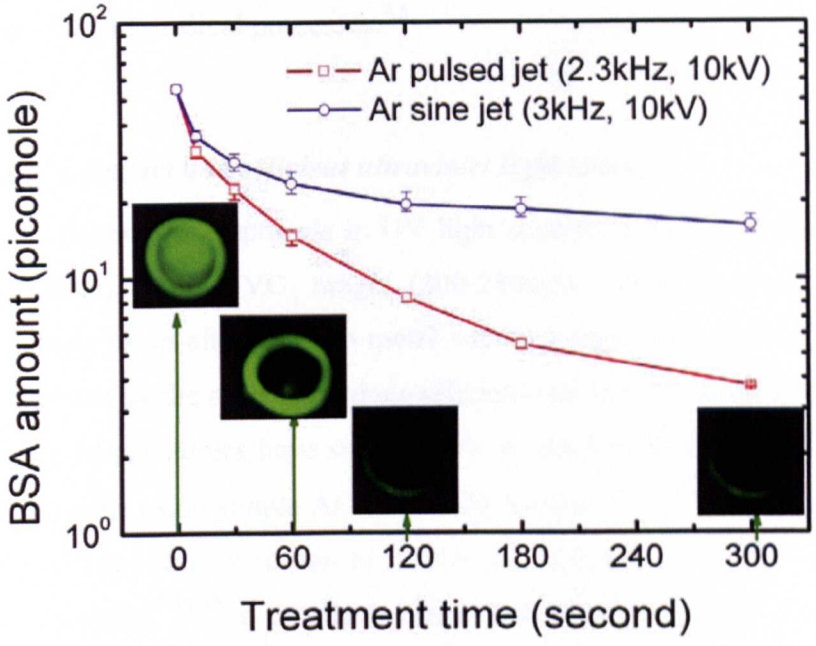

Fig 7-6: Removal rate of BSA protein on stainless steel disc with sinusoidal and pulsed excitation. Images show fluorescing protein sample after various plasma exposure times.

In order to achieve the protein removal rates equivalent to those published within reference 7.1 and 7.3 it would necessary to increase the pulse repetition rate into the tens of kilohertz range. While this is certainly possible it would require modification to the pulse generation system which is currently limited to a maximum pulse repetition rate of 5 kHz.

7.3 Nanosecond pulsed plasma for generation of intense UV

Plasmas employing rare gas and rare gas-halide mixtures are known to be efficient producers of incoherent UV and vacuum ultraviolet (VUV) radiation. In an argon discharge, narrow and intense VUV radiation centred at 190nm is efficiently produced without the need for hazardous chemicals such as mercury, which is commonly found in many commercial UV light sources. VUV and UV-C radiation is useful for breaking molecular bonds, modifying

surfaces, and initiating chemical reactions, hence is widely used in many industrial and medical processes.[7.5]

7.3.1 Compact and efficient ultraviolet light sources

Recent developments in UV light sources, emitting in the VUV range (10-200nm), and UVC range (200-280nm), have focused upon glow discharges as an alternative to metal vapour lamps. This shift in research has been driven by the need to produce efficient and environmentally friendly light sources. Many studies have successfully shown that efficient VUV production is achievable using simple AC driven discharges.[7.6,7.7,7.8] Pulsed excitation has been considered as a means to further increase the efficiency of AC driven VUV sources;[7.9,7.10] a detailed comparison between pulsed and AC driven DBD lamps showed efficiency could be increased three fold by employing sub-microsecond pulses compared to a kHz AC source.[7.9] The remainder of this section explores the effects of pulse duration on VUV production. By employing very short pulses (<100ns) it is possible to do away with the dielectric barrier hence the light source becomes a simple bare electrode parallel plate configuration. As discussed in Chapter 6, barrier-free pulsed discharges are capable of attaining substantially higher instantaneous peak powers than dielectric barrier or radio-frequency discharges. Increased peak power is known to be directly linked to enhanced UV production and is likely to yield a higher output efficiency.[7.10]

7.3.2 Experimental procedure and results

In order to produce high voltage pulses with nanosecond durations a transistorised Marx bank pulse generator was developed; details of which are discussed within Chapter 2. The device was capable of delivering pulses with a FWHM (Full Width, Half Maximum) of less than 5ns, rise and fall times around 2ns, and a peak magnitude of -8kV. Such a pulse generator is an ideal candidate for a compact pulsed VUV source as it is constructed from low cost,

small scale semiconductor devices; no magnetic components are required unlike a sinusoidal source that may require some kind of bulky 'step-up' transformer. When dealing with nanosecond pulses special attention must be directed toward the effect of voltage probe loading and signal propagation delay. A Tektronix P5100 voltage probe was used to measure the applied voltage, having a 100:1 attenuation and 250MHz bandwidth it is well suited to the task. Unfortunately, the P5100 has an input capacitance of 2.75pF, when measuring an edge transition of 4kV with a rise time of 2ns a displacement current of over 5A is produced, this adds further stress to the pulse generator and increases heating within the transistors. Another issue is the signal propagation delay between voltage and current probes. Without careful calibration the oscilloscope displays a current pulse several nanoseconds before the start of the voltage pulse, this is obviously erroneous. Using a 50Ω RF dummy-load it was possible to determine the actual propagation delay between the current and voltage signals thus enabling an accurate calibration to be performed. Figure 7-7 shows a current and voltage trace of a 5ns FWHM 4kV voltage pulse and resultant discharge current (total current less displacement current). The electrode unit comprised of two bare metallic discs of 3cm diameter with a gap separation of 2mm, the electrodes were housed within a polycarbonate enclosure with a quartz window permitting optical access (polycarbonate strongly attenuates UV light). Gas was fed into the housing unit through perforations on the surface of one of the electrodes; this has the added advantage of improving uniformity as gas flow is no longer from one side of the electrodes.

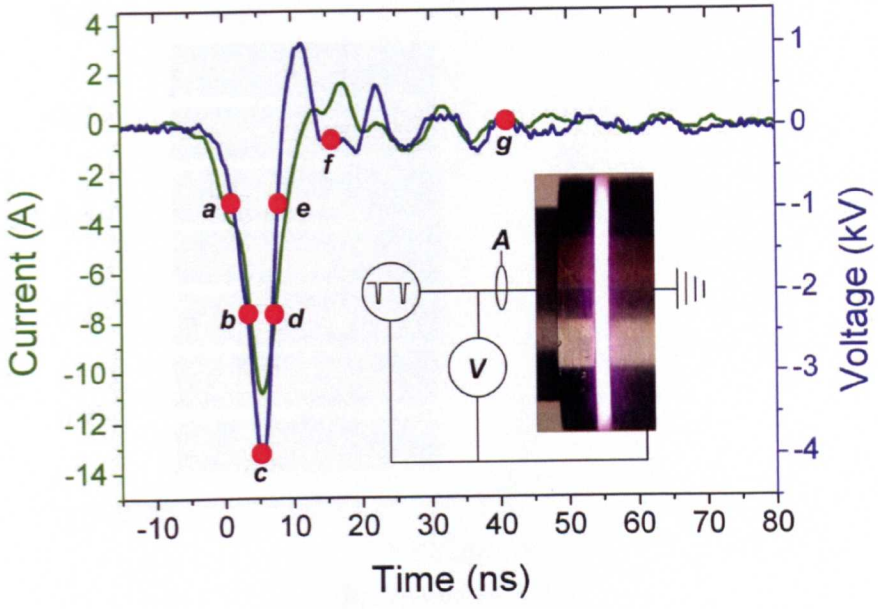

Fig 7-7: Current and voltage data for a nanosecond pulsed discharge, insert shows schematic of system and digital image of plasma.

Nanosecond imaging reveals a similar breakdown mechanism as that observed in discharges generated with longer pulses. Due to the reduced timescales and increased applied voltages involved in barrier free nanosecond pulsed discharges the breakdown event occurs much faster than those observed in Chapter 6. Figure 7-8 shows the breakdown process using 1ns exposure iCCD images taken every two nanoseconds. It should be noted that the images shown are taken in a single shot, not an accumulation of many images overlaid. A difficulty associated with imaging such rapid pulses is that an inherent delay in triggering of the iCCD means this it is likely the discharge event will be completely missed by the camera. This issue was overcome by triggering the iCCD using a logic level pulse generator and then passing the trigger pulse through a 100ns coaxial delay line to trigger the high voltage pulse generator which initiates the discharge. Consequently the iCCD camera was triggered 77ns before the discharge event, thus overcoming the 23ns propagation delay within the camera and ensuring no part of the discharge event was missed.

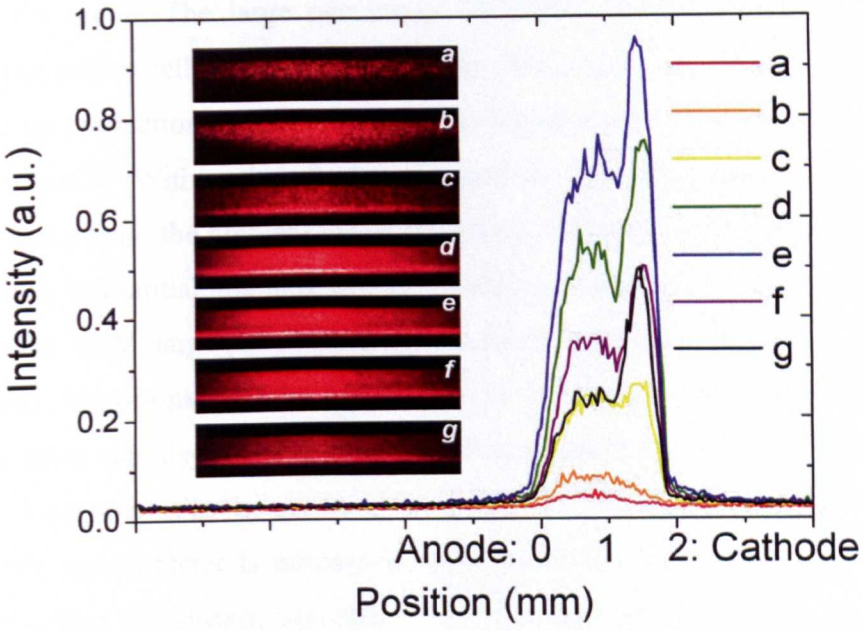

Fig 7-8: Intensity profile of nanosecond pulsed discharge. Insert shows single-shot 1ns exposure images, anode at top and cathode at bottom of each image.

Figure 7-8 clearly shows a breakdown process that is similar to that reported in Chapter 6, ions accumulate near the anode and are accelerated toward the cathode (images a to c), a sheath region forms, above which appears a negative glow region (images c to f). Finally, as the driving voltage is removed the discharge intensity gradually extinguishes over several hundreds of nanoseconds. The whole breakdown process (time from a to f) takes approximately 8ns, this is in stark contrast to the process detailed within Chapter 6, which lasts over 140ns when generated with a 250ns pulse. A likely cause of this difference in timescale is the difference in the applied electric field. In the nanosecond case the applied electric field was 20kV/cm (4kV across 2mm), whereas in the 192ns (figure 6-19) case the applied electric field was only 4kV/cm, correspondingly, ions are able to move much faster in the nanosecond discharge. The ability to generate uniform gas discharges using fast rising electric fields well in excess of the breakdown voltage of the gap is a distinguishing feature of pulsed excitation unobtainable using other excitation methods and will be discussed in the next section.

The working gas used in this investigation consisted of 99% helium and 1% argon. The large percentage of helium ensured a low breakdown voltage and excellent discharge stability. The argon impurity was added to enhance production of VUV, namely the Argon dimer 3rd continuum, centred at 190nm.[7.7] Within the discharge chamber further nitrogen and oxygen impurities from the ambient air were present. Nitrogen and oxygen impurities produce substantial amounts of NO which emits strongly in the UV-C range. [7.7] In the VUV range (10-200nm) atomic nitrogen emits strongly at 149nm and 174nm. Unfortunately, the sensitivity of a standard optical spectrometer diminishes rapidly below 190nm due to the absorption of short wavelength UV by air present in the optics of the device. For measurements below 190nm a VUV spectrometer is necessary, such a device uses nitrogen to purge air from within the system. As only a standard spectrometer was available the only measurable portion of the VUV spectrum was between 190-200nm, fortunately the small argon impurity added produces a strong emission of the argon dimmer 3rd continuum thus giving an indication of VUV production.

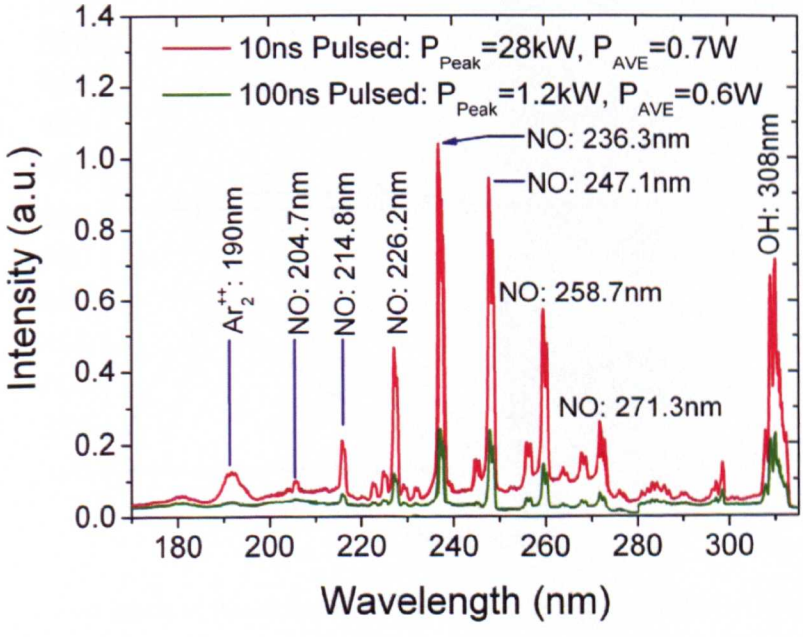

Fig 7-9: Optical emission data showing UV emission obtained from a 10ns and 100ns pulsed APGD.

Figure 7-9 shows two emission spectra overlaid, the green line shows the emission produced by a 100ns pulse, the red line shows the emission from the nanosecond pulse shown in figure 7-8. It should be noted that each discharge consumed a very similar amount of electrical energy; however the peak powers measured in each discharge were significantly different. Clearly, both UV-C and VUV production is enhanced by reducing pulse width, a likely explanation for this is the increased instantaneous power dissipated within the nanosecond discharge. Higher peak powers, resulting from large over-voltages are likely to produce a greater number of high energy electrons. A high energy electron transfers more energy when colliding with a neutral thus resulting in a shorter wavelength photon being emitted. To summarise, a reduction in pulse width allows for a higher over voltage to be applied to the gas gap whilst maintaining a uniform discharge, the resultant breakdown is rich in high energy electrons which yield a higher proportion of UV photons than a discharge consisting of many low energy electrons.

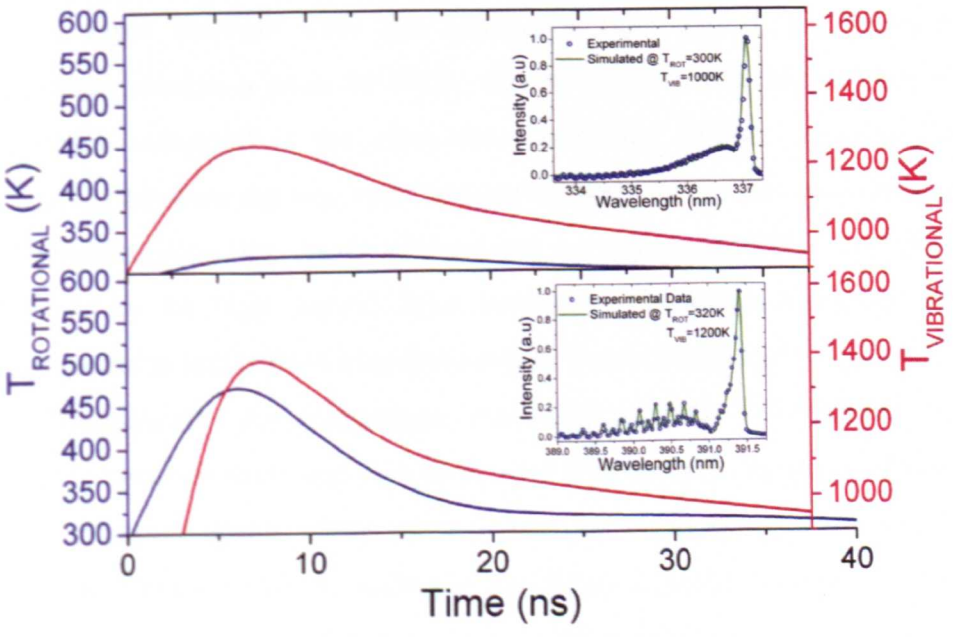

Fig 7-10: Time-resolved Rotational and Vibrational temperatures calculated using N_2 emission at 337nm, and N_2^+ emission at 391nm. Insert shows time-averaged temperatures.

For any potential light source it is essential that the temperatures generated remain at a manageable level, high temperatures necessitate complex cooling systems which are often costly. Figure 7-10 shows the time-resolved rotational and vibrational temperatures obtained via optical emission. The upper graph shows the temperature measured using the molecular nitrogen line at 337nm, during each applied voltage pulse a steep rise is observed in the vibrational temperature whereas the rotational temperature only increases by a few tens of Kelvin. The insert shows a time-average optical emission profile and simulated profile, as expected, the rotational temperature is found to be very low, only 300K. As mentioned previously the gas temperature is likely to be very similar to the rotational temperature meaning the nanosecond pulsed discharge is an ideal candidate for a low temperature, efficient UV source. The lower graph in figure 7-9 shows the rotational and vibrational temperatures obtained using the ionic nitrogen line at 391nm, the temperature profile is markedly different from that obtained using the 337nm emission line. Both rotational and vibrational temperatures show a rapid increase over the applied voltage period, the rotational temperature reaches a peak of 475K, this is almost 150K higher than the temperature measured at the same time using the 337nm emission. The discrepancy between the two measurements is likely due to the ionic nature of the 391nm emission line. As the nitrogen ion is a charged particle it is strongly influenced by the high electric fields present in the pulsed discharge. The 337nm emission line is from a neutral particle, hence unaffected by the electric field; consequently the temperature measured is lower. The temperature difference between ionic and neutral species highlights a drawback of using optical emission spectroscopy as a means of temperature measurement. Variations in temperature depending on the choice of emission line have been observed in other studies,[7.11] however, the difference is greater in the case of pulsed discharges due to the large electric fields present. Despite the large differences observed in the time-resolved temperature profiles, the time-averaged temperatures are found to be very similar. The high peak temperatures observed from the 391nm emission are only apparent over 20ns;

this is insufficient time to have any significant heating effect on the background gas or electrodes.

7.4 Nanosecond pulsed APGD for polymer treatment.

Cold gas plasmas are used extensively as a means to enhance the surface characteristics of polymer films. Through plasma-polymer interaction the surface energy of a sample is increased which enhances wettability, printability and adhesion. As polymer films become thinner it is essential that any plasma processing does not cause undue thermal burden which may irreparably modify the bulk properties of the polymer or perforate the film itself. For large scale industrial treatment of polymers it is desirable to use low cost gases such as nitrogen or air, however molecular gases tend to produce hot plasma which is often filamentary in nature. Voltage pulses with durations less than 100ns are shown to produce low temperature, diffuse discharges which are ideally suited for the uniform treatment of thermally sensitive polymer films. It is shown that nanosecond pulsed air discharges are capable of greatly increasing oxygen-containing functional groups on the surface of polymeric films which are know to significantly enhance the hydrophilic properties.

Polymeric materials are used extensively in food packaging, protective coatings and sealing applications because of their excellent bulk properties, such as transparency, high strength to weight ratio, and good thermal resistance.[7.12] Unfortunately, it is often the case that polymer films exhibit several undesirable characteristics such as poor wettability, poor printability, and poor adhesion to secondary phases.[7.13] In many applications it is necessary to increase the surface energy of the polymer thus enhancing wetting and adhesion properties whilst maintaining the bulk characteristics of the material. Chemical activation of the polymer surface is the most utilized method; however the use of aggressive solvents, caustic solutions, and acids on an industrial scale has detrimental ecological consequences. An environmentally

benign surface treatment, such as cold gas plasma treatment, is a highly attractive alternative for industrial scale processing.[7.14]

To date many studies have been conducted into the surface treatment of polymers using low pressure plasma systems, typically 1-10Pa. The additional cost and complexity of the vacuum equipment makes such systems unattractive for industrial use. Atmospheric pressure plasma sources offer a chamber-less method for the treatment of polymers which is easily integrated into existing production lines.[7.12,7.15] Typically, sinusoidal excitation sources from 50Hz up to many MHz are used to produce non-equilibrium plasma in various inert gases such as helium and argon.[7.15,7.16,7.17] Noble gases tend to produce very stable plasmas at the expensive of chemical reactivity, in order to achieve efficient surface modification it is necessary to enhance reactivity whilst maintaining stability which is a considerable challenge. Chemically reactive molecular gases such as nitrogen and air have been used as the working gas in various studies; however the plasma produced tends to be filamentary in nature.[7.12,7.13] Filamentary discharges are very inhomogeneous, consisting of many micro-discharges lasting tens of nanoseconds which are randomly distributed over the polymer surface thus yielding a non-uniform treatment. [7.16]

This section focuses upon the use of a pulsed excitation source to produce cold and diffuse atmospheric pressure plasma in ambient Air. By maintaining short pulse widths, typically less than 100ns, the discharge is free from potentially damaging streamers and is uniform across the entire electrode region. Diffuse operation in gases such as nitrogen and air are typically obtained using low frequency sinusoidal sources with a wire mesh placed between electrode and barrier, such discharges are very sensitive to the excitation frequency which is often prohibitively low.[7.18] Pulsed excitation introduces two additional stabilisation mechanisms that are not possible with sinusoidal excitation and as such the diffuse nature of the discharge can be maintained over a wide frequency range without the aid of a wire mesh. The

short pulse width ensures there is insufficient time for instabilities such as thermal runaway to occur, similar pulsing techniques are employed in the laser community to produce glow discharges at current densities above the threshold for glow to arc transition.[7.19] A further stabilizing mechanism is associated with the fast rise and fall times of the voltage pulse, charges uniformly trapped on the dielectric surface are spontaneously expelled during the rapid transition phase (typically > $500V.ns^{-1}$) and initiate a homogenous high current discharge across the entire electrode surface.[7.20] Electrical and optical measurements are employed to demonstrate that pulsed excitation is capable of producing highly uniform glow like discharges over large areas which allow for uniform surface treatment of polymer films at temperatures less then 80°C. X-ray photoelectron spectroscopy (XPS) and scanning electron microscopy (SEM) are used to detect changes in the polymer surface properties.

The pulsed excitation source employed in this investigation was capable of delivering voltage pulses up to 5kV, at pulse widths from 50ns to 10μs, with rise and fall times typically less than 10ns. Pulse repetition rates can be varied from 1Hz to approximately 20 kHz depending on the load conditions. Voltage pulses were applied to a rectangular metallic anode measuring 4cm by 0.8mm, a dielectrically coated ground plate was placed 0.5-2.5mm below the anode to form the cathode. Polymer films were placed on the dielectrically coated cathode and exposed directly to the plasma. The electrode unit was housed within in a Perspex box which allowed the background gas to be controlled; however, in the case of air plasma the box was opened and allowed to fill with the ambient laboratory air. Current and voltage were measured with a Pearson 2877 current probe (200MHz Bandwidth with 2ns useable rise time) and a Tektronix P5100 voltage probe (250MHz Bandwidth with 1.75ns useable rise time), signals were recorded on a Tektronix DPO 4104 oscilloscope with a 1GHz bandwidth. Optical emission spectra were obtained using an Andor Shamrock spectrometer with a focal length of 0.3 m and a grating of 2400 grooves/mm.

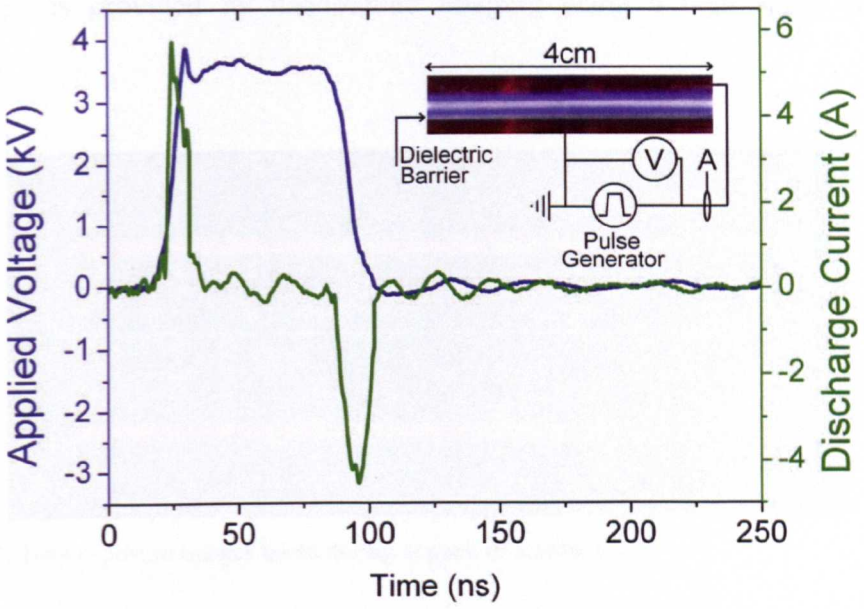

Fig 7-11: Current and voltage of a pulsed air DBD, schematic shows experimental setup and digital image of the discharge.

Figure 7-11 shows electrical measurements of a kHz pulsed DBD operating in ambient air. As reported in previous studies, two current pulses are observed for each applied voltage pulse.[7-21,7-22] The first current pulse is produced as the applied voltage exceeds the breakdown voltage of the gas; the second current pulse always occurs on the falling edge of the voltage pulse and represents a secondary discharge. The second current pulse is a direct consequence of charges stored on the dielectric barrier from the preceding discharge reigniting the discharge during the voltage falling phase.[7-21] The shape of the current pulses gives an indication of the diffuse nature of the discharge, typically, if the discharge is filamentary the current trace will consist of many small current pulses each representing a single filament. A large continuous current pulse is highly indicative of a diffuse discharge however it is not conclusive proof, potentially a lack of temporal resolution in the current transducer could give the appearance of a single continuous current pulse as it is unable to resolve the individual filament pulses. In this study the current probe bandwidth was 200MHz which should be sufficiently high to

capture individual filaments. Further evidence of the diffuse nature of the discharge is provided by nanosecond imaging using a high speed iCCD camera.

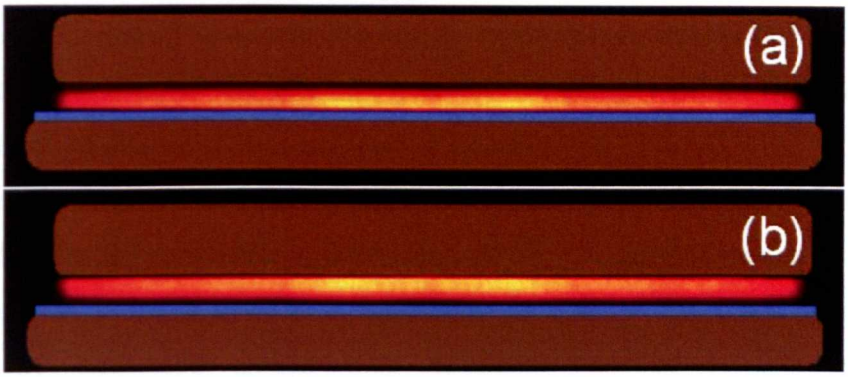

Fig 7-12: 10ns exposure images taken during at peak of current pulse.

Figure 7-12 shows single shot iCCD images taken during each current pulse with an exposure time of 10ns. Clearly it can be seen that the discharge is entirely streamer free and homogenous across the entire electrode area, it is also interesting to note that during the positive current pulse the peak intensity is positioned above the grounded lower electrode and in the negative current pulse the peak intensity is closer to the upper electrode. This phenomenon is due to the negative glow formation above the instantaneous cathode. As the gas voltage changes polarity the top electrode becomes an instantaneous cathode and consequently a negative glow region forms, hence giving the appearance of the discharge alternating between the electrodes over the applied voltage pulse. For surface treatment of polymer films it is highly advantageous to have a streamer free discharge, not only because uniform surface treatment can be ensured but also because streamers can cause rapid localized heating of the polymer surface which may lead to damage to the bulk material or even film perforation.

The electrical efficiency of pulsed DBD's is significantly higher than conventional AC driven discharges, primarily due to a second discharge, which essentially occurs without any additional power from the power

source.[7.21] The peak discharge current is 5.9A yielding a current density of 18.4A.cm^{-2}, this is unusually high for a DBD where typical current densities are in the mA.cm^{-2} range. Using the current density and calculated gas voltage it is possible to estimate the electron density within the discharge using $n_e = (J/E_g)/(e.\mu_e)$, where J is current density, E_g is electric field, e is the charge of an electron and μ_e is the electron mobility of the gas used. The electron mobility of air at atmospheric pressure is known to be 592 cm^2.V^{-1}.s^{-1} [7.23] and the electric field is obtained by using the gas voltage calculated from the method described previously and dividing by the gas gap distance. It is found that the peak electron density is approximately $1.4x10^{13}$cm^{-3}; this is several orders of magnitude greater than densities observed in conventional sinusoidally driven barrier discharges at atmospheric pressure.[7.28] Furthermore, the value calculated is likely to be significantly underestimated due to the nonuniformity of the electric field across the gas gap. In practice, the cathode sheath is a region of high electric field which accounts for most of the voltage drop across the gas gap. The bulk of the discharge is in a region of low electric field, consequently the acceleration of electrons towards the anode is low resulting in a higher concentration of electrons in the plasma bulk.

In nonequilibrium plasmas sustained by DC or oscillating electric fields the electron energy distribution function (EEDF) is strongly non-Maxwellian and electron temperatures defined by the EEDF slope at low energy are usually in the 1-3eV range.[7.24] Under such conditions only a very small number of electrons are capable of ionization which typically requires electron energies in the 10-15eV range. The majority of electrons have insufficient energy to cause ionization during collisions, consequently almost all collisions result in inelastic or elastic energy losses. Electrons with energies in the 1-3eV range are highly effective in exciting the vibrational states of gas molecules, in many cases up to 90% of the discharge power is consumed through vibrational excitation yielding a very low ionization efficiency.[7.24] It is clear that in order to improve ionization efficiency it is necessary to produce a shift in the EEDF resulting in a far higher proportion of high energy electrons

that are capable of ionization. One approach is to accelerate electrons in a vacuum where inelastic losses are minimized, alternatively the same effect can be achieved using fast rising voltage pulses that are greater in magnitude than the minimum breakdown voltage of the gas. The strong field increases ionization rate and reduces the energy cost per electron, such operation is only possible in a pulsed discharge as high over-voltages rapidly lead to the formation of instabilities within the discharge, only through short pulse widths can such instabilities be avoided.

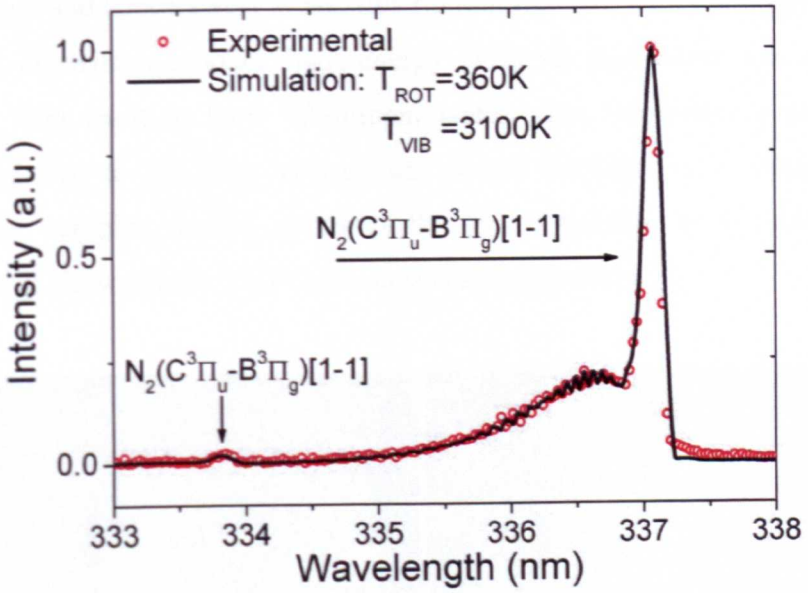

Fig 7-13: Measured and simulated optical emission data of 337nm Nitrogen emission line.

Figure 7-13 shows experimental and simulated spectral data for a pulsed air discharge, the voltage pulses used were approximately 3.5kV in amplitude with a pulse width of 70ns. A repetition rate of 5kHz was used to sustain the discharge, light emission from the discharge was directed into the spectrometer via fibre optic cable and measurements were obtained using a 1ms exposure time. By comparing the measured spectrum to the simulated spectrum of the nitrogen 2nd positive system it is possible to obtain an estimate of the rotational and vibrational temperatures of the discharge. Due to the highly collisional nature of an atmospheric pressure discharge it can be

assumed that the rotational temperature is very close to the actual gas temperature, many studies have made use of such techniques and found agreement to be excellent, errors as low as 2.4% have been reported.[7-25] Speacair, a program specifically designed for modelling of air discharges, was used to model the emission data, the best fit between experimental and simulated data was obtained at T_{rot} = 360K and T_{vib}=3100K in ambient air. The temperatures determined are uncharacteristically low, for example, DC discharges operated at low currents (tens of mA) typically have gas temperatures above 1000K.[7.11] The emission line at 334nm is a vibrational transition and appears very weak, this finding fits well with the suggestion that pulsed discharges produce high energy electrons that ionise gas molecules rather than exciting their vibrational states. Gas temperatures are further reduced due to the long voltage off period between each voltage pulse, polymer samples treated continuously for 5 minutes in a stationary air discharge showed only a 10°C rise in surface temperature.

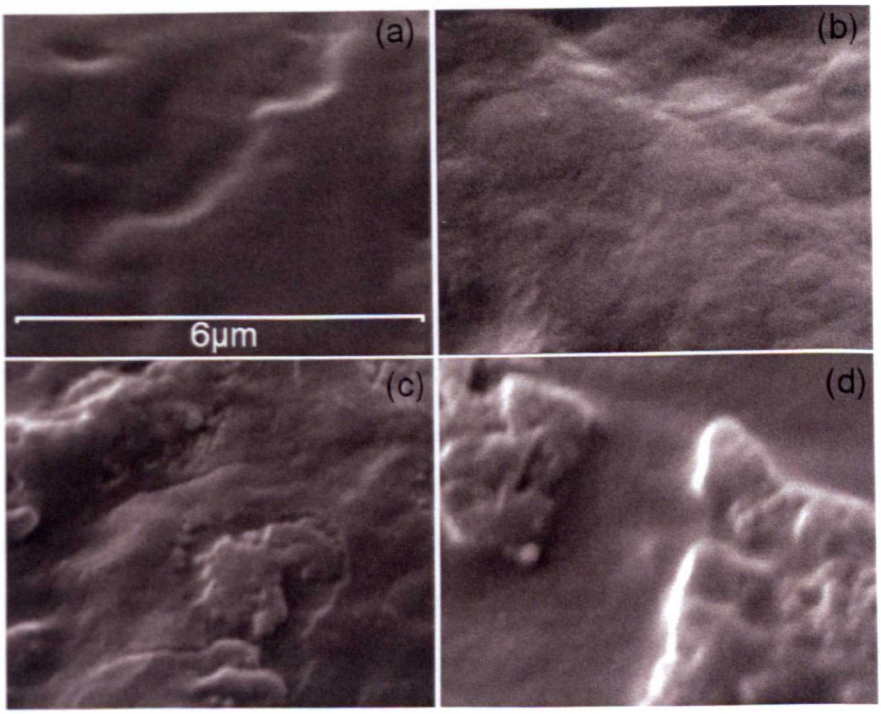

Fig 7-14: SEM images of polymer surfaces after a)0s, b)60, c)180, and d)300s of plasma treatment. 10,000 magnification.

Figure 7-14 shows a series of scanning electron microscope (SEM) images of a polypropylene film treated with a 5kHz 3.5kV pulsed air discharge. Following plasma treatment each sample was sputter coated with a nanometer layer of gold to prevent surface charging and observed using a Cambridge Instruments steroscan 360 SEM operating at an accelerating voltage of 10kV. Image 7-14(a) shows the untreated polymer sample, it is clear from the image the surface is quite uneven, this is a likely result of the manufacturing process, at higher magnifications the surface appears relatively smooth. Figure 7-14(b) shows the surface after 1 minute of continuous plasma treatment, this is likely to be significantly longer than any viable industrial treatment time. Very few changes in surface morphology can be observed, this was also the case in samples treated from 10-50 seconds (data not shown). After several minutes of plasma treatment the surface changes significantly, the entire treated area is covered predominantly in raised formations. Similar structures have been reported previously in studies involving plasma treated polypropylene,[7-26] several explanations are proposed for the appearance of such structures including recrystalisation processes initiated by the plasma or the appearance of additives introduced during the production process, however more research is needed before a conclusion can be reached.

The chemical composition of polypropylene film was investigated by an X-ray photoelectron spectroscopy system (XPS) employing Aluminium X-rays with an anode voltage of 8kV and current of 20mA. Figures 7-15 and 7-16 show de-convoluted XPS spectra from untreated polypropylene and a sample exposed to 5 minutes of pulsed air plasma. The de-convolution process was performed using a program called XPS-Peak, the software allows XPS spectra to be dissected into its constituent parts allowing elements with similar binding energies to be determined from a single spectral peak.

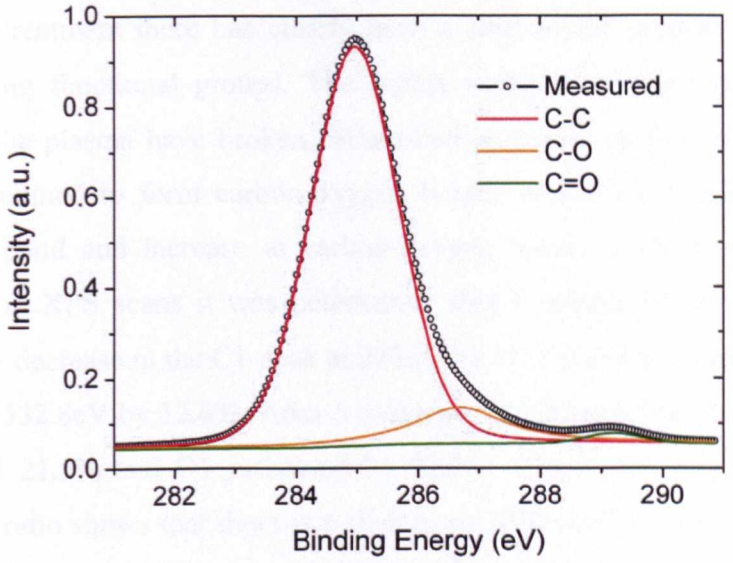

Fig 7-15: De-convoluted XPS spectra of untreated polypropylene sample.

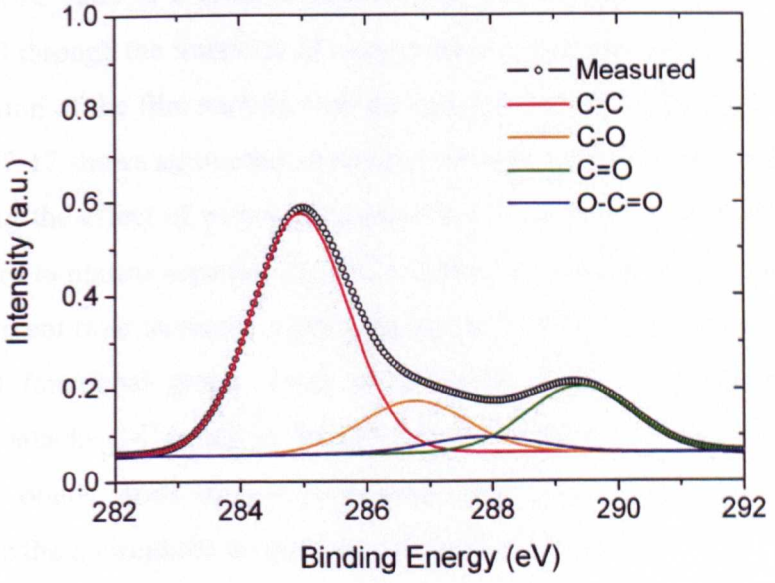

Fig 7-16: De-convoluted XPS spectra of polypropylene sample plasma treated for 300s.

Polypropylene has one of the simplest chemical compositions of all polymers, consisting of only hydrocarbon chains, with no other chemical elements present. The XPS spectrum shown in Figure 7-15 clearly indicates the presence of small amounts of oxygen containing functional groups on the polymer surface. Such impurities are a likely consequence of surface

contamination incurred since the time of manufacture. After 5 minutes of plasma treatment there has clearly been a shift of the proportion of oxygen containing functional groups. The highly energetic oxygen species present within the plasma have broken carbon-carbon bonds on the polymer surface and combined to form carbon-oxygen bonds, hence a reduction in carbon-carbon bond and increase in carbon-oxygen bonds is observed. From low resolution XPS scans it was determined that 1 minute of plasma treatment causes a decrease in the C1 peak at 285eV by 11.2% and an increase in the O1 peak at 532.8eV by 12.6%. After 5 minutes of treatment time the C1 peak had dropped 21.5% and O1 increased by 22.8%. Calculation of the Oxygen to Carbon ratio shows that there is a shift from 10% to 47.2% after 5 minutes of treatment, this is highly consistent with other studies where the O/C ratio has been raised from a few percent to a saturation point of 47.9%.[7-12] A large shift in the O/C ratio is a clear indication that surface functionalization is being induced through the interlock of oxygen based polar species resulting from the interaction of the film surface with the species present in the gas discharge.[7-17] Figure 7-17 shows an overlay of several detailed XPS spectra of the C1s peak, allowing the effect of plasma treatment to be observed. It is clear to see that exposure to plasma significantly reduces the C1s peak at 285eV. Additionally, as treatment time increases a peak appears at 289.3eV, this corresponds to the O-C=O functional group. From these results it can be concluded that the plasma attacks C-C bonds in the polypropylene chains to form various carbon oxygen bonds, such oxygen-containing groups are known to substantially improve the hydrophilic properties of polymeric materials.[7.12,7.13,7.14,7.15]

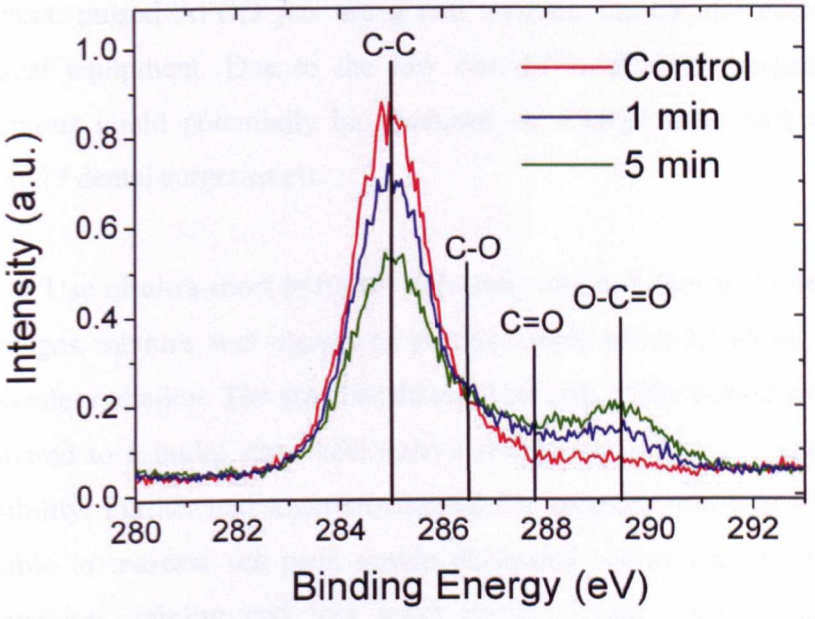

Fig 7-17: Overlaid XPS spectra showing increases in oxygen containing functional groups.

In conclusion, monopolar high voltage pulses with durations less than 100ns are capable of sustaining diffuse Air plasma over a wide area which has an uncharacteristically low temperature. A consequence of pulsed excitation is an increase in electron density and an enhancement of ionisation efficiency which is unobtainable using conventional CW excitation methods. It is shown through SEM images and XPS analysis that pulsed air plasma treatment greatly enhances the surface characteristics of polymeric films.

7.5 Summary

This chapter has shown how pulsed excitation can be applied to several real-world applications and highlighted numerous advantages gained over conventional excitation sources. In the field of biomedicine it was demonstrated that pulsed excitation of an atmospheric pressure dielectric barrier jet offers a low cost and environmentally sound means of decontaminating surgical instruments. The pulsed jet was shown to remove almost four times as much protein than a comparable sinusoidal excited

plasma jet. Coupled with the enhanced efficiency discussed in previous chapters, pulsed APGD jets are a real solution for the decontamination of surgical equipment. Due to the low cost of solid state components pulse generators could potentially be produced on a large scale and stationed in hospital / dental surgeries etc.

Use of ultra-short (<100ns) duration voltage pulses to excite a helium-argon gas mixture was shown to produce high levels of short wavelength ultraviolet radiation. The small scale and low cost of the pulsed power supply compared to a bulky sinusoidal source makes compact VUV sources a real possibility. Further investigation showed that as pulse width is reduced, it is possible to increase the peak power dissipated within the discharge whilst maintaining stability and low input power. These findings indicate that nanosecond duration pulses, or perhaps even shorter, are the most suitable candidate for the generation of VUV emissions.

Finally, a pulsed, large area, dielectric barrier discharge was highlighted as an ideal means of modifying the surface characteristics of polymeric films. The excellent stability and low operating temperature associated with ultra-short pulsed excitation means even thermally liable polymer films could be treated in ambient air. SEM and XPS were used to detail the surface changes due to plasma treatment, it was found that plasma treatment introduced significant amounts of oxygen containing functional groups which are typically associated with better wettability and printability.

References

[7.1] Deng, X.T, Shi, J.J, Kong, M.G, 'Protein destruction by a helium atmospheric pressure glow discharge: Capability and mechanisms' Journal of Applied Physics, Vol.101, Iss.7, No.074701, 2007.

[7.2] Smith D, Dickson M, Aitken J, Bagg J, 'Contaminated dental instruments', Journal of Hospital Infection, Vol.51, Iss.3, pp.233-235, 2002

[7.3] Deng, X.T., Shi, J.J, Chen, H.L, Kong, M.G, 'Protein destruction by atmospheric pressure glow discharges', Applied Physics Letters, Vol.90, Iss.1, No.013903, 2007.

[7.4] Ena, J, 'Prions: Who should worry about them?', Archives of Medical Research, Vol.36, Iss.6, pp.622-627, 2005.

[7.5] Rahul, R, Stan, O, Rahman, A, Littlefield, E, Hoshimiya, K, Yalin, A.P, Sharma, A, Pruden, A, Moore, C.A, Yu, Z., Collins, G.J, ' Optical and RF electrical characteristics of atmospheric pressure open-air hollow slot microplasmas and application to bacterial inactivation', Journal of Physics D-Applied Physics, Vol.38, Iss.11, pp.1750-1759, 2005.

[7.6] Guivan, N.N, Janca, J, Brablec, A, Stahel, P, Slavicek, P, Shimon, L.L, 'Planar UV excilamp excited by a surface barrier discharge', Journal of Physics D-Applied Physics, Vol.38, Iss.17, pp.3188-3193,2005.

[7.7] Rahman, A, Yalin, A.P, Surla, V, Stan, O, Hoshimiya, K, Yu, Z, Littlefield, E, Collins, G. J, 'Absolute UV and VUV emission in the 110-400 nm region from 13.56 MHz driven hollow slot microplasmas operating in open air', Plasma Sources Science & Technology, Vol.13, Iss.3, pp.537-547, 2004.

[7.8] Ricconi, B. J, Park, S. J, Sung, S. H, Tchertchian, P. A, Eden, J. G, 'Ultraviolet emission from OH and ArD in microcavity plasma devices', Electronics Letters, Vol.43, Iss.22, pp.1194-1196, 2007.

[7.9] Carman, R.J, Mildren, R.P, 'Computer modelling of a short-pulse excited dielectric barrier discharge xenon excimer lamp (lambda similar to 172 nm)', Journal of Physics D-Applied Physics, Vol.36, Iss.1, pp.19-23,2003.

[7.10] Lu, X. P, Laroussi, M, 'Optimization of ultraviolet emission and chemical species generation from a pulsed dielectric barrier discharge at atmospheric pressure', Journal of Applied Physics, Vol.98, Iss.2, No.023301, 2005.

[7.11] Staack, D, Farouk, B, Gutsol, A.F, Fridman, A.A, 'Spectroscopic studies and rotational and vibrational temperature measurements of atmospheric pressure normal glow plasma discharges in air', Plasma Sources Science & Technology, Vol.15, Iss.4, pp.818-827, 2006.

[7.12] De Geyter, N, Morent, R, Leys, C, Gengembre, L, Payen, E, 'Treatment of polymer films with a dielectric barrier discharge in air, helium and argon at

medium pressure', Surface & Coatings Technology, Vol.201, Iss.16-17, pp.7066-7075, 2007.

[7.13] Morsy F.A, Elsayad S.Y, Bakry A, Eid M.A, 'Surface properties and printability of polypropylene film treated by an air dielectric barrier discharge plasma', Surface Coatings International Part B-Coatings Transactions, Vol.89, Iss.1, pp.49-55, 2006.

[7.14] Egitto, F.D, Matienzo, L.J,'Plasma modification of polymer surfaces for adhesion improvement', Ibm Journal of Research and Development, Vol.38, Iss.4, pp.423-439, 1994.

[7.15] Cheng C, Zhang L.Y, Zhan R.J, 'Surface modification of polymer fibre by the new atmospheric pressure cold plasma jet', Surface & Coatings Technology, Vol.200, Iss.24, pp.6659-6665, 2006.

[7.16] Massines, F, Gouda, G, 'A comparison of polypropylene-surface treatment by filamentary, homogeneous and glow discharges in helium at atmospheric pressure', Journal of Physics D-Applied Physics, Vol.31, Iss.24, pp.3411-3420, 1998.

[7.17] France, R.M, Short, R.D, 'Plasma treatment of polymers: The effects of energy transfer from an argon plasma on the surface chemistry of polystyrene, and polypropylene. A high-energy resolution X-ray photoelectron spectroscopy study', Langmuir, Vol.14, Iss.17, pp.4827-4835, 1998.

[7.18] Golubovskii Y.B, Maiorov V.A, Behnke J.F, Tepper J, Lindmayer M, 'Study of the homogeneous glow-like discharge in nitrogen at atmospheric pressure', Journal of Physics D-Applied Physics, Vol.37, Iss.9, pp.1346-1356, 2004.

[7.19] Takaki K, Hosokawa M, Sasaki T, Mukaigawa S, Fujiwara T, 'Production of atmospheric-pressure glow discharge in nitrogen using needle-array electrode', Applied Physics Letters, Vol.86, Iss.15, No.151501, 2005.

[7.20] Kogelschatz, U, 'Filamentary, patterned, and diffuse barrier discharges', IEEE Transactions on Plasma Science, Vol.30, Iss.4, pp.1400-1408, 2002.

[7.21] Lu, X.P, Laroussi, M, 'Temporal and spatial emission behaviour of homogeneous dielectric barrier discharge driven by unipolar sub-microsecond square pulses', Journal of Physics D-Applied Physics, Vol.39, Iss.6, pp.1127-1131, 2006.

[7.22] Walsh J.L, Shi J.J, Kong M.G, 'Contrasting characteristics of pulsed and sinusoidal cold atmospheric plasma jets', Applied Physics Letters, Vol.88, Iss.17, No.171501, 2006.

[7.23] Raizer Y.P, 'Gas Discharge Physics', Springer, Page 11, 1991.

[7.24] Macheret, S.O, Shneider, M.N, Miles, R.B, 'Modeling of air plasma generation by repetitive high-voltage nanosecond pulses', IEEE Transactions on Plasma Science, Vol.30, Iss.3, pp.1301-1314, 2002.

[7.25] Moon, S.Y, Choe, W, 'A comparative study of rotational temperatures using diatomic OH, O-2 and N-2(+) molecular spectra emitted from atmospheric plasmas' Spectrochimica Acta Part B-Atomic Spectroscopy, Vol.58, Iss.2-3, pp.249-257, 2003.

[7.26] Warren, J.M, Mather, R.R, Neville, A, Robson, D, 'Gas plasma treatments of polypropylene tape', Journal of Materials Science, vol.40, *Iss.20, pp.*5373-5379, 2005.

[7.27] Walsh J.L, Kong M.G, '10 ns pulsed atmospheric air plasma for uniform treatment of polymeric surfaces' Applied Physics Letters, Vol.91, Iss.25, No.251504, 2007.

[7.28] Kim J.H, Choi Y.H, Hwang Y.S, 'Electron density and temperature measurement method by using emission spectroscopy in atmospheric pressure nonequilibrium nitrogen plasmas', Physics of plasmas, Vol.13, Iss.9, No.093501, 2006.

PAGE NUMBERS CUT OFF IN ORIGINAL

8 Conclusions

8.1 Key findings and contributions

This work has detailed the generation of non-thermal atmospheric pressure gas discharges by means of ultra-short high voltage pulses. As stated in the introduction chapter, the structure of the thesis follows a natural progression starting with the technology behind generating high voltage pulses, through detailed analysis of the plasma generated using ultra-short pulses, and finally highlighting several applications where pulsed gas discharges offer real benefits compared to sinusoidally excited plasma. The work described within this thesis has proved the basis for five, first author, journal publications, three oral presentations at international conferences, and numerous poster presentations. The key findings and contributions are summarised in the following sub-sections.

8.1.1 Pulsed Power Technology

Chapter 2 briefly details several pulsed power technologies and discusses their potential for generating the sub-microsecond, high repetition rate pulses necessary for generation of stable atmospheric pressure glow discharges. Many of the common pulsed power technologies discussed were found to be inadequate due to limited repetition rates or slow rise and fall times. It was determined that MOSFETs and BJT transistors are well suited to the task. Both devices have limited current and voltage handling abilities but are easily combined to form high current and high voltage switches. Rise and fall time's less than ten nanoseconds coupled with repetition rates of many kilohertz are achievable with careful layout design and adequate cooling.

Three pulse generator topologies were discussed; the first employed four 1kV switching MOSFETs to form a switch with a hold-off voltage of 4000V and fall time less than 100ns. The second topology examined employed MOSFETs in a push-pull configuration, this topology has many of the benefits of a stacked MOSFET pulse generator but has fast rise and fall times. A drawback of any push-pull topology is that twice as many switching devices are required for a given hold-off voltage, for example, a 4kV pulse generator requires 8 x 1kV MOSFETs. The final pulse generator topology examined was an avalanche transistor Marx bank. It is often thought that operating transistors in the avalanche mode is highly destructive and should be avoided, however this is a misconception, when the maximum collector-emitter voltage is exceeded many BJT devices non-destructively avalanche. The avalanche breakdown within a device is on a picosecond time scale thus enabling extremely rapid switching times of high voltages to be achieved. By employing transistors in a Marx bank configuration it is possible to produce kilovolt pulses with rise times of a few nanoseconds at repetition rates of many kilohertz.

8.1.2 Pulsed Plasma Jet Topologies

Chapter 3 focuses upon a comparison between pulsed and sinusoidal excitation of a plasma jet. The plasma jet is widely used in many industrial applications and research laboratories as it is easy to construct and allows plasma to be generated in one region and transported to another region for processing applications. For the first time a direct comparison between pulsed and sinusoidal excitation of a plasma jet is presented. It was shown that pulsed discharges are not only electrically more efficient than a sinusoidal equivalent but also that for a fixed input power considerably more excited oxygen species are produced. Many of the findings were published in the article 'Contrasting characteristics of pulsed and sinusoidal cold atmospheric plasma jets' which appeared in Applied Physics Letters. 88, 171501 (2006).

Chapter 4 investigates the effects caused when the pulse width of the excitation voltage is reduced from a microsecond scale to a sub-microsecond scale. It was shown that a reduction in pulse width necessitates a higher excitation voltage; this translates in to a higher instantaneous peak power while maintaining a fixed input power. As peak power is increased electron density is higher and consequently a higher flux of excited species is produced. The benefits of sub-microsecond are further demonstrated when argon is used as the working gas, typically argon plasma is considerably hotter than an equivalent helium plasma. Employing pulsed excitation with a very low duty cycle enables the stable generation of an argon discharge with an uncharacteristically low temperature. The shift to argon from helium represents a substantial economic benefit as helium is prohibitively expensive for use in many industrial applications. Many of the findings detailed within this chapter were published in the article 'Room-temperature atmospheric argon plasma jet sustained with submicrosecond high-voltage pulses' which appeared in Applied Physics Letters. 91, 221502 (2007).

Finally, chapter 5 focuses upon the possible propagation mechanisms behind the plasma jet. To date, very few studies have investigated the physical means by which the plasma plume propagates in a region of low or no electric field. A definitive proof remains elusive; however it is hoped that the work covered contributes to the readers understanding and provides a basis for any future work undertaken. The effect of excitation frequency upon the plasma bullet is accepted for publication in IEEE transaction on plasma science, due to appear June 2008.

8.1.3 Pulsed Parallel Plate Topologies

Chapter 6 sees a change in emphasis from a jet configuration to a parallel plate configuration. While the jet configuration is focused toward applications the parallel plate configuration is well suited to experimental investigation due to its simplistic geometry. It was shown for the first time that high voltage pulses with sub-microsecond durations are capable of generating

stable and diffuse glow discharges at kilohertz frequencies without the aid of a dielectric barrier. Previously barrier free operation was limited to high frequency excitation which produces hot plasma; or kilohertz excitation over a very small operating range. It was demonstrated that the pulsed barrier free discharges were highly uniform, had a very low gas temperature, and were stable over many hours of continuous operation. Using various diagnostic techniques a detailed understanding of the pulsed barrier free discharge and its breakdown mechanism was presented; it was also shown that the high peak power involved produces sharp bursts of excited species during each voltage pulse. Many of the findings detailed within chapter 6 were published in the articles 'Submicrosecond pulsed atmospheric glow discharges sustained without dielectric barriers at kilohertz frequencies' which appeared in Applied Physics Letters. 89, 161505 (2006), and 'Sharp bursts of high-flux reactive species in submicrosecond atmospheric pressure glow discharges' which appeared in Applied Physics Letters. 89, 231503 (2006).

8.1.4 Applications of pulsed APGD

The penultimate chapter of this thesis highlights various applications where pulsed APGD's offer real benefits compared to the sinusoidal excited plasmas typically used. It is shown that a pulsed plasma jet is far more efficient at removing protein contamination from medical instruments compared to an equivalent sinusoidally driven APGD jet; this fits well with the findings detailed in previous chapters where it was shown that the high peak powers associated with pulsed discharges produce significantly more excited oxygen species.

Nanosecond duration voltage pulses were employed in a parallel plate helium-argon discharge to produce intense UV-C and VUV light, which is often used in many industrial materials processing applications. It was shown that a reduction in pulse width from hundreds of nanoseconds to less than ten nanosecond introduces a shift in light emission into the high energy, short wavelength region. For a fixed input power, a 10ns pulsed APGD produced

substantially more UV than a 100ns discharge whilst maintaining excellent uniformity and stability.

Finally, a pulsed DBD was used for the surface modification of polymeric materials. Unlike the applications discussed previously air was used as the working gas, this introduces further difficulties when attempting to produce cold and uniform gas discharges. Through pulsed excitation it was possible to produce a cold and uniform air discharge at atmospheric pressure over a wide area. It was demonstrated that the short pulse duration enhances stability as there is insufficient time for instabilities to form within the discharge. Application of the pulsed air discharge to polymeric materials resulted in significant changes of the surface properties; after plasma treatment XPS was used to show that several oxygen containing functional groups had been introduced. Such a system could easily be integrated into existing industrial processes as a low cost means of in-situ surface enhancement. Many of the results from this section were published in the article '10 ns pulsed atmospheric air plasma for uniform treatment of polymeric surfaces' which appeared in Applied Physics Letters. 91, 251504 (2007).

8.2 Future Work & Improvements

Several pulsed power sources have been designed and constructed over the past three years, while they have proved sufficient to produce the results detailed within this thesis they are still experimental in nature and would be unsuitable for long term usage in an industrial setting. For the work detailed within this thesis to be truly useful further efforts need directing toward enhancing the reliability and efficiency of the pulse generators required. Additionally, the work discussed within this thesis covers a very few of the numerous applications which could benefit from an atmospheric pressure gas discharge generated with ultra-short voltage pulses. There is sufficient scope for several follow up studies focused upon applications alone. The following sub-sections are intended to give the reader an idea of what could be achieved

in the future and where improvements could be made to the work detailed within this thesis.

8.2.1 Alternative pulse generator topologies

Many of the pulse generators discussed within this thesis are considered because of their ability to produce kilovolt pulses with nanosecond rise times at kilohertz repetition rates. Future efforts could be directed towards producing discharges with sub-nanosecond pulses, the result are likely to be even higher peak powers and electron densities than those considered within the scope of this work. The physics behind a sub-nanosecond gas discharge is likely to become increasingly complex as the pulse duration becomes much shorter than the electron transition time through the gas gap. A further complication of reducing pulse width is the added complexity of the necessary diagnostic equipment. For example, an iCCD camera with minimum exposure time of 1ns would be insufficient to gain any real understanding of the breakdown mechanism of a 1ns pulsed discharge.

Several published studies make use of non-linear transmission line transformers as a means of reducing pulse width.[8.1] Such devices are relatively simple to construct, consisting only of inductors and diodes, and would be an ideal choice for 'sharpening' nanosecond duration pulses into sub-nanosecond pulses. In theory a simple 1kV MOSFET could be used to produce a pulse at a high repetition rate (hundreds of kilohertz) which the non-linear properties of the line would transform into a sub-nanosecond, high magnitude, high rep-rate pulses which would be ideal for plasma generation. Another promising pulse generator technology is the drift step recovery diode (DSRD).[8.2] Commercially available pulse generators employing DSRD's are capable of producing sub-nanosecond duration pulses up to 10kV at 100kHz, however they are prohibitively expensive for many applications. (http://www.fidtechnology.com/).

8.2.2 *Improved diagnostic techniques*

Several diagnostic techniques have been employed within this thesis, primarily electrical diagnostics such as current - voltage measurements, and optical techniques such as optical emission spectroscopy and iCCD imaging. While such techniques allow many aspects of a gas discharge to be explored in depth there are certain limitations to the detail of the data obtained. Ideally, more sophisticated diagnostic techniques, such as laser induced fluorescence (LIF),[8.3] would be employed to determine electron density, electron temperature, and absolute densities of chemical species. Unfortunately, the expense and complexity involved in LIF diagnostics means very few research groups have the necessary equipment and expertise required. Other diagnostic techniques such as stark broadening and line ratio methods can be employed to measure electron density and electron temperature, such methods are less accurate than LIF, but are much simpler and can be performed using a standard spectrometer. Stark broadening is known as a line shape technique and involves the observation of a single emission line, typically a hydrogen line; as electron density increases the profile of the line changes due to Stark broadening.[8.4] Unfortunately, Stark broadening in low density plasma ($<10^{14}cm^{-3}$) is limited and it is difficult to distinguish between the various broadening mechanisms present (Doppler, instrumental, etc).[8.5] It is likely that Stark broadening would not be too useful for the diagnostics of sub-microsecond pulsed discharges as rough calculations suggest they have electron densities around $10^{13}cm^{-3}$. Due to the high peak powers involved in nanosecond discharges there may be sufficient energy to produce electron densities above $10^{14}cm^{-3}$ which could be measured using Stark broadening.

Another promising technique suitable for measuring electron density and electron temperature is the helium line ratio method. This method is based on a collisional–radiative (C–R) model and is a well-established technique used to estimate electron density in the range of 10^{10}–10^{13} cm^{-3} and temperature in the range of 1–20 eV.[8.6] The availability of well-known helium atomic data, strong visible lines, and many density- or temperature-sensitive

line pairs makes this technique ideal for the moderate density helium plasmas produced using ultra-short pulsed excitation. Future efforts should be directed toward developing and validating the C-R model for use with pulsed gas discharges, potentially the method could be time resolved to show the evolution of electrons within the discharge, this would add great value to the current body of work

8.2.3 Increasing and decreasing discharge dimensions

The scale of the discharges investigated within this thesis are typically on the order of mm^3 to cm^3, these could best be described as laboratory scale. It is likely that the volumes considered are too small to be used on an industrial scale, and too large to be classed as a micro-plasma. Future efforts should be directed toward increasing / decreasing the dimensions of the discharge. For industrial applications the solution should simply be a process of scaling up, employing larger input powers to produce ever increasing volumes of plasma. The field of micro-plasma is growing rapidly; very small scale discharges introduce physical mechanisms which are not observed in larger scale plasmas, such as the possible breakdown of 'pd scaling' and the role of boundary-dominated phenomena.[8.7] Many novel and exciting applications are emerging from the field and these could benefit considerably from the insights gained within this thesis.

8.3 Concluding remarks

Finally, it is hoped that the reader has found reading this thesis an enjoyable experience and has gained a detailed understanding of the generation, mechanisms, and potential applications of ultra-short pulsed, atmospheric pressure, gas discharges. Through publication in journals and presentations at conferences the work detailed within has hopefully contributed to the ever expanding body of knowledge on atmospheric pressure gas discharges and will in some way prove useful to others working within the field.

References

[8.1] Ibuka, S, Abe, K, Miyazawa, T, Ishii, A, Ishii, S, 'Fast high-voltage pulse generator with nonlinear transmission line for high repetition rate operation', IEEE Transactions On Plasma Science, Vol.25, No.2, 1997.

[8.2] Pemen A.J.M, Grekhov I.V, van Heesch E.J.M, Yan K, Nair S.A, Korotkov S.V, 'Pulsed corona generation using a diode-based pulsed power generator', Review of Scientific Instruments, Vol.74, No.10, 2003.

[8.3] Niemi K, Schulz-von der Gathen V, Dobele H.F, 'Absolute atomic oxygen density measurements by two-photon absorption laser-induced fluorescence spectroscopy in an RF-excited atmospheric pressure plasma jet', Plasma Sources Science & Technology, Vol.14, No.2, 2005.

[8.4] Torres J,van de Sande M.J, van der Mullen J.J.A.M, Gamero A, Sola A, 'Stark broadening for simultaneous diagnostics of the electron density and temperature in atmospheric microwave discharges', Spectrochimica ACTA Part B-Atomic Spectroscopy, Vol.61, No.1, 2006.

[8.5] Wang Q, Koleva I, Donnelly V.M, Economou D.J, 'Spatially resolved diagnostics of an atmospheric pressure direct current helium microplasma', Journal Of Physics D-Applied Physics, Vol.38, Iss.11, pp.1690-1697, 2005.

[8.6] Srivastava A.K, Garg M.K, Prasad K.S.G, Kumar V, Chowdhuri M.B, Prakash R, 'Characterization of Atmospheric Pressure Glow Discharge in Helium Using Langmuir Probe, Emission Spectroscopy, and Discharge Resistivity', IEEE Transactions on Plasma Science, Vol.35, No.4, 2007.

[8.7] Becker K.H, Schoenbach K.H, Eden J.G, 'Microplasmas and applications', Journal Of Physics D-Applied Physics, Vol.39, Iss.3, 2006.